5G Programmable Infrastructure Converging disaggregated network and compUte REsources

D2.3 Vertical services, architecture and final evaluations

This project has received funding from the European Union's Framework Programme Horizon 2020 for research, technological development and demonstration

5G PPP Research and Validation of critical technologies and systems

Project Start Date: 1st June 2017 **Duration**: 33 months

Call: H2020-ICT-2016-2 **Date of delivery**: 11th November 2019

Topic: ICT-07-2017 **Version** 1.0

Project co-funded by the European Commission
Under the H2020 programme

Dissemination Level: Public

Grant Agreement Number:	762057
Project Name:	5G Programmable Infrastructure Converging disaggregated network and compUte REsources
Project Acronym:	5G-PICTURE
Document Number:	**D2.3**
Document Title:	Vertical services, architecture and final evaluations
Version:	1.0
Delivery Date:	September 30th 2019 (**November 11th 2019**)
Responsible:	University of Bristol (**UNIVBRIS**)
Editor(s):	Anna Tzanakaki (**UNIVBRIS-HPN**)
Authors:	Markos Anastasopoulos (**UNIVBRIS-HPN**), Arash Farhadi Beldachi (**UNIVBRIS-HPN**), Thierno Diallo (**UNIVBRIS-HPN**), Anna Tzanakaki (**UNIVBRIS-HPN**), Vaia Kalokidou (**UNIVBRIS-CSN**), Laura Serra (**TIM**), Andrea di Giglio (**TIM**), Alessandro Percelsi (**TIM**), Ioanna Mesogiti (**COS**), Elina Theodoropoulou (**COS**), George Lyberopoulos (**COS**), Salvatore Pontarelli (**CNIT**), Sevil Dräxler (**UPB**), Jesús Gutiérrez (**IHP**), Nebojsa Maletic (**IHP**), Darko Cvetkovski (**IHP**), Daniel Camps (**I2CAT**), Azahar Machwe (**ZN**), Jens Bartelt (**AIR**), Adrian Sasu (**ADVA**), Peter Legg (**BWT**), Kostas Katsalis (**HWDU**).
Keywords:	Flexible functional splits, Disaggregated RAN, hardware programmability, network softwarisation, Physical Network Functions, Virtual Network Functions, Performance Evaluation, Techno-Economic Analysis, multi-tenant and multi-operator services.
Status:	Final
Dissemination Level	Public
Project URL:	http://www.5g-picture-project.eu/

Revision History

Rev. N	Description	Author	Date
0.1	First draft shared with the Consortium	Anna Tzanakaki (UNIVBRIS-HPN)	01.07.2019
0.2	Contributions to Section 2 and Section 6	Ioanna Mesogiti (COS), Elina Theodoropoulou (COS), George Lyberopoulos (COS), Andrea di Giglio (TIM), Laura Serra (TIM), Alessandro Percelsi (TIM)	05.09.2019
0.3	Contributions to Section 3.4 Section 4	Sevil Dräxler (UPB), Azahar Machwe (ZN)	09.09.2019
0.4	Contributions to Section 3.1	Anna Tzanakaki (UNIVBRIS-HPN), Markos Anastasopoulos (UNIVBRIS-HPN)	10.09.2019
0.5	Contributions to Section 5	Anna Tzanakaki (UNIVBRIS-HPN), Markos Anastasopoulos (UNIVBRIS-HPN), Vaia Kalokidou (UNIVBRIS-CSN)	19.09.2019
0.6	Contributions to Section 3.2	Salvatore Pontarelli (CNIT), Adrian Sasu (ADVA), Jens Bartelt (AIR), Arash Beldachi (UNIVBRIS-HPN), Daniel Camps (I2CAT), Nebojsa Maletic (IHP), Jesús Gutiérrez (IHP)	20.09.2019
0.7	Revisions to Section 4	Sevil Dräxler (UPB), Azahar Machwe (ZN)	20.09.2019
0.8	Contributions to Section 3.3	Daniel Camps (I2CAT), Peter Legg (BWT), Kostas Katsalis (HWDU), Thierno Diallo (UNIVBRIS-HPN), Darko Cvetkovski (IHP), Jesús Gutiérrez (IHP)	08.10.2019
0.85	Revisions of all sections by all Partners involved	ALL	21.10.2019
0.9	Final revision of the deliverable	Anna Tzanakaki (UNIVBRIS-HPN), Jesús Gutiérrez (IHP)	05.11.2019
1.0	Submission of the deliverable	Jesús Gutiérrez (IHP)	11.11.2019

Table of Contents

List of Figures

List of Tables

Executive Summary

This deliverable reports on the refined 5G-PICTURE architecture together with a detailed evaluation of its performance through modelling and simulations focusing on network performancel Key Performance Indicators (KPIs), including energy consumption and cost.

5G-PICTURE has focused on the development and demonstration of a converged fronthaul and backhaul infrastructure integrating advanced wireless and novel optical and packet network solutions. To address the limitations of the current Distributed-Radio Access Network (D-RAN) and Centralised/Cloud-RAN (C-RAN) approaches, 5G-PICTURE proposed a novel and advanced transport network solution and exploited the concept of flexible functional splits that can be dynamically selected, to optimise resource and energy efficiency. Within this framework, the project's main architectural principles include convergence and integration of network and compute technologies, network softwarisation, hardware programmability and dissagregation of compute/storage and network resources. Adopting these concepts, the project has proposed the architectural approach of Disaggregated - Radio Access Network (DA-RAN) to facilitate provisioning of any service across the infrastructure by flexibly and efficiently mixing-and-matching network, compute and storage resources. "Resource disaggregation" allows decoupling of network and compute/storage components, creating a common "pool of resources" that can be independently selected and allocated on demand to compose any infrastructure service with increased efficiency.

The overall architectural approach of the project involves a layered structure comprising a programmable data plane that exposes a set of physical and virtual funtions to the control plane. Services are provisioned through the orchestration layer responsible to combine physical and/or virtual functions adopting the notion of service chaining. In this generic framework, 5G-PICTURE relies on a set of hardware and software innovations associated with the data plane, the control plane and the orchestration layer. In addition, to the principles described above, one of the central objectives for the 5G-PICTURE architecture is to support multi-tenancy. The overall 5G-PICTURE architecture has been evaluated using mathematical models, simulation frameworks as well as experimental platforms. In addition, 5G-PICTURE will showcase converged fronthaul and backhaul services in: a) a smart city environment in Bristol, UK, b) a 5G railway experimental testbed showcasing seamless service provisioning and mobility management in moving environments in Catalonia, Spain and c) a stadium with ultra-high user density, supporting media services in a stadium in Bristol, UK.

This deliverable summarises the vertical services planned to be demonstrated by the project including also some high-level discussion on the KPIs to be evaluated. In addition, it describes the 5G-PICTURE layered architecture, and discusses the functionality, capabilities and features of the individual layers. A detailed discussion on how the overall 5G-PICTURE architecture and approach supports multi-tenancy and multi-operator envronments is also provided. It also concentrates on the theoretical evaluation of the proposed architecture. The data plane related evaluation focused on performance assessment of 5G wireless access communications to trains and the adoption of Sub-6 GHz LTE Massive MIMO technologies, multi-technology access network solutions in railway systems and the benefits these can provide in terms of reliability and throughput. Architectural solutions to support resilient C-RAN services are also proposed and analysed. Possible approaches for efficient dynamic placement of softwarised RAN functions in Data Centres adopting the disaggregated 5G-PICTURE architecture have been studied and evaluated and suitable solutions are proposed. Emphasis is also given on the scalability challenges associated with the proposed solution and a novel service chaining approach is proposed that can significantly reduce service provisioning times. Suitable approaches to enable scalable service chaining in MEC-assisted 5G Networks exploiting Artificial Intelligence (AI) and scalable multi-service placement are also examined. The performance of the proposed schemes is examined over realistic topologies using actual traffic data. The performance of the 5G-PICTURE architecture has also been assessed in terms of cost efficiency through a detailed techno-economic analysis taking into consideration real traffic statistics and equipement costs.

1 Introduction

Digital technologies have been identified by the EU as key in addressing some of its fundamental challenges associated with societal and economic objectives, such as improved quality of living for citizens, sustainable development and economic growth. This approach will create new opportunities for governments, businesses and individuals. In this context, 5G infrastrucutres will play a fundamental role in bringing these technologies to society, organizations and countries transforming their every day's life in the way services are provided, and businesses are run. The effect of this approach is expected to influence a large variety of sectors through the ability to offer connected goods, collaborative and automated processes within and across sectors, optimized processes, new and improved services with regards to security, user experience, etc.

However, this transformation will require new service capabilities that network operators need to support including: i) connectivity for a growing number of very diverse devices, ii) ubiquitous access with varying degrees of mobility from low to high in heterogeneous environments and, iii) mission critical services currently handled by closed specific purpose networks, supporting highly variable performance attributes in a cost and energy-efficient manner. Typical examples include networks used to provide end user and operational services in mobile telecommunication networks, vertical industries such as communication networks used by railway operators, media services, etc. These demanding and diverse requirements bring the need of a paradigm shift to support the upcoming service requests imposing enormous capacity requirements, following new service models such as cloud-based solutions. Only future proof infrastructures adopting flexible architectures offering converged services across heterogeneous technology domains deploying unified software control will be able to address a wide range of vertical industry services.

In this context, 5G-PICTURE, in aligment with the overall 5G vision, targeted to develop a generic architecture that is able to support a set of stringent requirements in terms of latency, reliability and density, along with tight constraints on geographical and population coverage and high-speed mobility capabilities. The project focuses on the development and demonstration of a transport network infrastructure supporting converged fronthaul and backhaul services integrating advanced wireless and novel optical and packet network solutions. The requirements that the architecture needs to support have been identified and studied through the generic 5G KPIs defined as part of the 5G PPP KPI Working Group (part of the Technical Board) activites and also the specific use cases planned to be showcased in the framework of the project. These use cases include a Rail related demonstration in Catalonia, Spain; a Smart City demonstration in the city wide test-bed in Bristol, UK; and a Stadium event demo also located in Bristol, UK exploiting the generic 5G-PICTURE architecture and technology developments.

The main architectural principles that 5G-PICTURE have focused on include convergence and integration of network and compute technologies, network softwarisation, hardware programmability and dissagregation of compute/storage and network resources. Adopting these concepts, the project has proposed the architectural approach of Disaggregated - Radio Access Network (DA-RAN), to facilitate provisioning of any service across the infrastructure by flexibly and efficiently mixing-and-matching network, compute and storage resources. The overall architectural approach of the project involves a layered structure comprising a programmable data plane that exposes a set of physical and virtual funtions to the control palne. Services are provisioned through the orchestration layer responsible to combine physical and/or virtual functions adopting the notion of service chaining. In this generic framework, 5G-PICTURE relies on a set of hardware and software innovations associated with the data plane, the control plane and the orchestration layer.

One of the very central targets for the 5G-PICTURE architecture is to support multi-tenancy, different strategies can be applied to support slicing for both the RAN and transport network. Specifically, for the RAN, slicing can rely on slicing at the spectrum level, the Inter-Cell Interference Coordination (ICIC) level, the packet scheduling level, and at the admission control level. In 5G-PICTURE slicing related use cases will be shown as part of the Bristol stadium and the Spanish Rail demonstrations.

Mathematical models and simulation frameworks have been specifically developed for the overall 5G-PICTURE architecture evaluation. The data plane related architecture evaluation focused on the assessment of the performance of 5G wireless access communications to trains and the adoption of Sub-6 GHz LTE Massive MIMO technologies, multi-technology access network solutions in railway systems and the benefits these can provide in terms of reliability and throughput. Transport network solutions to support resilient C-RAN services are also proposed and analysed. Possible approaches for efficient dynamic placement of softwarised RAN functions in Data Centres adopting the disaggregated 5G-PICTURE architecture have been studied and evaluated and suitable solutions are proposed. Emphasis is also given on scalability challenges associated with 5G in general and the 5G-PICTURE specific solution. In this ontext, a novel service chaining approach is proposed to significantly reduce service provisioning times. Suitable approaches to enable scalable service chaining in MEC-assisted 5G Networks exploiting Artificial Intelligence (AI), and finally scalable multi-service

placement have been also examined. The performance of the proposed schemes is examined over realistic topologies using actual traffic statistics. Finally, the 5G-PICTURE architecture has been also assessed in terms of cost efficiency through a detailed techno-economic analysis taking into consideration real traffic statistics and equipement costs.

1.1 Organisation of the document

This document comprises seven sections. Following the Executive Summary and Introduction sections, Section 2 summarises the vertical services planned to be demonstrated by the project including also some high level discussion on the KPIs to be evaluated. Section 3 focuses on the 5G-PICTURE layered architecture, and discusses the functionality, capabilities and features of the individual layers. Section 4 discusses how the overall 5G-PICTURE architecture and approach supports multi-tenancy and multi-operator envronments. Section 5 focuses on the evaluation of the proposed architecture, involving the description of purposely developed models and simulation tools as well as detailed results produced to analyse and benchmark the 5G-PICTURE solution against alternative approached. Section 6 provides a detailed technoeconomic analysis based on a techno-economic model developed specifically for the 5G-PICTURE solution using a realistic scenario and actual cost and traffic data. Finally, in Section 7 the conclusions of the deliverable are summarised.

2 Vertical service to be demonstrated and KPIs

2.1 Overview of 5G networks and services KPIs

During the last years, standardisation bodies such as 3GPP, ETSI and ITU, as well as industry alliances and regulatory bodies, have focused on the definition of the application and networks services [9] and the required Quality of Service (QoS) to be delivered by 5G network deployments [10]. The work of these bodies has also led to the definition of the various service-level KPIs and target values to assess the 5G infrastructure (user and network equipment capabilities) and network deployments [3],[4],[5],[6],[7],[8].

In particular, Vertical applications to be served by 5G networks (and benefit from their advancements) correspond to Service Classes categorized by 3GPP and ITU-T as follows: enhanced Mobile BroadBand (eMBB), massive/enhanced Machine Type Communications (m/eMTC) and Ultra Reliability Low Latency Communications (URLLC). For these service classes, the critical network service-related KPIs and the target values to be achieved by 5G equipment and network deployments have been identified by 3GPP [3],[4],[5],[6],[7],[8], indicatively as follows:

- **eMBB KPIs** (taking into consideration services like video streaming, video conferencing and virtual reality):
  - High DL/UL Data Rates: from 20 to 100 Mbps per user (exploiting statistical multiplexing at network deployment level).
  - Low Latency: $\leq$10 ms End-to-End (data plane) and at 2-4 ms control plane for highly interactive and mission critical eMBB services.
  - Traffic Density: 3.75 Mbps DL/m^2 and 7.5 Mbps/m^2 UL; for Crowdsourced video the requirement is >10,000 users/km^2 (METRO-HAUL project) [16].
  - Mobility: for users' speed in vehicles at 60-100 km/h for CDN video services, and at 50 km/h for Live TV distribution, as defined by METRO-HAUL project [16], while there may be cases with speed reaching 200 km/h).
- **m/eMTC KPIs** (for *massive IoT* like metering sensors and for *enhanced MTC* like automotive sensors):
  - High Coverage for the huge number of metering sensors, typically about 200,000/km^2, at highest density reaching 1M/km^2 (connection density reflects active devices that are exchanging data, assuming a single operator in the considered area per km^2).
  - Positioning accuracy around 0.3 m (and preferably of 0.1 m for eMTC).
- **URLLC KPIs** (for "mission critical" communications in industry automation, medical application, etc.):
  - Ultra High Reliability: 10^{-5} successfully delivered packets at 32 bytes within 1 ms.
  - Connection Availability: 99.999% of available time for a transport connection (imposed also by 5G-PICTURE).
  - Communication Service Availability: 99.999% of available time for an end-to-end service with agreed QoS (imposed also by 5G-PICTURE).
  - Ultra Low Latency: 0.5 to 1 ms control plane latency, $\leq$10 ms data plane latency.
  - Packet or Frame Loss: 10^{-4} (considered also as 5G-PICTURE target).
  - Jitter 10-100 μs.

It is obvious that there are KPIs that depend highly on network equipment capabilities, such as the aggregate and per user data rate which depend on radio network equipment performances or the high mobility that depends on network equipment abilities to mitigate Doppler and high BER effects, and there are KPIs that are deployment-specific such as broad coverage, service availability; or other KPIs that are both equipment and deployment dependent such as Packet/Frame Loss, Traffic Density, Jitter, etc.

At the same time, in the context of 5G-PPP activities (projects and collaborative works), the infrastructure and services' KPIs defined by standardisation bodies and industry alliances have been compiled and high-level, operational 5G network deployment KPIs have been derived in comparison to existing technologies deployments as follows [11], [13]:

- 1,000 times higher mobile data volume per geographical area reaching a target of 0.75 Tbps for a stadium.

- 1,000 times higher number of connected devices reaching a density ≥ 1M terminals/km^2.
- 100 times higher user data rate reaching a peak terminal data rate ≥ 1 Gbps for cloud applications inside offices.
- 10 times lower energy consumption compared to 2010.
- 5 times lower end-to-end latency reaching delays ≤ 5 ms.
- 5 times lower network management Operational Expenditure (OPEX).
- 1,000 times lower service deployment time for reaching a complete deployment in ≤ 90 minutes.
- Guaranteed user data rate ≥50 Mbps.
- Capability to support ≥ 1 trillion IoT terminals.
- Service reliability ≥ 99.999% for specific mission critical services.
- Mobility support at speed ≥ 500 km/h for ground transportation.
- Accuracy of outdoor terminal location ≤ 1m.

These 5G-network deployment KPIs and targets essentially reflect the network service requirements expected from operational 5G network deployments. They can be translated as requirements to be fulfilled by the network operators as stakeholders undertaking the role of delivering the network service, either enforced by regulation or by the market they address, irrespective of the underlying technological specifics of the system that is deployed. It becomes obvious that some of these KPIs are very tightly related to the network architecture and real network deployment options besides the capabilities of the individual network nodes; thus shall be considered in the definition of any 5G network architecture and deployment options.

For the purposes of assessing 5G network equipment/architectural solutions/deployments towards these KPIs, a parallel 5G-PPP Working Group exercise has led to further decomposition – for the time being- of the Latency and Service Deployment Time performance KPIs [12].

Latency

Towards having a common reference for assessing the generic latency KPI, given the fact that latency depends on equipment as well as application and network deployment specificities, the end-to-end latency has been decomposed into the following network segment-specific latency contributions (Figure 2-1):

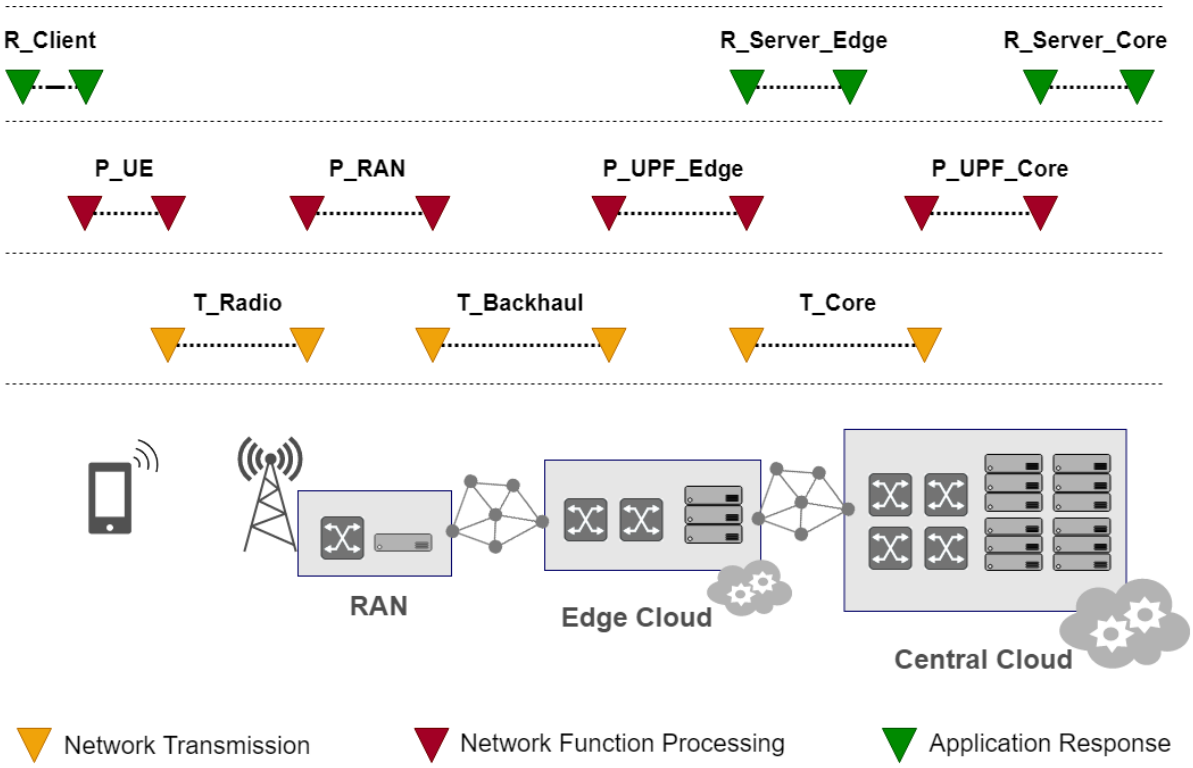

Figure 2-1: Reference framework of delay contributions of an end-to-end latency [12].

Service Deployment Time

Similarly, towards having a common reference for assessing the generic service deployment time KPI, given the fact that service deployment is a procedure involving a number of different processes depending on the service/application and network deployment/setup, the generic KPI has been decomposed into sub-KPIs referring to the following phases [12]: Platform Provisioning, Service/Application Onboarding, Service Instantiation/Configuration and Activation, Service Modification and Service Termination, as detailed in Table 2-1.

Table 2-1: Reference framework of service deployment time contributions to an end-to-end service deployment time ([12]).

Service Deployment Time KPIs	Time components
Phase 0. Platform Provision	Platform configuration
	Platform deployment
Phase 1. Onboarding	Network Slice Template (NEST)
	Network Service Descriptor (NSD)
	VNF package (VNFD)
	MEC Application Descriptor (MEC AppD)
	Other applications
Phase 2. Instantiate, Configure & Activate	Instantiate Network Slice (NSI)
	Instantiate & Activate Network Service (NS)
	Instantiate & Configure VNFs in service chain (VNF)
	Instantiate & Configure MEC Application (MEC App)
	Instantiate & Configure other applications
	Configure other NFVI elements
	Configure SDN infrastructure
	Configure Optical WAN
	Configure satellite backhaul
Phase 3. Modify	Modify Network Slice configuration
	Modify Network Service configuration
	Detect scale out/in decision
	Implement manual scale out/in
	Implement autoscale out/in
	Modify VNF configuration in service chain
	Modify MEC App configuration
	Modify configuration of other applications
	Modify configuration of other NFVI elements
	Modify configuration of SDN infrastructure
	Modify Optical WAN circuit
	Modify satellite backhaul configuration
Phase 4. Terminate	Terminate Network Slice (NSI)
	Terminate Network Service (NS)
	Terminate VNFs in service chain (VNF)
	Terminate MEC Application (MEC App)
	Terminate other applications
	Remove configuration of other NFVI elements
	Remove configuration from SDN infrastructure
	Terminate Optical WAN circuit
	Terminate satellite backhaul circuit

It shall be noted that, besides the service-related KPIs, 5G network technologies/architecture/deployments shall also address a number of telecom operator-defined requirements and KPIs, such as multitenancy, interoperability with various technologies, resilience, security, scalability and so on, as already presented in [14].

5G-PICTURE has contributed to the aforementioned work through participation to the relevant 5G-PPP KPIs and Architecture WG discussions, and it has equally considered the WGs work in the equipment/ architecture/ reference deployment to be delivered by the project and the associated evaluation.

2.2 KPIs Evaluation through 5G-PICTURE Network Architecture Options' Analysis

Considering the 5G network and service requirements and KPIs, the 5G-PICTURE architecture has been refined, and deployment options have been defined as it will be further detailed in Chapter 3. The architecture and deployment options have been further evaluated from the perspective of the architecture and deployment-specific KPIs as follows:

- Multitenancy support, considering the telecom operator multitenancy requirements, with regard to:
  - Capabilities to have versatile tenant profiles.
  - Isolation.
  - QoS guarantees.
- Mobility, towards achieving seamless service provisioning for eMBB and Critical Communication services at train speeds – considering the high mobility KPI.
- Service provisioning workflows, considering the service provisioning and deployment time KPIs.
- Co-existence of heterogeneous processing capabilities (GPPs, GPUs, FPGAs, HW accelerators) through the disaggregated 5G-PICTURE approach, considering the interoperability with various technologies requirement.
- Scalability, considering the devices density (control plane) and traffic density (user plane) KPIs.
- Resilience and security, considering the relevant telecom operator requirements and reliability/ availability KPIs.

2.3 KPIs Evaluation through 5G Network Deployment Modelling Tools

In addition, targeted analysis tools have been extended/developed for the purposes of evaluating deployment-specific aspects, such as Network CAPEX/OPEX and network Energy Efficiency.

In particular, a techno-economic analysis of the 5G-PICTURE technologies and architecture alternatives has been performed considering real network deployments, towards evaluating the aforementioned network CAPEX/OPEX minimisation KPI. The latter is highly dependent on the running equipment prices, as well as on the deployment options, thus the aim of this work has been the identification of the key parameters affecting the YTCO (Yearly Total Cost of Ownership).

Energy Efficiency has been also evaluated with these tools, given the fact that this KPI highly depends not only on the equipment characteristics but also on the network deployment specifics.

Details of these analyses and the obtained results are provided in Chapter 6.

2.4 KPIs Evaluation through 5G-PICTURE demonstrations

At a third stage, equipment capabilities and short scale network deployment options are evaluated through 5G-PICTURE demonstrators, in terms of their capability to achieve the KPI targets related to vertical services. Details regarding the demonstrators, the evaluation procedures and the KPIs are provided in [15], and will be further processed and refined in 5G-PICTURE deliverable D6.3.

2.4.1 Railway Demonstrator

Considering the Railway Vertical sector in the context of 5G-PICTURE, the combination of mmWave radio links (for high quality mobile broadband connections) and Passive WDM, which provides point-to-point logical connections through a physical point-to-multipoint network topology, has been considered as the most appropriate technology deployment option for building the vertical's telecommunications infrastructure named Train Access Network (henceforth abbreviated as TAN), represented in Figure 2-2. The main idea is to provide broadband connectivity to the passing trains along the railway track, towards delivering high performance network services at train speeds.

For this purpose, also a new and faster on-board communication network, traditionally named as Train Communications Network (TCN) must also be developed to take advantage of the capabilities of this new TAN, allowing aggregated traffic in the order of Gbps. More information can be found in [15].

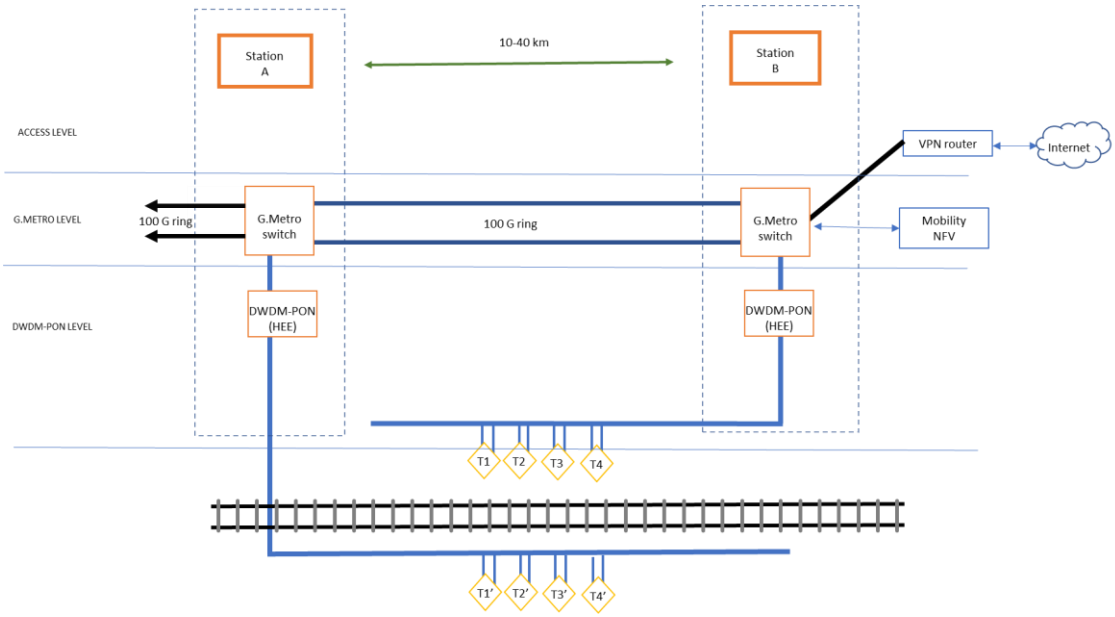

Figure 2-2: TAN components.

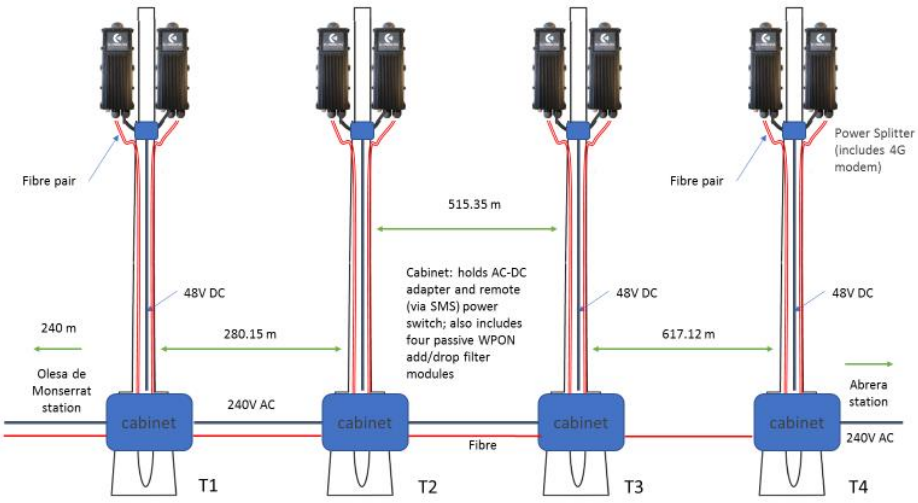

Figure 2-3: Towers location.

In the medium term, this network solution would aim to be valid for any generic railway deployment, regardless of the type or nature of rail services (from High Speed Long Distance to High Frequency Urban Metro), it iwould be dedicated to both passenger and freight transport and it would prove itself to be valid for all types of environments (including tunnels and adverse weather situations).

In the context of 5G-PICTURE, the capabilities of these solutions will be evaluated in the context of a limited railway demo environment, thus showing the enormous potential of this new architecture. In particular, testing will be done in one **FGC** line, from Llobregat to Anoia, locations that surround Barcelona metropolitan area. The track section selected to develop the 5G-PICTURE demo is placed between Olesa and Martorell stations. The information sent by the 5G network will be sent to Martorell station where it will be placed the simulated control centre.

Four stanchions, near the Olesa de Monserrat station, are equipped with a pair of mmWave AP's each one. The distances between the towers and the area to be provided with mmWave coverage are shown below in Figure 2-3.

Martorell station has its own Internet Access and will host the video recorder and the CCTV screens, as well as all the equipment needed to perform the Handover Management Network Function for Session Continuity.

One FGC train will be equipped with a TCN represented by two on-board mmWave units, mounted at the front and rear of the train and Host Processor Modules that will be connected to both ends of the 10G Ethernet ring, as shown in Figure 2-4.

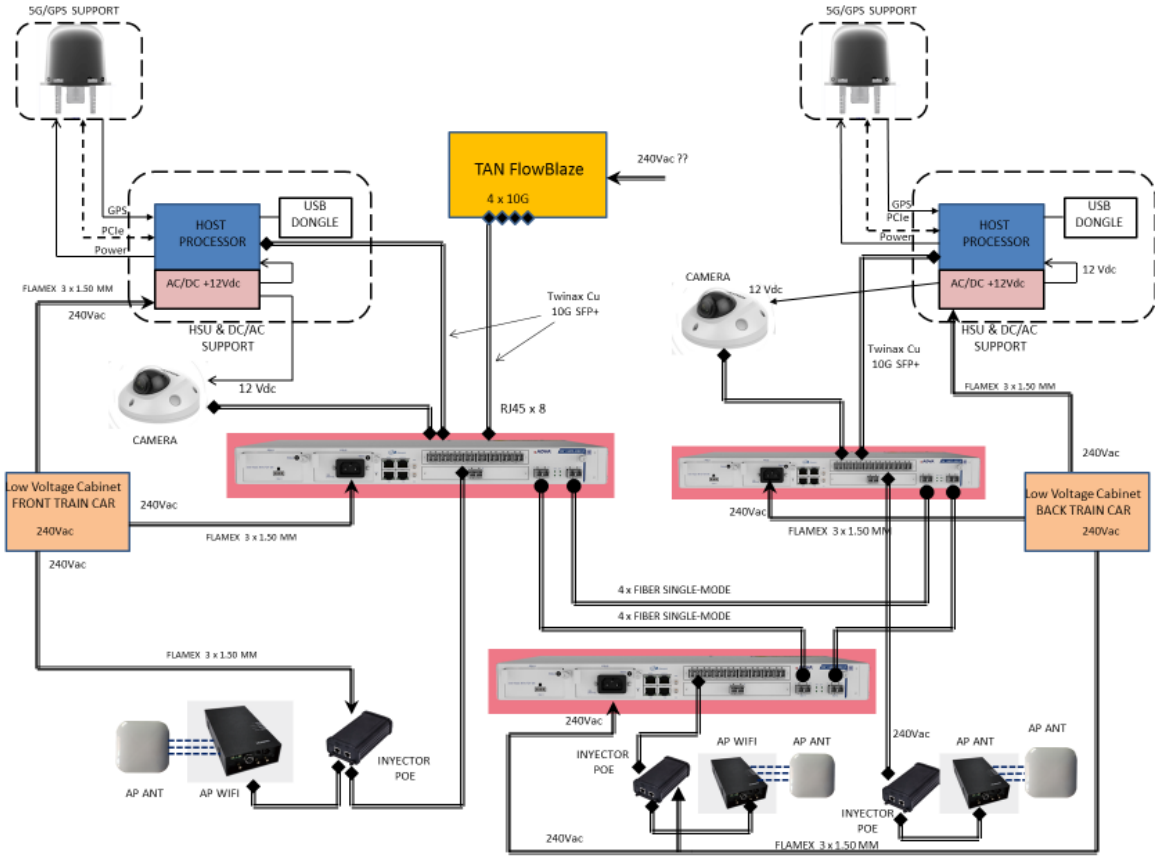

Figure 2-4: On-board equipment for TCN.

This 10G ring will consist of three Ethernet switches interconnected by two fibres; each of them in a vehicle. One Wi-Fi AP will be connected to each switch to provide the Internet Access service to passengers. A CCTV camera will be attached to the TCN. These will be the services used to test the broadband transparent connection.

The vertical service KPIs to be evaluated through this demonstrator (as indicative railway 5G network deployment option) are described in Table 2-2.

Table 2-2: Railway Demonstrator KPIs Evaluation.

KPI	Type & Comments
Users data rate	Equipment & Deployment-specific (Through ftp transfers between devices connected to the on-board Wi-Fi AP's and a server located at Martorell station). Considering the services 20-100 Mbps/user is expected.
Radio Network node capacity	Equipment-specific 1 – 3.5 Gbps to the train is expected taking into account the deployment.
Data rate for train communication services	Deployment-specific (Through live-recording of CCTV files produced by the images captured by the on-board high definition cameras)

End-to-end latency for train communication services	Equipment & Deployment-specific
High Reliability	Deployment-specific (Through monitoring Data BER, packet loss rate, CRC errors)

2.4.2 Smart City Demonstrator

As already discussed in 5G-PICTURE deliverables D2.2, D6.1 and D6.2, **UNIVBRIS'** 5G testbed is a multi-site and multi-technology test network connected via city wide fibre and wireless links along with several active switching nodes and access points. This test network is managed from the Smart Internet Lab at Merchant Venturers Building (one of the University of Bristol sites). This site is connected with fibre towards the "We The Curious" and "MShed" locations in the heart of the city of Bristol.

The state-of-the-art radio access technologies (RATs) deployed in Millennium Square will deliver high-bandwidth, high-bitrate and high-reliability connections to the user equipment, therefore enabling the usage of the network-intensive distributed applications for the 5G-PICTURE demonstration. In particular, the availability of LTE-Advanced (LTE-A) and installations of 5G access points (Nokia 5G NR) will be especially important in 5G-PICTURE to demonstrate applications that require mobility while keeping user experience continuity.

The SDN capabilities supported by the NetOS controller will facilitate network slicing through optical, electrical and radio technologies via on-demand SSID creation, demonstrating another key concept in the 5G architecture that will be explored by 5G-PICTURE to provide a multi-tenant environment, where the multiple demonstrators, or even final users, can coexist independently with different connectivity specifications.

The high performance and edge computing capabilities will power resource-intensive applications developed for the 5G-PICTURE demonstrators. In these applications, hardware acceleration and GPU-processing will be used to deliver enhanced performance and enable low-latency/real-time user interaction.

Finally, the University of Bristol 5G testbed will deliver an automated and programmable environment, which will be used by the 5G-PICTURE southbound interface to create fully integrated orchestration for both application components and network services.

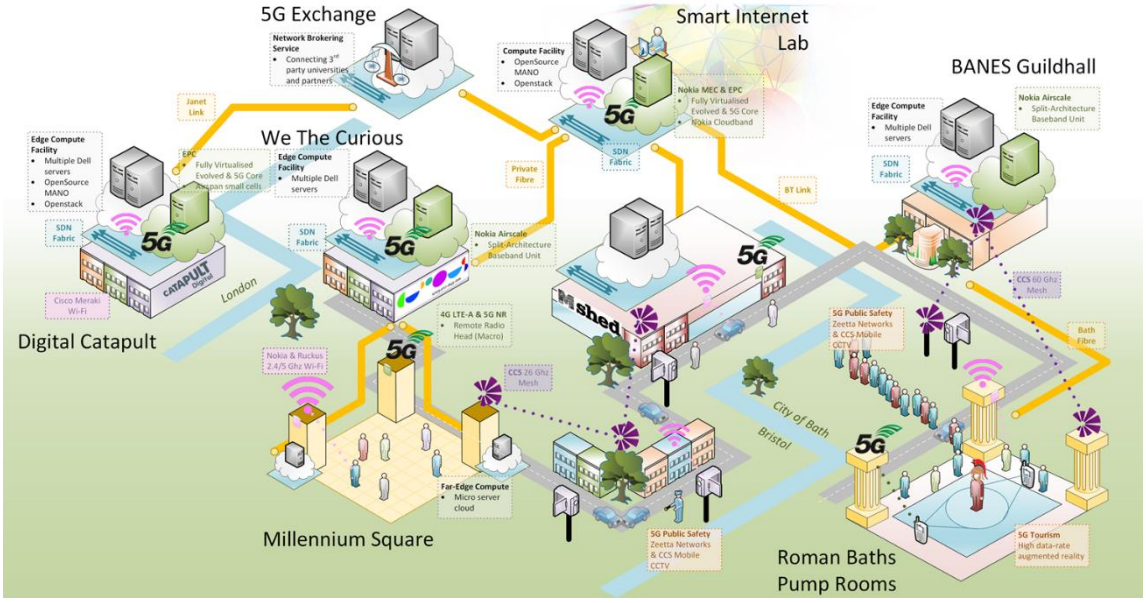

Figure 2-5: 5GUK University of Bristol's Network Connectivity.

2.4.2.1 Use Cases to be demonstrated

The Use Cases and Services that have been identified to be demonstrated over the 5G UK test-bed extended to include the 5G-PICTURE technologies are listed below.

2.4.2.1.1 Use Case1: VR /AR

This creative & production processes includes visual and audio data capture of an artist performing in a private space in Bristol. The use case creation will involve working with the artists and development team in order to expand the visuals into a real-life environment around Millennium Square in Bristol. An audio specialist will work on the soundtracks so it adapts to the environment; while the development team further creates the data into an Augmented Reality experience.

The music artist leads the ritual-like audio experience through her holographic persona, whilst each participant assumes the virtual form of an anthropomorphic character. The experience allows a group of guests wearing VR headsets and headphones to get lost within a 10-metre virtual space, alongside the holographic capture of Devi herself. Individual instrument tracks from the featured music piece are scattered around the environment, making the music sound different from every position; whilst guests can playfully interact with each other through their virtual avatar alter-egos.

Target performance from the use case

Table 2-3: Virtual Reality Demonstrator KPIs Evaluation.

KPI	Type	Target value
Radio Network node capacity	Equipment – Specific to the Access Technology	≥ 30 Mbps (DL) ≥ 1 Mbps (UL)
Throughput	Equipment – specific to the cameras used	< 3 Mbps (DL) < 100 Kbps (UL)
Latency	Between the Device and the Cloud serving node	< 35 ms (UL or DL)

2.4.2.1.2 Use Case 2: Smart City Safety

This use case looks for monitoring the city with audio and video sensors. These sensors are deployed in a bike helmet and they are attached to a Raspberry PI (RP) that communicates via Wi-Fi to the Cloud or Edge (MEC – Mobile Edge Computing). The RP sends video and audio to be processed in a DC. Using VNFs, the overall ecosystem should be able to perform audio and video transcoder a long of the network. In addition, audio and video processing using machine learning to detect suspicious activities in the city should take place. Once the suspicious activities have been detected the system is able to notify the security department with the right information. Based on the information the security guards spread in different location will be able to take the right action.

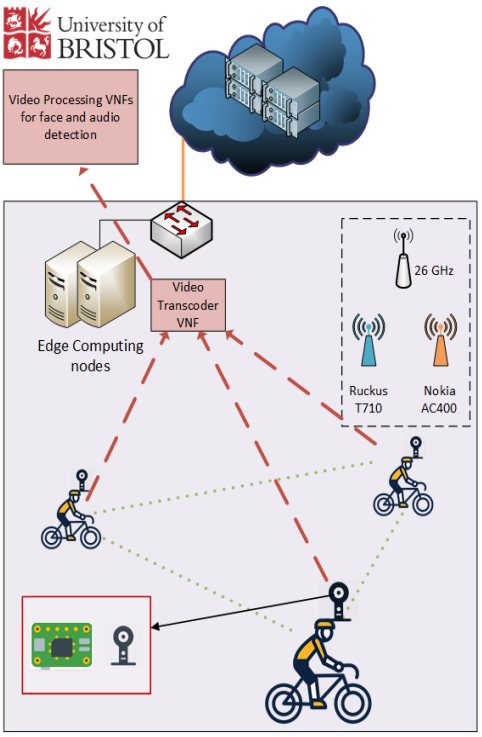

The setup may be equipped with 3 x 360-degree cameras on 3 bike helmets with each attached to a Raspberry Pi. The camera is sending audio and video to the cloud storage and the face detection software ready to process data from the cloud. The VNFs are not yet available.

The Safety Use Case use case will be carried out in 5G Bristol Testbed. It will involve the Harbour side area of the Bristol City Centre, adjacent to the Millennium Square, where a significant part of 5G Bristol testbed's RAN is located, using either Wi-Fi, LTE or 5GNR air interfaces while testing the 5G-PICTURE fronthaul technologies from IHP mmWave or Airrays radio demonstration access technology.

Table 2-3: Smart City Safety Demonstrator KPIs Evaluation.

KPI	Type	Target Value
Radio Network node capacity	Equipment – Specific to the Access Technology	≥ 50 Mbps
Throughout	Equipment – specific to the cameras used Expected to be greater than 3 Mbps per device	≥ 3 Mbps per device
Latency	Between the Device and the Cloud serving node	< 50 ms

2.4.3 Stadium and mega event

The stadium demo aims at evaluating the 5G-PICTURE solution and architecture with view to the Service Deployment Time (sub-) KPIs. In practice, it is validating service creation over an heterogeneous network, consisting of wireless access and fixed transit network, using the 5G OS defined in WP5. The demo will also show the use of VNFs and programmable networks to improve the utilisation of access networks. Network slicing is used to provide isolation in the transit network.

Figure 2-6 shows the demo outline. I2CAT provides Wireless Access Points and Wireless Fronthaul, which represent an access network at the Mega-Event/Smart Venue. Zeetta Networks (ZN) provides the fixed network, which represents a transit network providing connectivity to multiple tenants including the Mega-Event/Smart Venue.

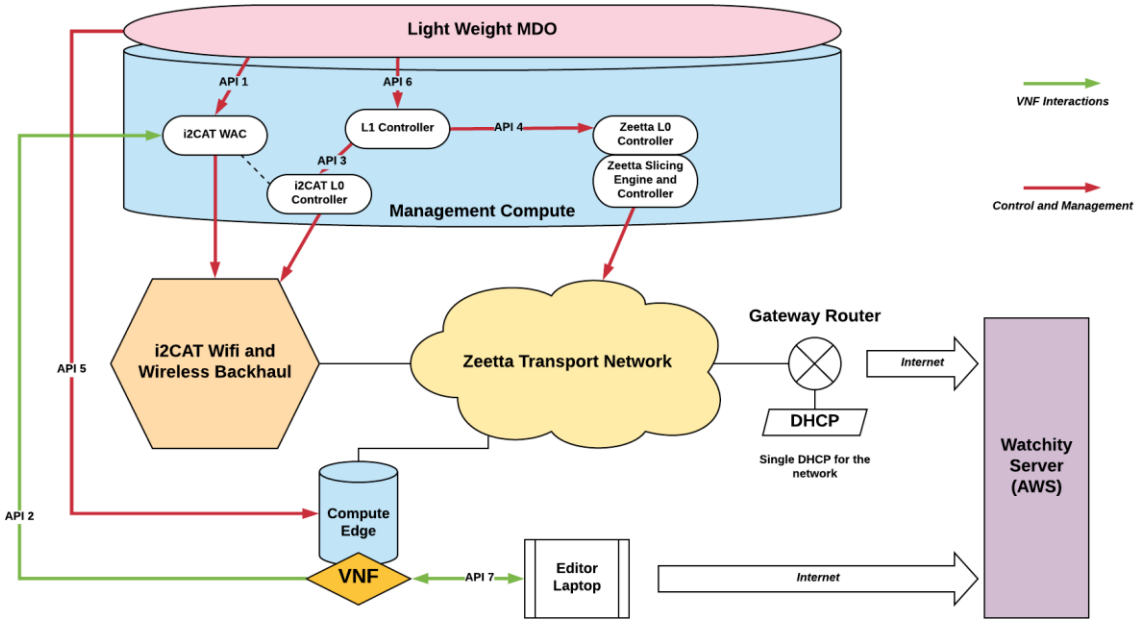

Figure 2-6: Demo network setup showing Data Plane, Control Plane and Integration Points (APIs).

The demo of this vertical consists of three separate test scenarios:

- Scenario 1: End-to-end service setup consisting of connectivity and functions over wireless and transit networks, addressing the service deployment time (sub-) KPIs.
- Scenario 2: Showcase of how programmable networks can enable services to operate in conditions of reduced resource availability (by using VNFs), addressing the service deployment time (sub-) KPIs, and partially the KPIs relate to user data rate and number of connected devices.
- Scenario 3: Show of how different classes of services can be created over shared infrastructure, addressing the service deployment time (sub-) KPIs and partially the KPIs relate to user-experienced QoS.

The KPIs to be evaluated in these use cases are reported in the following Table 2-3.

Table 2-3: Stadium and mega event Demonstrator KPIs Evaluation (first set).

KPI	Type
Users data rate **(also under reduced resource availability)**	Equipment & Deployment-specific Targeting 5-15 Mbps/user considering the Watchity application.
Radio Network node capacity	Equipment-specific Expected to be 1~3 Gbps
Number of connected devices (number of offered services by devices under reduced resource availability)	Equipment & Deployment-specific
Service Setup Time	Deployment-specific
Ubiquitous access	Deployment-specific Over the expected coverage area.

Physical Access at the Edge

The other challenge during a mega-event (sport, concert and so on) is that the edge access is required to provide connectivity to many users in a small area. Novel access technologies such as massive MIMO (mMIMO) can solve this problem. The latter will be demonstrated at the University of Bristol (**UNIVBRIS-CSN**).

In this specific vertical use case, the KPIs to be achieved are shown in Table 2-4.

Table 2-4: Stadium and mega event KPIs Evaluation (second set).

KPI	Type	Target Value
Radio Network node capacity	Equipment-specific Targeting 1 – 3.5 Gbps	1 – 3.5 Gbps
Number of connected devices	Equipment & Deployment-specific	12
Service Setup Time	Deployment-specific	1 Minute

3 Refined overall 5G-PICTURE architecture

3.1 Generic Layered Structure

The generic 5G-PICTURE architecture has maintained its aligment with the overall 5G vision and the requirements and KPIs of the use cases and services described in deliverable D6.1 (Specification of Vertical Use cases and Experimentation) and section 2 of this document. In view of this and the fundamental objective of the project to provide a common transport solution for backhaul and fronthaul services relevant to the ICT and a number of vertical industires, 5G-PICTURE proposed a next-generation converged infrastructure **integrating a variety of wireless network technologies with optical and packet transport network solutions**.

This infrastructure aims to to enable provisioning of any ICT or vertical industry service in a flexible an efficient manner addressing the increased dynamicity of the service requests. Thereore, the main architectural principles of 5G-PICTURE have remained **convergence and integration of network and compute technologies**, **network softwarisation**, **hardware programmability** and **dissagregation** of compute/storage and network resources. Adopting these concepts, the project has proposed the architectural approach of Dissagggregated - Radio Access Network (DA-RAN). “Resource disaggregation” allows decoupling of network as well as compute and storage components, creating a common “pool of resources” that can be independently selected and allocated on demand to compose any infrastructure service. Thereofre the concept of DA-RAN can facilitate provisioning of any service across the infrastructure by flexibly and efficiently mixing-and-matching network, compute and storage resources.

To achieve this, 5G-PICTURE relies on a set of hardware and software innovations covering the data, the control plane and the orchestration layer.

In 5G-PICTURE the data plane includes the following capabilities:

a) integrated optical, wireless and packet-bsed transport network,
b) compute resources required for both BH and FH services, and
c) enhanced functionality through novel programmability features.

To address the challenge of managing and operating this type of complex heterogeneous infrastructure in an efficient manner, 5G-PICTURE proposed to merge the SDN and NFV approaches to address function programmability. This takes advantage of SDN’s separation of control and data plane via open interfaces, exploiting limited reconfigurability of high-performing switching HW; and NFV’s full programmability of network functions via SW on commodity platforms that, in general, does not rely on open programming interfaces. However, the architecture proposed by 5G-PICTURE utilises a programmable data plane (which will be described in the following sections) and relies on the creation of functions needed for the required service compositions. These functions are then exposed to the higher layers through suitable interfaces. Functions can then be selected and combined together in the form of service chains by the orchestration capabilities offered through the 5G Operating System (5G OS) developed in the framework of the project (WP5).

The overall architectural approach of the project involves a layered structure comprising a programmable data plane that exposes a set of physical and virtual funtions to the control palne. Services are provisioned through the orchestration layer responsible to combine physical and/or virtual functions adopting the notion of service chaining. A schematic representation of the proposed architecture and the mapping of the associated work to the relevant project activities is shown in Figure 3-1. A more detailed discussion on the functionality of the individual 5G-PICTURE architectural layers is provided in this section.

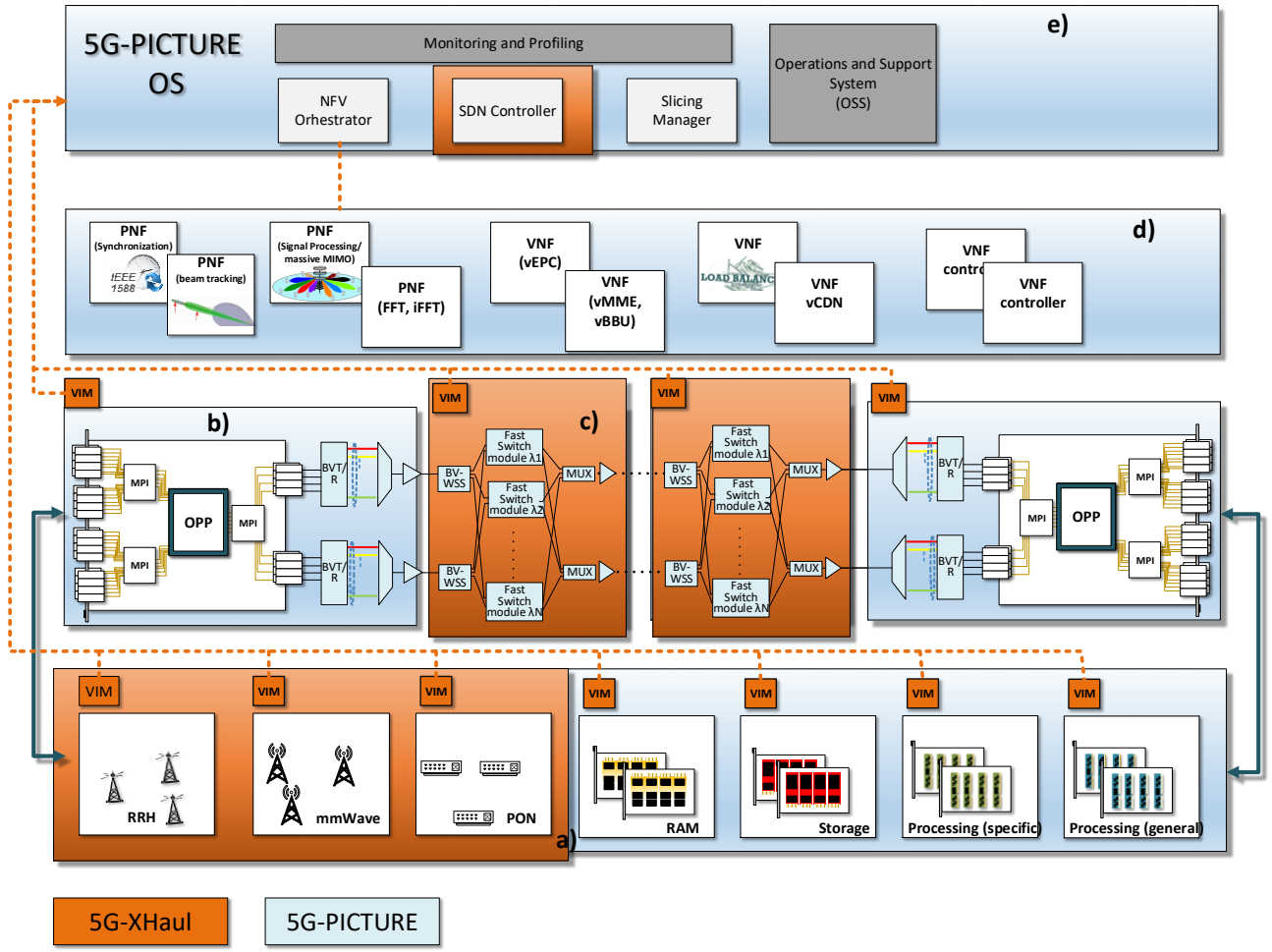

Figure 3-1: The 5G-PICTURE architecture and project activities mapping.

3.2 Programmable data plane

In this section, we briefly summarise the characteristics of the programmable data planes, giving an architectural overview, while the implementation details will be described in deliverable D3.3 [17]. 5G-PICTURE envisioned the data plane as a set of highly configurable wired/wireless infrastructures and interfaces, integrated in a single transport solution. We recall that the 5G-PICTURE network is highly heterogeneous, being composed by passive and high capacity elastic optical networks, packet/Ethernet based networks, mmWave and massive MIMO wireless transport technologies. Since this heterogeneity can be a limiting factor to the integration of the various network segments, 5G-PICTURE leverages the concept of data plane programmability to seamlessly merge the various technologies and to offer a set of network functions that can be deployed among the programmable elements of the network to efficiently realize the required network services.

In the rest of this section we give an overview of the various programmable data planes developed in the project, describing the latest developments achieved with respect to what reported in deliverable D2.2.

3.2.1 Optical Transport

5G technology requires a generic edge interface that can be programmed both at transport protocol level and at the network function level. Such an interface can be deployed anywhere at the edge of the network, can interface any access technology at any backhaul/metro/core network and also host network functions that are sensitive to latency. A high-level architecture of the interface is shown in Figure 3-2. This interface needs to be designed with convergence capability to deliver agility, programmability, and flexibility for interfaces between heterogeneous transport technologies, i.e. optical and wireless, and different networks, e.g. optical core, metro, access; wireless cellular, and wireless local area networks.

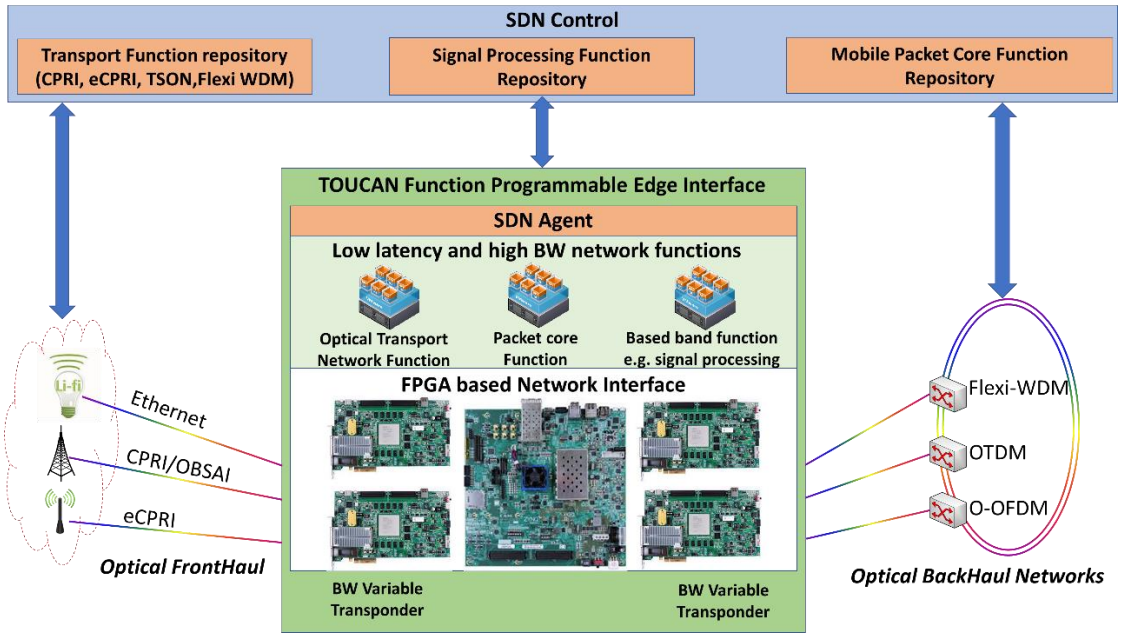

Figure 3-2: A high-level architecture of the edge interface.

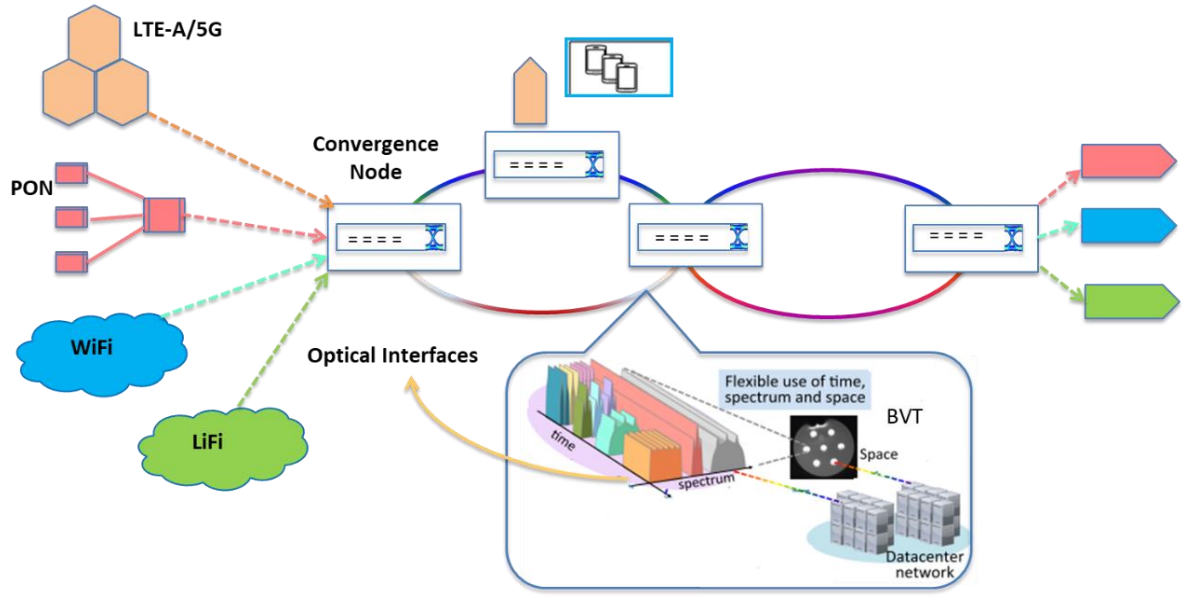

Figure 3-3: The generic convergence-node architecture.

Figure 3-3 presents the architecture of the generic convergence-node with multiple interfaces. In this scenario, the node is implemented on Field-Programmable Gate Arrays (FPGAs) to provide the flexibility and the requests for future network convergence. In addition, the node interface takes advantage of the huge Input-Output (IO) resource and hardware programmability of FPGAs. Through high speed transceivers, the FPGA could process the incoming traffic from Ethernet, access, wireless cellular, and other networks. Then, the FPGA could use its computing power to perform traffic parsing, protocol framing/mapping, traffic aggregation, and other operations. Moreover, the convergence node aims to allocate resources elastically in time, spectrum, and space, in order to accommodate a large range of traffic profiles and granularities in an efficient way and providing low latency based on considered vertical technology interfaces. Finally, the processed data traffic will drive different Bandwidth Variable Transmitters (BVTs) to generate optical signals for transmission towards different networks.

Time Shared Optical Network (TSON) has been adapted to support the convergence node proposed in Figure 3-3. The TSON technology is an active optical transport network solution to provide high bandwidth and low-latency connectivity in support of the 5G technology requirements. The TSON solution is a proven active WDM

solution which is providing variable sub-wavelength switching granularity and the ability to dynamically allocate optical bandwidth elastically to achieve the required Quality of Service (QoS). 5G-PICTURE deliverable D3.2 [21] presented the TSON architecture in detail.

The TSON extension maintained all previous features of TSON and added increased functionality and flexibility. The TSON extensions over the course of 5G-PICTURE are summarised as:

- A set of Intellectual Property (IP) cores has been created to ease and shape the TSON system integration.
- The TSON pipelines are designed to be extendable. The only limitation factor is the FPGA chip density and IOs for implementation.
- Aggregation of 10Gb clients to 40/100Gb is added to the architecture.
- The TSON frame format is changed. In this content each TSON frame slice carries the incoming client frame format. This means if the client data is Ethernet packets, the TSON frame slices are shaped by Ethernet frames. This feature makes the TSON frames transparent for other packet processing devices, but the time-slices frames are visible for them for processing.
- All the TSON wavelengths (i.e. 10G, 40G, and 100G) are supporting elastic bandwidth allocation mode.
- The TSON supports the frame format of the eCPRI protocol, which is either native Ethernet frame with VLAN, IPV4 packet with VLAN, or IPV6 packet with VLAN with eCPRI Ethertype (IEEE1914.3).
- A set of IP cores has been created to support Network Coding for Resilient C-RANs.

Figure 3-4 presents the latest TSON data plane architecture. This architecture is fully programmable using Software-Defined Networking (SDN). The functions for the operation of TSON domains has been implemented in internal modules, within the SDN controller, that collaborate for the on-demand provisioning of connectivity between TSON nodes. The ingress TSON edge nodes are responsible for parsing, aggregation, and mapping of any input traffic combination with different bandwidth (in this implementation less than 10 Gbps) into either 10 Gbps TSON output or converged 4 0/100 Gbps output with different granularity, while the egress edge nodes have the reverse functionality. This architecture follows the TSON architecture legacy described in D3.2 [21] with the some extra features that will be described below.

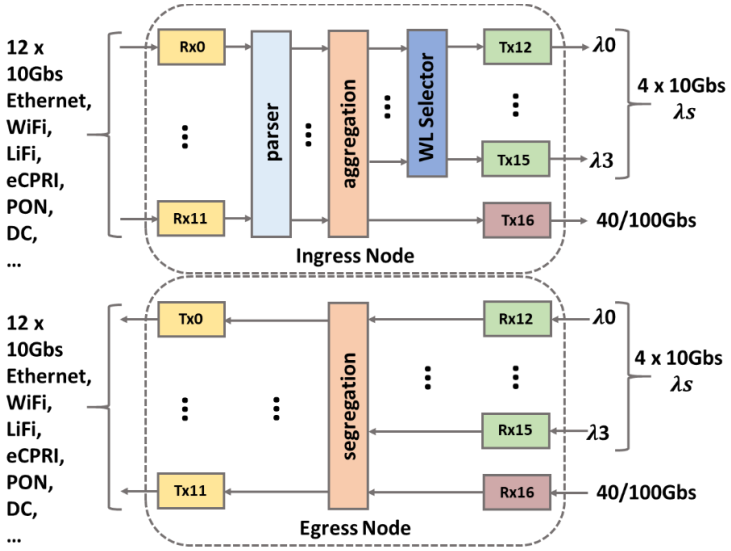

Figure 3-4: The latest TSON data plane architecture.

These include advanced signal processing functionalities (such as Network Coding – NC) to enable resilience in C-RAN environoments. Given that C-RAN services have with very high bandwidth requirements, this approach can be adopted to protect the network from possible optical network and/or BBU failures. However, in order to adopt NC based resilient FH networks there are three main challenges that need to be addressed:

- Coding: Providing module-2 sum and replication operation at FH line rate as these factors may degrade the performance of C-RANs in practical systems.

- Storage: The operation of the decoding process at the edge imposes significant buffering requirements due to the high data rate of FH streams.
- Synchronisation: Synchronisation between flows reaching decode nodes.

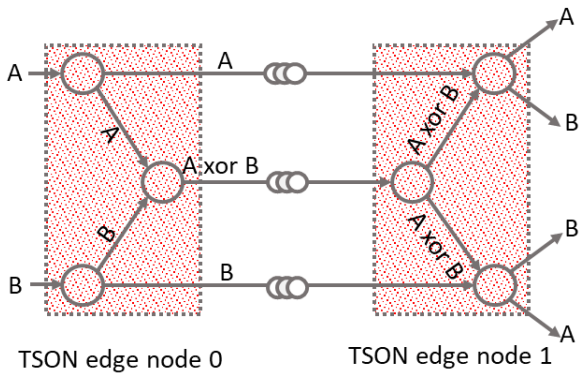

Figure 3-5: A butterfly network composed by of two TSON nodes.

TSON is extended to address these challenges and execute the coding and decoding processes at line rate as well as minimising buffering requirements adopting a purposely developed synchronisation scheme to make it suitable for C-RAN implementation. A simple topology that can clearly illustrate the principle of the NC solution is a butterfly network. Figure 3-5 presents an example of a butterfly network comprising two TSON nodes. In this scenario, each TSON node maps three source nodes of a butterfly network for NC. The TSON node 0 receives two different FH traffic streams (A and B) and sends the streams A, B, and their modulo 2 sum (XOR) of both traffic streams to the TSON node 1. The TSON node 1 receives the three traffic streams and transmits each traffic stream A and B simultaneously to two destinations of the TSON node 1.

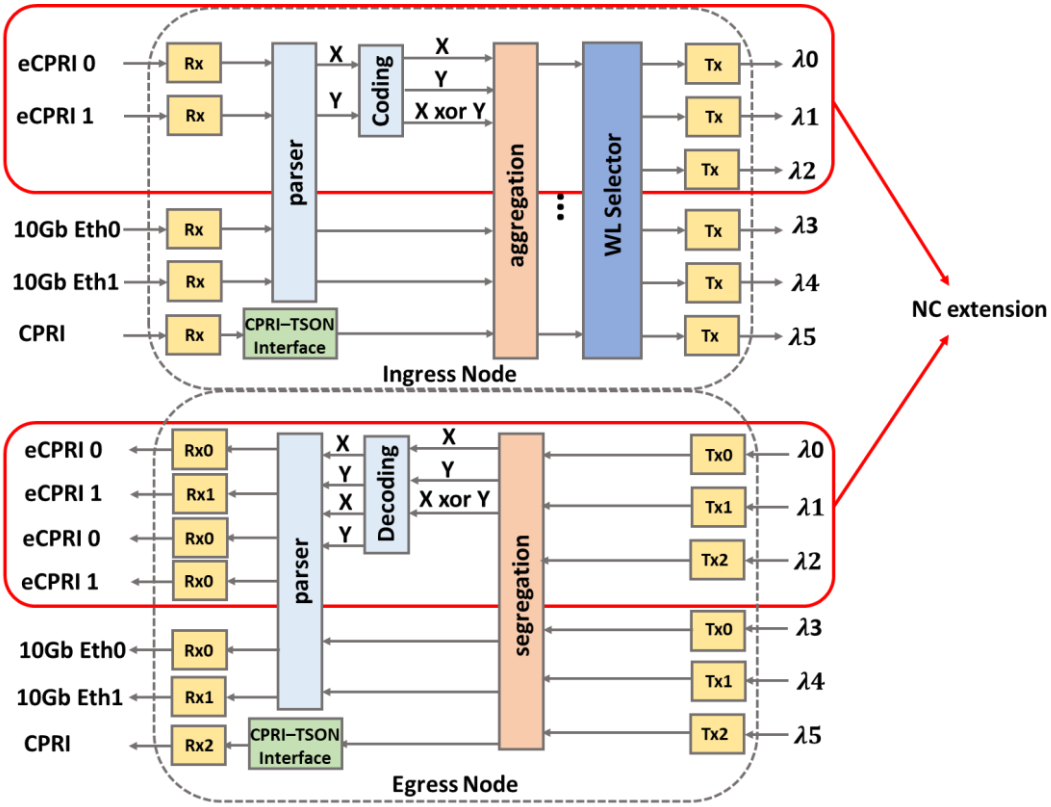

Figure 3-6: The TSON data plane architecture supporting NC.

Figure 3-6 presents the TSON data plane architecture with extra pipelines to support NC for FH considering the butterfly network for 10G lines. The marked extended pipelines in the figure are following the other TSON pipelines legacy with extra coding/decoding capability. In ingress node of these pipelines, the incoming traffic parses to two flows: X and Y. The output ingress node contains three different wavelengths (X, Y, and X XOR

Y) that can be configured on the fly using SDN to address different programmable parameters. The egress edge nodes include the reverse functionality with extra replication outputs to support a butterfly network. The IEEE-1588 synchronisation is employed for accurate synchronisation.

3.2.2 Wireless Technologies

As already presented in deliverable D2.2 [18], the 5G-PICTURE wireless transport and access network adopt massive MIMO, millimetre wave (mmWave), and Sub-6 technologies that leverage much greater numbers of antennas at the radio units to improve data rates, reliability as well as energy efficiency. In 5G-PICTURE, these technologies feature programmability and upgradability, with the goal of being able to satisfy the demands of 5G.

3.2.2.1 High speed RAN featuring programmable Massive MIMO

Massive MIMO plays an important role in the 5G-PICTURE architecture, as well as in 5G in general. By utilising spatial multiplexing via large antenna arrays, massive MIMO can deliver a large increase in RAN capacity. One of the goals in 5G-PICTURE is to introduce a higher degree of flexibility to the RAN and massive MIMO in particular, for which a new concept for Sub-6 massive MIMO radio units (RUs) was developed.

Such an RU, as shown in Figure 3-7, consists of 4 Radio Subunits (RSUs) and one Interface Subunit (ISU). Each of the modules carries an MPSoC, consisting of an FPGA and an ARM-processor subsystem. The RSUs in addition carry analog processing hardware like filters and amplifiers. This concept offers programmability both in the form of FPGAs and GPP processors (ARM subsystem).

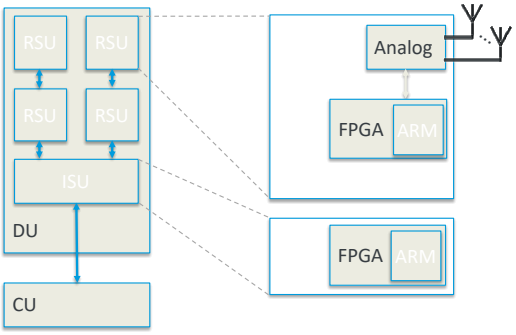

Figure 3-7: Concept for radio unit architecture.

However, as stated in deliverable D2.2 [18], RUs are function specific nodes, mainly performing lower physical layer as well as analog processing, for which non-programmable hardware is required. Hence it cannot be expected that an RU offers the same amount of programmability as other network nodes and cannot be seen as a programmable platform that can be utilized for different tasks. Nonetheless, with the developed concept, the platform offers a far greater flexibility compared to conventional 4G Remote Radio Heads (RRHs).

Conventional RRHs are based on the CPRI protocol, a very rigid interface implementing functional split option 8 having limited configurability and programmability. The RU concept developed in 5G-PICTURE is now based on the ORAN standard [19] [20], which implements functional split 7.2. This new interface differentiates four so-called planes, denoted User-Plane (U-Plane), Synchronization-Plane (S-Plane), Control-Plane (C-Plane) and Management-Plane (M-Plane) (see Figure 3-8). A plane basically is a logical link for a specific task. Several planes can be multiplexed over the same physical fronthaul interface.

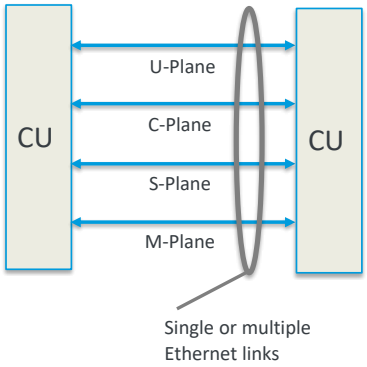

Figure 3-8: Radio unit interfaces.

The **U-Plane** is responsible for transporting I/Q-samples. The main benefit here lies in the new functional split 7.2, which offers the benefit of reduced fronthaul capacity requirement, but no real flexibility. The developed concept targets a 16-layer MIMO RU, which offers approximately eight times the maximum capacity of a 4G RRH, while requiring only about three times the fronthaul capacity. Also, because of the packet-based approach in combination with a frequency-domain split, the latency requirements can be drastically relaxed. While CPRI required a delay variation of 5 µs, with the targeted concept delay variations of more than 100 µs can be tolerated.

The **S-Plane** utilizes SyncE ant IEEE 1588 for synchronizing RUs and CUs in the network, while CPRI used the line rate from the CU to synchronize. The new approach offers a higher flexibility in terms that due to the packet-based approach of IEEE 1588, different synchronization sources can be used. As an example, the CU could be equipped with GPS, which could be utilized as primary source. In case of outage, a holdover oscillator or another GPS-based clock deeper in the network (i.e. in the central office) could be used as fallback.

With the use of the **C-Plane**, especially beamforming becomes more dynamic than in former CPRI-based RRHs. With CPRI beamforming weights had to be transferred via the very low-data rate control channel (1/16 of the CPRI line rate, e.g. ~150 Mbps for CPRI line rate 3), which could take several 10s of ms. Accordingly, beamforming could be only done semi-static. With the C-Plane, beamforming weights are transferred via the same link as IQ data and can hence make use of the full interface speed (typically 10 Gbps or 25 Gbps). Accordingly, it can be updated as in less than one millisecond, allowing for truly flexible beamshaping, be it for user-specific beams or to change the overall cell-shape.

Finally, the **M-Plane** offers a large set of standardized function to control the behavior of the antenna. This includes, adding/removing carriers, configuring carriers (bandwidth, frequency, power), software updates, or reporting alarms (overheating, hardware defects), to which a management system can react to optimize network performance.

In summary, the mMIMO RU architecture developed in 5G-PICTURE provides the following benefits:

- Peak capacity up to 8x compared to 2x2 RRH.
- FH capacity requirement only 3x of CPRI 2x2 RRH, or 1/3 of 16x16 CPRI RRH.
- Maximum allowed delay variation increased from 5 µs to >100 µs.
- Beamforming weight update time reduced by 10x.
- High degree of reconfigurability, updatability, alarm reporting through M-Plane.

3.2.2.2 Millimetre Wave at 60 GHz

3.2.2.2.1 IHP's digiBackboard programmability

The digiBackBoard FPGA platform presented in deliverables D3.1 and D3.2 is a custom System-on-chip (SoC) software-defined radio (SDR) platform. In 5G-PICTURE addresses the rapid prototyping in the micro- and millimeter wave frequency region using an SDR approach. This is supported by the real-time capabilities that feature this platform makes it a good candidate for use in running and upcoming 5G-related projects.

The platform comprises a SoC with an extensive programmable logic resources, and a high-performance dual-core ARM-based software processing system. For data converters - two ADC and two DAC – with sampling rates up to 2.5 GSps are integrated on the same board, together with four Gigabit Ethernet interfaces and additional general purpose input/output (GPIO) connectors. A firmware / operating system on the SoC together

with a PC software framework with example applications are available to easily control and use the prototyping platform. Hardware abstraction layers have been included for a simplified control and usage.

The digibackboard has been featured with a Medium Access Control (MAC) processor for 60 GHz, involving a general medium access scheme and link establishment using beam steering/beamforming antennas with very narrow (pencil) beam characteristic. These features are presented in deliverable D3.3 [17] and, in the context of WP6, the mmWave nodes including an Analogue Fron-End (AFE), will be part of the Smart City use case demonstration that will be held in Bristol in March 2020.

3.2.2.2.2 Line-of-Sight (LoS) MIMO configuration at mmWaves

In Section 4.7 of D3.2 [21] we discussed the theoretical background for mmWave Line-of-Sight (LoS) MIMO systems and the criterion for obtaining a near-orthogonal wireless channel with optimal inter-antenna spacing. An optimally arranged LoS MIMO can provide full spatial multiplexing gain, i.e., the transmission of parallel data streams even in pure LoS channels, making it interesting for, e.g., wireless backhaul applications. An exemplary link budget and achievable data rates were derived for different orders of LoS MIMO setups at mmWave carrier frequencies. It has been shown that rates in the order of tens of Gbps are achievable with a relatively low number of streams and compact antenna arrays of up to 1 m^2 for link ranges in the order of 100 m. Finally, a basic 2x2 LOS MIMO experimental evaluation was performed in an anechoic chamber at a link range of 5.5 m and carrier of 60.48 GHz, providing a verification of the discussed LoS MIMO concept.

The LoS MIMO research was extended in a number of directions by performing a new measurement campaign whose results will be reported in 5G-PICTURE's deliverable D3.3. First, the experimental setup is expanded from a 2x2 to a 4x4 array in a Uniform Rectangular Array (URA) configuration, in order to test if the orthogonality criterion holds for a larger number of streams. Furthermore, measurements are performed in three different environments (lab and anechoic chamber at 3 m, and a narrow hallway at 15 m, see Figure 3-9) to evaluate the effect of possible NLoS components to the conditioning of the LoS MIMO channel. Lastly, a transmit waveform structure similar to the one used in 802.11ad Single-Carrier mode is introduced, in order to evaluate linear equalization for LoS MIMO in a frame-based transmission. In all cases, the inter-antenna spacing is set optimally according to the LoS MIMO orthogonality criterion, e.g., at 0.335 m for a link range of 3 m and a carrier frequency of 60.5 GHz.

Measurement Setup Description

Measurements were conducted using hardware-in-the-loop (HIL) methodology with an offline post-processing of the captured frames, in order to obtain a performance benchmark for the given LOS MIMO system. An arbitrary waveform generator (AWG5208) was used to repetitively and synchronously generate the pre-compiled waveforms at the baseband inputs of the 4 transmitting AFEs, whereas a mixed signal oscilloscope (MSO58) was used to capture the baseband outputs of 4 receiving AFEs. The transmitted frames are composed of a preamble of 25 repetitions of a PN127 training sequence, followed by QAM-modulated data blocks, each preceded by a single PN127 mid-amble sequence. Each of the 4 spatially multiplexed data streams was assigned a different and mutually orthogonal complex PN127 sequence and uncorrelated QAM-modulated data symbols. With a complex double-sided bandwidth of 1.25 GHz, 4-QAM modulation order and 4 spatially-multiplexed data streams, a combined maximum throughput of 10 Gbps could be achieved with the described experimental setup.

Receiver architecture

With respect to the applied receiver processing, in the first stage symbol timing and carrier frequency synchronization are performed in a standard fashion based on the cross-correlation of the preamble with the replicas of the training sequences. The next stage is the separation of the MIMO streams by linear equalization, i.e., zero-forcing, based on the pseudo-inverse of the averaged channel matrix estimate from the preamble. Under near-orthogonal and well-conditioned LoS MIMO channels, simple linear equalization methods are of interest since they yield low receiver processing complexity, especially for mmWave systems with wideband processing of the parallel data streams. After the MIMO stream separation, adaptive per-stream linear equalizers are considered, for removing ISI caused by the frequency selectivity of the AFEs, as well as possible NLoS channel taps from reflections. This stage can be performed either in the frequency domain (FDE) or using adaptive linear equalizers (e.g. LMS). Finally, I/Q impairment compensation can be considered for further improving the EVM of the equalized data streams.

Experimental evaluation / results

Initial results on the estimated channel matrix condition number, as an indicator of the orthogonality of the LoS MIMO channel, yield 1.6~1.7 for the indoor lab and anechoic chamber scenarios, and in the vicinity of 3.0 for

the narrow hallway scenario. It can be concluded that the narrow hallway is ill-conditioned, which can be attributed to the keyhole effect since the wireless sub-channels are highly correlated, making this specific scenario unsuitable for a LoS MIMO system setup. For the aforementioned two scenarios, it is verified that the LoS MIMO criterion holds for a 4x4 setup as well, since the condition number estimates are close to the optimal value of 1.

With respect to the equalizer performance, it can be shown that simple zero-forcing can provide full i.e. error-free separation of the four spatially multiplexed streams, however due to the presence of ISI, a per-stream ISI cancellation after the stream separation is needed to further improve the EVM.

Lab **Hallway** **Anechoic Chamber**

Figure 3-9: Environments where the LoS MIMO measurements are being performed.

3.2.2.2.3 Blu Wireless Technology (BWT) Typhoon platform

BWT uses its Typhoon Platform for data plane programmability investigations in WP3, for the investigation of virtualized synchronisation functions in WP4, as well as for the deployment of mmWave Typhoon nodes along the track as part of the Railway demonstration activities in WP6. BWT uses its DN101LC Gbit communication module, which is a member of the Typhoon family of highly programmable wireless communications modules, for multi-gigabit prototype 5G infrastructure links.

The Blu Wireless IP that is included within the Typhoon module consists in the patented HYDRA technology (Hybrid Defined Radio Architecture). A key feature of the HYDRA is that both the PHY and the MAC layer of its IEEE 802.11ad modem combine optimized hardware accelerators with programmable parallel processing. Namely both MAC and PHY are software-defined, which allows the performance of novel mmWave wireless algorithms to be explored and continuously tailored in the context of advanced research platforms.

The Typhoon utilises the latest integrated electronic beam steering phased array antenna, RF and baseband technologies and is available in various configurations, including single, dual and quad RF, with or without NPU support and in either the default unlicensed 60 GHz standard or other licensed bands. The RF module comprises a 60 GHz radio transceiver with phased array antenna including separate active Rx and Tx antenna arrays with 12 elements each. Note that the module can operate with an external host and a single mmWave radio-frequency integrated circuit (RFIC) device. It is as well upgradable to feature larger antenna sizes to achieve increased gain.

One additional use case where the Typhoon platforms are involved is in the development of synchronisation functions in WP4, which will be further extended with the use these nodes, as they support transmission and reception of IEEE 1588 Precision Time Protocol (PTP) messages with hardware timestamping of PTP event messages.

The architecture that is considered involves the clock synchronisation function to be performed in user space of a host running a PTP application. The application, in turn, requires specialized driver and network device hardware, such as the one provided by the BWT Typhoon's BH2 device. The PTP application is responsible for the communication with the device driver, with whom it agrees to gain control of a hardware clock (time counter) and negotiates the ability to receive departure and arrival timestamps of pre-defined packets (PTP event messages). The driver, in turn, communicates to the network adapter and ensures that clock and timestamp interactions become possible.

Such PTP network design considers the grandmaster architecture including fall-back plans. This relates to the best master clock (BMC) algorithm to automatically define the best clock to play the role of the grandmaster. Due to the BMC algorithm, the node that plays the role of the grandmaster is automatically defined, specifically by each node discovering its own role (and the grandmaster discovering that it should be it). However, the

network manager can exert some control on the results of this automatic definition. Additional functions will be able to override the BMC (setting it to work in the background).

3.2.2.3 Sub-6 technologies

Sub-6 GHz access/transport nodes were presented in presented in previous deliverables, concretely in deliverable D3.1 [22], where the Sub-6 platform Gateworks Ventana (GWV) was introduced. A high-level view of their configurability was provided, e.g. enabling different Sub-6 GHz network slicing functions. To that end, a GWV node has been equipped with multiple access/backhaul NICs (IEEE 802.11n/ac interfaces). Each NIC can support multiple wireless virtual interfaces (i.e. vifs) that belong to multiple tenants [18]. The technical component, as captured in deliverable D4.1, can be referred as SWAM: "SDN-based WiFi Small Cells with Joint Access-Backhaul and Multi-Tenant capabilities" [23]. SWAM is used to provide a wireless connectivity service over a distributed area, and it is instantiated over prototype Wi-Fi Small Cells being developed in WP3. The services investigated are a) Service 1: Instantiation of e an access connectivity service composed of virtual APs over a set of physical Aps and b) Service 2: allocation of a connection through the wireless backhaul, which transport the traffic from such access service until a fibre attachment point. More details are included in deliverable D4.1 [24].

3.2.3 Ethernet Transport

3.2.3.1 Flex-E

Flex-E enables Ethernet-based services to be mapped over a next-generation optical transport network with the most efficient utilization of capacity possible. It was originally conceived to meet the challenges of Internet Content Providers (ICPs) for higher capacities and dynamicity, and as a new mechanism for the data center interconnect (DCI). It was originally proposed by OIF in Interoperability Agreement (IA) OIF-FLEXE-01.0 on March 2016. A detailed description of the technology can be found in OIF in IA OIF-FLEXE-02.0(2018), IA OIF-FLEXE-01.1(2017) and IA OIF-FLEXE-01.0(2016). The forthcoming FlexE 2.1 project is about prototyping FlexE over 50Gbe PHY applications and extending the recently released FlexE 2.0 (IA). FlexE 2.1 will specify a 50G FlexE frame and multiplexing format and address applications with lower bandwidth needs. Flex-E neighbor discovery is discussed in IA OIF-FLEXE-ND-01.0(2018).

Flex-E introduces a Flex-E Shim layer that is responsible for the mapping of Flex-E clients (Ethernet flows) to groups of PHYs. From a layering perspective Flex-E Shim is introduced between the Ethernet MAC and the PCS sublayers. Flex-E technology is introduced as a thin layer, known as Flex-Shim, and being able to support data rates out of the conventional range offered by current Ethernet standards. The main idea behind Flex-E is to decouple the actual PHY layer speed from the MAC layer speed of a client. Flex-E is based on a time-division multiplexing mechanism that is able to drive the asynchronous Ethernet flows over a synchronous schedule over multiple PHY layers.

In deliverable D4.2 [25] we demonstrated and evaluated Flex-E technology, while verifying the theoretical framework proposed by OIF. The system demonstrator is implemented in a testbed with two Huawei Optix PTN 990 supporting IA OIF-FLEXE-01.0 (2016). From all the experiments performed, perfect isolation characteristics were obtained by means of throughput. However Flex-E is not able to provide delay guarantees. Our ongoing research activities are targeting ways to enhance Flex-E performance by means of delay in integrated scenarios.

3.2.3.2 X-Ethernet

X-Ethernet stands for extended distance, expanded granularity and extremely low latency. X-Ethernet introduces Ethernet PCS switching based on the interface offered by Flexible-Ethernet. The basic switching unit is FlexE Client. The switch device will redirect FlexE Clients (64B/66B block streams) from its inbound port to its outbound port without waiting for the arrival of the whole Ethernet frame for FCS checksum and forwarding decision with table lookup. Therefore, all the time consuming procedure, such as encapsulation/decapsulation, queuing and table lookup, can be removed. We give another name to the PCS switching that is PCS Non-Stop Switch (NSS). What's more, the remaining procedure processing time is predictable, which results in deterministic device latency. Idle insertion or deletion according to IEEE 802.3 may be performed to rate-adapt FlexE Client to the Flex Group.

A X-Ethernet testbed was used to carry demonstration activities, where for each X-Ethernet switch the solution is based on FPGA board, six 100G CFP2 optical module slots, two 10G SFP+ optical module slots, one Ethernet interface slot. The FPGA board is mainly composed by one Virtex UltraScale chip, one ZYNQ chip, two

DDR3 SDRAM chips, one DDR4 SODIMM, two Quad-SPI flashes and one Micro SD. In D4.2, we provided experimentation results from the execution of three test scenarios that were carried out and display the ability of X-Ethernet technology to satisfy challenging switching requirements for the integrated programmable network.

3.2.4 IEEE Time Sensitive Networking

On data link layer IEEE 802.1 Audio/Video Bridging (AVB) task group work was focusing on enabling isochronous and deterministic low-latency services over legacy Ethernet. However, this was intended for multimedia streaming applications. In order to widen the area of applications, this later evolved into the IEEE 802.1 TSN Task Group (TG). The IEEE 802.1 TSN TG focuses mainly on the physical and link layer techniques to achieve guaranteed delivery of data with bounded low latency, low delay variation and low loss.

In the context of forthcoming D4.3 [26] activities, we demonstrate how system and statistical parameters affect the performance of TSN-enabled network for carrying fronthaul traffic between multiple RRUs and BBUs endpoints. A IEEE TSN testbed was implemented supporting 802.1Qbv (Traffic Aware Scheduling) and 802.1Qbu (preemption) used a functional split compatible with the NGFI IF4.5 split implemented in OpenAirInterface v2019. In the network part we used prototype TSN switches based on the Huawei AR 550 gateway system design equipped with eight 1 GB ports each and supporting IEEE TSN data plane functionality.

3.2.5 Programmable Packet Processors

The packet level programmable dataplane aims to provide the following main capabilities:

1. protocol independence, thus managing programmable parsing of the protocol stack for generic field extraction,
2. extended rule matching capabilities providing programmable flow level stateful behaviors, and
3. programmable packet level actions for generic packet generation, encapsulation/decapsulation.

The 5G-PICTURE project developed several building blocks to achieve these objectives, namely (i) V-PMP, a VLIW (Very Long Instruction Word) processor called V-PMP tailored for packet manipulation task; (ii) FlowBlaze, a programmable data plane focused on the implementation of stateful per-flow functionalities based on eXtended Finite State Machine (XFSM) and (iii) a P4 compiler to configure high speed Mellanox Ethernet switches. A detailed description of the implementation of these technologies is available in Deliverable D3.3.

The V-PMP has been developed to provide packet level action programmability. This will solve the issue related to the growing number of packet action required by heterogeneous networks, which require complex functionalities such as encapsulation/decapsulation of VxLAN tags used in large cloud computing deployments, management of GPRS Tunnelling Protocol (GTP) termination used for tunnelling in the mobile edge [30]. We remark that in the last period the capabilities of the V-PMP processor has been extended and two main new features has been added. First of all, the V-PMP now support the eBPF instruction set [31]. This instruction set permit the V-PMP to seamlessly accelerate virtual network function developed for the linux kernel, thus allowing a fast and efficient offload of Virtual Network Functions (VNFs) originally designed for a software environment. Moreover, the V-PMP has been enhanced with flexible internal interface to add specific hardware accelerated blocks needed to provide high throughput specific computation on the packet payload. These blocks ranges from eBPF-like helpers (such as checksum computation) to more generic functionalities such as cryptographic primitives.

The second technology, namely the FlowBlaze stateful dataplane [32] has an almost defined architecture, thus in the last period we focused on the design of a specific high level programming language (called “XL, the XFSM Language”), to exploit the programmability features of FlowBlaze.

Finally, the P4 compiler for the Mellanox Ethernet switches is currently able to support the P4-16 version and has been integrated with the SAI flexible APIs and with several network operating systmes such as the SONIC Open Network OS and the Onyx OS [33]. The compiler also supports a hybrid mode, where standard concepts like L2 bridging and L3 routing are represented as fixed points in the hardware pipeline and are optimized for performance and resource usage, while the ASIC programmable blocks are bounded at discrete locations around these fixed hardware blocks.

3.3 Physical and virtual functions

The vision of 5G-PICTURE is to demonstrate how programmable hardware platforms can be used to instantiate several physical and virtual functions, which can then be dynamically orchestrated by an operating system (5G OS) to deploy connectivity services on demand.

WP4 focuses on the development of the aforementioned functions classified in three groups, namely: *RAN*, *Transport*, and *Synchronization* functions. The work carried out in WP4 has produced as outcome 17 different functions that have been described and evaluated in deliverables D4.2 [25] and D4.3 [26]. Table 3-1 describes 12 of these functions, which have been selected to highlight their relationship with the WP3 programmable platforms, and their integration with WP5. An update of the missing functions will be provided in deliverable D4.3.

Table 3-1 highlights that several WP4 functions have been developed that make use of specialized processors developed in WP3, e.g. the AIR Massive MIMO platform, various FPGAs platforms, the CNIT OPP, or the I2CAT Sub-6 and BWT mmWave wireless platforms. In addition, we have other software functions that make use of generic x86 compute resources. Looking at how the various WP4 functions are integrated with the 5G OS developed in WP5, we see three main cases:

- First, WP4 functions that are part of the 5G OS, i.e. a control function of the 5G OS.
- Second, physical network functions that are controlled by the 5G OS through a well-defined API or descriptor.
- Third, we also have software functions that are virtualized (VM/container) and are dynamically instantiated by the 5G OS. In addition, we have WP4 functions that are physical transmission technologies, and therefore do not interact with the 5G OS.

Finally, we have highlighted in the table (last column) the intended roadmap for the various functions until the end of the project. Here, we can see various functions that are going to be used to support the WP6 use cases (Smart City, Stadium and Railways). We also have several functions that will be further integrated within WP4 into three testbeds to demonstrate our vision on RAN, Transport and Synchronization. These testbeds are going to be reported in deliverable D4.3. A third case is a set of functions that will be delivered to WP5, in order to support the demonstration of the 5G OS prototype in Task 5.4.

Table 3-1. Relation between WP4 functions, WP3 platform and WP5 5G OS.

WP3 Platform	WP4 function	Integration in WP5 5G OS	Intended use
RAN FUNCTIONS			
AIR platform – D3.2 section	**Tech.Comp.#1:** Optimal Massive MIMO functional split	Descriptor describing Massive MIMO antenna configuration	
Generic x86 compute platform	**Tech.Comp.#2:** Software based RAN functions in OAI	VNF in VM/container plus associated descriptor	WP6: Smart City (D6.3) WP5: 5GOS demo (D5.4)
Generic x86 compute platform	**Tech.Comp.#3**: Control function to select optimal functional split in RAN	Control plane function belonging to 5G OS	WP4: RAN Integration (D4.3)
Generic x86 compute platform or FPGA Xilinx Zynq - D3.2	**Tech.Comp.#4**: RAN as a VNF for custom PDCP split and heterogeneous wireless DUs	VNF in VM/container/FPGA plus associated descriptor API for bootstrapping the functions	WP5: 5GOS demo (D5.4)
I2CAT Small Cell platform – D3.2	**Tech.Comp.#5**: Sub6 wireless for fronthaul-like RAN splits	No interaction with 5G OS (it is a physical technology)	
TRANSPORT FUNCTIONS			

Generic x86 compute platform	**Tech.Comp.#1:** TSON controller	Control plane function belonging to 5G OS (domain controller)	WP4: RAN Integration (D4.3) WP6: Smart City (D6.3)
Huawei routing function – D3.2	**Tech.Comp.#2:** Ethernet channel isolation through Flex-E	No interaction with 5GOS (it is a physical technology)	WP4: RAN Integration (D4.3)
Huawei routing function – D3.2	**Tech.Comp.#3:** Low latency cross-connect through X-Ethernet	No interaction with 5G OS (it is a physical technology)	
Huawei switching function	**Tech.comp.#** Low latency Ethernet switching	Interaction with 5GOS through JOX	WP4: RAN Integration (D4.3)
Generic x86 compute platform	**Tech.Comp.#4:** Segment routing	Control plane function belonging to 5G OS (domain controller)	
Open Packet Processor – D3.2	**Tech.Comp.#5:** Mobility function for railways scenarios	P4 based function onboarded into 5G OS	WP6: Railways (D6.3)
I2CAT Small Cell platform – D3.2	**Tech.Comp.#6:** On demand wireless slice on joint access/backhaul small cells	Controller is a control function in 5G OS (domain controller) On demand wireless slice, onboarded as descriptor warpping API call	WP6: Stadium (D6.3) WP5: 5GOS demo (D5.4)
SYNCHRONIZATION FUNCTIONS			
BWT Typhoon platform – D3.2	**Tech.Comp.#1:** 1588 over IEEE 802.11ad	No interaction with 5G OS (it is a physical technology)	WP4: Synchronization Integration (D4.3)
Generic x86 compute platform	**Tech.Comp.#4:** Synchronization Harmonizer	Control plane function belonging to 5G OS (domain controller)	WP4: Synchronization Integration (D4.3)

We next describe the planned RAN, Transport and Synchronization integrated demonstrators.

3.3.1 Integrated RAN demonstrator

The vision of 5G-PICTURE for the RAN segment was based on the following design principles:

- Have a software based implementation of open RAN functions supporting different types of functional splits (c.f. deliverable D4.2 [25] for details about the supported functional splits).
- Be able to instantiate different functional splits over the network in a dynamic manner, using software interfaces.

To illustrate the aforementioned concepts an integrated testbed has been proposed composed of the generic x86 compute nodes supporting the following functions:

- RAN functions implemented in OpenAirInterface - OAI (*RAN Tech. Component #2*).
- FlexRAN controller (*RAN Tech. Component #3*) to select the functional split at run-time.
- Ethernet IEEE TSN (a variant of *Transport Tech. Component #3*) to instantiate the transport network.

3.3.2 Data plane Integration activity

The IEEE 802.1 TSN TG focuses mainly on the physical and link layer techniques to achieve guaranteed delivery of data with bounded low latency, low delay variation and low loss.

The integration process is with respect to practical considerations. We demonstrate how system and statistical parameters affect the performance of IEEE TSN for carrying fronthaul traffic between RRUs and BBUs end-points. We quantify the performance through the average forwarding latency and average delay-variation (jitter) of the high priority traffic when in contention with lower priority traffic and background traffic.

Based on the area of application, TSN Profiles have been specified to explain which standards, protocols, features and options to use for a given use-case. The existing TSN Profiles are 802.1BA for Audio-Video Bridging (AVB) networks, IEC/IEEE 60802 TSN Profile for Industrial Automation, P802.1DG for Automotive In-Vehicle Ethernet Communications and IEEE 802.1CM TSN for Mobile Fronthaul networks. IEEE 802.1CM is a collaborative effort between the CPRI cooperation and IEEE 802.1. It describes how to meet the stringent fronthaul requirements in an Ethernet-based bridged network that besides fronthaul traffic it can support concurrently other traffic as well. In 802.1CM both CPRI and eCPRI splits are supported (Class 1 and Class 2 respectively).

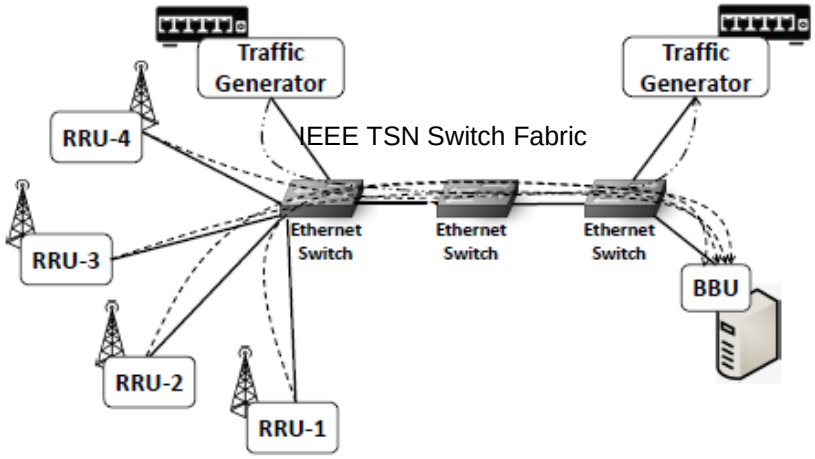

Figure 3-10: Considered testbed network topology.

Since eCPRI implementations are still not available, we used a functional split compatible with the NGFI IF4.5 split implemented in OpenAirInterface. We evaluate the performance of IEEE TSN 802.1Qbv & IEEE 802.1Qbu while carrying real fronthaul traffic and benchmark against Strict priority and Round Robin scheduling principles.

On the TSN network part we used prototype TSN switches equipped with eight 1 Gigabit ports each. For the end-stations, we use a traffic generator to emulate background traffic. In order to generate IEEE 802.1Qbv scheduled traffic we use Ixia traffic generator produced by Keysight Technologies, using IEEE 802.1AS with hardware time-stamping for verifying time-synchronization.

The key takeaway from the evaluations performed is high performance of 802.1Qbu (Preemption) and the tunable feature of 802.1Qbv, which allows the user to assign different schedules for different traffic flows. Since the traffic requirements varies based on traffic types, we showcase this feature could be used to prioritize different traffic flows thus ensuring the protection of the various traffic flows and a deterministic bounded worst-case delay.

3.3.3 Control plane Integration activity

In this integration activity we are exploiting a Netconf interface provided by the TSN switch prototype and we are integrating it in the JOX open source orchestrator. JOX, is an open-source orchestrator for the virtualized network that natively supports network slicing. Each slice supports one or multiple service offering tailored to specific business segment. Using JOX, each network slice can be independently optimized with specific configurations on its resources, network functions and service chains. Inside the JOX core, a set of services is used to operate and control each network slice, while at the same time support the necessary interplay between resource and service orchestration, Virtual Network Function Management (VNFM) and Virtual Infrastructure Management (VIMs) as these are defined in the ETSI MANO architecture.

In this integration activity we exploit JOX characteristics for slice-specific lifecycle management and its powerful northbound API in order to facilitate the optimization of end-to-end orchestration procedures. IEEE TSN is integrated by a message-bus based plugin framework is exploited for communicating with VIMs. JOX also

supports RAN specific plugins, like for example FlexRAN, in order to control the physical or virtualized LTE eNodeBs.

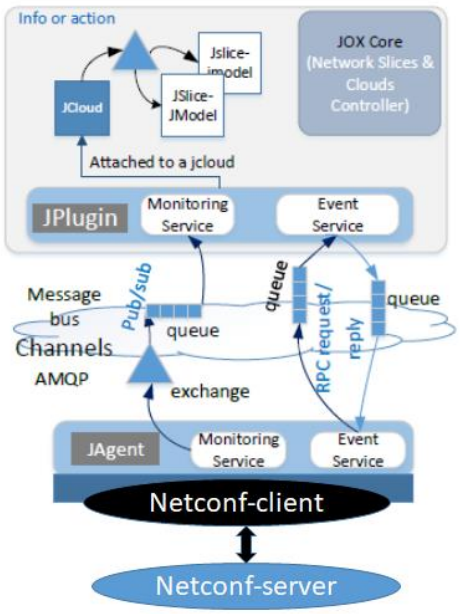

Figure 3-11: JOX plugin architecture.

Regarding the configuration of the TSN switch fabric inside JOX a specific plugin (referred as JPlugin) is loaded to interact with the JOX agent over the message bus and with the JOX core. Integrated demonstrators will be presented in deliverable D4.3.

3.3.4 Integrated Transport demonstrator

The vision of 5G-PICTURE in the Transport segment is to be able to dynamically provision end-to-end connectivity services, connecting physical or virtual RAN functions of different tenants, across a multi-technology and potentially a multi-operator transport network.

To address this heterogeneity the 5G-PICTURE architecture adopts a hierarchical control plane architecture where each transport domain is integrated through a specific SDN controller referred to as the “Level-0 controller”. Subsequently, several L0 Controllers are integrated through a “Level 1 Controller”, and the interface between L0 and L1 controllers is implemented using the Control Orchestration Protocol (COP) as proposed in the 5GXHAUL project. The interested reader is referred to D4.1 [24] for more details on this architecture.

The L1 controller is able to process end-to-end requests and partition them into individual requests for each of the impacted technology domains, which are then processed by the individual L0 controllers. Since each domain selects the connection identifiers individually, a data plane function known as Inter-Area Transport Node (IATN) is used to bind connections between domains. Finally, an edge function known as Edge Transport Node (ETN) is used to maintain per-tenant state (i.e. the MAC addresses of the P/VNFs) and bind it to the corresponding transport connection.

The purpose of the proposed integrated testbed is to benchmark the time required to provision end-to-end connectivity services across a multi-domain topology. For this purpose three technology domains, namely i2CAT instantiating a wireless transport based on *Transport Tech. Component #6*, UTH instantiating a wired transport segment based on OpenFlow switches, and UNIVBRIS instantiating an optical network segment based on *Transport Tech. Component #1*, will be connected through a domain provided by Zeetta Networks representing a different operator. The multi-operator approach will be presented in Section 4. The results of this test will be described in deliverable D4.3.

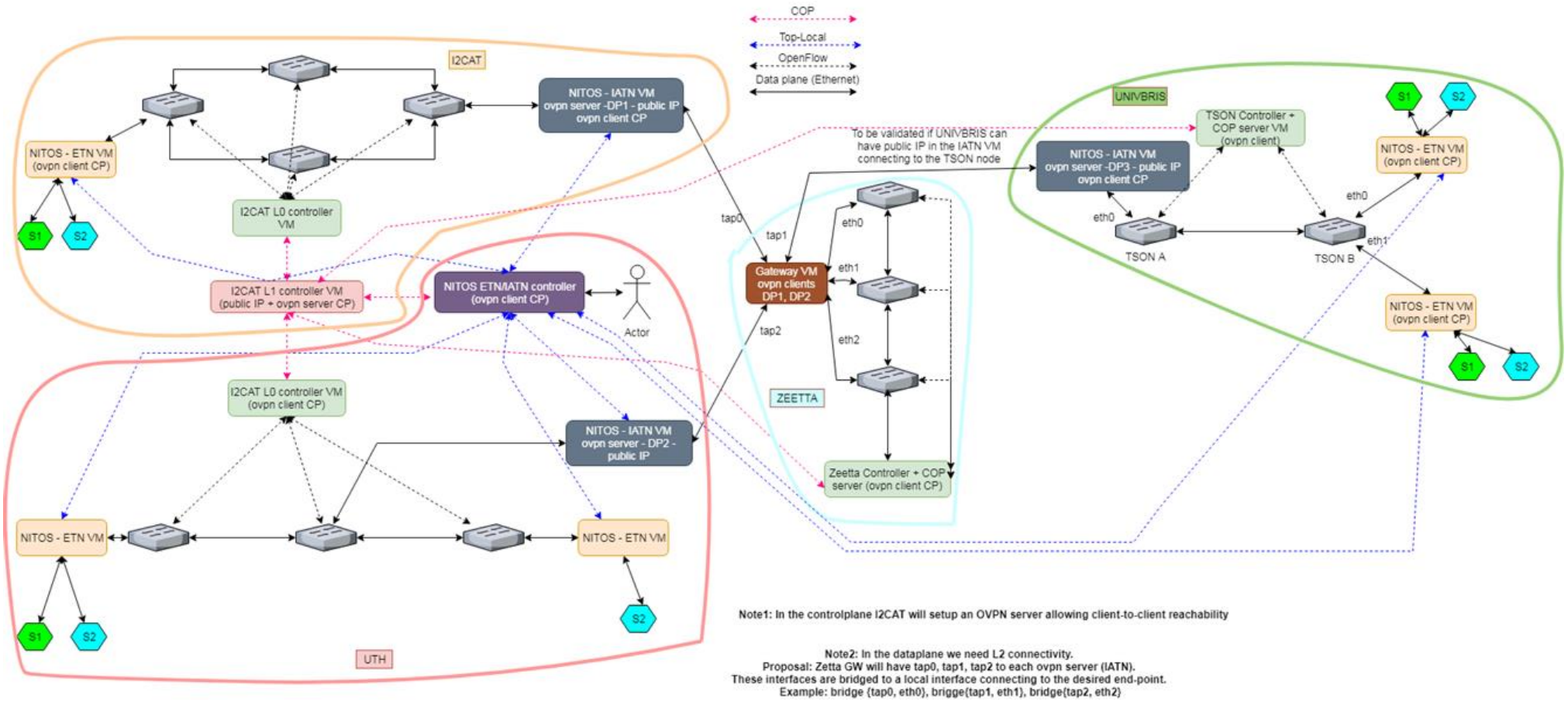

Figure 3-12: Planned multi-domain setup for Transport function integration.

3.3.5 Integrated Synchronization demonstrator

The vision of 5G-PICTURE in the synchronization domain was to be able to provide Synchronization as a Service when a tenant deploys a physical or virtual RAN function requiring clock distribution from the network. An important technical component developed to fulfil this vision is the Synchronization Harmonizer (*Sync. Tech Component #4*), which is collects synchronization capabilities from various devices in the network, and is able to influence on the clock distribution path. To demonstrate this capability the testbed depicted in Figure 3-13 is going to be setup, which features the BWT devices with the developed 1588 extensions (*Sync. Tech Component #1*), the TransPacket AS advanced Ethernet devices developed in WP3, and an external instrumentation to generate and recover clock signals.The testbed will demonstrate the capability of the Synchronization Harmonizer to select whether the clock signal is distributed through the wireless or the wired paths of the network. This work will be reported in deliverable D4.3, and additional measurements might be as well captured in deliverable D6.3.

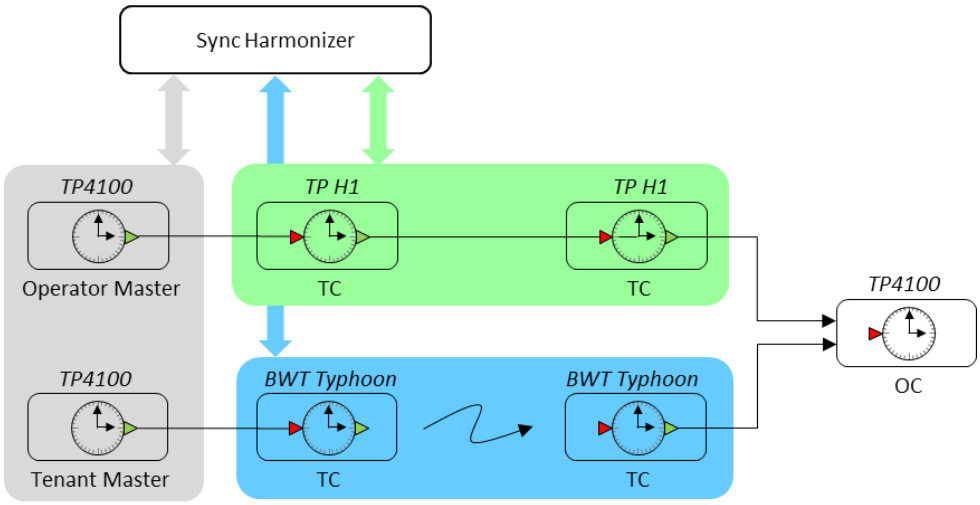

Figure 3-13: Planned integration of Synchronization functions.

3.4 5G OS

The 5G OS architecture presented briefly in deliverable D2.2 and more extensively in deliverable D5.1 [27] has been refined as tasks T5.2-T5.4 have been progressing. In this section, we describe the highlights of the refinements beyond the description provided in deliverable D2.2. More details on the approaches and concrete implementations are presented in the corresponding deliverables D5.1, D5.2 [28], and D5.3 [29].

The 5G OS architecture presented briefly in deliverable D2.2 and more extensively in D5.1 has been refined as tasks T5.2-T5.4 have been progressing. In this section, we describe the highlights of the refinements beyond the description provided in D2.2. More details on the approaches and concrete implementations are presented in the corresponding deliverables D5.1, D5.2, and D5.3.

3.4.1 Multi-PoP Orchestration

5G OS is designed to handle multiple domains and Points of Presence (PoPs) providing resources using different technologies. For this purpose, we have built upon and extended the state-of-the-art open-source tools like OSM[1], OpenStack[2], and OpenDayLight (ODL)[3]. We have extended the triangle of these three tools to support deploying VNFs of a NS over multiple PoPs and providing the required inter-connections. Our extensions exploit SDN-LAN and SDN-WAN controllers using ODL to handle networking beyond the existing OpenStack network management functionalities. These extensions have been described in detail in D5.2.

[1] https://osm.etsi.org

[2] https://www.openstack.org

[3] https://www.opendaylight.org

3.4.2 Multi-Domain Orchestration

5G OS supports orchestration of services that are distributed across different compute domains. In the case of our proof-of-concept design, Pishahang[4], these domains are managed by OpenStack and Kubernetes instances, orchestrating VM-based and container-based workloads, respectively. 5G OS carries out the inter-domain management tasks and can split and translate the service descriptors if necessary, to prepare the service deployment in the target domain. Pishahang has been described in more details in D5.3 [29].

3.4.3 RAN Slicing

Showcased by our proof-of-concept based on JoX[5], we have refined the 5G OS architecture for management and orchestration of the lifecycle of a network slice instance, including the preparation, instantiation, run-time, and decommissioning steps using novel slice management and monitoring functionalities, as well as VNF placement solutions that are described in D5.2 [28].

3.4.4 Transport Network Slicing

The Zeetta Slicing Engine (the Engine, for short) is a realization of the domain orchestration functionality, detailing the 5G OS architecture design from D2.2. Using an orchestrator component, the Engine maps the requested slice to an underlay network and using a virtualization engine, the slice is implemented in the underlay, exposing northbound APIs for the upper layers of slides. This solution is described in detail in D5.1 [27] and D5.2 [28].

3.4.5 Hierarchy of Controllers

5G OS provides a scalable SDN control plane architecture for multi-tenant, multi-domain (and multi-PoP) 5G transport networks. In this architecture, the Top-Level controller provisions per-tenant slices and orchestrates the interconnections among different domains. Level-0 controllers are technology-specific and are responsible for the orchestration of transport tunnels between Edge Transport Nodes (ETNs) and Inter-Area Transport Nodes (IATNs). Level-1 controllers are technology-agnostic and provide the connectivity among different areas and maintain the state at the area level. ETNs and IATNs at the edges of transport areas are controller by Local Agents. The details of the interactions among controllers in this hierarchy are described in D5.2.

3.4.6 Hierarchy of NFV MANO Frameworks

Within the Pishahang proof-of-concept implementation, we have defined and realized a hierarchical management and orchestration (MANO) of services. For this, we have introduced a uniform, standards-based Python wrapper library[6] for different MANO REST APIs to ease the communication among different MANO implementations. These communications include authorization, NSD management, NS fault management, lifecycle management, NS performance management, as well as VNF package management methods. Additionally, we have designed NSD splitter as well as NSD and VNFD translator components that enable delegating the deployment of a set of VNFs within a service to different MANO frameworks, possibly with different implementations, e.g., across OSM and SONATA[7] management and orchestration frameworks. More details on the hierarchical MANO solutions are provided in D5.2.

3.4.7 Orchestration of Multi-Version Services

We have refined the 5G OS architecture design to support the orchestration of multi-version services. The extensions include multi-domain orchestration functionality, showcased within the Pishahang proof-of-concept implementation, which can provision services across VM, container, and networking domains. We have used state-of-the-art NFV, SDN, and Cloud Computing tools for multi-version service orchestration. Within Pishahang, OpenStack and Kubernetes instances are used as Virtualized Infrastructure Managers (VIMs), supporting services that might contains multiple versions, each consuming different types of resources from

[4] https://github.com/CN-UPB/Pishahang

[5] http://mosaic-5g.io/jox/

[6] https://python-mano-wrappers.readthedocs.io/en/master/

[7] https://www.sonata-nfv.eu/

the underlying heterogeneous 5G-PICTURE infrastructure, e.g., VM or containers using CPUs, GPUs, or FPGAs. The details of this approach are described in D5.3.

3.4.8 Service instantiation

Instantiation of services (or slice) happens through 5G OS. The required procedures for service instantiation have been described in detail in D5.1. In this section, we give a brief overview of these procedures.

The required service and its corresponding service-level objectives enter the 5G OS in the form a 5G-PICTURE Descriptor, as shown in Figure 3-14. For instantiating a service, different components of a 5G OS instance need to process the descriptor. Figure 3-15 shows an overview of how a high-level slice descriptor is enriched and broken into slice, sub-slice, connectivity, and function descriptors by different components of 5G OS.

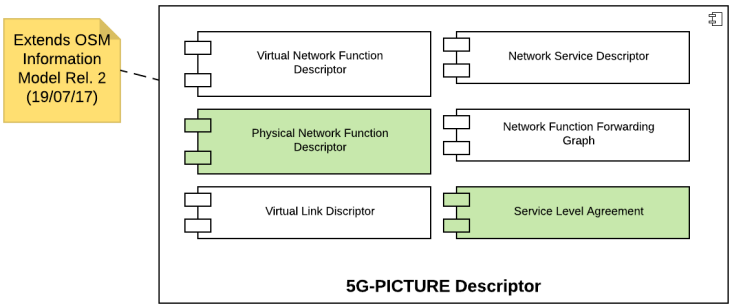

Figure 3-14: 5G-PICTURE Slice Descriptor (Extensions to the OSM Information Model are marked as green boxes).

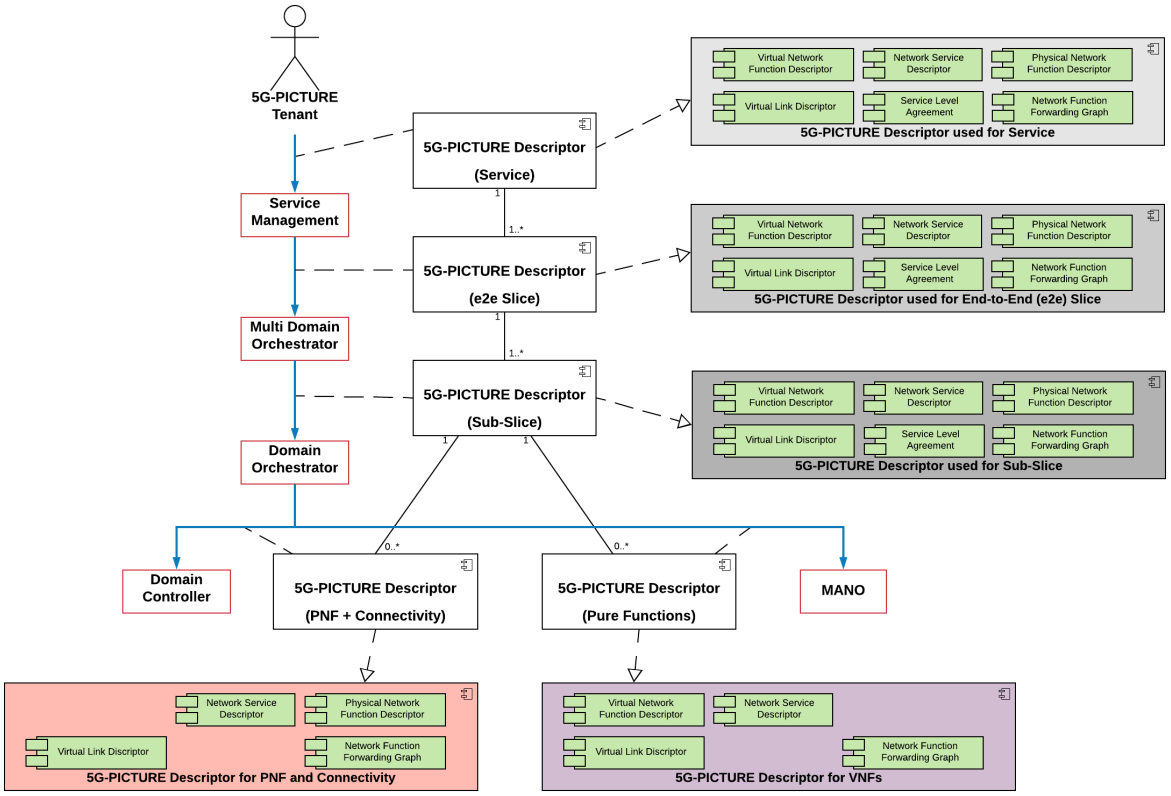

Figure 3-15: Processing a 5G-PICTURE descriptor by 5G OS components for service instantiation

Once the service is instantiated, a Slice Instance Descriptor is generated and travels back through the 5G OS components. This descriptor includes monitoring, management, and control information and the corresponding endpoints that allow the service requester to use and control the service, depending on the type of the slice (e.g., Base Slice, Guide Slice, or Generic Slice as described in deliverable D5.1).

As a concrete example, Figure 3-16 shows a connectivity service instantiation that is implemented as a one of project demonstrators within Task 5.4. The service request is received by the top domain controller, after traversing the Service Management and Multi-Domain Orchestrator components (not included in the demo for simplicity). Via the COP interface, the required service is communicated with the lower-level controllers (edge and transit controllers). Zeetta COP Adaptor enriches the service request and creates specific slice descriptors for the corresponding Domain Orchestrator and Domain Controller components that reside in the Zeetta domain. These components then instantiate the required slices that provide the required connectivity service.

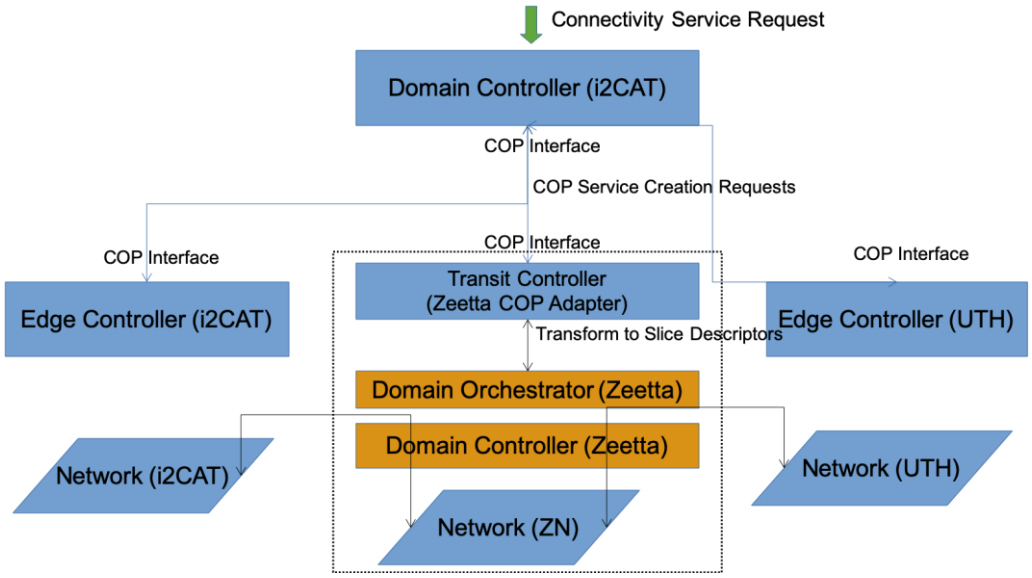

Figure 3-16: Components involved in an example service instantiation.

4 5G-PICTURE Architecture in support multi-tenant and multi-operator environments

4.1 Generic approach and technologies

Network slice instances include a set of network functions and resources spanning across multiple domains like CN and RAN, providing a customized logical network to meet the requirements of individual services. RAN slicing is a crucial part of realising an end-to-end control of different tenants or different operators on resources within a shared infrastructure.

To support multi-tenancy, different strategies can be applied for RAN slicing [34]. We briefly summarize the following four strategies as described in the work of Sallent et al. [34]:

- RAN slicing at the spectrum planning level: Spectrum resources of the RAN are grouped into a number of carriers and assigned to different tenants. Each tenant is allocated sufficient carriers to provide the required capacity and coverage. After assigning the carriers to the tenants, a tenant-specific spectrum planning function strategically decides how these carriers are utilized across different cells, considering the service and the traffic distribution of the corresponding user equipment.
- RAN slicing at the ICIC level: A number of different Resource Blocks (RBs) in each carrier are assigned to each tenant, ensuring transmissions without interference as well as radio-electrical and traffic isolation among different slices for different tenants. After RB assignment, tenant-specific ICIC strategies can be applied to mitigate inter-cell interference within a slice.
- RAN slicing at the packet scheduling level: Slicing is done at each cell by distributing the RBs among different tenants and by assigning specific RBs to each tenant, isolation among tenants is ensured. This method, however, may result in inter-cell interference among tenants.
- RAN slicing at the admission control level: A tenant-specific admission control process decides about resource requests, e.g., by prioritizing or rejecting certain types of resources when capacity limitations within the tenant slice are reached. The final decision about the request is, however, taken by the RAN slicing function that has an overall view of all tenants and all resources. With this level of slicing, inter-cell interference among tenants may happen and the packet scheduling within a cell is done for all tenants, without enforcing any tenant-specific requirements.

Figure 4-1 shows an overview of the differences of the mentioned slicing strategies, for example, with respect to isolation and customization possibilities. Depending on the requirements of the 5G-PICTURE Tenants and Operators, the right strategy can be selected for supporting multi-tenancy within the 5G-PICTURE architecture

	RAN slicing at the spectrum planning level	RAN slicing at the ICIC level	RAN slicing at the packet scheduling level	RAN slicing at the admission control level
Granularity in the frequency domain	One carrier (minimum 1.4 MHz in LTE)	1 RB (180 kHz in LTE)	1 RB (180 kHz in LTE)	Not applicable
Granularity in the time domain	Relatively long-term (several minutes)	Every ICIC period (typically hundreds of ms in LTE)	Every TTI (1ms in LTE)	Associated to RAB establishment request rate (in the order of seconds)
Granularity in the spatial domain	Whole scenario (might be less if sets of non-interfering cells are identified)	Whole scenario (might be less if sets of non-interfering cells are identified)	One cell	One cell
Degree of customization	Spectrum planning, ICIC, PS and AC can be tenant-specific	ICIC, PS and AC can be tenant-specific	PS and AC can be tenant-specific	AC can be tenant-specific
Radio-electrical isolation	High	High	Medium	Medium
Traffic isolation	High	High	High	Medium

Figure 4-1: Overview of RAN slicing strategies.

There are different existing architectures and frameworks for RAN slicing that also provide solutions for the multi-tenancy and isolation issues and the related problems. For example, the ORION architecture [35] enhances slice control by isolating virtual networks that share a physical infrastructure. This architecture is focused on providing multi-service mobile communication based on user specification. To ensure functional and performance isolation, RAN slices are managed using base station hypervisors, which provide virtual base

stations to services with their dedicated RAN controller as independent processes. Independent communication channels are used between the controllers and the hypervisor. Dedicated memory and compute resources can be provided in this way and the radio resources are distributed to slices after being virtualized by the hypervisor.

For a *disaggregated* RAN environment such as in the 5G-PICTURE infrastructure, in the work of Chang and Nikaein [36] three overlapping service levels have been identified. First, Infrastructure-as-a-Service, which provides programmable software-defined infrastructure for hosting RAN services. Second, Platform-as-a-Service that extends the former mentioned service in monitoring and orchestrating the functions of RAN slices. And finally, Software-as-a-Service including control applications such as radio resource management (RRM) and spectrum management application (SMA) to provide control logics. RAN runtime that belongs to the category of Platform-as-a-Service, provides a multiservice execution environment for customized functioning and sharing of radio resources at RAN. RAN runtime allows slice owner or service provider to perform the following tasks, providing individual control for multiple tenants or operators over their specific resources:

- Managing the RAN slices.
- Performing controlled logics.
- Operate on virtual resource level, e.g., resource block groups.
- Access the state of a plane revealed by RAN runtime.

FlexRAN [37], integrated in one of 5G OS prototypes as outlined in deliverable D5.1 [38], is a flexible and programmable platform that controls RAN in real time. One of the design goals of FlexRAN has been tackling the challenges of RAN management considering different requirements of different operators in terms of radio resources and the policies they might want to apply based on the needs of their tenants. FlexRAN enables sharing RAN with on-demand resource allocation capabilities. It defines interfaces, translates 3rd-party instructions to a set of commands and allows radio access network abstraction by programmability. The central FlexRAN controller interacts with the agents by using certain interfaces hosted by evolved nodes that perform critical-control functions, e.g., UE scheduling process.

Besides efficient slicing mechanisms, the right *business model* for network slicing is a deciding factor in multi-operator and multi-tenant environments. In this context, different business models have been described by NGMN [39], among which the following models may be used to derive new business models to fit the requirements of multi-tenant networks:

- Basic and enhanced connectivity model: The operator provides best-effort services to its tenants and can be enhanced to include QoS considerations, mobility, latency, etc., depending on the use case. With an instance of 5G Operating System (5G OS) as described in deliverable D5.1 [38], a 5G-PICTURE Operator can provide 5G-PICTURE Tenants with connectivity services using this model.
- Asset provider model: Depending on the asset that is available, in this model, the so-called “X-as-a-Service” approach is taken by the operator. For example, using 5G OS, Infrastructure-as-a-Service (realized by definition of two separate stakeholders in the 5G-PICTURE architecture as 5G-PICTURE Operator and Infrastructure Provider [38]), Platform-as-a-Service (supported by the hierarchical, cross-concept control and orchestration design in 5G OS [38]), as well Network-as-a-Service models are possible. Using this model, multi-operator scenarios can be realized, where operators share assets with other operators or operators are provided resources from different infrastructure providers.

Based on this model, different business models have been proposed in multi-tenant and multi-operator environments, from single-domain infrastructures to multi-domain setups. For example, Zhou et al. [40] propose a framework called Network Slicing as a Service (NSaaS) that can provide tailored network slices to the customers. They have identified different possible business models, for example a Business to Business to Customer (B2B2C) model, where a wholesale provider (e.g., an Infrastructure Provider) works with brokers who enable operators (e.g., different 5G-PICTURE Operators) to maintain a relationship with their customer (e.g., different 5G-PICTURE Tenants).

Another possible business model has been defined by 3GPP [40]. This model foresees roles like Communication Service Customer (equivalent to End Users 5G-PICTURE), Communication Service Provider (5G-PICTURE Tenants in 5G-PICTURE terms), Network Operator (5G-PICTURE Operator in 5G-PICTURE terms), and Virtualization Infrastructure Service Provider (Infrastructure Provider in 5G-PICTURE terms). The relationships defined in this business models among these roles have directly been considered and reflected in the design of the 5G OS architecture [38].

4.2 Use cases

In deliverable D5.1 [27] we have validated the 5G OS architecture using the mega-event/stadium as well as the rail use case of 5G-PICTURE project. In this section, we briefly highlight parts of these validation scenarios related to the multi-tenant/-operator/-provider matters.

4.2.1 Mega-event/Stadium Vertical

In a mega-event and/or stadium scenario, different services are expected to be running before, during, and after the event, for example, broadcast services (e.g. high-definition and standard-definition videos), infrastructure services (e.g. advertising, ticketing), and third-party services (e.g. betting, social media and personal communication applications). These services may be provided by different service providers (i.e., 5G-PICTURE Tenants) using resources from different Infrastructure Providers (such as cloud and edge compute resources, transport network and access network).

In this scenario, multiple 5G-PICTURE tenants may require a dedicated network or connectivity to be used by their devices and applications over the shared infrastructure. For this purpose, standard interfaces are needed to request access to shared resources owned by third-party Infrastructure Providers. Moreover, isolation, security, resilience, and control requirements of different 5G-PICTURE Tenants must be fulfilled. To ensure this, 5G-PICTURE Tenants are assigned slices of the shared infrastructure and make use of negotiation mechanisms to get the appropriate levels of isolation, security, resilience and control as well as their specific KPIs.

An example solution for realizing this scenario using a 5G OS instance (the 5G OS architecture and stakeholders are shown in Figure 4-2 for reference) is shown in Figure 4-3. In this example, we assume that a 5G-PICTURE Operator (5G Operator A in Figure 4-3) is running 5G OS Service Management (SM) and Multi-domain Orchestrator (MDO) components and allows different 5G-PICTURE Tenants (e.g., broadcasters) to deploy their own services on a shared infrastructure.

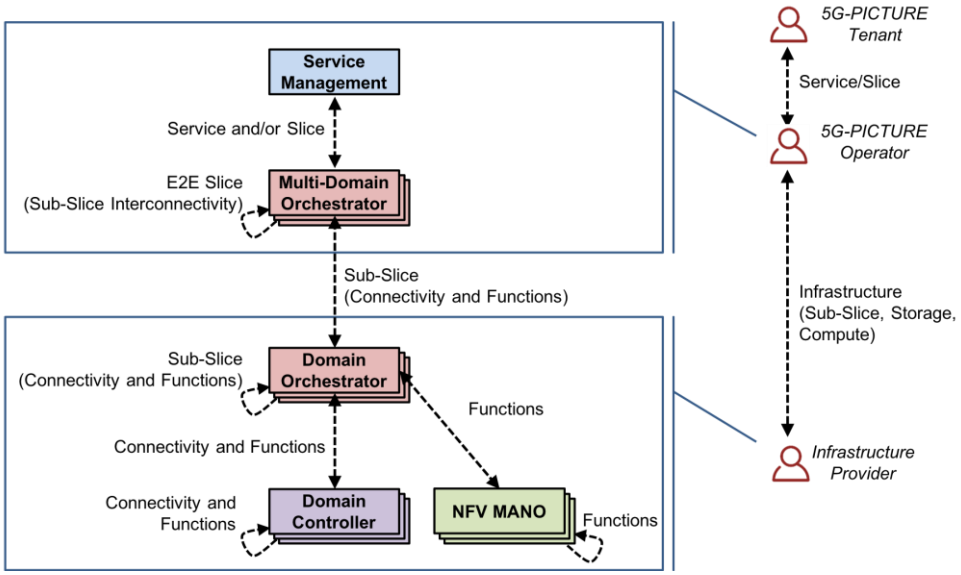

Figure 4-2: 5G OS major components and stakeholders.

The 5G Operator A has agreements with various Infrastructure Providers to provide connectivity (Domain B and Domain C), compute (Datacentre) and edge access network (Stadium). One of the infra-structure providers is the venue where the broadcaster is going to be telecasting live. Each Infrastructure provider is running a Domain Orchestrator (DO) and various Domain Controllers and MANO stacks. We assume a pre-provisioned connectivity exists between the 5G OS Operator A and the Stadium.

To create individual end-to-end slices for different tenants, the following steps need to be taken in this scenario, as described in more details in D5.1:

1. 5G-PICTURE Tenant activates a service via the 5G Operator A's SM component, requesting specific Access Points at the stadium together with the required QoS and Network Access device whitelist.
2. SM enriches the service request and passes to MDO.

3. MDO maps and translates the request to various infrastructure providers it knows to obtain optimal resource allocation.
4. Once resource allocation is confirmed, the functions are deployed and the connectivity initiated; which marks the completion of the end-to-end slice creation process.
5. Once the end-to-end slice has been created the service is considered to be 'alive' and corresponding monitoring, management and configuration interfaces can be brought on-line to allow the Tenant (broadcaster) to fully control their service.

For creating the end-to-end slice, two different approaches are possible: The Base Slice approach and the Guide Slice approach. We briefly recap the required steps using each of these approaches to create tenant slices. The Base Slice approach involves creating one or more end-to-end slices across all the available domains to be used as a base for different types of tenant slices. In turn, the Guide Slice approach involves creating a guide slice consisting of domains and links between them. This guide slice is used as a reference to create slices at run-time based on services requested by the 5G-PICTURE Tenant. This requires stitching sub-slices together to create an end-to-end slice, where each sub-slice lives in a separate domain. The advantage of the guide slice approach is that while it does not possess the flexibility of a base slice, it simplifies the MDO orchestration and placement problem by removing the problem of domain interconnect (which is pushed to the layer below in case of Base Slice approach).

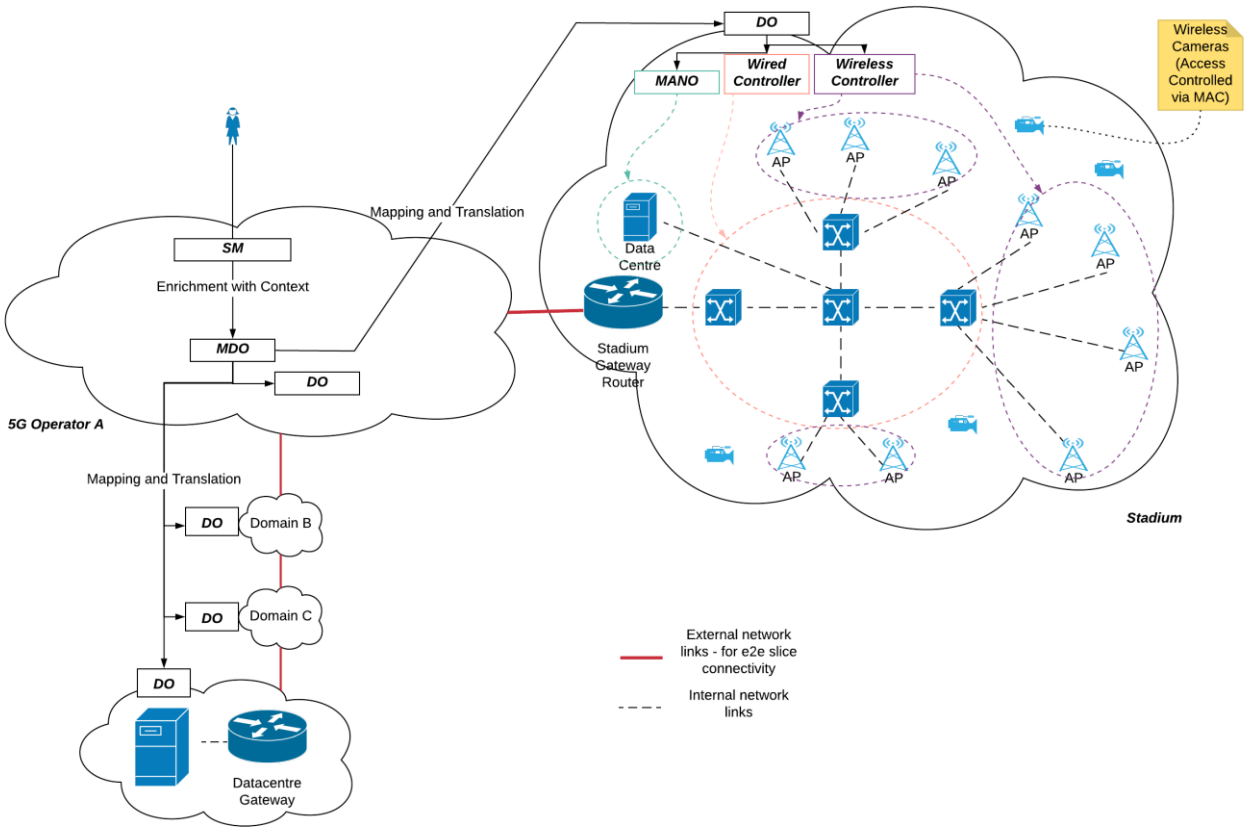

Figure 4-3: 5G OS in the stadium use case [38].

Base Slice approach:

1. In preparation for tenant requests, the 5G Operator A (in Figure 4-3) creates *one or more base-slices* from the resources provided by the infrastructure provider. These provide an abstraction for resources held across every domain. For example, in this case the base slice would contain resources assigned to 5G Operator A from the following domains:
    a. Stadium – providing edge access and compute at that location.
    b. Domain A – its own domain, where resources are earmarked for Tenant use – separate from resources required for internal and other uses.
    c. Domain B – providing connectivity to Datacentre.
    d. Domain C – providing connectivity to Datacentre.

e. Datacentre – providing compute facility.

2. The Slicing Engine operates upon the base slice to create a service specific slice for the 5G-PICTURE Tenant (Broadcaster) with the required functions chained as per the service definition.

Guide Slice approach:

1. In preparation for tenant requests, the 5G Operator A creates a *guide slice* from the resources provided by the infrastructure provider. This contains reservations for all available resources for tenant use, across every connected domain.
2. The Slicing Engine, which is part of the Orchestrator component (MDO and/or DO), looks up the guide slice and allocates sub-slices in each domain to provide required connectivity and functions.
3. The sub-slices are connected, based on the pre-defined domain interconnect, to create a service specific slice for the Tenant (Broadcaster) with the required functions chained as per the service definition.

4.2.2 Rail Vertical

In the Rail vertical, a wide variety of services may be operating in parallel. Some examples include infrastructure services (e.g., rail network monitoring, CCTV, advertising, tills, signalling, and sensors) and third-party services (e.g., mobile broadband, content distribution, and telephony).

Similar to the mega-event/stadium scenario, these services are provided either directly by the rail company or by third-party providers. In both cases, external resources may be required for compute and connectivity.

In some regions, the track and associated infrastructure are owned and operated by a separate Infrastructure Provider. In this case, even the access side will span across separate domains. For simplicity, we assume there is a single monolithic rail company in the rest of this description but we consider both scenarios for the actual validation.

Similar to the stadium scenario, in this case also multiple service providers (5G-PICTURE tenants) require their dedicated network or connectivity to their virtual/physical devices and applications over the shared network infrastructure. Apart from that, some other non-trivial aspects of this network are highlighted below:

1. The geographical spread of the network.
2. The mobility of the trains and associated use of wireless.
3. Safety critical nature of some of the services operating on the network.
4. The possibility of the transition between different administrative domains as part of a rail journey.

We assume a scenario, where trains are likely to transit through different regions where other rail providers control the infrastructure. Therefore, as a minimum requirement to provide un-interrupted service, connectivity to the End Users (e.g., passengers on the train or the train itself) must be provided across all the regions the train travels through. To support multiple 5G-PICTURE Tenants to provide their services in this setup over a rail network, a standard interface is required to allow the tenants to request resources. The network should also provide strong isolation guarantees to ensure different services running on top of the same infrastructure do not disrupt each other.

In deliverable D5.1, we have analysed two different cases to realize such a scenario using a 5G OS instance, which we briefly summarize in the following sections, focusing on the concerns regarding multiple tenants.

4.2.2.1 Rail Company as the 5G-PICTURE Operator

In this case, as shown in Figure 4-4, the Rail Company operates the Service Management and Multi-Domain Orchestrator components to provide end-to-end network virtualisation (i.e., slices) as well as Domain Orchestrators (for their network) and Domain Controllers to allow access to network resources.

The MDO interacts with DOs of other networks – whether those are other rail networks operating in different transit regions (Rail Company B in Figure 4-4) or compute infrastructure providers (Data-centre in Figure 4-4) or connectivity providers (Domain B and C in Figure 4-4).

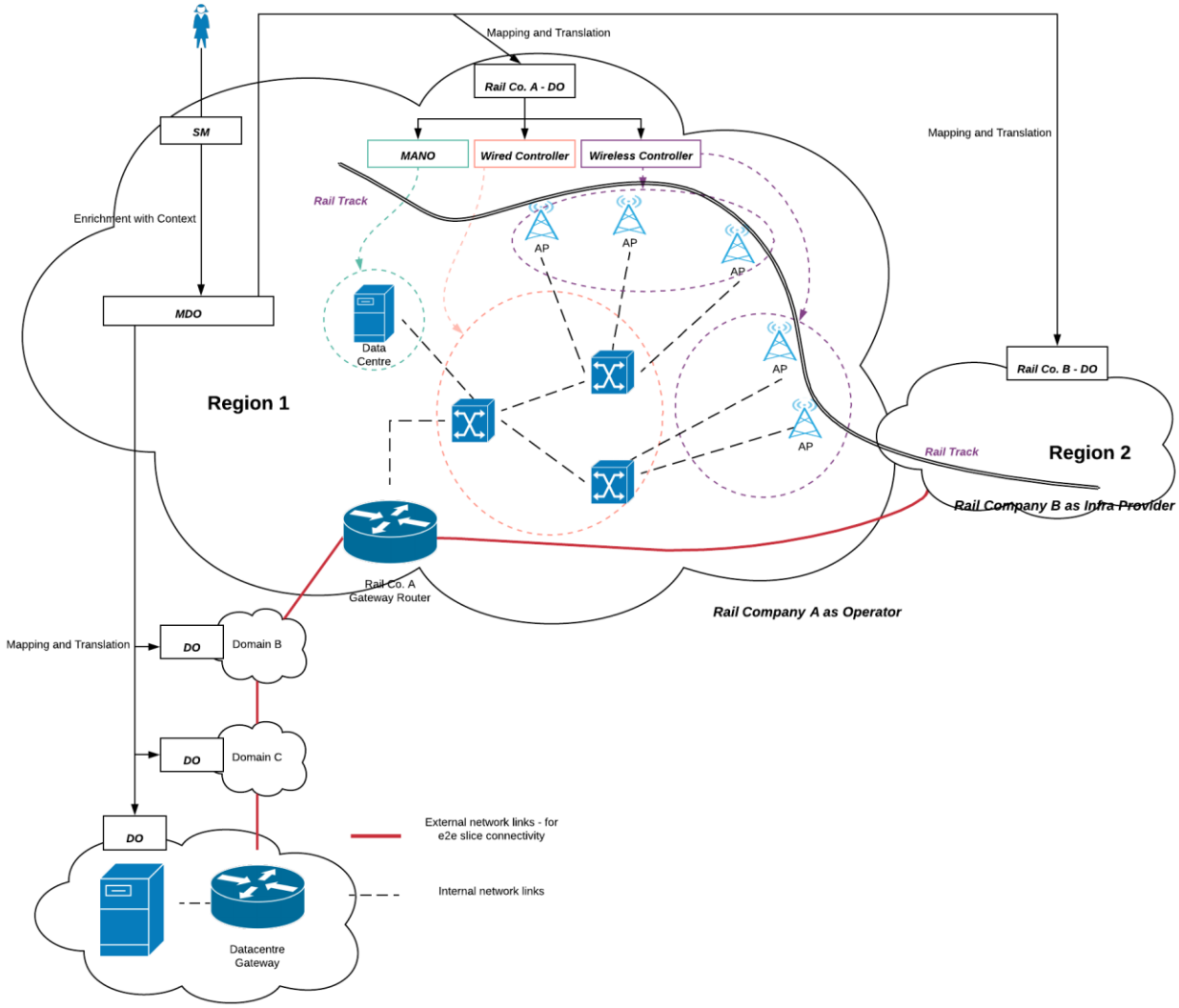

Figure 4-4 Rail company as the 5G-PICTURE Operator [38].

In this scenario, similar to the stadium scenario, the Base Slice and Guide Slice approaches can be used to create specific slice for different 5G-PICTURE Tenants. We summarize the required steps as follows.

Base Slice approach:

1. In preparation for tenant requests, the rail company (running the SM and MDO components of 5G OS as shown in Figure 4-4) would have created *one or more base slices* from the resources provided by the Infrastructure Provider. These provide an abstraction for resources held across every domain. For example, in this case the base slice would contain resources assigned to Rail company A from the following domains:
    a. Rail Company A – own domain, providing edge access and compute for the Rail network (Region 1), earmarked for Tenant use.
    b. Rail Company B –infrastructure provider providing edge access in Region 2 to allow full route coverage for users of Rail Company A.
    c. Domain B – providing connectivity to Datacentre.
    d. Domain C – providing connectivity to Datacentre.
    e. Datacentre – providing compute facility.
2. Tenant via the Service Management system requests a Service to be initiated which contains all edge access points in Region 1 and Region 2, application servers to be deployed in the cloud and edge, connectivity with QoS constraints.
3. The request is passed to the MDO which in turn maps and translates service request into requests for compute, connectivity and access while ensuring constraints related to QoS and placement.

4. The Slicing Engine operates upon the base slice to create a service specific slice for the Tenant (third-party Service Provider or Rail company A) with the required functions chained as per the service definition.

Guide Slice approach:

1. In preparation for tenant requests the 5G-PICTURE Operator (Rail company A in Figure 4-4) would have created a *guide slice* from the resources provided by the Infrastructure Provider. This contains reservations for all available resources for tenant use, across every connected domain.
2. The 5G-PICTURE Tenant, via the Service Management system, requests a service to be initiated which contains all edge access points in Region 1 and Region 2, application servers to be deployed in the cloud and edge, connectivity with QoS constraints.
3. The request is passed to the MDO which in turn maps and translates service request into requests for compute, connectivity and access while ensuring constraints related to QoS and placement
4. The Slicing Engine looks up the guide slice and allocates sub-slices in each domain to provide required connectivity and functions.
5. The sub-slices are connected, based on the pre-defined domain interconnect, to create a service specific slice for the Tenant (third-party Service Provider or Rail company A) with the required functions chained as per the service definition.

4.2.2.2 Rail Company as the Infrastructure Provider

With a rail company acting as an Infrastructure Provider, third-party 5G-PICTURE Tenants can provide their services to their passengers and other classes of End Users, operated by a 5G-PICTURE Operator running an instance of 5G OS. The Service Management and MDO components will be operated by a 5G-PICTURE Operator.

There are two possible options to implement such services given the requirement for the connectivity to span multiple regions with different Rail companies owning the infrastructure there:

1. Primary rail infrastructure provider fronts for other rail infrastructure providers in the regions of interest (Figure 4-5).
2. Each rail infrastructure provider (per region) interacts directly with the 5G-PICTURE Operator (Figure 4-6).

In both cases, slice creation for different tenants can be done using Base Slice or Guide Slice approaches, summarized as follows.

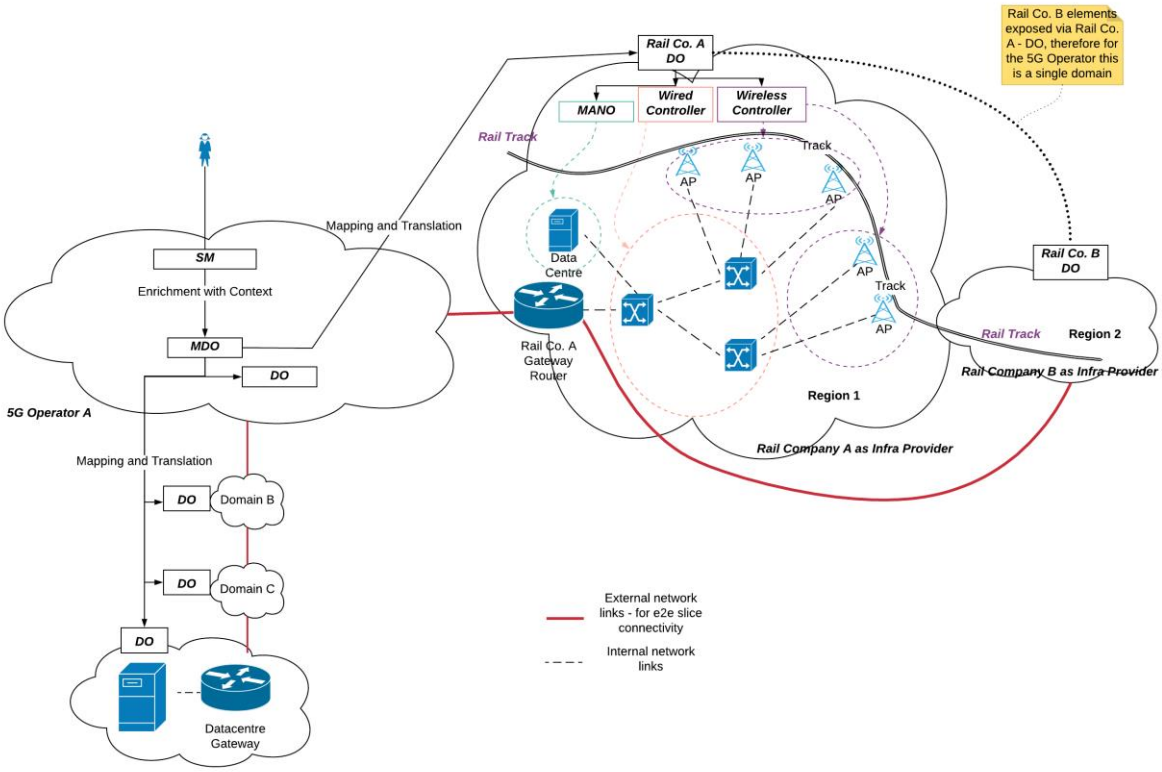

Figure 4-5: Rail Company as the Infrastructure Provider [38].

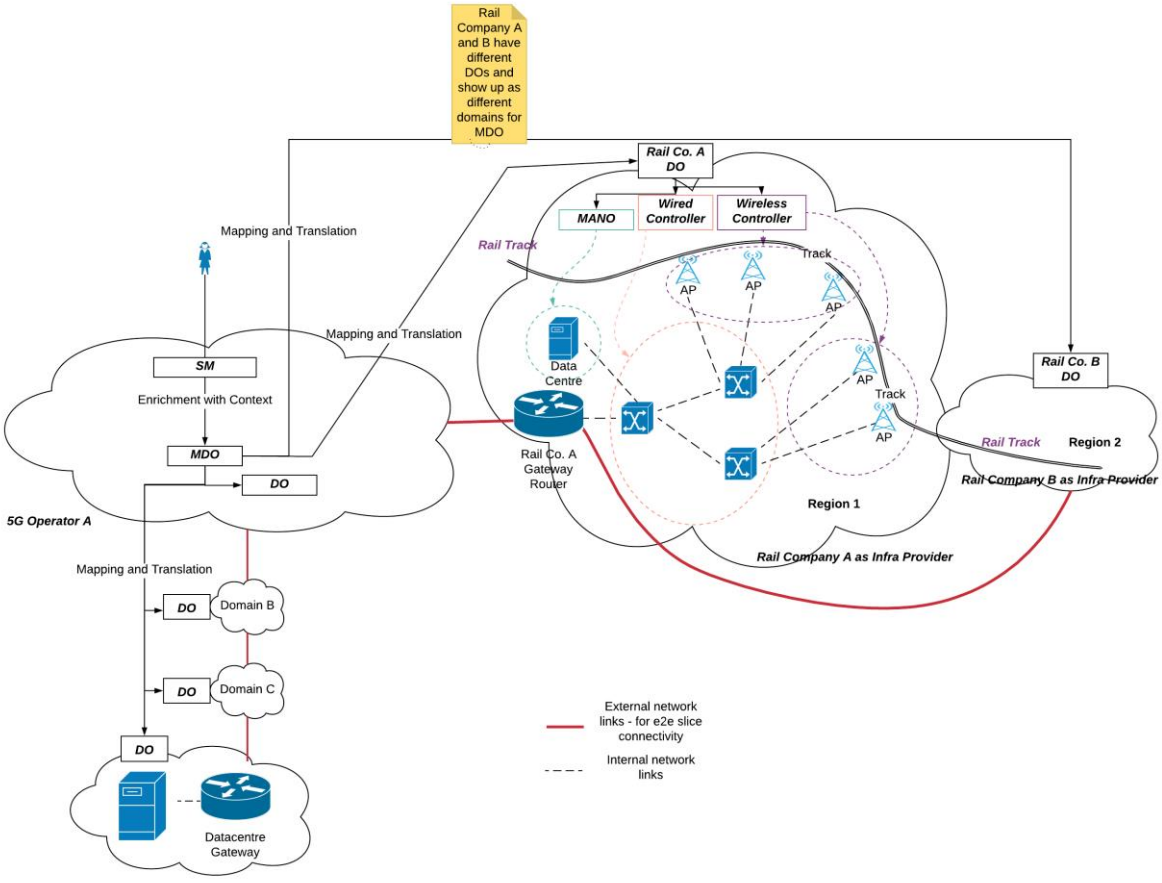

Figure 4-6: Rail Company as an Infrastructure Operator - Individual integration with each rail network – single point of interaction with different rail networks [38].

Base Slice approach:

1. In preparation for tenant requests, the 5G-PICTURE Operator A (running the SM and MDO components of 5G OS) would have created one or more base slices from the resources provided by the Infrastructure Provider. These provide an abstraction for resources held across every domain. For example, in this case the base slice would contain resources assigned to Rail company A from the following domains:
    a. Rail company A – own domain, providing edge access and compute for the Rail network (Region 1), earmarked for Tenant use.
    b. Rail company B –infrastructure provider providing edge access in Region to allow full route coverage for users of Rail company A, in case of single interface Rail company B resources would be exposed via Rail company A's Domain Orchestrator.
    c. Domain B – providing connectivity to Datacentre.
    d. Domain C – providing connectivity to Datacentre.
    e. Datacentre – providing compute facility.
2. The 5G-PICTURE Tenant, via the Service Management system, requests a service to be initiated which contains all edge access points in Region 1 and Region 2, application servers to be deployed in the cloud and edge, connectivity with QoS constraints.
3. The request is passed to the MDO which in turn maps and translates service request into requests for compute, connectivity and access while ensuring constraints related to QoS and placement.
4. The Slicing Engine operates upon the base slice to create a service specific slice for the 5G-PICTURE Tenant (third-party service provider) with the required functions chained as per the service definition.

Guide Slice approach:

1. In preparation for Tenant requests the 5G-PICTURE Operator would have created a guide slice from the resources provided by the Infrastructure Provider. This contains reservations for all available resources for tenant use, across every connected domain.
2. 5G-PICTURE Tenant, via the Service Management system, requests a service to be initiated which contains all edge access points in Region 1 and Region 2, application servers to be deployed in the cloud and edge, connectivity with QoS constraints.
3. The request is passed to the MDO which in turn maps and translates service request into requests for compute, connectivity and access while ensuring constraints related to QoS and placement
4. The Slicing Engine looks up the guide slice and allocates sub-slices in each domain to provide required connectivity and functions.
5. The sub-slices are connected, based on the pre-defined domain interconnect, to create a service specific slice for the 5G-PICTURE Tenant (third-party service provider) with the required functions chained as per the service definition.

5 Final Architecture Evaluation

This section of the deliverable focuses on the final evaluation and benchmarking of the 5G-PICTURE architecture using mathematical models, simulation frameworks as well as experimental platforms. In this deliverable we provide our final evaluation tools as they have been developed in the second year of the project, and a set of scenarios and use cases that have been defined and analysed using these tools.

In view of this, the architecture evaluation focuses on the data and control planes proposed by the generic 5G-PICTURE architecture. In terms of data plane the topics/scenarios considered address performance of the 5G wireless access communications to trains and the adoption of Sub-6 GHz LTE Massive MIMO technologies, multi-technology access network solutions in railway systems and the benefits these can provide in terms of reliability and throughput. In terms of the optical transpot the extension of TSON to provide rellient C-RAN services is also discussed and the performance of the corresponding solution is assessed experimentaly in a lab environment and, theoretically, at network level. Emphasis is also given on scalability topics where a novel service chaining approach is proposed that can significantly reduce service provisioning times. Investigation and proposal of suitable approaches to enable scalable service chaining in MEC-assisted 5G Networks exploiting Artificial Intelligence (AI), and finally scalable multi-service placement is also examined.

The performance of these schemes is examined over realistic topologies using actual traffic statistics.

5.1 Mobility Considerations

In 5G-PICTURE deliverables D3.1, D3.2 and D2.2, we have presented initial work considering a railway environment. We have stated that two technologies would be investigated: a) mmWave APs (at 26 GHz, 60 GHz), and b) Massive MIMO (at 3.51 GHz). Two real railway environments were investigated: a) Bristol Temple Meads, and b) London Paddington. In this section, we present our final results along with our conclusions and recommendations regarding the two scenarios.

5.1.1 Sub-6 GHz LTE Massive MIMO coverage cell

In this scenario, 5G connectivity to trains could be achieved by Massive MIMO technology. Access Points (APs) on the train will be served by a Sub-6 GHz LTE Massive MIMO station per cell (Figure 5-1 (left)). High data rates are expected due to the multiplexing gain as well as the array gain that a Massive MIMO system offers. Massive MIMO stations could be connected via CPRI to co-ordinate connectivity as the train moves from one cell to another, i.e. hand-over.

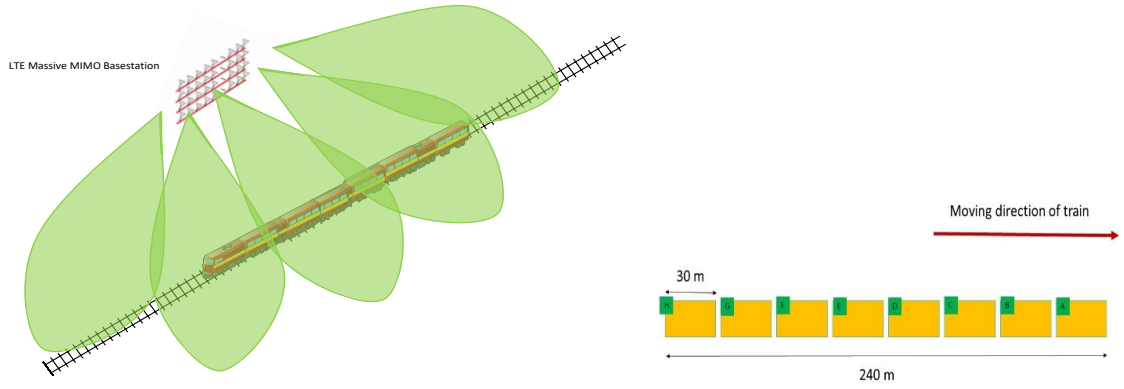

Figure 5-1: Vertical Rail – (left)Sub-6 GHz LTE Massive MIMO cell, (right) train considered.

For this scenario, we consider a BS at a height of 25 m and APs on the train at 2.5 m high. Considering a 1.4 km long railway track in Bristol (Temple Meads), and 1.6 km in London (Paddington), and frequency 2.6 GHz (MIMO) and 3.5 GHz (Massive MIMO), the channels were modelled with the ray-tracer simulator, in the University of Bristol (CSN group). Moreover, with the Received Bit mutual Information Rate (RBIR) LTE Matlab simulator and a Matlab Massive MIMO simulator, the spectral efficiency and Bit Error Rate (BER) were investigated, in a rail environment, using the ray-tracer acquired channels. We have considered a 240 m long 8-vehicle train moving along the pre-designated route, with one antenna mounted on each vehicle, as shown in Figure 5-1 (right).

In previous deliverables (D2.2 and D3.2), we have presented results considering point-to-point (P2P) links for SISO and MIMO at 2.6 GHz. In this deliverable we present results considering Massive MIMO and an actual train travelling on the rail track at a speed of 120 km/h, thus considering when we acquire our channels, the Doppler Effect due to mobility.

5.1.2 Massive MIMO results and final evaluation

We considered the two routes (Bristol Temple Meads and London Paddington) shown in Figure 5-2 .For both routes, we have placed a Massive MIMO BS in a distance of 500 m-700 m from the route for Temple Meads and a distance of 1.2 km-1.9 km from the route for London Paddington. In the BS, we have considered two cases: a) 64 antennas, and b) 128 antennas. The EIRP was estimated as 43 dBm in UL, as suggested widely in LTE systems. On the train, we have considered 8 antennas (one per vehicle).

Figure 5-2: Vertical Rail – (left)Bristol Temple Meads route, (right) London Paddington route.

At first, we look at the throughput and spectral efficiency performance for the Temple Meads route scenario. As shown in Figure 5-3 and Figure 5-4, the difference between having 64 or 128 antennas at the BS does not have a major impact on the performance. The resulting throughput was found around 3000 Mbps and the spectral efficiency around 150 bps/Hz.

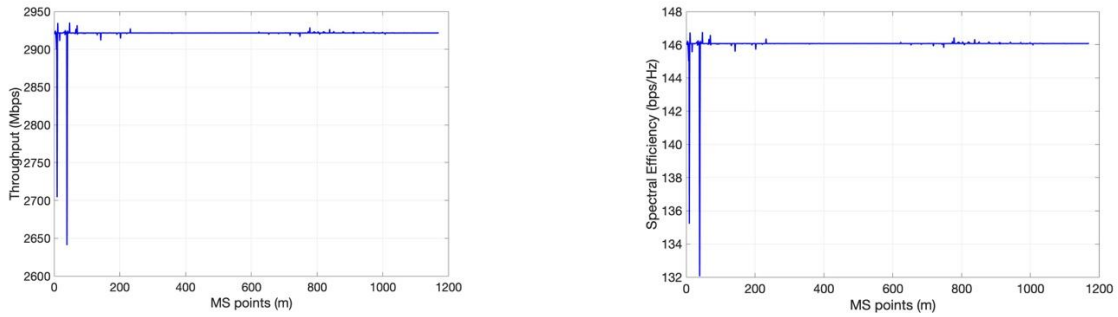

Figure 5-3: Temple Meads Massive MIMO 64 antennas: Throughput (left) and Spectral Efficiency (right).

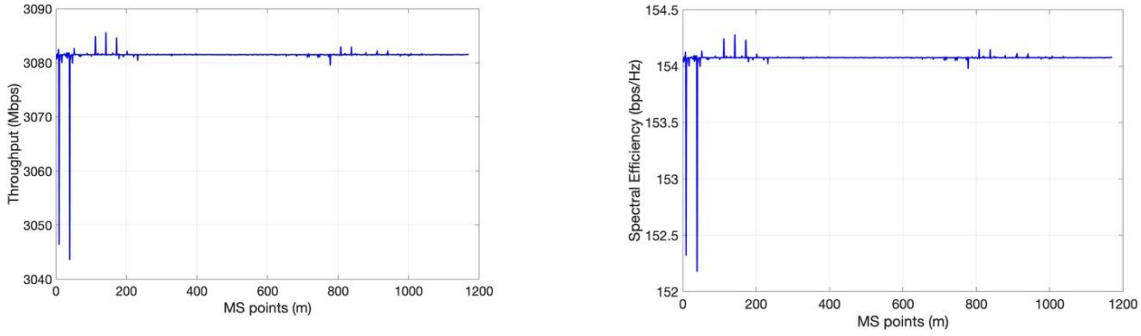

Figure 5-4: Temple Meads Massive MIMO 128 antennas: Throughput (left) and Spectral Efficiency (right).

We have also investigated the BER performance, using different modulation schemes (QPSK, 16-QAM and 64-QAM). We have considered Doppler Effect and channel aging in our model, since we are investigating a mobility scenario. Thus, we compare the resulting performance with the ideal case, that no channel aging is considered, in order to evaluate the amount of impact channel aging has on the system's performance. Figure 5-5, Figure 5-6, Figure 5-7 and Figure 5-8 show the BER results for both 64 and 128 antennas at the BS for the Temple Meads environment. It can be seen that as we use a higher modulation scheme, the BER performance, as expected, gets worse. For matters of space not all results are presented, i.e. ideal (no channel aging for QPSK and 16-QAM). In Figure 5-6 and Figure 5-8 we observe that channel aging has a considerable effect on the BER performance with 64-QAM. However, this difference was not that obvious at the BER results for QPSK and 16-QAM, concluding that the higher the modulation scheme the greater the impact of channel aging in the performance of our system.

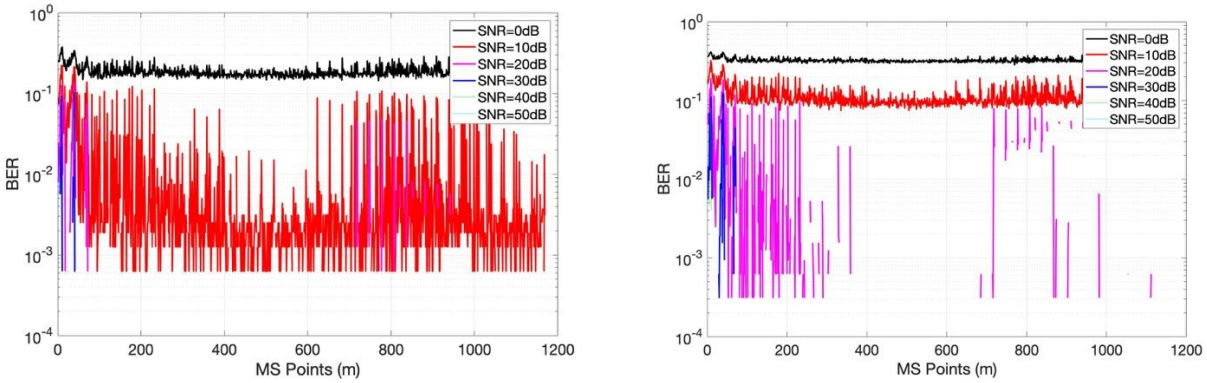

Figure 5-5. Temple Meads Massive MIMO 64 antennas: BER with QPSK (left) and 16-QAM (right).

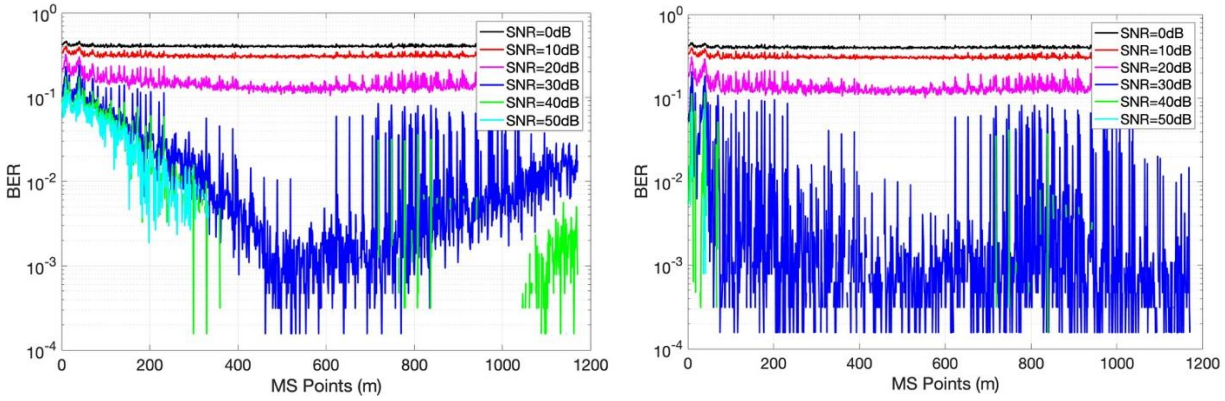

Figure 5-6. Temple Meads Massive MIMO 64 antennas: BER with 64-QAM (left) and 64-QAM-Ideal (right).

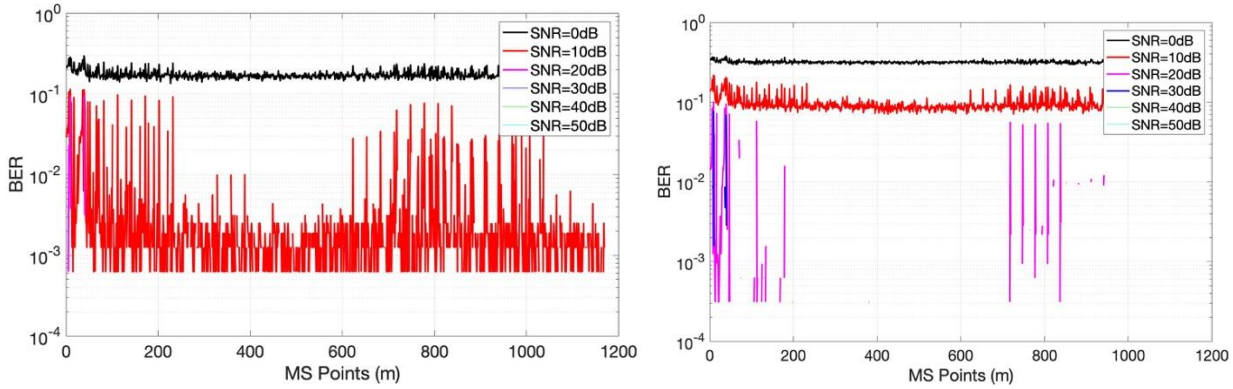

Figure 5-7. Temple Meads Massive MIMO 128 antennas: BER with QPSK (left) and 16-QAM (right).

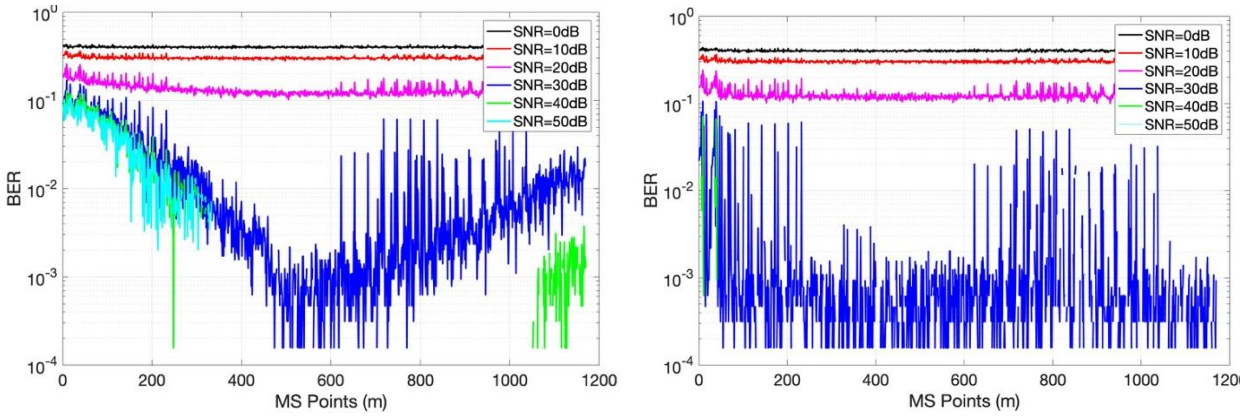

Figure 5-8. Temple Meads Massive MIMO 128 antennas: BER with 64-QAM (left) and 64-QAM-Ideal (right).

Similar simulations were run for the London Paddington route. In Figure 5-9 and Figure 5-10, we can observe that the average throughput is around 1500 Mbps and the spectral efficiency around 80 bps/Hz. The results are worse compared to the results acquired for the Temple Meads route. This us due to the different environment and position of the BS. Again, the performance is slightly better when the BS is mounted with 128 antennas.

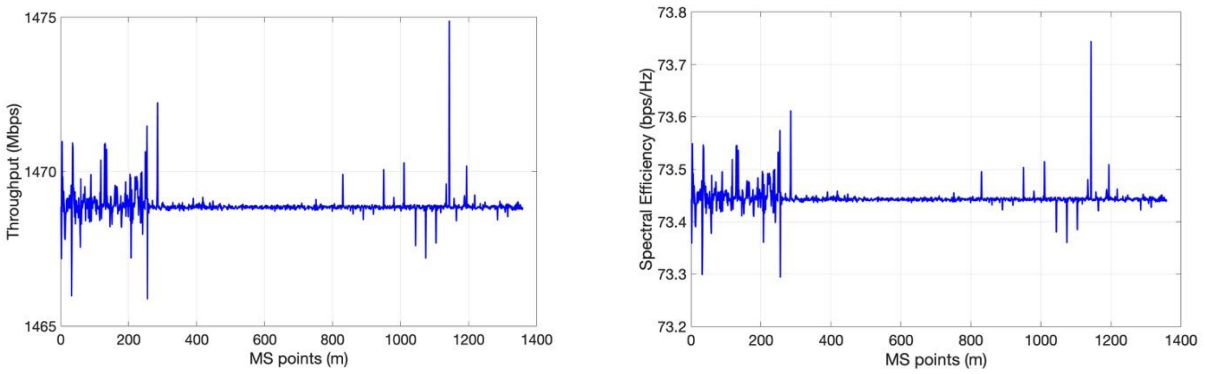

Figure 5-9. Paddington Massive MIMO 64 antennas: Throughput (left) and Spectral Efficiency (right).

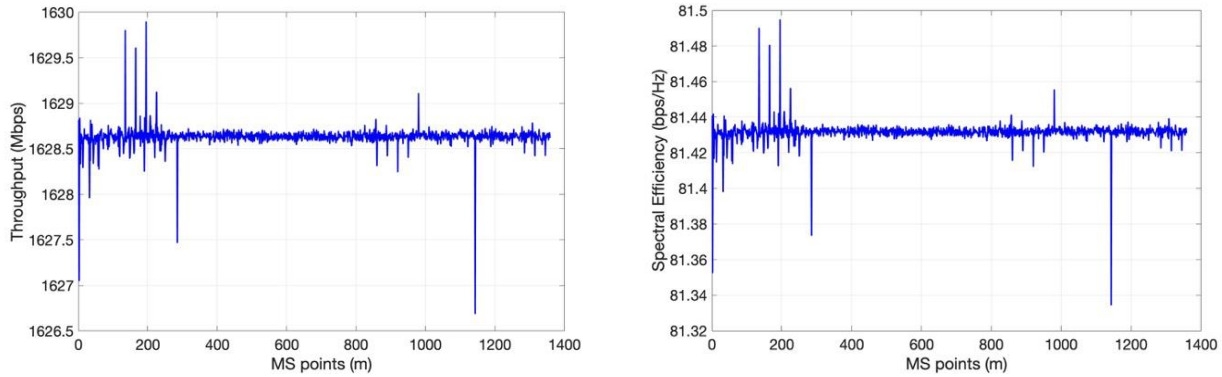

Figure 5-10. Paddington Massive MIMO 128 antennas: Throughput (left) and Spectral Efficiency (right).

We have also investigated the BER performance, using different modulation schemes (QPSK, 16-QAM and 64-QAM). We have considered Doppler Effect and channel aging in our model, since we are investigating a mobility scenario. Thus, we compare the resulting performance with the ideal case, that no channel aging is considered, in order to evaluate the amount of impact channel aging has on the system's performance. Figure 5-11, Figure 5-12, Figure 5-13 and Figure 5-14 depict the BER results with both 64 and 128 antennas mounted at the BS for the London Paddington environment. Results follow similar trend to the ones for the Temple Meads route. It can be observed that as we 'move' to a higher modulation scheme, the BER performance gets worse. Channel aging has a considerable effect on the BER performance with 64-QAM, as for an SNR=30dB,

with channel aging the BER performance drops at 10^{-2} around point 600, whereas it drops at 10^{-4} for the same point when perfect channel state information is considered.

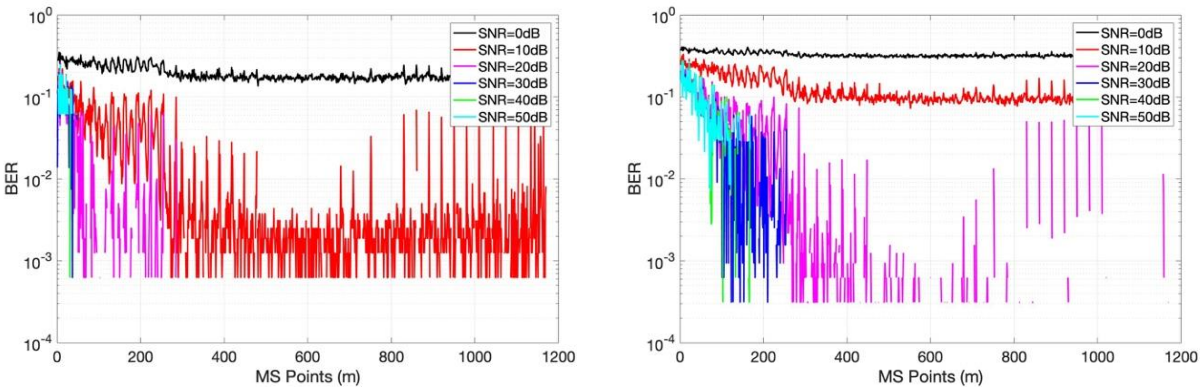

Figure 5-11. Paddington Massive MIMO 64 antennas: BER with QPSK (left) and 16-QAM (right).

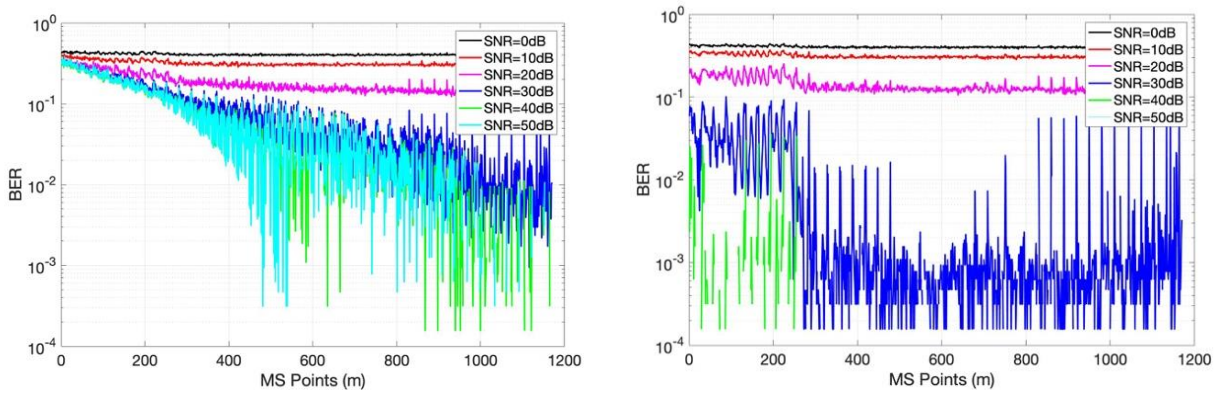

Figure 5-12. Paddington Massive MIMO 64 antennas: BER with 64-QAM (left), 64-QAM-Ideal (right).

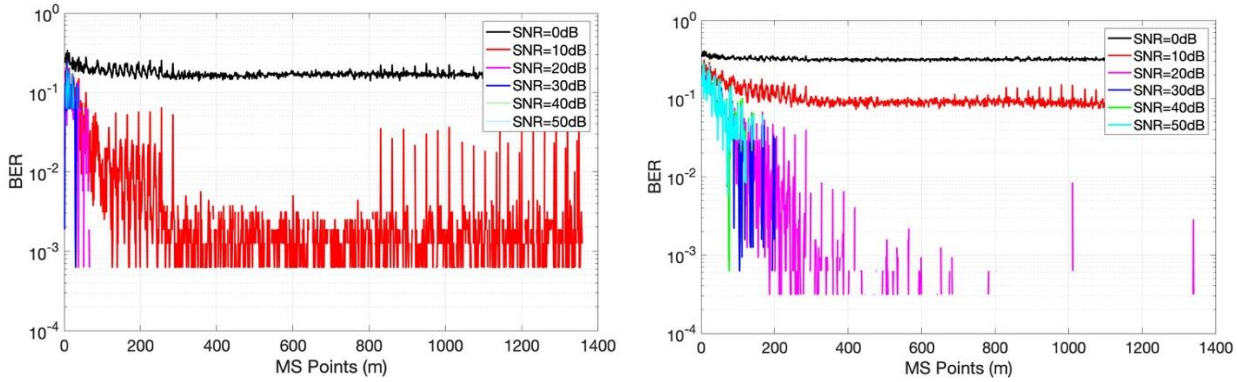

Figure 5-13. Paddington Massive MIMO 128 antennas: BER with QPSK (left) and 16-QAM (right).

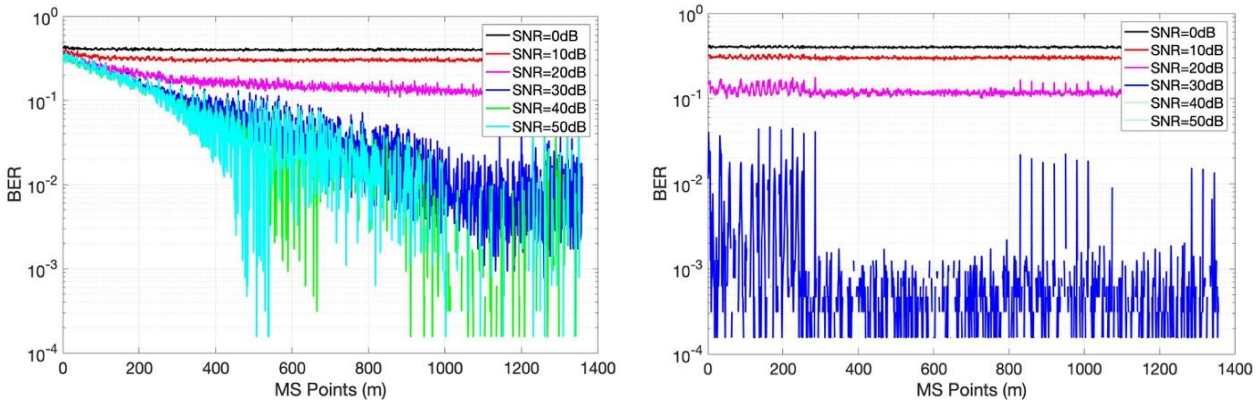

Figure 5-14. Paddington Massive MIMO 128 antennas: BER with 64-QAM (left) and 64-QAM-Ideal (right).

Overall, we have seen that a Massive MIMO deployment scenario in a railway environment can considerably increase throughput. However, there are many parameters, such as channel aging, modulation order, number of antennas at BS, etc. that can affect the performance. Based on our investigation, via Matlab simulations with the aid of our Massive MIMO Simulator, we have observed that the employment of 128 antennas at the BS does not result in major throughput performance. In addition, as we increase the modulation order, the BER performance gets worse and channel aging has also a greater impact on the performance. Finally, as the results between the Temple Meads and London Paddington routes are following the same trend but are not at the same level, we can see how the environment can have a major impact, and thus it should be greatly accounted for when designing a system like this.

5.1.3 mmWave Access Points (APs) along the trackside

For the mmWave scenario, we consider several mmWave APs, at a height of 3 m, placed along the trackside, initially 400 m - 800 m apart and around 3-5 m away from the tracks, and mmWave APs on the train, all at a height of 2.5 m, as shown in Figure 5-15 (left). Thus, FH will be based on mmWave, whereas the BH, i.e. connection between the APs on the trackside, could be connected via CPRI. We will consider both 26 GHz and 60 GHz frequencies.

Again, we have considered a 1.4 km long railway track in Bristol (Temple Meads), and 1.6 km in London (Paddington). Like in the Massive MIMO scenario, the channels were modelled with the ray-tracer simulator, in the University of Bristol (CSN group). In addition, beamforming was introduced, selecting beam width in azimuth and elevation. Then, the spectral efficiency was evaluated, based on the modelled channels, using an RBIR mmWave simulator. We have considered a 240m long 8-vehicle train moving along the pre-designated route, with one antenna mounted on the front and one at the rear of the train, as shown in Figure 5-15 (right).

In previous deliverables (D2.2 and D3.2), we have presented results considering P2P links for both 26 GHz and 60 GHz. In this deliverable we present results considering both frequencies and an actual train travelling on the rail track, considering the Doppler Effect, and choosing the best of the two antennas on the train, i.e. employing receive diversity we choose to serve the train with the antenna receiving the highest-power signal resulting in the highest throughput.

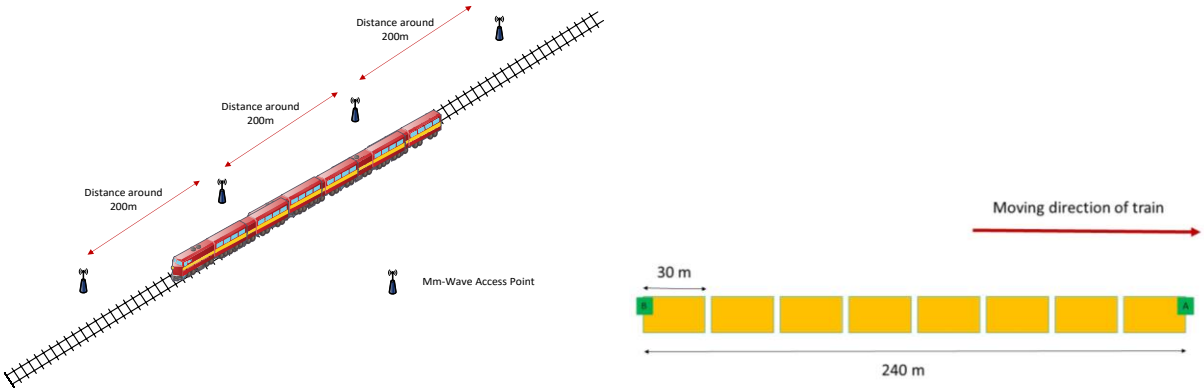

Figure 5-15: Vertical Rail – (left) mmWave APs along trackside, (right) train considered.

5.1.4 mmWave Results and Final Evaluation

Our investigation in mmWave technology deployed in a rail environment, considered both 26GHz and 60GHz frequencies for the rail environments in Bristol Temple Meads and London Paddington (Figure 5-16). The transmit power was 22 dBm. Every mmWave BS placed along the trackside is shown with a different colour.

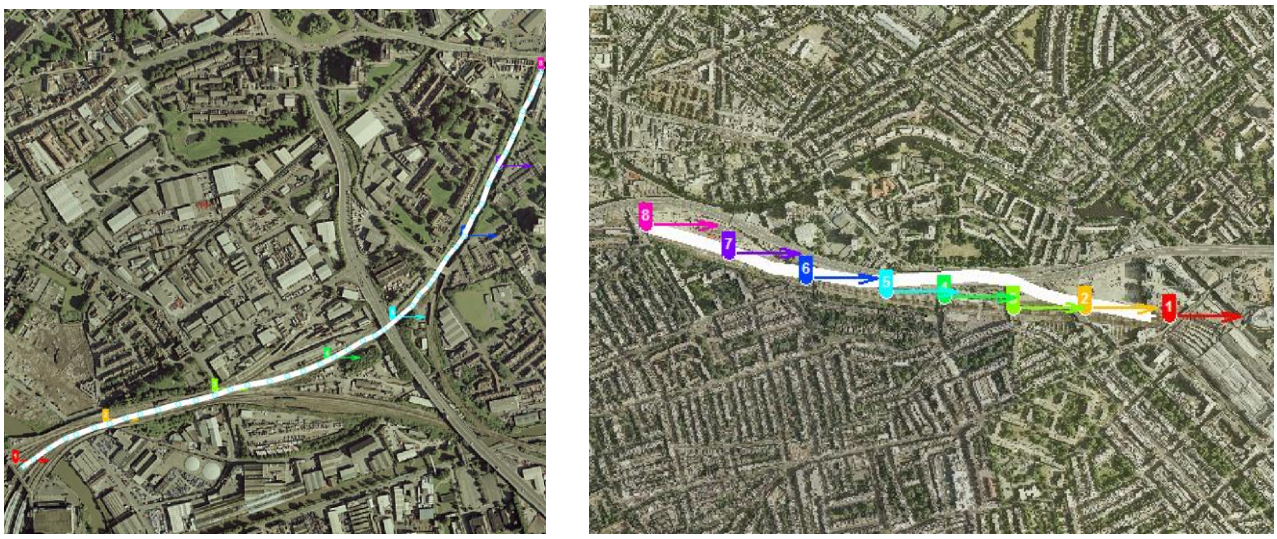

Figure 5-16: Vertical Rail – (left)Bristol Temple Meads route, (right) London Paddington route.

Considering the train moving along the track, we investigated the throughput performance, for both Temple Meads and Paddington, with and without beamforming (max ray selection), with 7.5° beamwidth at both ends, and for APs distance 400/600/800 m, at 26/60 GHz.

Figure 5-17 and Figure 5-18 depict the throughput achieved with and without beamforming respectively, choosing the best of the two mounted antennas on the train, for both rail environments. Overall, for the Paddington scenario, results are slightly worse for the case that APs are placed 800 m apart. In Figure 5-19, the Cumulative Distribution Functions (CDFs) can be observed. For both environments, without BF, with a 300 m radius mmWave cells, we can achieve around 4.7 Gbps with 45% certainty. When BF is applied, with a 400 m cell radius, a throughput of 4.7 Gbps can be achieved almost certainly. Figure 5-20, Figure 5-21 and Figure 5-22, show the achievable throughput for the APs placed at 400 m, 600 m, and 800 m distance respectively. We can observe that as mentioned above, for the environment investigated in the Paddington station the resulting throughput is lower than the one achieved in the Temple Meads scenario. Moreover, as expected, as the APs distance gets larger, the performance deteriorates.

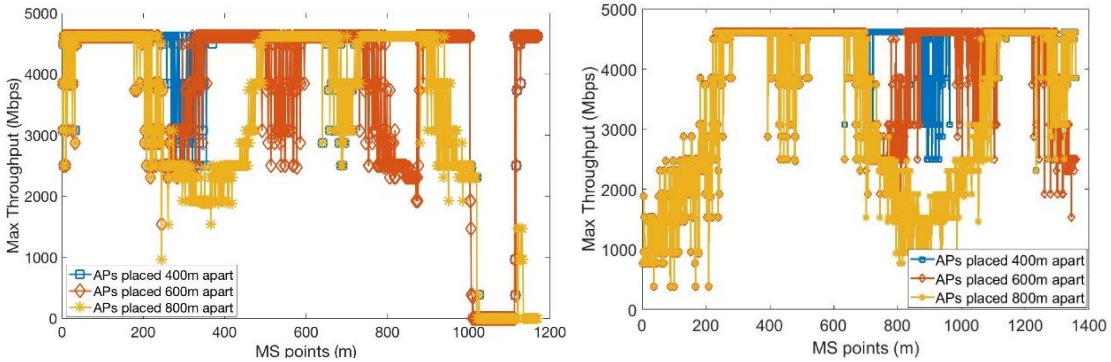

Figure 5-17. Throughput (best antenna) without BF at 60 GHz (left) Temple Meads, (right) Paddington.

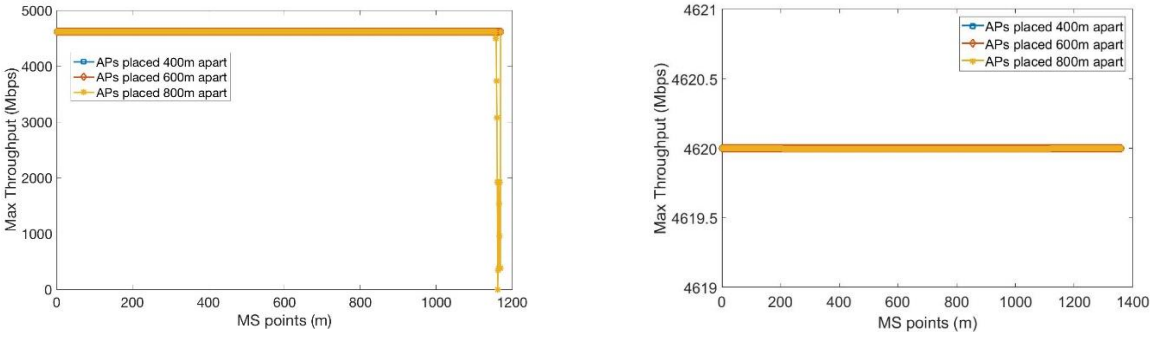

Figure 5-18. Throughput (best antenna) with BF at 60 GHz (left) Temple Meads, (right) Paddington.

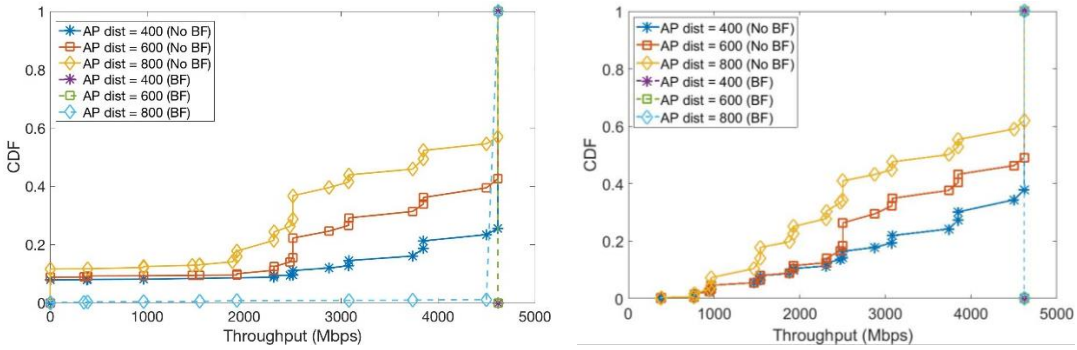

Figure 5-19. CDF of throughput at 60 GHz (left) Temple Meads, (right) Paddington

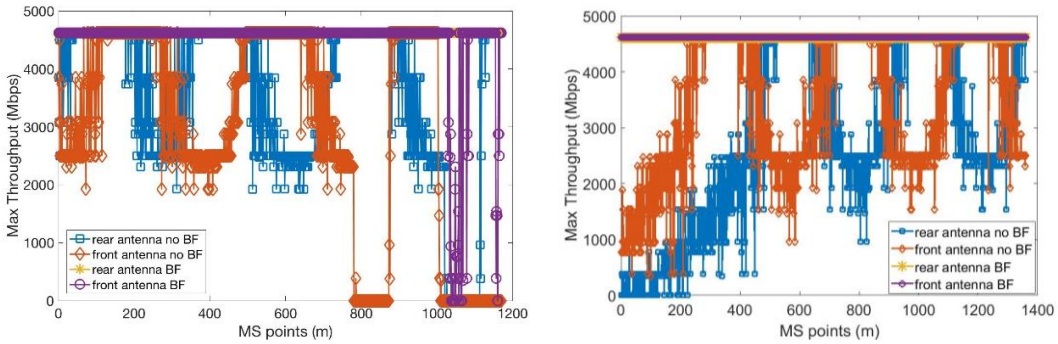

Figure 5-20. Throughput with 400 m AP distance at 60 GHz (left) Temple Meads, (right) Paddington.

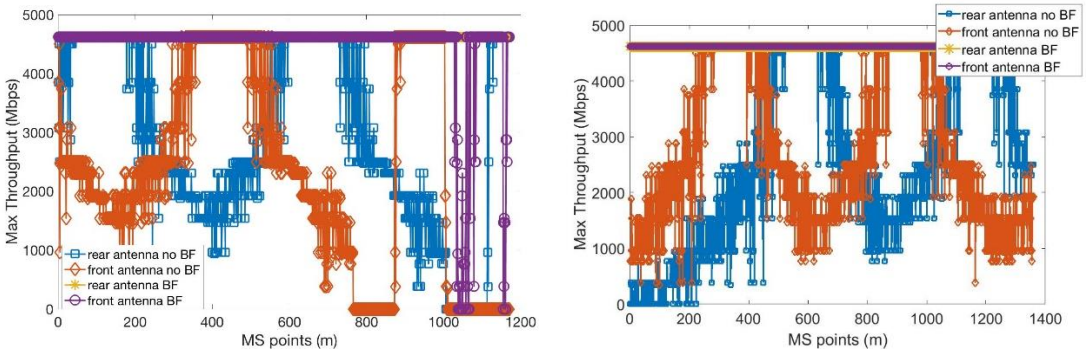

Figure 5-21. Throughput with 600 m AP distance at 60 GHz (left) Temple Meads, (right) Paddington.

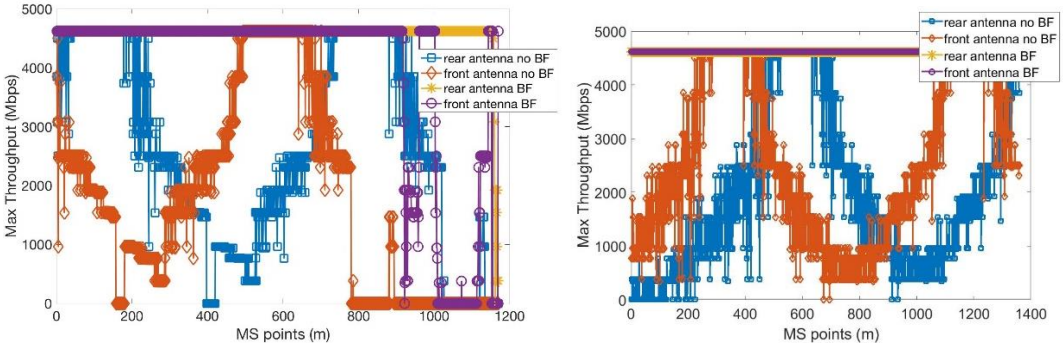

Figure 5-22. Throughput with 800 m AP distance at 60 GHz (left) Temple Meads, (right) Paddington.

From Figure 5-23 up to Figure 5-28, similar results are depicted for Temple Meads and Paddington stations, with the centre frequency now being 26 GHz. The results trend is very similar to the case of 60 GHz. We can comment that when no BF is applied, then the route designated in London Paddington station results in lower throughput performance. Looking at the CDF of the throughput for the two centre frequencies (60 GHz and 26 GHz), we can observe that results are very similar, for 26 GHz and 60 GHz, at the Temple Meads station.

However, this is not the case for London Paddington. At 26 GHz, in the case of no BF, considering 800 m AP distance, the chance of achieving 4.7 Gbps drops from 60% to 30%.

Overall, based on the fact that we cannot compare rail environments, we could conclude that 60 GHz and 26 GHz provide, in most cases, similar throughput performance. Most importantly, the employment of mmWave cells, with 400 m cell radius, looks a viable 5G solution, since with the application of BF 4.7 Gbps can be achieved, whereas without BF, there is an average of 45%-50% possibility to achieve 4.7Gbps.

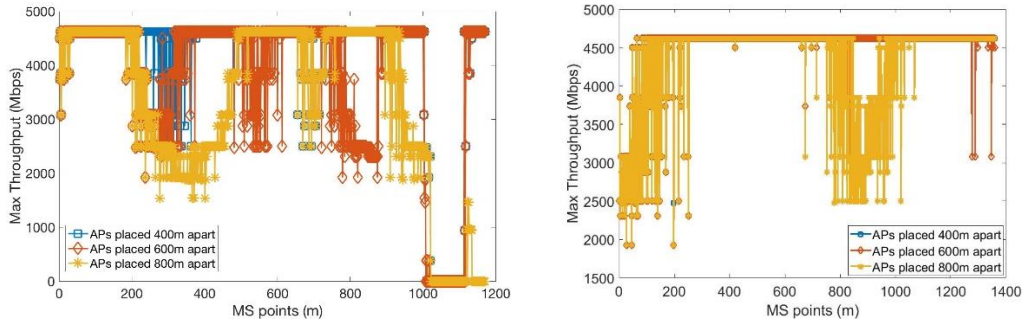

Figure 5-23. Throughput (best antenna) without BF at 26 GHz (left) Temple Meads, (right) Paddington

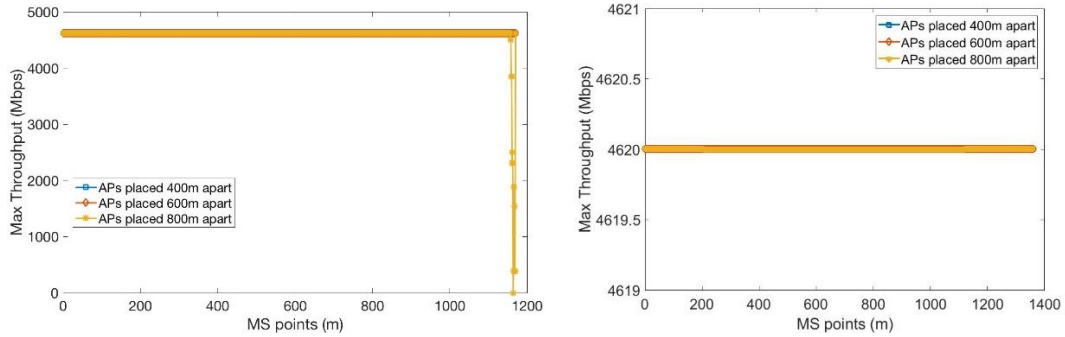

Figure 5-24. Throughput (best antenna) with BF at 26 GHz (left) Temple Meads, (right) Paddington

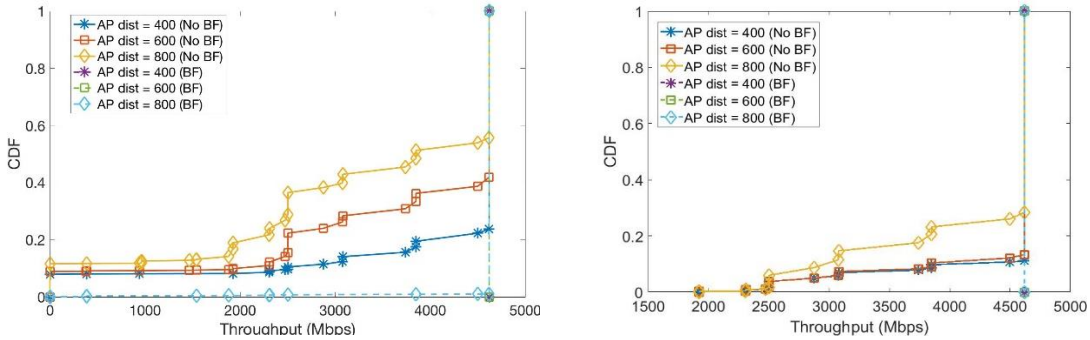

Figure 5-25. CDF of throughput at 26 GHz (left) Temple Meads, (right) Paddington

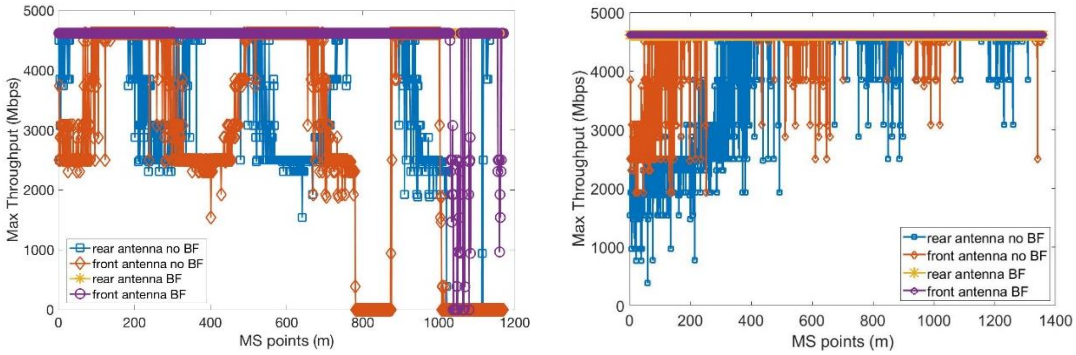

Figure 5-26. Throughput with 400 m AP distance at 26 GHz (left) Temple Meads, (right) Paddington

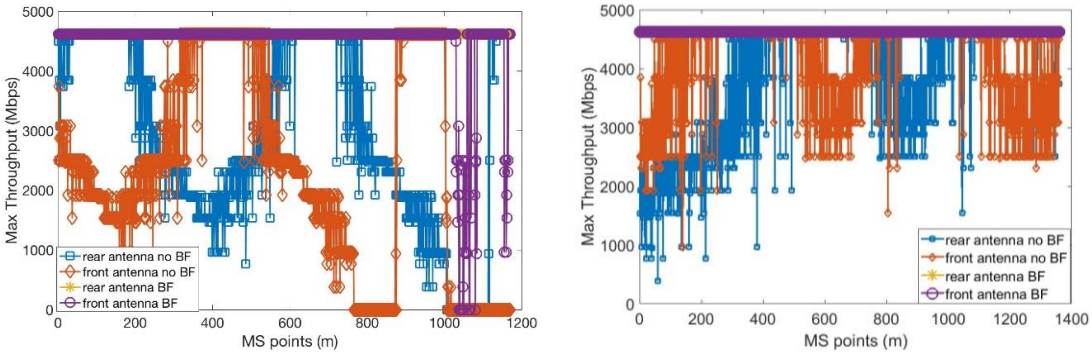

Figure 5-27. Throughput with 600 m AP distance at 26 GHz (left) Temple Meads, (right) Paddington

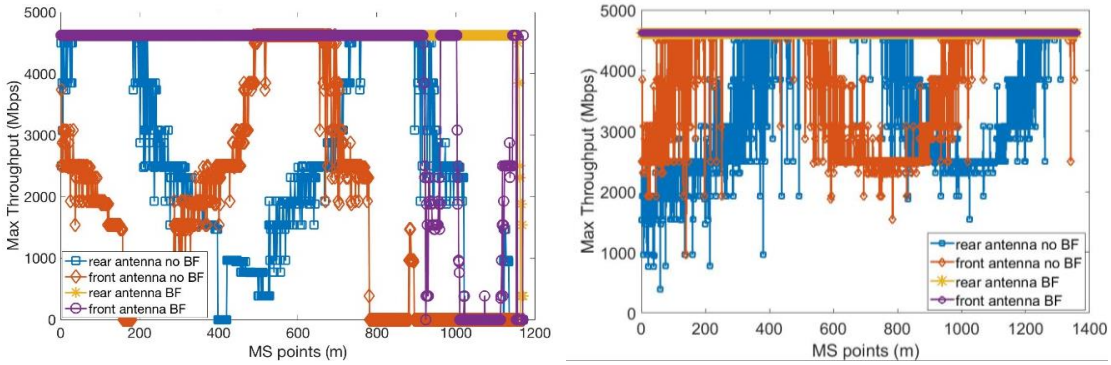

Figure 5-28. Throughput with 800 m AP distance at 26 GHz (left) Temple Meads, (right) Paddington

Finally, an examination on the AoA/AoD of the rays, per MS point, was performed to conclude on the ideal beamwidth for the Temple Meads station route, at 60 GHz This examination reveals a pattern that can be seen around every AP in the route. As seen in Figure 5-29, there is no substantial variation in the transmitted and received angles for the majority of the route. At distances, larger than 30m from the AP a connection can be maintained with beamwidths of 20°. A further increase to 30° allows the AP to serve the MS up to a distance of 10m without a change in the beam pattern.

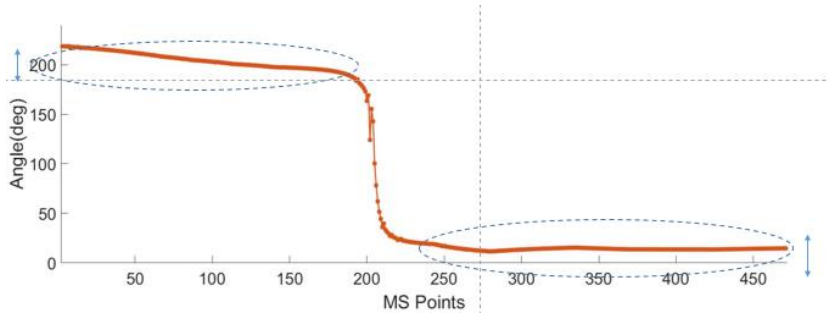

Figure 5-29: AoA/AoD profile for Temple Meads at 60 GHz.

5.2 Heterogenous access network for railways

This section provides a high level description of the design and development of a converged infrastructure integrating a variety of technologies to improve the efficiency of cabin services in railway systems. This solution is inline the work conducted under the Future Railway Mobile Communication system (FRMCS). Adopting the 5G-PICTURE various access technologies (i.e. LTE, Wi-Fi, RUs, LiFi etc) can be intergrated resuling in improvement of the efficiency and reliability of in-cabin railway services. A challenging problem in this enviroment is associated with the optimal design of the onboard railway communication system. To address this problem, a novel modelling framework based on Integer Linear Programming is proposed that tries to minimize the overall capital and operational expenditures (CAPEX and OPEX). These costs are minimized subject to requirements imposed by rail-specific applications such as, UHD video streaming to passengers, in-cabin surveillance and monitoring services, metering/monitoring applications etc. Once the topological problem has

been identified, its performance in terms of throughput, latency and reliability is examined using analytical models based on Markov Chain analysis.

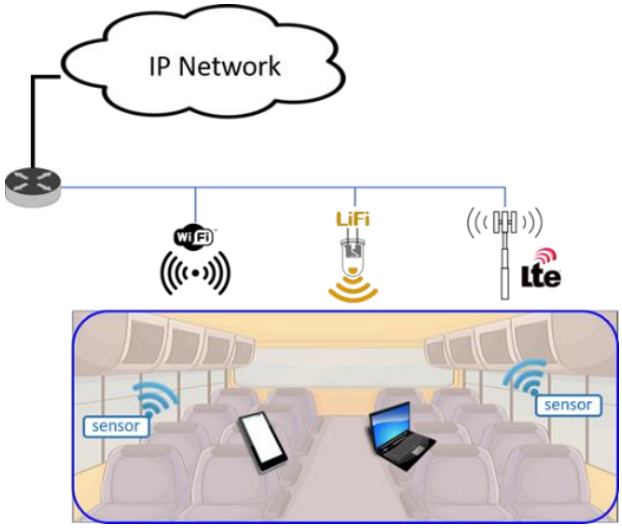

Figure 5-30: HetNet consisted of LTE, Wi-Fi and LiFi.

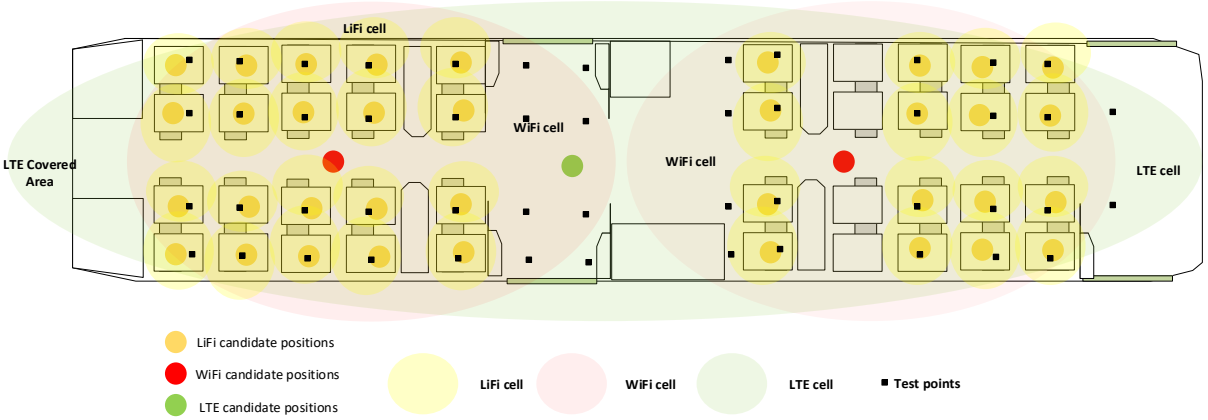

Figure 5-31: On-board multi-technology access network.

5.2.1 Planning of the on-board communication network

5.2.1.1 Topological design

We consider an on-board wireless access network comprising cellular LTE, Wi-Fi and LiFi technologies. To optimally design the onboard railway network, we consider a deployment area where traffic source points, named test points, generate demands. Each test point can either represent a passenger and/or a sensing/monitoring device generating traffic requests according to the desired planning scenario. The set of test points is denoted by $\mathcal{P}$ and $\mathcal{D}_i$ is the demand volume generated at test point $i \in \mathcal{P}$. The LiFi, WiFi and LTE APs can be installed at discrete sets of candidate sites $\mathcal{S}_{LF}, \mathcal{S}_{WF}, \mathcal{S}_{LT}$, respectively. Due to wiring issues, these devices can be placed only at specific locations. Furthermore, each test point $i \in \mathcal{P}$ can be served by a specific set of APs. Now let $\mathcal{A}_i^{LF}$, $\mathcal{A}_i^{WF}$ and $\mathcal{A}_i^{LTE}$ be the set of candidate sites in $\mathcal{S}_{LF}, \mathcal{S}_{WF}, \mathcal{S}_{LT}$ that can be reached from test point i. A graphical illustration of this setting is provided in Figure 5-31.

In order to identify the optimal placement of the various APs, an Integer Linear Programming (ILP) model is constructed minimizing the combined CAPEX/OPEX:

$$\min \left[\sum_{j \in \mathcal{S}_{LTE}} \mathcal{C}_j^{LTE} y_j^{LTE} + \sum_{j \in \mathcal{S}_{LF}} \mathcal{C}_j^{LF} y_j^{LF} + \sum_{j \in \mathcal{S}_{LF}} \mathcal{C}_j^{WF} y_j^{WF} \right]$$
$$+ \sum_{i \in \mathcal{P}} \mathcal{D}_i \left[\sum_{j \in \mathcal{S}_{LTE}} \mathcal{E}_{ij}^{LTE} x_{ij}^{LTE} + \sum_{j \in \mathcal{S}_{LF}} \mathcal{E}_{ij}^{LF} x_{ij}^{LF} + \sum_{j \in \mathcal{S}_{LF}} \mathcal{E}_{ij}^{WF} x_{ij}^{WF} \right]$$

where in the above equation parameters $\mathcal{C}_j^{LTE}$, $\mathcal{C}_j^{LF}$, and $\mathcal{C}_j^{WF}$ denote the deployment costs of LTE, LiFi, Wi-Fi APs, respectively, for site j. In the numerical evaluations, these costs are assumed to be equal for all technologies as they require the same installation effort and rely on the same wired interface (ethernet based) for backhaul. $\mathcal{E}_{ij}^{LTE}$ is related to operational costs (i.e. consumed power) when test point i transmits its demands $\mathcal{D}_i$ to the LTE AP hosted in site j. A similar definition holds for $\mathcal{E}_{ij}^{LF}$ and $\mathcal{E}_{ij}^{WF}$.

This cost function is minimized subject to a set of constraints, including:

- *Association constraints*: This set of constraints indicate that each test point can be served by a single antenna. Hence, at every time instance any user or monitoring device can be interconnected with a single wireless interface.
- *Wireless Access Point Variables:* This set of equations is used to introduce a set of binary variables indicating whether an AP will be installed at the candidate position j or not
- *Access traffic constraints:* This set of constraint enforces each test point to transmit its data using at any time instant one of the available air interfaces. Each test point can use an AP only if this is active.
- *Capacity constraints*: This constraint limits the total traffic requests generated by the test points connected to a specific AP technologies (WiFi, LiFi and LTE) below the capacity of the individual access technologies ($\mathcal{V}^{\mathrm{LTE}}$, $\mathcal{V}^{\mathrm{LF}}$, $\mathcal{V}^{\mathrm{WF}}$).

5.2.1.2 Extension: Design with delay constraints

To address the great diversity of requirements introduced by the upcoming services in a cost-effective and energy efficient manner, optimal resource assignment considering the unique application and device characteristics is needed. In achieving this goal, the development of intelligent optimization algorithms considering different Key Performance Indicators (KPIs), i.e. capacity, latency, energy consumption, for network providers can play a key role. Apart from the network and capacity and service constraints discussed in the previous sub-section, *end-to-end delay* is an important KPI that needs to be also considered in the analysis. In highly loaded heterogeneous networks, end-to-end delay can be greatly influenced by queuing delays associated with the interfaces. Therefore, applying specific queuing policies and scheduling strategies at these locations is very important. Significant delay benefits can be achieved by instantiating the necessary network functions and reserving the required virtual/physical resources. End-to-end delay can be mathematically modelled through queuing models and the adoption of closed form approximations derived by modelling the different network domains as open, closed and/or mixed queuing networks.

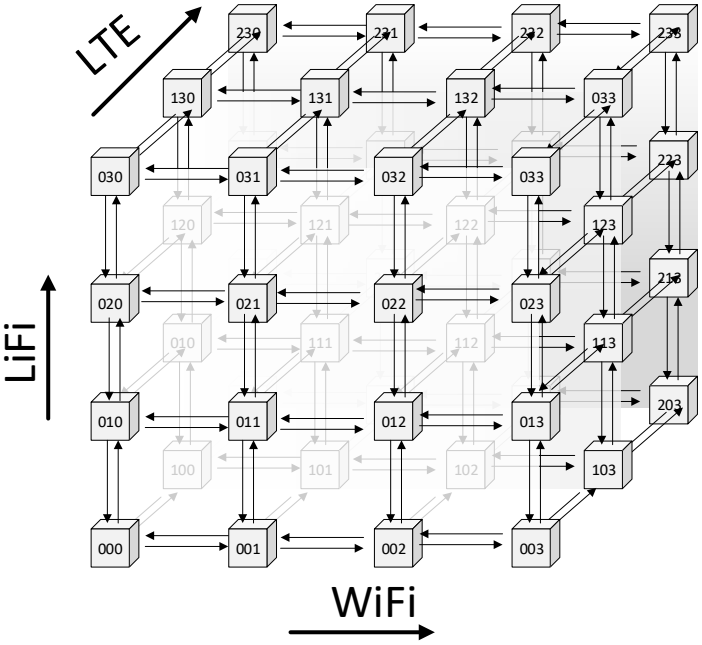

Figure 5-32: Modelling queuing delays in converged network environments: three-dimensional Markov chain for estimating delays in virtualized wireless access network.

An example is illustrated in Figure 5-32, where a three-dimensional Markov chain is adopted to model the three wireless access technology domains i.e. LTE, LiFi and Wi-Fi. Each dimension of the Markov chains corresponds to a different virtualized wireless access domain with its state space defined as:

$$\mathcal{S} = \{(i,j,k) | i \leq \mathcal{I}, j \leq \mathcal{J}, k \leq \mathcal{K}\},$$

where i, j and k correspond to the virtualized resources used across the LTE, LiFi and Wi-Fi dimension respectively and (i,j,k) is a feasible state in $\mathcal{S}$. Note that $\mathcal{I}$, $\mathcal{J}$ and $\mathcal{K}$ correspond to the maximum set of resources that can be allocated to a specific provider. A key characteristic of the proposed scheme is that it allows modelling of traffic offloading decisions from one entity to another, i.e. LiFi to Wi-Fi or LTE, as well as modelling of the arrival of a new service request by modifying the corresponding state, i.e. $(\mathrm{i},\mathrm{j},\mathrm{k}) \rightarrow (\mathrm{i}+1,\mathrm{j},\mathrm{k})$, when a new forwarding decision is applied through the LTE network. The steady state probabilities of the Markov process can be determined in a unique way using the well-known matrix-geometric solution techniques and the corresponding service delay can be determined.

5.2.1.3 Design with resilience considerations

Apart from delay, an additional requirement is resilience. To ensure resilience, the Markov chain model shown in Figure 5-32 is extended to cover the case of failure of LTE, LiFi or Wi-Fi APs. The key idea behind the proposed protection scheme is that in case of failure of an AP, services are redirected to the remaining operational APs. The overall process is modelled through the Markov Chain shown in Figure 5-33. As previously described, under normal operational conditions users may be served by any of the APs available in their corresponding areas. However, in case of failure of an LTE, LiFi or WiFi AP, demands will be served by the remaining working devices. For example, assuming that the system is in state (i,j,k), in case of failure of an LTE AP, the i users that are currently served by the LTE will be redirected to the Wi-Fi AP. This will increase the number of users served by WiFi to $k+i$ and the new state of the system will be $(0,j,k+i)$. Similarly, in case of failure of LiFi, the j users that are currently served by the LiFi APs will be redirected to LTE increasing the number of LTE users to $i+j$. The new state of the system will be $(i+j,0,k)$.

In this study, we assume that the failed APs can be either repaired after a predefined interval or remain out of order. Furthermore, in case of failure of all APs an immediate repair is scheduled.

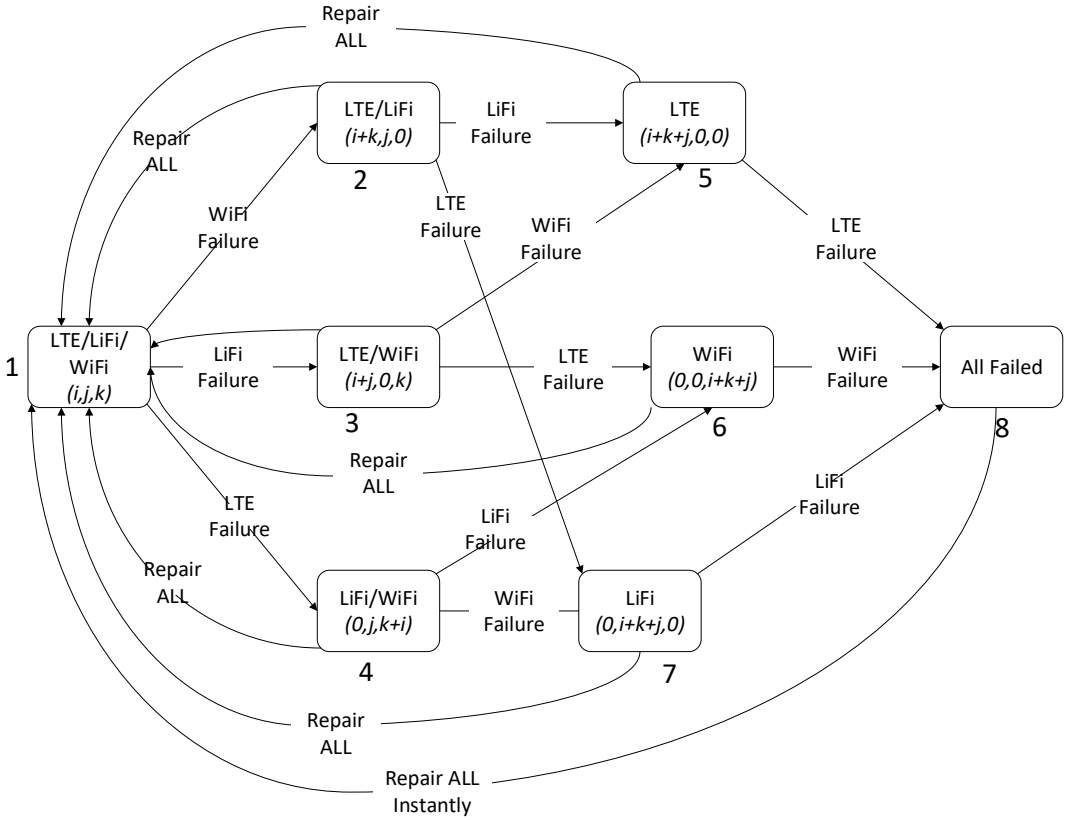

Figure 5-33 Repair/failure transition states of the on-board multi-technology access network comprising LTE/LiFi/Wi-Fi.

The transmission matrix of the state diagram shown in Figure 5-33 is given by an 8x8 matrix **P** with elements $p_{\ell m}$ $\ell, m \in \{1,2,\dots,8\}$ indicating the transition probability from state ℓ to state m defined as follows:

$$\mathbf{P} = \begin{bmatrix} 0 & F & F & F & 0 & 0 & 0 & 0 \\ R & 0 & 0 & 0 & F & 0 & F & 0 \\ R & 0 & 0 & 0 & F & F & 0 & 0 \\ R & 0 & 0 & 0 & 0 & F & F & 0 \\ R & 0 & 0 & 0 & 0 & 0 & 0 & F \\ R & 0 & 0 & 0 & 0 & 0 & 0 & F \\ R & 0 & 0 & 0 & 0 & 0 & 0 & F \\ R & 0 & 0 & 0 & 0 & 0 & 0 & 0 \end{bmatrix}$$

where R denotes the repair rate and F the failure rate. For simplicity we assume that the failure rate of all technologies is equal. However, the analysis can be easily extended to cover different failure rates. The proposed multi-technology access scheme is compared in terms of resilience with the traditional solution based on Wi-Fi/LTE solution. The state diagram of the LTE/Wi-Fi solution is shown in Figure 5-34.

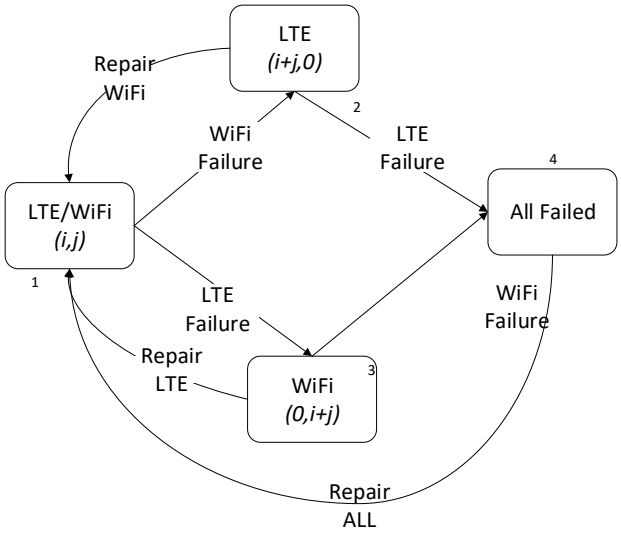

Figure 5-34: Repair/failure transition states of the on-board multi-technology access network comprising LTE/Wi-Fi.

with state transition probabilities given by the following 4x4 matrix **P**:

$$\mathbf{P} = \begin{bmatrix} 0 & F & F & 0 \\ R & 0 & 0 & F \\ R & 0 & 0 & F \\ R & 0 & 0 & 0 \end{bmatrix}$$

5.2.2 Numerical Results

5.2.2.1 Topological design

In order to evaluate the performance of the proposed ILP scheme and carry out the associated sensitivity analysis, the topology shown Figure 5-31 has been considered. The optimization problem has been solved considering the parameters shown in Table 5-1.

Table 5-1: Parameters used in the dimensioning study.

Technology	Relative Operational Cost over 5-year time Span (Normalized)	Relative Installation costs (Normalized)	Capacity Per AP (Mbps)
LTE	5	1	100
Wi-Fi	20	1	100
LiFi	40	1	43

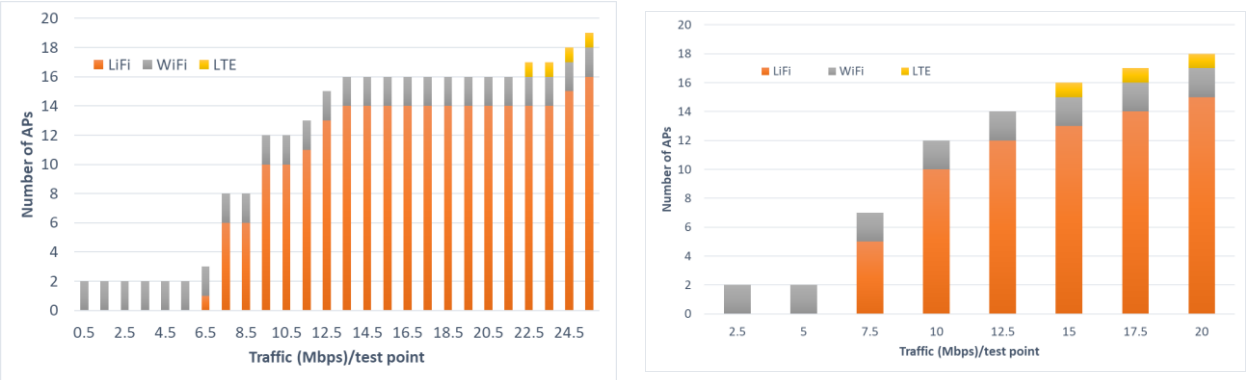

Figure 5-35: Optimal Number of APs/per technology as a function of traffic requests per test point a) for low (σ=0.5) and b) high traffic (σ=2) variability.

We also assume that traffic demands generated by each test point are uniformly distributed taking values in a specific range [Min Traffic -Max traffic]. The number of test points is equal to 32 and they are uniformly distributed across the cabin. Numerical results are provided in Figure 5-35. It is observed that when the average traffic per test point is low, the WiFi network is sufficient to handle the generated demands. However, as the traffic increases, LiFi access points need to be installed in order to provide the necessary capacity to address users' requirements. Under very high demands, the LTE APs are also activated to support the generated traffic.

5.2.2.2 Reliability analysis

A numerical example showing the probability for all APs to fail for the case where the average failure rate per AP is 1/1000h and the average repair time varies between 10 and 2000h is shown in Figure 5-36. As expected, the probability of APs to fail increase with the time interval between repairs. From Figure 5-36 we observe that by integrating all technologies through the 5G-PICTURE approach the probability of all on-board technologies to fail reduces. Therefore, the same reliability level can be ensured with less frequent repairs leading to lower operational costs.

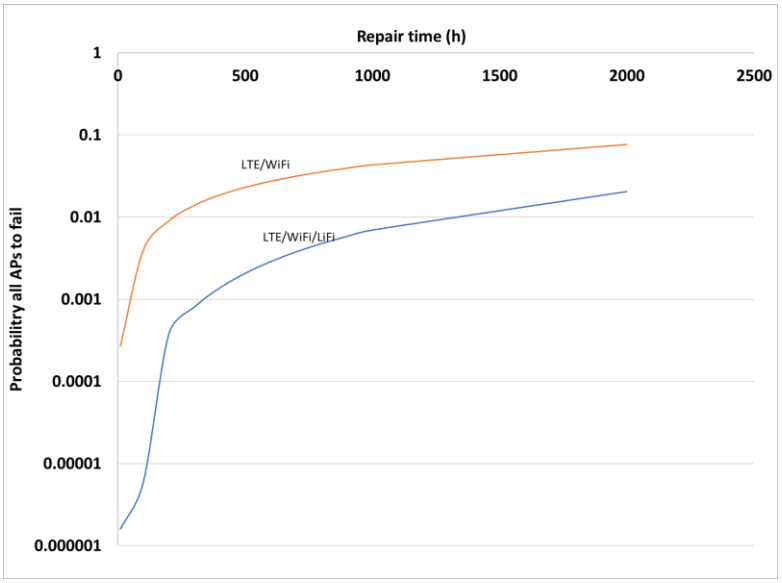

Figure 5-36: Failure probability of all APs as a function of the repair frequency for the LTE/Wi-Fi vs the converged LTE/LiFi/Wi-Fi solution.

5.2.2.3 Service dropping analysis

Figure 5-37 shows the dropping probability (service disruption) as a function of the arrival rate per AP for different average repair time. As expected, for higher values of repair times service disruption probability increases as the probability for the APs to fail also increase. Service disruption also increases with the offered load as in case of failure for high values of service requests the remaining capacity is not sufficient to cover all demands. In this case, call dropping is performed. The dropping probability (service disruption) as a function

of the arrival rate per AP for different access technologies is shown in Figure 5-37 b). As expected, the introduction of complementary technologies increases overall capacity and reliability of the system leading to lower service disruption probabilities.

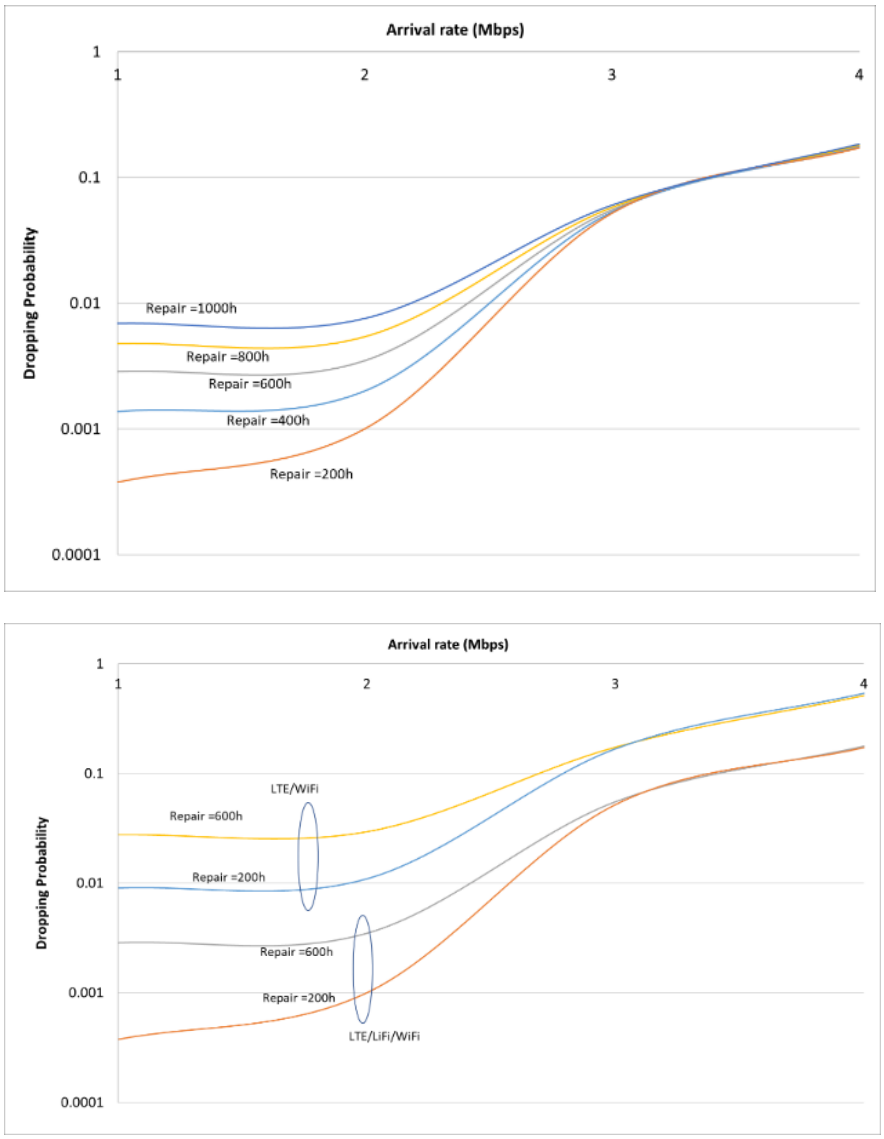

Figure 5-37: Dropping probability as a function of the arrival rate per AP for various repair time intervals. b) Dropping probability as a function of the arrival rate per AP for the LTE/WiFi and the LTE/WiFi/LiFi system.

5.3 Dynamic Softwarised RAN function placement in Optical Data Centre Networks through the disaggregated 5G-PICTURE approach

When adopting the centralized architectural model proposed by C-RAN as is the case in 5G-PICTURE it is very important to identify the optimal allocation of functions comprising the BBU function chain to the appropriate servers hosted by the CU. The concept of compute resource disaggregation approach allows individual allocation of these processing functions, associated with a specific FH service, to different servers depending on the nature and volume of their processing requirements. In addition, dynamic access and efficient sharing of compute resources for BBU processing, through the adoption of Cloud Computing, takes advantage of the notion of virtualisation that has become key technology for Data Centre (DC) resource management. In this context, virtualisation can assist in improving performance and reliability as well as operational costs reduction. Virtual Machine (VM) migration is one of the features provided through virtualization. Migration of operating system instances across different servers is a crucial tool, which is used to achieve different performance goals.

To quantify the benefits of live VM migration in the 5G-PICTURE architecture employing centralized BBU processing, a heuristic that is able to assign different functions composing the BBU chain to an appropriate set of servers at the CU, was developed. A set of experiments where the developed heuristic was called to allocate the incoming FH traffic to suitable DC resources for the required processing were conducted. Each experiment assumed different initial DC loading conditions referring not only to the absolute processing load, but also to the load distribution to different servers within the DC. Our results show that when we are able to redistribute the load of the compute resources within the DC, considerable benefits can be achieved, in terms of resource as well as energy efficiency and therefore operational cost reduction.

5.3.1 Problem Statement

The generic 5G PICTURE architecture is considered, where compute resources located at the CU support the processing requirements of a group of RRHs. The compute resources at the CU comprise a set General Purpose Processors (GPPs). These servers are arranged in a simple tree topology shown in Figure 5-38 The required compute capacity to support FH service provisioning, is supplied by these servers. These employ an implementation of softwarised BBU processing that executes the baseband signal processing to support the operation of RRHs. The requirements, in terms of compute resources, for the baseband processing of an RU, can be estimated as the sum of all compute elements performing the BBU functions. These functions include: Single Carrier - Frequency Division Multiple Access (SC-FDMA) Demodulation, Subcarrier Demapping, Frequency Domain Equalizer, Transform Decoding, Constellation Demapper, Descrambling, Rate Matching and Turbo Decoding. It should be noted, these functions need to be performed in a specific order.

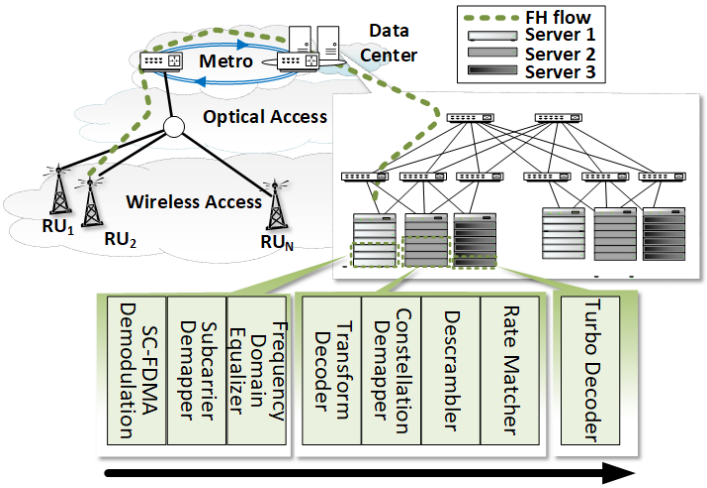

Figure 5-38: Centralized processing of softwarised-RAN functions on a data center hosting different type of servers.

5.3.2 Heuristic Design

To address scalability limitaitions of multi-sage Integer Linear Programming (ILP) solutions, a heuristic algorithm with low computational complexity is proposed that tries to identify the optimal compute resources required to support the most energy efficient processing of the BBU Service Chain within the DC.

The analysis of the LTE uplink application, provided by the WiBench suite [43], showed that different construction elements of the BBU chain have different requirements in terms of processing. From the 8 different functions, Turbo Decoder was proven to be the one with the dominant contribution to the total BBU service chain instruction requirements, as shown in the Figure 5-39 and Figure 5-40.

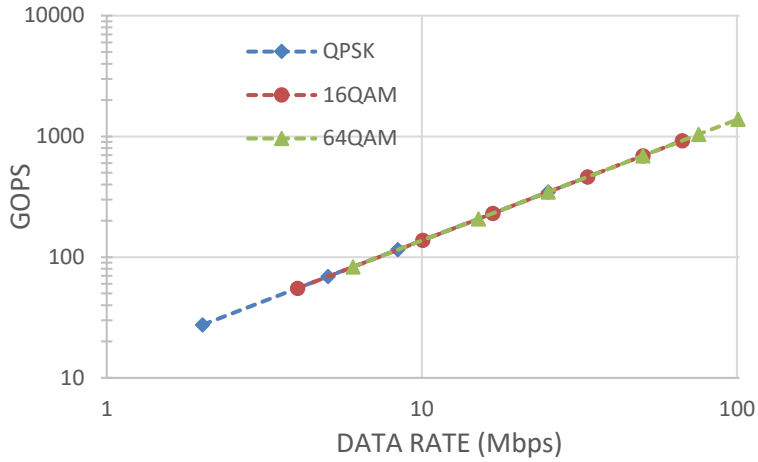

Figure 5-39: Operations per second, measured in GOPS, under various data rates for the Turbo Decoder.

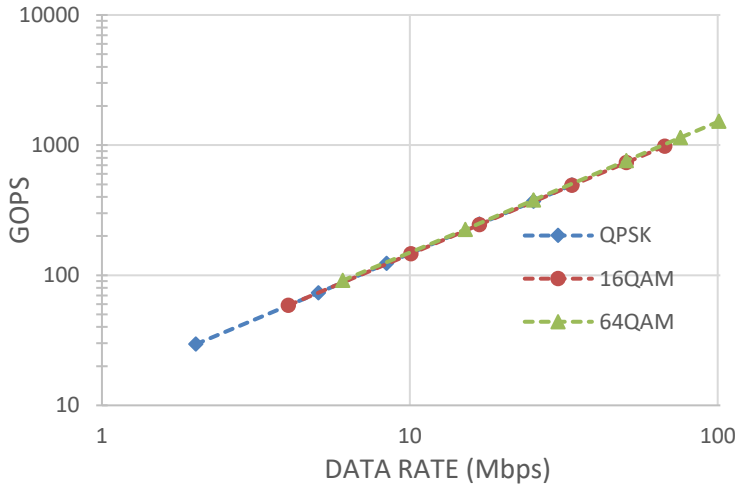

Figure 5-40: Operations per second, measured in GOPS, under various data rates for the Total BBU Service Chain.

Taking this information into consideration, in order to limit the complexity of the heuristic, we divide the 8 different BBU processing functions into two sub-sets of functions (1st and 2nd sub-set, as shown in the figure below). To satisfy the requirements of the BBU Service Chain, the order of these processing functions is always maintained within and across the 2 different sets of functions defined. The proposed grouping policy has been selected as it requires a relatively small amount of network resources for the interconnection of the first (1st) with the second (2nd) sub-set of functions while the computational requirements of the 2nd sub-set is still very high.

The main objective of the proposed heuristic is to allocate an input BBU service chain to the most energy efficient servers that have sufficient capacity to process it. The input service can be split and allocated to a set of servers, in case that splitting the service across servers is a more energy efficient option.

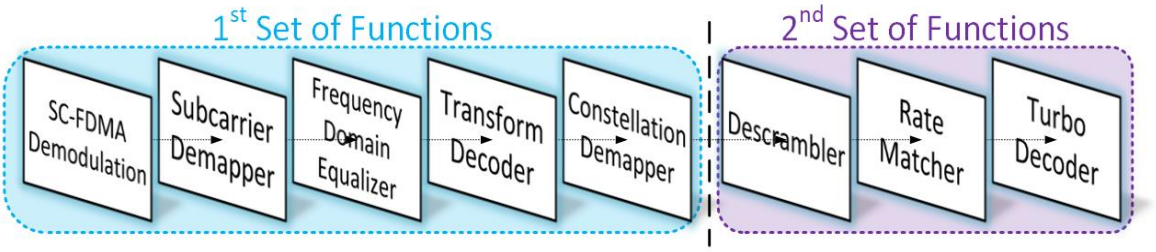

Figure 5-41: Reduction of complexity through grouping of BBU functions into 2 sets.

In our analysis, we were aiming at always serving the input traffic, independent of the volume of incoming data to be processed, satisfying at the same time, the time constraints associated with the service. Therefore, we are considering the ratio of the number of instructions required for the 2nd sub-set of functions to be performed, over the number of instructions of the 1st sub-set of functions.

5.3.3 Live VM Migration

Although VM migration comes with great benefits for the DCs, it also contains the risk of service disruption and as such Service Level Agreement (SLA) violations. In order to migrate a VM, one must contemplate the total time during which the services, supported by this VM, would be unavailable and try to maintain this below an acceptable threshold. A second aspect to consider is the total migration time in which both machines are synchronizing their states and therefore reliability might be affected. Finally, one must ensure that the active services running on the DC would not be disrupted due to the resources allocated to the VM migration.

The duration between the initiation of the live VM migration and the moment during which the original VM can be discarded is defined as the total migration time and can be divided in three phases. The first phase referred to as “image-copy” phase, is the phase where all the memory pages from the source VM are copied to the destination VM. During this process, a number of memory pages may change. At the pre-copy phase, the memory pages that have changed are re-copied. At the stop-copy phase, also known as downtime, the source VM is suspended, the remaining dirty pages are transferred to the destination VM, the device drivers are reattached to the new VM, the moved IP addresses are advertised and then the destination VM is becoming operational.

The total migration time is vastly affected by the volume of the VM and the network capacity, since migration involves the transfer of the entire VM volume from one physical server to another. While this transfer takes place, the rest of the services already running at the DC will have to be supported without disruption, thus maintaining the relevant resources. This implies that the DC network capacity that can be used for migration purposes is only the one remaining unused by the rest of the running services. In addition, for scenarios in which more than one VMs need to migrate in a short-time window, there is a clear need for identifying suitable migration scheduling schemes to avoid DC network congestion situations. Furthermore, the additional CPU overhead during migration may cause service disruption. This leads to the introduction of a threshold to the CPU utilization, in order to be able to manage the CPU overhead caused by migration.

The main elements that affect the downtime are the dirty page rate and the network’s bandwidth allocated for the migration. The rate at which the memory of the source VM is being written, during the migration process, is called dirty page rate, measured in pages per second, or dirty rate, measured in MBps and in the case in which the dirty rate is similar with the transfer rate, the result is the increase of the downtime. But the total overhead of the VM migration procedure is not restricted to the total migration time. There is also a Pre-Migration Overhead which is constituted from operations that are not part of the Live VM migration phases. It is introduced through the selection of the destination host, the initialisation of a VM and the reservation of the appropriate resources. The Pre-Migration overhead has no connection with the size of the VM and can be considered as static overhead.

5.3.4 Experiments Description

The scenario considered assumes the DC topology illustrated in the figure below. This topology includes 6 racks with each rack incorporating 48 servers. The connectivity between the racks is assumed to be provided by an optical switching solution described in [44]. For the numerical calculations, four different server types were randomly placed within each rack. The technical specifications of the servers assumed are provided in Table 5-2. These servers can be classified according to their performance in terms of energy efficiency, with type 1 server being the most energy efficient, while type 4 the least energy efficient server.

Considering this assumption, we calculate the ratios of the capacity of the larger type of server (type 4 server, least energy efficient) over the capacities of the rest of the servers (type 1, type 2 and type 3). Based on these ratios and the time constraints associated with the LTE upload service (in total <1ms per sub-frame), we define a set of thresholds that can be used to identify whether an incoming service chain (including a set of functions) can be split between the larger server type and any other of the smaller available type of servers.

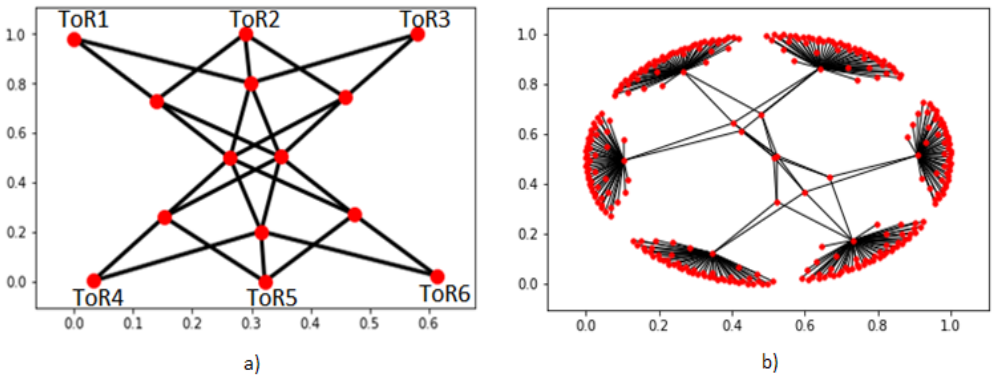

Figure 5-42: DC Topology used for the experiments: a) ToRs interconnection in the DC and b) total intra-DC network, including the servers under each ToR.

For the specific functional split and the set of servers considered in this study, the numerical values of the thresholds we have identified are: a) 68% of type 4 server processing capacity if the 1st sub-set of functions is allocated to server type 1, b) 69% of type 4 server processing capacity if the 1st sub-set of functions is allocated to server type 2 and c) 70% of type 4 server processing capacity if the 1st sub-set of functions is allocated to server type 3. It should be noted that in our calculations additional processing margins of the order of 2% have been allowed.

Table 5-2. Technical specifications of the servers used in the numerical evaluations

SERVER TYPE	COMPUTER/ DEVICE	SERVERS	CHIPS	CORES	THREADS	GOPS	POWER (Watt)	GOPS / Watt	IDLE (Watt)
S1	SuperMicro X11DPi-N(T) SMC X11	2x Intel Xeon Plat-inum 8160	2	48	96	1071.37	360	2.976	53.4
S2	SuperMicro X11DPG-QT	2x Intel Xeon Gold 6140	2	36	72	888.52	336	2.644	52.4
S3	SuperMicro X10Dai SMC X10	2x Intel Xeon E5-2683 v4	2	32	64	700.94	288	2.434	81
S4	Sugon I908-G20	8x Intel Xeon E7-8860 v3	8	128	256	2510.56	1344	1.868	269

5.3.5 Numerical Results

To quantify the benefits of the VM migration, the simple DC network topology described above is considered. Four different types of servers were randomly placed inside each rack.

We experimented with various initial DC loads (10%, 15%, 20% and 25%), for 2 different scenarios. In the first scenario, the initial load was distributed on a small number of servers (80 servers). This scenario will be referred to as “compact”. In the second scenario, the initial load was allocated to a large number of servers (180 servers). This scenario will be referred to as “spread”. Figure 5-43 illustrates the differences of the DC’s state under these two scenarios. In both scenarios the heuristic that was developed was used to assign the incoming traffic to the remaining DC resources.

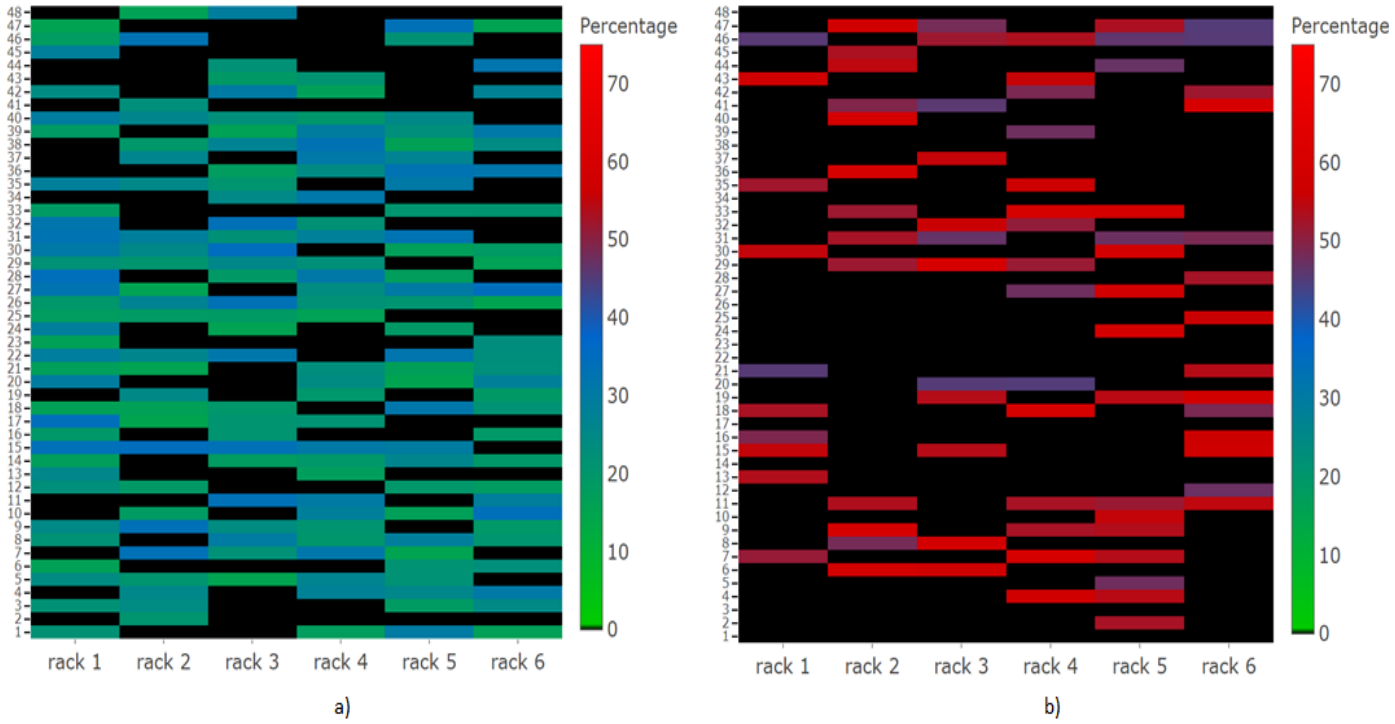

Figure 5-43: Heatmaps showing the CPU utilisation of each server at the DC, for 15% initial DC load. In a) is presented the DC state for the "spread" scenario while in b) the DC state for the "compact" scenario.

Through our experiments we calculated the total power consumption of the DC, the average CPU utilisation of the switched-on servers, as well as the total DC utilisation. The total DC utilisation is defined as the percentage of the switched-on servers compared to the total number of DC servers. All the experiments showed that the scenario with the "compact" initial load had much better utilisation of the DC resources and much lower power consumption than the "spread" scenario.

Figure 5-44 presents the benefits, in terms of power consumption, in the case where live VM migration is applied. It also shows that by migrating the initial DC load, a great reduction of the number of switched-on servers can be achieved. In the figure illustrating "Utilisation vs Data Rate" we observe that the average CPU utilisation of the switched-on servers is much higher in case of the "compact" scenario compared to the "spread" scenario. It can be also noted that the CPU utilisation reaches a maximum value introduced due to live VM migration. In order to migrate a VM in real time, some of its resources have to be used to support the migration process itself. To address this requirement, a threshold of 75% of CPU usage was adopted.

The difference in the power consumption of the schemes under evaluation observed in the figure below, is due to the minimization of the power achieved when setting servers to the idle state. The idle state consumes less power but still adding a fair amount to the total power consumption. In the "spread" scenario most of the switched-on servers had low CPU utilization, which means that they spend a considerable amount of time idle. On the other hand, in the "compact" scenario the number of switched-on servers were significantly reduced, which led to the high CPU utilisation of these servers and the reduction of their time spent in the idle state.

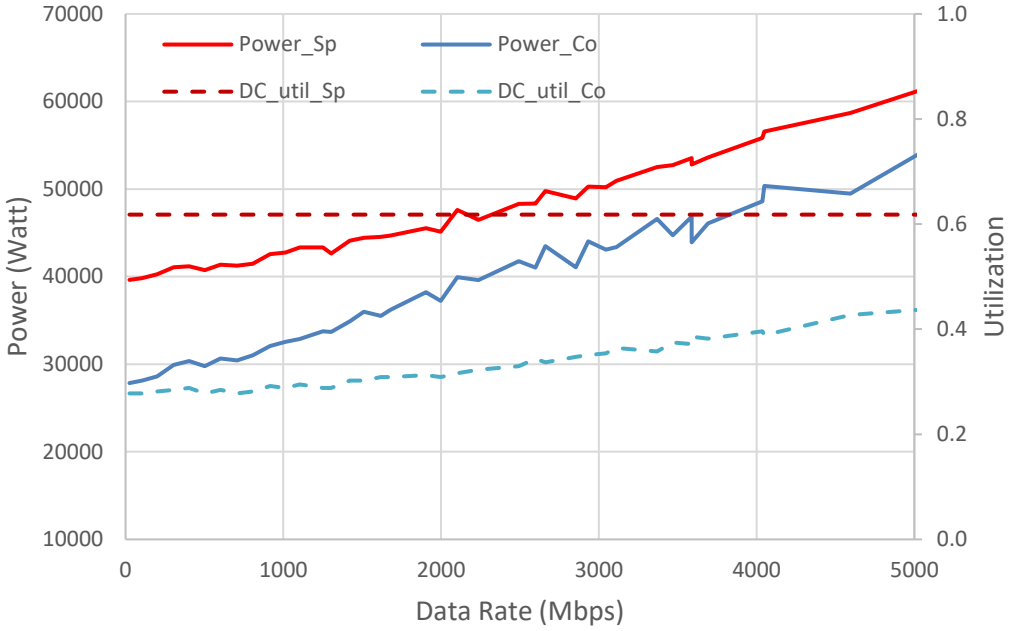

Figure 5-44: Power consumption and DC utilisation for 15% initial DC load for various Data Rates. Dotted lines correspond to the DC's utilisation while solid lines to the Power consumption. Red corresponds to the "spread" scenario while blue to the "compact".

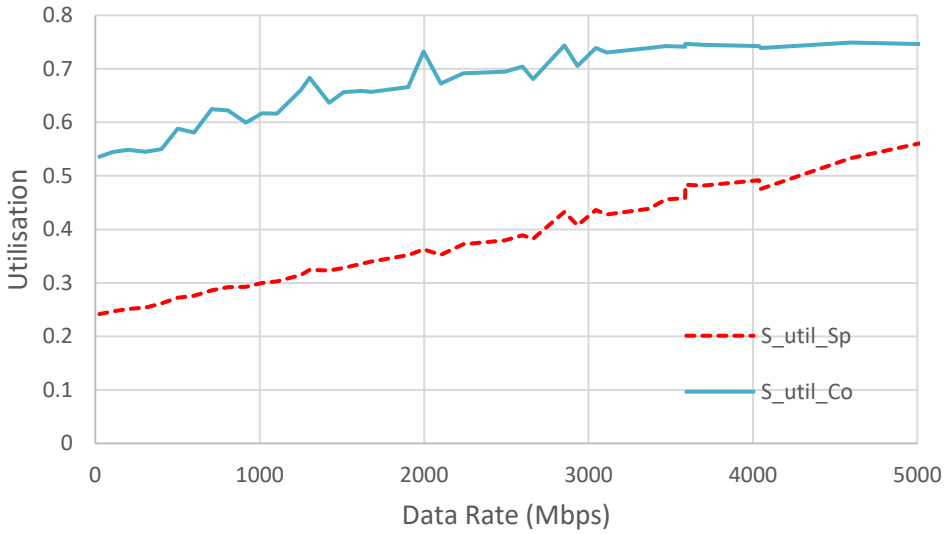

Figure 5-45: Switched-on servers' utilisation for 15% initial DC load for various Data Rates. The red dotted line corresponds to the "spread" scenario while the blue solid line to the "compact".

Live VM migration is not instant and for therefore introduces energy overheads. In the figure below a comparison between the power consumption when considering these overheads and when not is presented. The following graph is produced under the assumptions that a) each VM consists of 4 virtual cores and 8GB RAM, b) over-commitment of virtual cores and RAM is not allowed, and c) the total migration time overhead is 250s (migration transfer rate was considered at 0.5 Gbps).

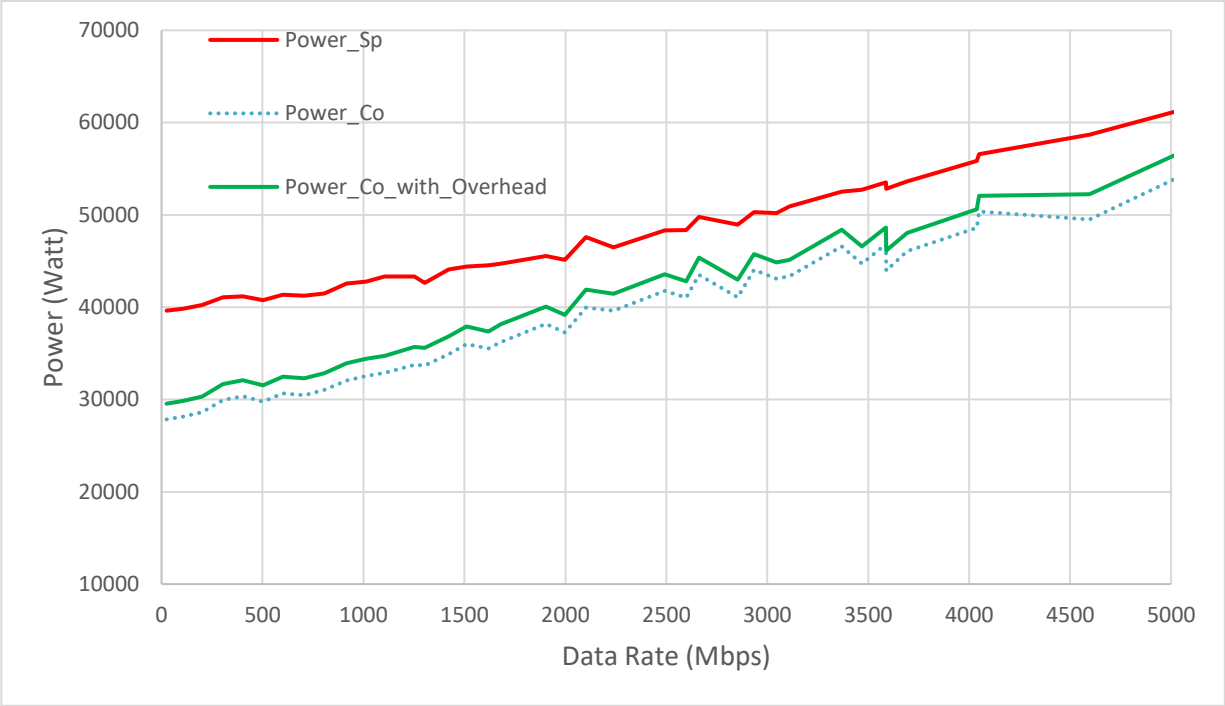

Figure 5-46: Power consumption for 15% initial DC load for various Data Rates. The red solid line corresponds to the "spread" scenario. The blue dotted line to the "compact" scenario without taking into consideration the VM migration overheads while the green solid line is taking the overheads into consideration.

The traffic variation has great impact on the type and the number of servers that are used to process the incoming requests. For the wireless access, we considered the Bristol is Open (BIO) smart city testbed. The traffic statistics for the duration of five days for a random RU is presented in Figure 5-47. We consider two different scenarios. In the first scenario, we use the Live VM migration once every hour ("migration-on"), while in second we do not use VM migration at all ("migration-off"). In Figure 5-47 b) we depict the number of the active servers that support the BBU processing as afunction of time for both scenarios. Figure 5-47 c) presents the power consumption as a function of time for both "migration-on" and "migration-off" scenarios. As it can be seen the difference between the two scenarios and the benefits of the VM migration are substantial.

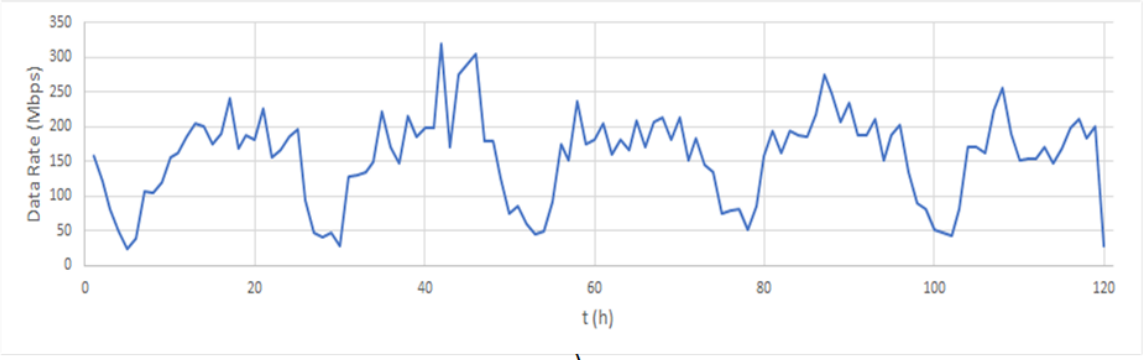

a)

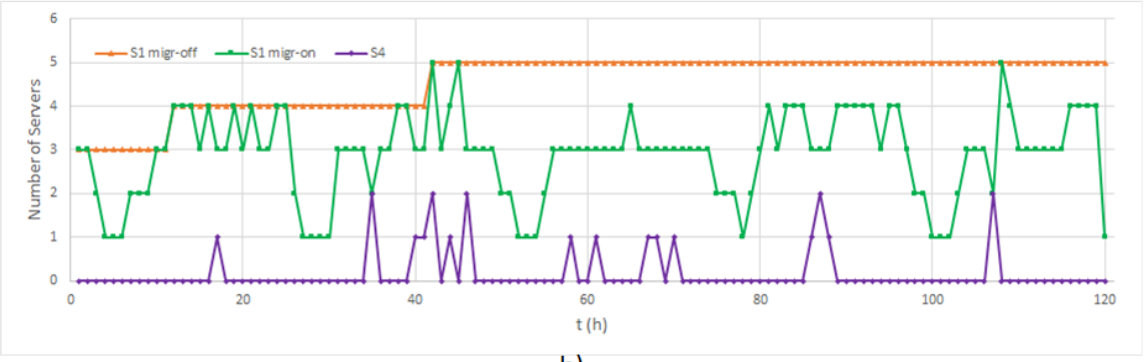

b)

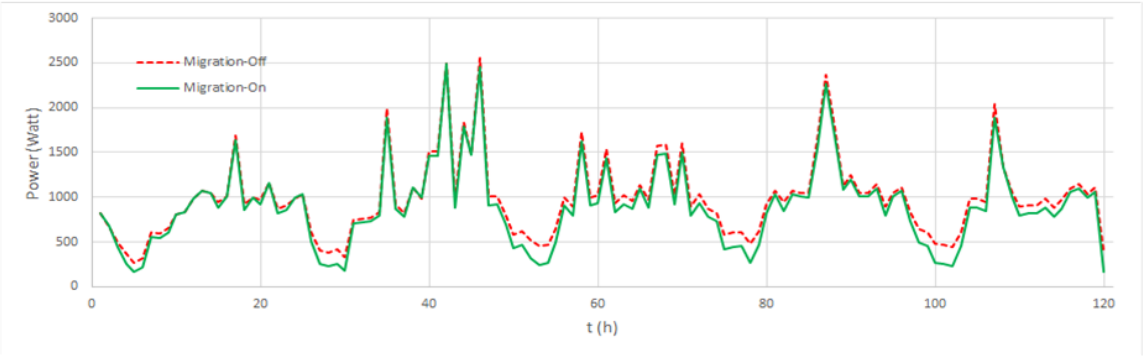

c)

Figure 5-47: a) Wireless access demands over time, b) Number of active servers supporting the BBU processing for both migration-on and migration-off scenarios, c) Power consumption as a function of time for both migration-on and off scenarios.

As expected during peak hours the DC power consumption is increased due to the allocation of additional servers. In the “migration-off” scenario after the peak hours the power consumption is immediately decreased but there is still a high number of servers activated due to the previous peak. These servers are not all required to process the incoming traffic and that adds an extra overhead in the power consumption, which can be mitigated if Live VM migration is enabled as shown in Figure 5-48.

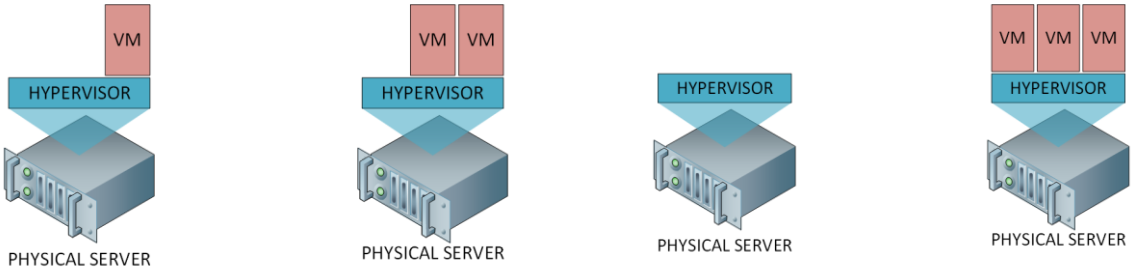

a)

b)

Figure 5-48: State of the hosts at the DC without using VM migration, b) state of the hosts at the DC when Live VM migration is enabled where the host at the left can be turned-off.

5.4 Scalable Service Chaining in MEC-assisted 5G Networks extension

This study focuses on a MEC-assisted 5G network architecture employing an optical transport network to interconnect MEC servers to process low layer functions and Central Cloud servers for processing of the upper layer functions of the LTE protocol stack as shown in the figure below. This architectural approach manages to simultaneously:

- maximize traditional C-RAN coordination and resource sharing gains, as processing is still performed by commonly shared compute resources and,
- minimize the volume of traffic that traverses the metro/core network, releasing resources for other services (i.e., fixed).

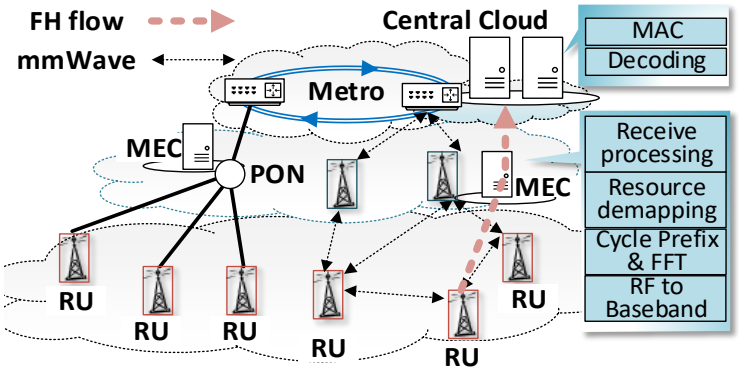

Figure 5-49: MEC-assisted 5G network. Functions up to "Receive Processing" are handled by MEC servers and the remaining by the Central Cloud, releasing network resources at the core.

Adopting this architecture, the problem of optimizing the vBBU service chaining (SC) in large scale 5G networks needs to be addressed. In this context, we propose a Multi-Layer Integer Linear Programming (ML-ILP) formulation that identifies the optimal locations where BBU functions will be placed.

We consider a 5G network, modelled as a undirected graph $G(N, E)$ where N is the set of nodes and E the set of links. In this network, vBBU SCs generated by a set $\mathcal{R}$ of R RUs are supported by a set of heterogeneous compute resources, located both at the edge (MEC) and at the metro/core (Central Cloud). Connectivity between these two endpoints is provided through a multi-technology transport network comprising point-to-point microwave links and optical network technologies. For the wireless transport we consider links operating in the Sub-6 GHz and 60GHz frequency bands, while for the optical transport, WDM network platforms [45] combining both active and passive optical elements. Active frame based WDM optical networks offer very low latency, transparent synchronization and service differentiation at the edge while WDM-PONs are used for the interconnection of the RUs with the metro/core optical network and the BBUs (see Fig.1) [45]. Now, let Σ_{r1}, Σ_{r2} be the processing requirements of the lower and upper-layer functions, respectively, of RU $r \in \mathcal{R}$. As shown in Fig. 1, Σ_{r1} includes BBU functions ranging from "RF-to-basedband" conversion up to "receive processing" whereas Σ_{r2} includes the "decoding" and "MAC" functions. Let also S be the set of all servers (MEC, central cloud) and S^t be the set of MEC and central cloud servers hosting BBU functions at stage $t, t = 1,2$ of the optimization process with $S^1 \cup S^2 \subseteq S$.

In the present deliverable, a multi-stage framework is developed where during *Stage 1* ($t = 1$) of the optimimization process, the first set of functions of all fronthaul flows in the service chain (i.e., functions with processing requirements Σ_{r1}) are assigned at servers $s \in S^1$. This is achieved by minimizing the total compute and network resource power consumption, approximated through the following cost function.

$$f_1(\mathbf{x_1}, \mathbf{z_1}) = \sum_{s \in S^1} \mathcal{E}_{S^1} \left(\sum_{r \in \mathcal{R}} x_{rs1} \Sigma_{r1} \right) + \sum_{e \in E} \mathcal{E}_e \left(\sum_{r \in \mathcal{R}, s \in S^1, p \in P_{rs}} \delta_{rpe} z_{rp1} \right) \quad (\mathbf{Eq.}\ 5\text{-}1)$$

TABLE I

Parameters and Variables used in the Optimization framework

Symbol	Description
N	Set of Nodes in the 5G network
E	Set of Links
$\mathcal{R}$	Set of Remote Units (RUs)
T	Set of stages of the optimization problem $T = \{1,2\}$
S^t	Set of servers used at stage $t, t \in T$
P_{rs}	Set of candidate paths interconnecting RU $r \in \mathcal{R}$ with server $s \in S$
$P_{rss'}$	Set of candidate paths interconnecting server $s \in S^1$ hosting the lower layer functions of RU $r \in \mathcal{R}$ with server $s' \in S^2$ hosting the upper layer functions.
Σ_{r1}	Processing requirements of the lower layer functions of the BBU chain of RU $r \in \mathcal{R}$
Σ_{r2}	Processing requirements of the upper layer functions of the BBU chain of RU $r \in \mathcal{R}$
$h_{\Sigma_{r1}}$	Transport network bandwidth requirements of function Σ_{r1} for RU $r \in \mathcal{R}$
$h_{\Sigma_{r2}}$	Transport network bandwidth requirements of function Σ_{r2} for RU $r \in \mathcal{R}$
C_s	Total processing capacity of server s.
C_{st}	Available processing capacity of server s at stage $t, t \in T$.
C_{et}	Available capacity of link $e \in E$ at stage $t, t \in T$
δ_{rpe}	Binary coefficient indicating whether link e belongs to path $p \in P_{rs}$ realizing transport network demands of RU r or not
D_r	Delay threshold for RU r.
D_{rst}	Processing time of BBU functions of RU r at server s and stage t.
D_{rpt}	Propagation delay of FH flow originating from RU r across path p at stage t.
$\mathbf{H}_t$	Matrix with elements h_{rt}
$\mathbf{C}_{et}$	Matrix with elements C_{et}
$\mathbf{D}_r$	Matrix with elements D_r
$\mathbf{C}_s$	Matrix with elements C_s
$\mathbf{C}_e$	Matrix with elements C_e,
x_{rs1}	First stage $(t = 1)$ binary decision variable indicating whether function Σ_{r1} of RU $r \in \mathcal{R}$ is processed at server $s \in S^1$ or not
x_{rs2}	Second stage $(t = 2)$ binary decision variable indicating whether function Σ_{r2} of RU $r \in \mathcal{R}$ is processed at server $s \in S^2$ or not
z_{rp1}	First stage $(t = 1)$ variable indicating the capacity allocated in support of the transport network requirements of RU r over path $p \in P_{rs}$
z_{rp2}	Second stage $(t = 2)$ variable indicating the capacity allocated in support of the transport network requirements of RU r over path $p \in P_{rss'}$

In Eq. (5.1) the summation $\sum_{r\in\mathcal{R}} x_{rs1}\Sigma_{r1}$ captures the total processing load of all Σ_{r1} functions processed at server s, x_{rs1} is a binary decision variable indicating whether function Σ_{r1} of RU $r \in \mathcal{R}$ is processed at server s or not, $\mathbf{x}_1$ is a vector containing all first stage decision variables x_{rs1} and $\mathcal{E}_s$ is the power consumption model of server s. $\mathcal{E}_e$ is the power consumption model for links e [45]. Network-related costs capture the costs of creating flows with rate, $h_{\Sigma_{r1}}$, transmitting the lower BBU functions Σ_{r1} from RU r, to the MEC. P_{rs} denotes the set of candidate paths interconnecting RU r with a server $s \in S^1$ and δ_{rpe} is a binary coefficient indicating whether link e belongs to path p realizing transport network demands of RU r or not. Now let z_{rp1} be a variable indicating the network capacity allocated to path $p \in P_{rs1}$ for flow r and $h_{\Sigma_{r1}}$ the transport network bandwidth requirements of function Σ_{r1}. $h_{\Sigma_{r1}}$ can be directly estimated using the analysis descibed in [78]. Note that the second part of the objective function ($\mathbf{Eq}.5\text{-}1$) captures all network load that is transferred through link e. The notation used in the formulation is summarized in Table I.

During *Stage 1* of the optimization process, the objective function should be minimized subject to a set of network and processing demand constraints described through the following set of equations:

$$\sum_{s\in S^1} x_{rs1} = 1, \qquad \forall\, r \in \mathcal{R} \tag{5-2}$$

$$\sum_{r\in \mathcal{R}} x_{rs1}\Sigma_{r1} \le C_{s1}, \qquad \forall\, s \in S^1 \tag{5-3}$$

$$\sum_{s\in S^1}\sum_{p\in P_{rs}} x_{rs1} z_{rp} = h_{\Sigma_{r1}}, \forall\, r \in \mathcal{R} \tag{5-4}$$

$$\sum_{r\in \mathcal{R}}\sum_{s\in S^1}\sum_{p\in P_{rs}} \delta_{rpe} z_{rp1} \le C_{e1}, \forall\, e \in E \tag{5-5}$$

Constraint (5-2) limits the number of servers where Σ_{r1}-type of functions can be processed to one, (5-3) indicates that the total number of tasks that can be assigned to server $s, s \in S^1$ cannot exceed its available processing capacity C_{s1} at stage 1, while equations (5-4) - (5-5) introduce network demand and capacity constraints, respectively. In (5-5), C_{e1} is the available capacity of network link e at stage 1. After the solution of the first stage optimization problem, the remaining server and network capacity that can be used for the subsequent functions in the chain will be equal to:

$$\boldsymbol{C_s} - \sum_{\boldsymbol{r\in \mathcal{R}}} \boldsymbol{x_{rs1}\Sigma_{r1}} = \boldsymbol{C_{s2}} \tag{5-6}$$

$$C_e - \sum_{r\in \mathcal{R}}\sum_{s\in S^1}\sum_{p\in P_{rs}} \delta_{rpe} z_{rp1} = C_{e2} \tag{5-7}$$

In *Stage 2*, the second set of functions of the FH service chain (Σ_{r2}) are forwarded to server $s \in S^2$ for processing. Now, let x_{rs2} be the second stage binary decision variables taking value equal to 1 if functions Σ_{r2} of RU $r \in \mathcal{R}$ are processed at server $s \in S^2$, 0 otherwise. Connectivity between servers $s \in S^1$ hosting Σ_{r1} of RU r and servers $s' \in S^2$ hosting Σ_{r2} is provided through a set of candidate paths $P_{rss'}$. The decision variables of the second stage optimization problem that are responsible to forward and allocate the second set of functions of the FH service chain to the optimal servers for processing, depend on the results of the first stage problem. Typical example incudes the set of path $P_{rss'}$ that can be used to forward the output of the first function in the chain to the subsequent one (i.e., Σ_{r1} to Σ_{r2}). This set depends on the decisions taken by the first stage problem regarding the servers where Σ_{r1} functions can be placed. Other examples include the available capacity at the servers and network links. All this unknown information is revealed gradually as we proceed deeper in the processing of the service chain. The optimal compute and optical network resource assignment problem in 5G environments can be solved through the minimization of the following nested cost function:

$$\min_{\mathbf{x}_1\in\mathcal{X}_1} f_1(\mathbf{x}_1, \mathbf{z}_1) + \mathbb{E}\left[\inf_{\mathbf{x}_2\in\mathcal{X}_2} f_2\left(\mathbf{x}_{2,}\mathbf{z}_2\right)\right] \tag{Eq. 5-8}$$

where extending (5.1)

$$f_t\left(\mathbf{x}_t,\mathbf{z}_t\right) = \sum_{s\in S^t} \mathcal{E}_{S^t}\left(\sum_{r\in R} x_{rst}\Sigma_{rt}\right) + \sum_{e\in E} \mathcal{E}_e\left(\sum_{r\in\mathcal{R}, s\in S^t, p\in P_{rs}} \delta_{rpe} z_{rpt}\right) \tag{Eq.5-9}$$

The multi-stage linear programming model described through (5.1)-(5.9) can be decomposed into a Master Problem (MP) and a sub-problem (SP) and solved using BD [55].

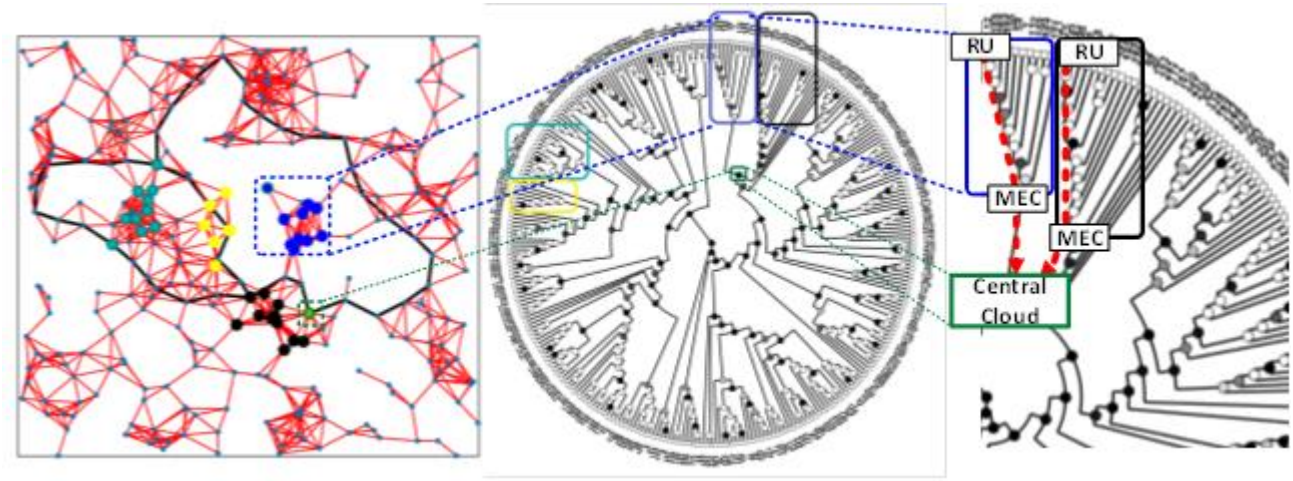

a) *b)* *c)*

Figure 5-50: a) Network with 300 RUs. Black lines indicate optical and red lines wireless links, b) HRG graph of the random topology in (a), c) vBBU SC in the HRG domain: RUs forward their low-level BBU functions to the MEC and then to the central cloud.

5.4.1 Accelerating Convergence Using Hierarchical Random Graph (HRG) theory

The BD-based algorithm successfully solve the service provisioning problem in MEC-assisted 5G environments. However, its computational complexity is still significant as the number of parameters involved in the process increase exponentially with the size of the network making it unsuitable for large optimization scenarios. In response to this we propose a decomposition technique based on HRGs that reduces the computational complexity of the SC process and accelerates the convergence process. Through HRG, the network graph over which the optimization is applied can be simplified reducing the number of variables included in the optimization model. However, a prerequisite for the successful implementation of HRG is the development of algorithms that can detect, in a cost-effective manner, a dendrogram that reflects with high probability the generic topological properties of 5G networks. This hierarchical structure can simplify the SC embedding process as it exposes to the ML-ILP problem a limited set of well-defined candidate paths that can support these flows. To apply HRG-theory the following steps are adopted:

Step 1: 5G topology decomposition using HRG

5G networks comprise access networks domains with densely interconnected devices (i.e., V2V, IoT etc) and transport optical networks sparsely interconnected with optical network nodes. HRGs capture these properties through parameter, p_n, $n \in N$ indicating the interconnection probability of any two nodes in the network. p_n takes high values in densely interconnected network (i.e. an RU servicing multiple users) and low values for optical nodes with limited connectivity. Assuming that e_n is used to denote the number of links interconnected to node n, C_n the total capacity of the node, and R_n, L_n the number of links of all nodes in the subtrees that are right and left, respectively, of node n, then, the likelihood of an HRG graph G^* is given by [56].

$$L(G^*, p_n) = \prod_{n \in G^*} p_n^{e_n/C_n}(1-p_n)^{L_n R_n - e_n/C_n} \quad \text{Eq.5-10}$$

Equation (5.10) indicates that the connection probability of two nodes in the HRG increases with e_n/C_n . For higher values of e_n, the probability a randomly selected node to be attached to n increases. Similarly, the probability that a randomly selected RU is directly attached to an optical transport node is very low and reduces with $L_n R_n$. As $L_n R_n$ increases, the number of elements that are low in the hierarchy increase. It can be easily shown that (5.10) is maximized at

$$p_n^* = \frac{E_n}{C_n L_n R_n} \quad \text{Eq.5-11}$$

taking values equal to

$$L(G^*, p_n) = \prod_{n \in G} p_n^{*\,p_n^*}(1-p_n^*)^{C_n L_n R_n} \quad \text{Eq.5-12}$$

or in log scale

$$\log L(G^*, p_n) = -\sum_{n \in D} C_n L_n R_n \mathcal{H}_n(p_n^*) \qquad \text{Eq.5-13}$$

where the $\mathcal{H}_n(p_n^*)$ function denotes the Shannon entropy.

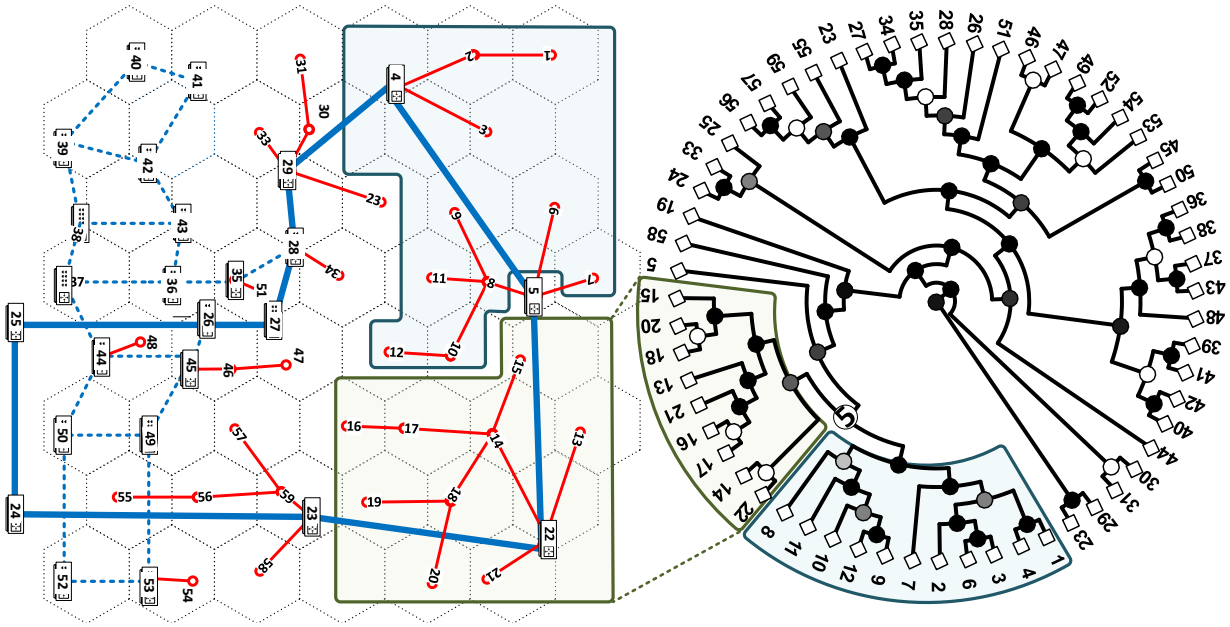

Figure 5-51: a a) Bristol Is Open (BIO) Converged 5G Network, b) Hierarchical Random Graph (HRG) of the BIO Infrastructure.

Step 2: Optimal Fitting of the HRG to the 5G network

Once the likelihood of the possible HRGs has been determined, a sampling technique based on the Markov Chain Monte Carlo (MCMC) approach can be applied. MCMC samples the candidate HRGs proportionally to their likelihood and identifies the HRG with the maximum $L(D, p_n)$ value [56]. The maximum likelihood HRG fits the real world 5G graph with high accuracy. An example of this process for a 300 node network (Figure 5-50 a)) is shown in Figure 5-50 b. Once fitted, the optical transport nodes appear high in the hierarchy of the generated HRG (close to the center). On the other hand, RUs are low in the hierarchy and are embedded at the edge of the disk (Figure 5-50 c).

Step 3: Optimal Service Chaining in the HRG space

After decomposing the 5G network into a hierarchical graph, a solution for the SC problem in MEC - assisted 5G environments can be obtained. The ML-ILP problem described in Section II can be easily solved in the HRG space as the number of candidate paths that interconnect RUs with servers $s \in S$ that support processing of the requested SCs has been drastically reduced. A graphical representation of this benefit is shown in Figure 5-50 c. It is observed that employing this methodology, central clouds servers which are directly attached to the core have been placed close to the root of the HRG whereas MEC servers have been embedded low in the hierarchy providing an intuitive solution to the problem. During this step, the BD algorithm described in Sec. III is executed over the simplified graph and the optimal allocation strategies are obtained.

Step 4: Service re-provisioning

HRGs are updated frequently to better fit the topological changes of the 5G network (i.e. link failures, beam steering, mobility, insufficient capacity etc). Given that these topological changes are observed mostly at the edge, the likelihood of the updated 5G graph is very similar to the original one. Therefore, during the re-provisioning phase, MCMC samples only a small subset of graphs with likelihood values close to those of the original graph. Once the updated graph has been determined, Step 3 is executed.

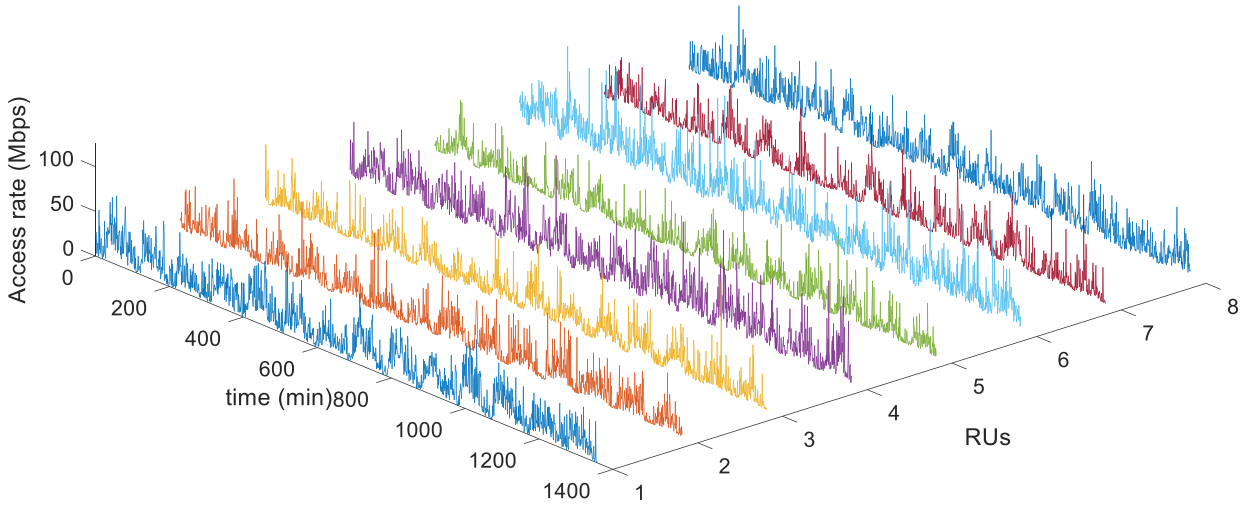

Figure 5-52: Sample of the traffic statistics used in the numerical evaluations for RUs 1-8.

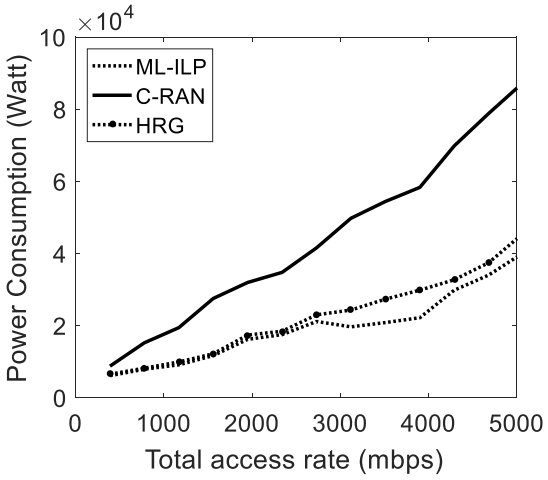

Figure 5-53: Comparison between C-RAN, ML-ILP and the HRG schemes for the BIO topology.

5.4.2 Numerical Results

We evaluate the performance of the proposed optimization framework under various topologies (including the BIO topology shown in Figure 5-51 a) for the scenario where RUs offload their signal processing functions to the MEC-assisted 5G Network. For the BIO topology we consider a set of 48 RUs evenly distributed across a 10x10 km^2 area. RUs are backhauled through microwave point-to-point links and a dynamic frame based optical network solution [45]. This solution deploys a single fiber per link, 4 wavelengths of 10Gbps each per fiber and minimum bandwidth granularity of 100 Mbps. Power consumption figures for the optical network can be found in [45]. The bandwidth of the microwave transceivers considered is 2Gbps and their associated power consumption is 45 Watts. We assume the realistic traffic statistics reported in [79]. A sample of this dataset corresponding to 8 out of 48 RUs is shown in Figure 5-52. For BBU processing, two types of servers have been considered: a) small scale MEC servers close to the RUs and, b) central cloud servers hosted by large scale DCs. MEC servers have an average cost equal to 2 Watts/GOPS while the processing cost for the central cloud servers is 1.6 Watts/GOPS [78]. We also consider that MEC servers are placed in all optical network edge nodes whereas central cloud servers are placed in nodes 4, 22, 26 and 42.

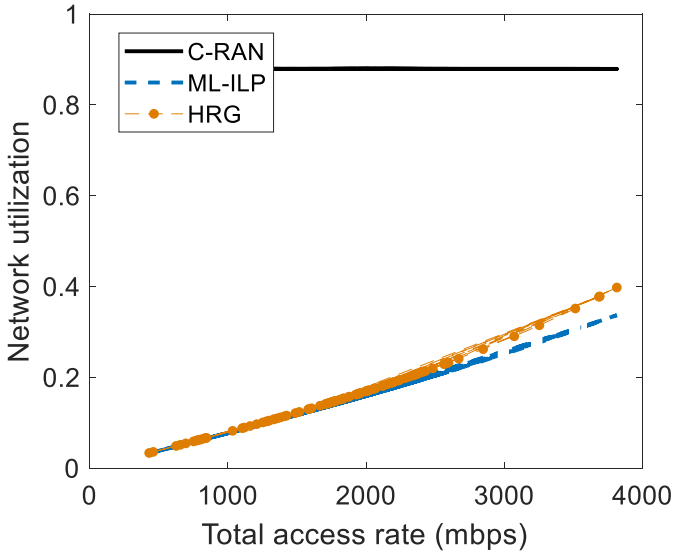

Figure 5-54: Comparison between C-RAN, ML-ILP and the HRG schemes for the BIO topology in terms of network utilization.

We initially compare the proposed ML-ILP scheme with the traditional C-RAN approach where all tasks are processed by fixed BBUs placed in the central cloud, with and without the adoption of HRG. Sizing of BBUs in this case is performed under maximum traffic demands. In Figure 5-53 it is shown that the HRG-based optimization scheme outperforms C-RAN in terms of power consumption and achieves very close performance to the optimal ML-ILP approach. In C-RAN all BBU functions are offloaded to the central cloud having significant FH network requirements and, therefore, increased power consumption. Through the introduction of the proposed scheme and the processing of some functions in MEC, FH network requirements are drastically reduced leading to lower network utilization (Figure 5-54) and reduced power consumption level. We also observe that the introduction of the HRG approach introduces minimal performance degradation compared to the optimal solution of the ML-ILP approach without the HRG simplification. As previously mentioned, HRG reduces the number of the available paths interconnecting the RUs with the compute nodes leading in some cases to sub-optimal solutions. However, compared to the benefits obtained from the reduction of the computational complexity this impact is negligible.

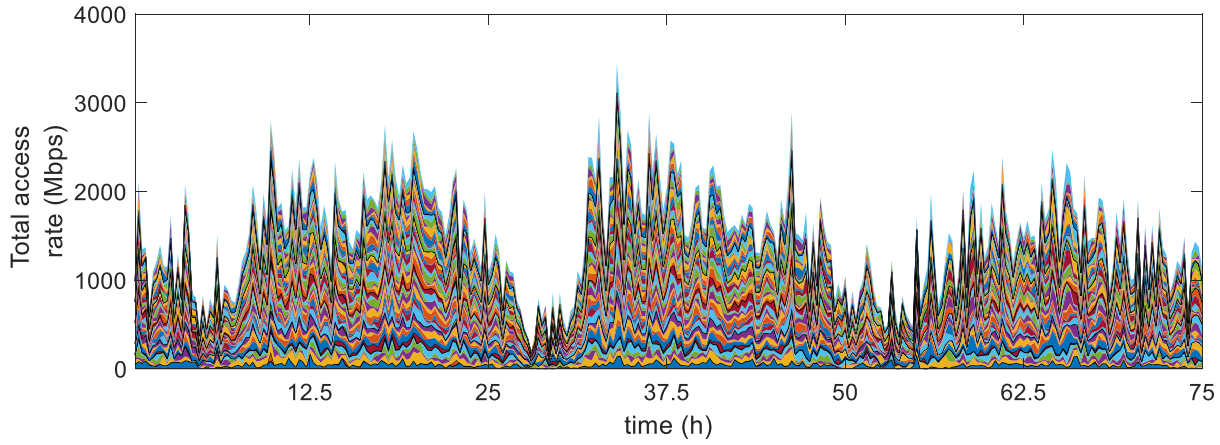

a)

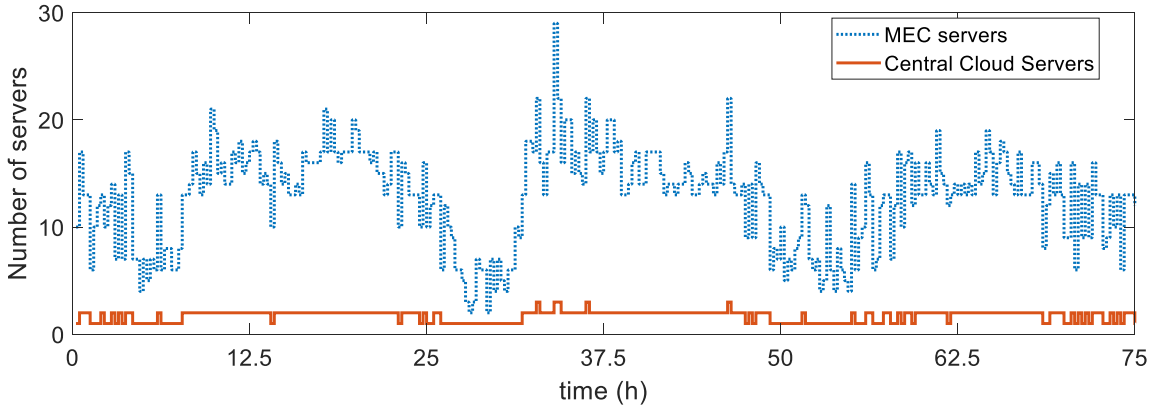

b)

Figure 5-55: a) Aggregated wireless access generated by the 48 RUs, b) Number of MEC and Central Cloud servers used for BBU functions' processing.

From Figure 5-54 it is also observed that the optical network resource utilization increases at a larger pace for HRG theory compared to the optimal solution provided by the ML-ILP scheme. This is attributed to the fact that for higher access rates the optimal paths interconnecting the RUs with the servers are not always detected by the HRG scheme. However, this difference is marginal.

Figure 5-55 a) shows a snapshot of the aggregated wireless access rate generated by all RUs as function of time. We observe that during peak hours the wireless traffic increases. This in turn increases the BBU processing requirements, leading to an increase to the number of MEC and central cloud servers required to support the generated traffic demands. Under off-peak hours, the majority of the servers are switched off to minimize the overall power consumption.

Figure 5-56 shows the impact of the number of samples taken during the MCMC process to identify the graph that reflects with high probability the properties of the 5G topology. As expected, for higher number of tree samples, the optimality gap of the solution obtained adopting HRG is reduced as the probability to detect a hierarchical graph with higher likelihood increases. The optimality gap also increases with the size of the 5G network topology. Therefore, for larger 5G network topologies a higher number of samples should be taken to achieve the same optimality gap. At this point it should be mentioned that the HRG detection process can be carried out offline (or in parallel to the ML-ILP problem) without affecting the speed of convergence of the SC allocation process.

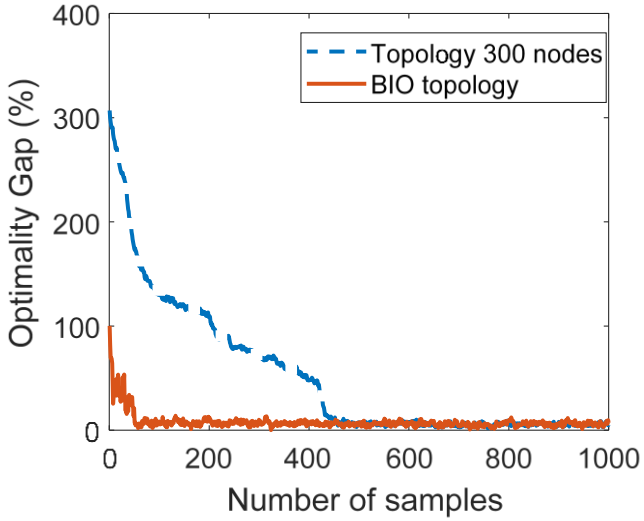

Figure 5-56: Optimality gap as a function of the number of HRG samples, c) Number of paths used in the ML-ILP and the HRG.

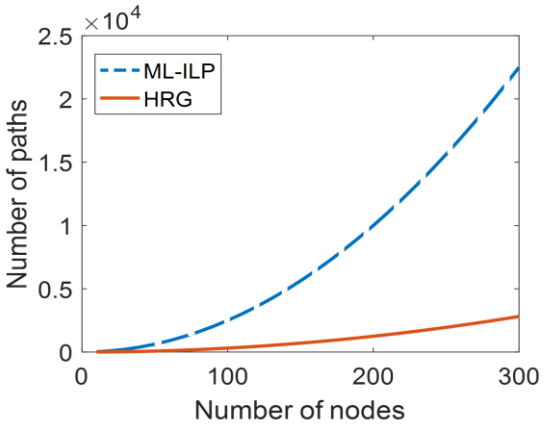

Figure 5-57: Number of paths used in the ML-ILP and the HRG.

From Figure 5-57 it is observed that that with the adoption of HRG the complexity of the BBU function allocation is reduced. This is due to that using HRG the number of candidate paths, and consequently the number of variables, that are used to interconnect the RUs with the compute resources are minimized. This has a direct benefit on the reduction of the time required to solve the optimization problem. The total exuction time for the HRG scheme for up to 300 nodes is less than 20 sec for whereas for the ML-ILP scheme the same value reaches 600 sec.

5.5 Resilience and Security considerations

The C-RAN concept has been proposed to address the inefficiencies of traditional RAN systems and support services requiring very low latency, high reliability, density and mobility. Through its pooling and coordination gains, C-RAN can address the increased capital and operational costs, as well as the limited scalability and flexibility of traditional RAN. However, it requires tremendous transport bandwidth and impose strict latency and synchronization constraints [60]-[61]. To address the need for a flexible transport network offering the required capacity levels we have proposed TSON solution [60]. However, the transport capacity problem is further exaggerated under survivable C-RAN deployments (see i.e. [62]-[67]). In many protection schemes, the optical network capacity is duplicated in size [67] to make possible realistic survivable C-RAN deployments.

A typical example of systems offering protection to any kind of failures (either at the optical transport or the compute domain where BBUs are hosted) is shown in Figure 5-58a). Specifically, in case of failure of the main paths interconnecting the RUs with the BBUs (i.e. paths 1-6, 3-5), FH flows are routed to their destination through a set of secondary (protection) paths (1-2-4-5, 3-2-4-6). A similar approach is taken for the C-RAN protection against BBU failures [65]. It is clear that under this scenario, multiple FH flows need to be transferred over a set of links introducing even higher transport bandwidth requirements.

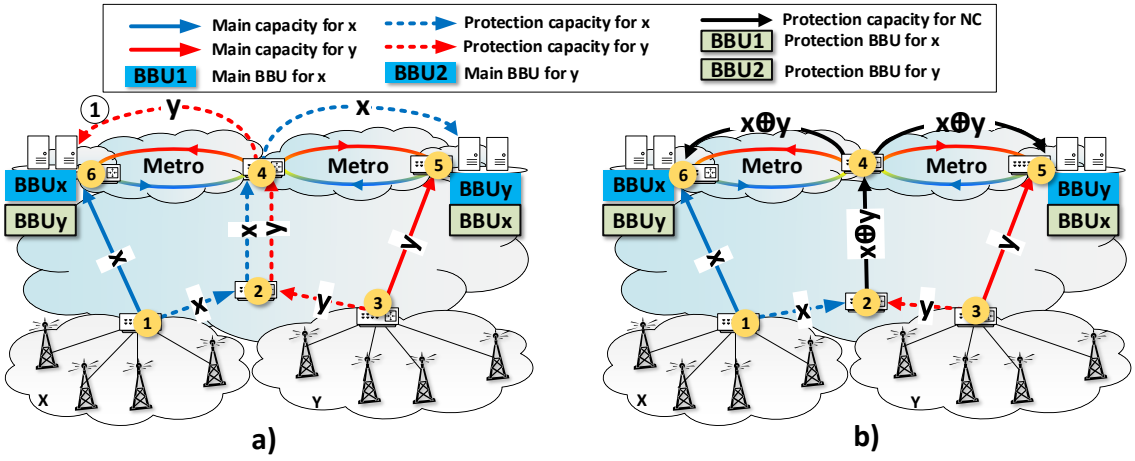

Figure 5-58. Protection of a C-RAN network from failures of compute and/or network elements. a) In the traditional approach, working and protection capacity for regions x, y are establishes over common links causing bottleneck, b) Protection of C-RAN adoting NC. FH flows from regions x, y are multiplexed ($x \oplus y$) at ingress edge node and replicated at the reducing bandwidth requirmens by half.

As mentioned in Section 3.2.1, to address this issue the concept of Network Coding (NC) [69] is proposed with the aim offer resilient FH services by multiplexing FH flows and therefore reducing the volume of the transmitted I/Q streams. Using NC, different FH traffic streams with the same source and destination nodes are routed through the network following diverse paths. These can be protected through their modulo-two sum that is generated at the source node and forwarded to the common destination node. This allows reconstruction of each one of the two initial streams at the destination node, in case of the occurrence of a failure along one of the two paths that the initial two streams are traversing. This approach offers 1+1 protection capabilities without having to transfer separately the working and protection copies of the two FH streams across the optical transport network. This reduces the overall protection bandwidth requirement by half (see link 2-4 in Figure 5-58 b). Through this approach, simultaneous protection against optical network and/or compute elements can be achieved.

Although NC has been extensively used to protect networks against link failures, its application in resilient FH networks has not been proposed before. This can be attributed mainly to the overhead that the application of the modulo-two sum and the replication operations of NC introduce in practical systems that may degrade the performance of C-RANs. At the same time, the operation of the decoding process at the edge imposes significant buffering requirements due to the high data rate of FH streams. To quantify the benefits of the proposed approach at a network level and further improve performance, an optimization framework is proposed. The proposed scheme focuses on optimally placing the NC-enabled edge nodes to minimize the overall deployment cost and protect the system from possible network or compute element failures. The performance of the proposed scheme is experimentally validated over the Bristol city testbed considering the requirements imposed by an operating open source LTE platform.

5.5.1 Implementation Aspects

To apply NC in 5G operational environments, two main practical aspects should be resolved: 1) implementation of the modulo-two sum and the replication operations at the FH line rate and, 2) synchronization between flows reaching decode nodes (flows $x, x \oplus y$ and flows $y, x \oplus y$ of Figure 5-58b). In the following subsections, the implementation details together with experimental demonstration of an NC-enabled optical edge node is presented.

5.5.1.1 NC operations implementation at TSON

TSON [72][73] is a multi-wavelength fully bi-directional synchronous, and flexible active optical transport network technology. Its network implementation consists of Field Programmable Gate Array (FPGA) optoelectronics platforms integrated with advanced optical components to enable high performance processing and transparent switching and transport. TSON provides a multiple protocol programable interface that meets 5G Key Performance Indicators (KPIs) such as high bandwidth and sub-millisecond end-to-end latency [73]. Although natively TSON allows handling Ethernet frames, its configuration can support a broad range of framing structures and communication protocols including CPRI, either natively or through their packetized versions.

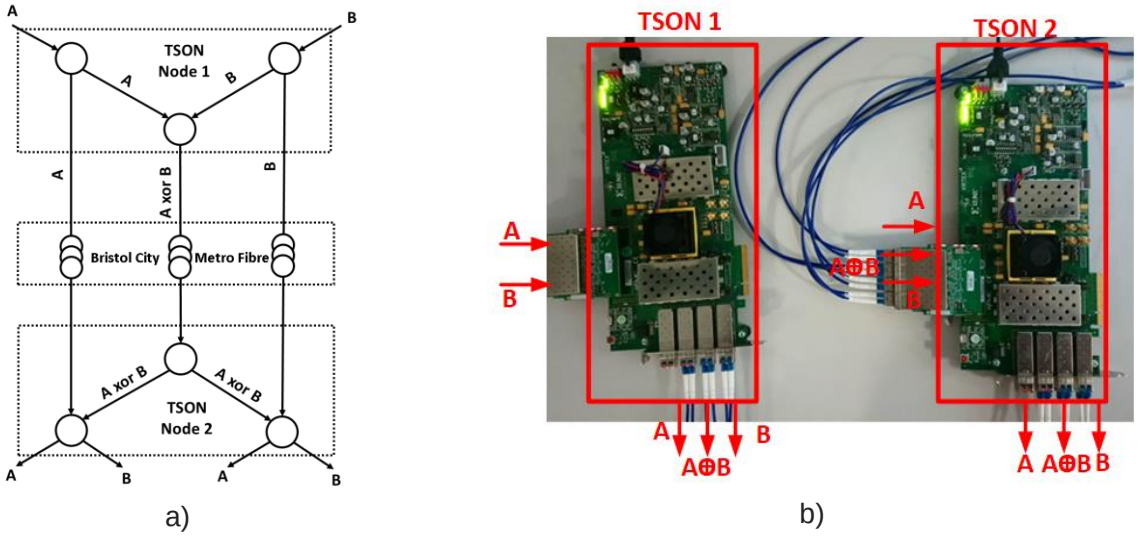

Figure 5-59. TSON Implementation architecture for evaluation concept, b) TSON edge node setup for the experimental implementation.

Figure 5-59 shows the TSON architecture implemented to solve this problem. The ingress TSON node is responsible for traffic coding and mapping. Its ports consist of two clients: X and Y. The output ingress node contains three different wavelengths that can be configured on the fly using Software Defined Networking (SDN) to address different programmable parameters. The egress edge nodes include the reverse functionality and ports. For the implementation of our experimental configuration we have employed two Xilinx VC709 evaluation boards. These contain 4XSFP/SFP+ cages. FM-S18 modules are used to expand the number of SFP+ cages as more than 4X10Gbs ports are required for the experiment. The FM-S18 is an FPGA Mezzanine Card (FMC) module that provides up to eight SFP/SFP+ module interfaces directly into Multi-Gigabit Transceivers of the FPGA. Figure 5-59 shows the implementation architecture for the evaluation of the proposed concept with two TSON nodes. Each TSON node emulates three source nodes of a butterfly network, with the aim to create a proof of concept experiment and showcase the concept of linear network coding. TSON node 1 receives two different traffic streams (A and B) and sends the streams A, B, and their modulo 2 sum (XOR) of both traffic streams to TSON node 2. TSON node 2 receives the three traffic streams and transmits each traffic stream A and B simultaneously to two destinations of TSON node 2.

5.5.1.2 Synchronization of Network Coded flows

To reduce buffering requirements during the coding/decoding phase of the FH flows, high synchronization accuracy across the network is needed. An early TSON prototype with local synchronization capabilities is described in [70]. To address the system wide strict synchronization requirements of the NC implementation, a subsystem relying on separate developed time stamper has been developed. Figure 5-60 shows the Subsystem architecture for the NC-enabled TSON nodes. The time stamper unit is located between the MAC and PCS/PMA IP cores, uses the Timer Syns clock and follows the IEEE 1588 protocol. In addition, the time stamper considers the physical layer delay for stamping.

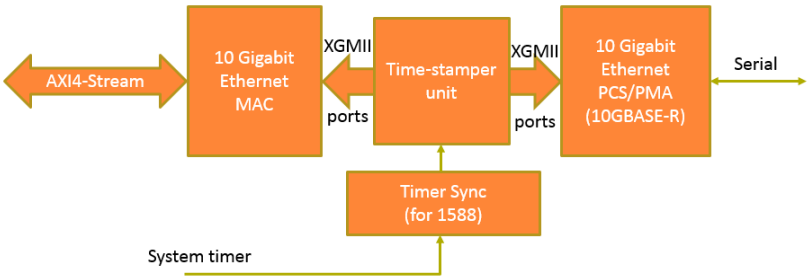

Figure 5-60: Synchronization subsystem for the NC implementation.

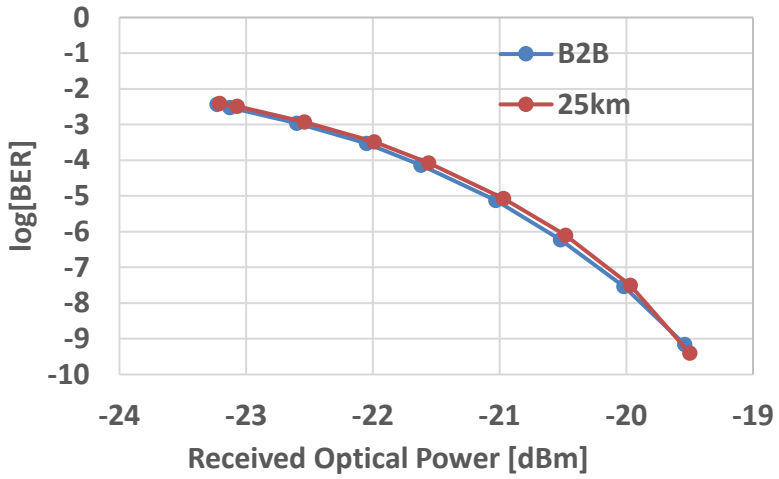

Figure 5-61. BER measurements.

5.5.2 Subsystem experimental validation

Two different scenarios are considered for experimental evaluation of the subsystems responsible for the NC-operations, including the modulo-two sum and synchronization accuracy. The first scenario includes both FPGAs connected back-to-back with short fibre lengths. In the second scenario, the proposed technologies are evaluated over the Bristol City test-bed Fibre with 25 km of standard single-mode fibre (SSMF). An Anritsu traffic analyser generates two Ethernet traffic streams to the TSON edge node 1 at 9 Gbps. The traffic is received from the TSON node 2. The performance parameters under consideration include Bit Error Rate (BER) and latency. Latency is defined as the time difference between the arrival of a frame at the analyser, and its departure from the analyser.

Figure 5-61 shows the BER measurements as a function of received optical power for the different scenarios under consideration. The BER curves show that the penalty observed for the case of 25 km of SSMF transmission over the Bristol City Infrastructure compared to the back-to-back (B2B) performance is less than 1dB. Table 5-3 displays the end-to-end latency for the transmitted flows. The TSON nodes latency for the 25km transmission is less than 2% of total latency.

Table 5-3: End-to-end flow latency.

latency	μs
B2B	1.979
25 km	125.4

5.6 Optimal 5G Network design with resilience considerations

In the previous section, the implementation details of NC-enabled TSON nodes have been described. In this section, the problem of optical placement of these nodes at a metro environment to support resilient operation

of C-RANs is provided.

5.6.1 Traditional Optimization framework

This section provides a description of the modeling framework used to identify the optical network resources for the interconnection of the RUs with the compute resources where the BBU are hosted. This formulation extends the work in [60] to address resilience and protect the 5G network from a possible failure of optical and/or DC network elements. Taking into account both FH network and BBU processing demands, let $\mathcal{P}_r$ be the set of paths interconnecting RU $r \in \mathcal{R}$ with server s where BBUs are hosted with $\in \mathcal{P}_r$. Now let x_{rp} be the rate at which FH demand originating from r flows through path p. The following demand constraints should be satisfied:

$$\sum_{s \in \mathcal{S}} \sum_{p \in P_r} \boldsymbol{\alpha_{rs} x_{rp} = h_r}, \qquad \forall \boldsymbol{r \in \mathcal{R}} \qquad \text{Eq. 5-14}$$

where α_{rs} is a binary coefficient taking values equal to 1 if RU $r \in \mathcal{R}$ is supported by server s.

In order to protect the planned network from a possible server failure hosting the BBU, a backup mechanism is introduced. This mechanism ensures that in case of failure of the primary server s, FH flows are routed to an alternative server s' $(s' \neq s)$ through the candidate path p' $(p' \in \mathcal{P}_r)$ with corresponding flow $x_{rp'}$. To formulate this requirement the binary coefficient $\alpha_{rss'}$ is introduced to indicate whether FH flow originating from RU r is assigned to servers s, s' or not. This coefficient equals to 1, if BBU of RU r is processed at server s or in case of its failure on server s'; 0 otherwise. In order to protect the operation of an RU from a possible server s failure, the following FH flow protection constraints should be satisfied:

$$\sum_{\substack{s', s' \neq s \\ s, s' \in \mathcal{S}}} \sum_{p' \in P_r} \alpha_{rss'} x_{rp'} = h_r, \forall\, r \in \mathcal{R}, s \in \mathcal{S} \qquad \text{Eq. 5-15}$$

Summing all FH flows over the optical network link e $(e \in \mathcal{E})$, the necessary link e capacity, denoted as u_e, is determined. Apart from server failures, optical network link failures are also addressed by forwarding FH flows to their destination via alternative paths. In order to protect the network from a possible link failure, a mechanism routing flows through alternative paths is introduced. Now, let $\mathcal{Q}_{rp}$ be the set of paths that can be used to protect a path $p \in \mathcal{P}_r$ from a possible failure, y_{rq} the rate at which FH demand originating from r flows through path $q_p \in \mathcal{Q}_{rp}$ protecting main path $p \in \mathcal{P}_r$ (with p, q being disjoint) and $u'_e = \mathcal{C}_e - u_e$ the remaining link e capacity. Adopting the same rationale as in the previous equations, path-protection constraints are introduced.

So far, the proposed model ensures that the network capacity is adequate to support the transmission of the FH flows to the servers where BBUs are hosted. However, once the information arrives at its destination, server s should have adequate capacity to support of BBU processing. To evaluate this capacity, h_r is mapped from a network type of requirement to a computing resource through the introduction of parameter $\mathcal{M}_{rs}$. This parameter specifies the computational requirements (usually in Instructions Per Second - IPS) to support FH flow r on server s.

To evaluate this parameter, an extensive benchmarking campaign utilizing OpenAirInterface (OAI) has been carried out. OAI is an open source software-based implementation of the LTE architecture for 5G experimentation and prototyping that encompasses the full protocol stack both in the E-UTRAN and the Evolved Packet Core (EPC) that runs in a commodity x86-based Linux Personal Computer or data center. In this system, the transceiver functionality is realized via a software radio frontend (such as the Ettus USRP B210). The combination of the open-source software and the inexpensive hardware involved, makes OAI a very attractive platform for experimentation and research towards the forthcoming 5th Generation. The platform comprises two components: i) openairinterface5g which implements the E-UTRAN, that is, eNodeB and UE and, ii) openair-cn which implements the Core Network, that is, the MME HSS, S-GW and P-GW. Based on OAI, the parameters $\mathcal{M}_{rs}$ for various wireless access network configurations has been evaluated.

Besides the working capacity, a spare set of resources should be reserved at each server s for protection purposes. As already mentioned, the primary objective of the proposed scheme is to minimize the total power consumption of the resulting network configuration. Let k_e being the cost of the capacity of link e of the optical network and PC_s the power consumed at server s. The following cost function should be minimized:

$$\boldsymbol{min\ \mathcal{O}(p,x) = \sum_{e\in\mathcal{E}_o} k_e(u_e(x) + u'_e(x)) + \sum_{s\in\mathcal{S}} PC_s(v_s(x) + v'_s(x))} \quad \text{Eq. 5-16}$$

subject to the constraints mentioned above

5.6.2 Extension: Integration of NC

In the previous section, a modeling framework enabling resilient operation of the C-RAN system by protecting it from possible optical network and/or compute failure has been proposed. To address the very high bandwidth requirements that are imposed by this approach, an alternative formulation employing NC is proposed. To demonstrate the potential of NC in resilient C-RAN networks let us consider the simple 5G topology of Figure 5-58. Adopting the traditional approach, multiple source-destination paths must be established double-sizing the necessary network bandwidth is some parts of the optical network. This may act as bottleneck considering that in FH networks this capacity may be extremely high. The adoption of NC, however, resolves this issue as it multiplexes FH streams originating from the two RUs. At the edge, FH streams are replicated (nodes 1, 3) and transmitted through disjoint paths 1-2, 1-3. Then, at node 2 instead of forwarding protection FH flows from regions x and y, the modulo-two sum $x \oplus y$ is transmitted over links 2-4, 4-6 and 4-5. At the egress nodes where BBUs are connected, the operations $x \oplus (x \oplus y)$ and $y \oplus (x \oplus y)$, are performed for BBU1 and BBU2, respectively, recovering FH flows y and x, respectively. Thus, by enabling encoding and decoding processes at the edge, throughput in survivable C-RAN architectures can be increased by a factor of 2.

An architectural decision in NC-enabled C-RANs is associated with the placement of the modulo-two sum and replication operations at the edge nodes. To optimize the operation of resilient NC-enabled C-RANs, a suitable set of constraints enabling NC is introduced. Let $\mathcal{N}_1$, $\mathcal{N}_2$, be the set of nodes where the modulo sum and replication operations are performed. To keep the analysis tractable, we assume that RUs are located in regions, x, y, as shown in Figure 5-58b), however, it can be easily extended to multiple nodes. Now, let $\mathcal{R}_x$, $\mathcal{R}_y$ be the set of RUs belonging to regions x, y, respectively with $\mathcal{R} = \mathcal{R}_x \cup \mathcal{R}_y$ and δ_{n1} a binary variable taking value equal to 1 if the protection flows of RUs originating from regions x, y are multiplexed at node $n_1 \in \mathcal{N}_1$. The following flow constraints should be satisfied:

$$\sum_{n_1\in\mathcal{N}_1} \sum_{q\in\mathcal{Q}_{rn_1}} \boldsymbol{\delta_{n1} y_{rq} = h_z}, \qquad \forall\, \boldsymbol{r \in \mathcal{R}_z, z = x, y} \quad \text{Eq. 5-17}$$

$$\sum\nolimits_{r\in\mathcal{R}_x} \sum\nolimits_{\substack{k\in\mathcal{R}_y, \\ k\neq r}} \sum_{n_1\in\mathcal{N}_1} \boldsymbol{\delta_{n1} = 1} \quad \text{Eq. 5-18}$$

where $\mathcal{Q}_{rn_1}$ denotes the set of paths interconnecting an RU r with node n_1. Eq. **5-18** indicates that the encoding process of all RUs will be performed at a single node. The encoded multiplexed stream $y_{n1} = y_{rq} \oplus y_{kq}$ is then forwarded to node $n_2 \in \mathcal{N}_2$ where the replication operation is performed. Flows are transmitted over candidate paths $q \in \mathcal{Q}_{n1n2}$ interconnecting nodes n_1 and n_2 with capacity z_q, $q \in \mathcal{Q}_{n1n2}$. The replicated flows are then routed to the locations where BBU are hosted over the shorted available paths. Finally, taking the summation of all FH flows over the optical network link e, the necessary protection capacity at e, u'_e, is determined. Finally, the NC-enabled C-RAN network is optimized by minimizing the cost function Eq. 5-16 subject to the constraints mentioned above.

5.6.3 Network level evaluation

To evaluate the performance of the overall system, the processing requirements of the virtualized BBUs, and, consequently parameter $\mathcal{M}_{rs}$, are determined. To achieve this, an extensive set of experiments has been carried out using OAI. Performance analysis includes CPU Utilization and instructions' measurement for different data rates as well as the application profiling. The measurements where performed with the use of the top command, which monitors the running processes in Linux systems and perf which is a collection of tools for system profiling. More specifically, the OAI profiling was done with the record command, which summarizes where CPU time is spent. Measurements were performed in the idle mode (LTE device phone not connected) and while downloading with different data rates (100 Kbps, 200 Kbps, 500 Kbps, 1 Mbps and 2 Mbps). The results are given in Figure 5-62. The measurement was performed with the perf stat command. As we can see, the instructions are clearly increasing in proportion to the data rate.

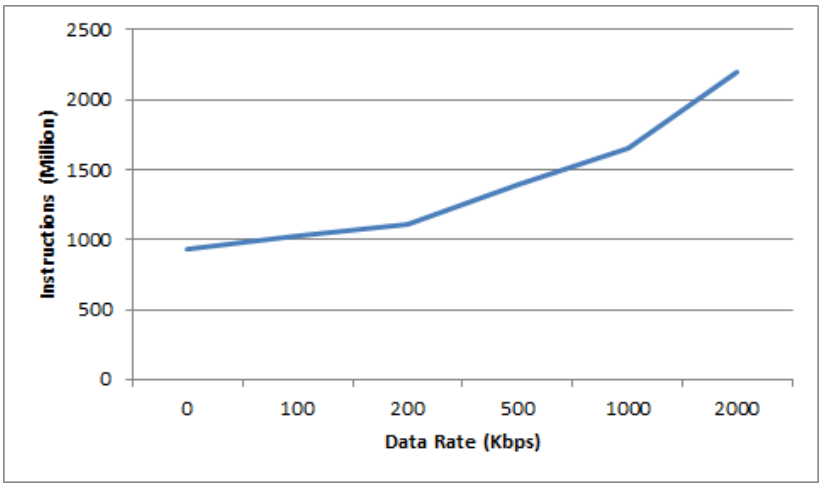

Figure 5-62: Total instructions per second for OAI as a function of access data rate.

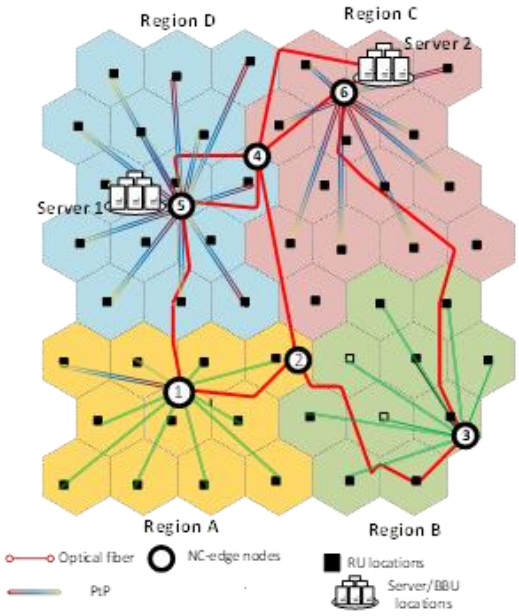

Figure 5-63: Modified Bristol city topology with NC enabled nodes.

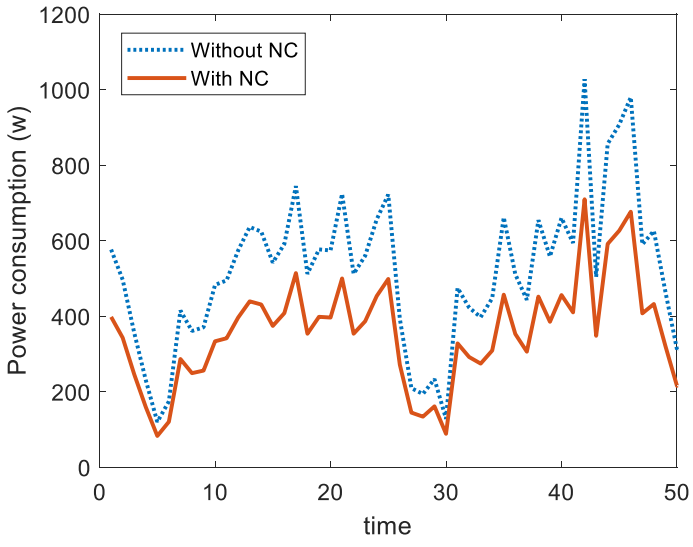

Figure 5-64. Bristol City Optical Network Power Consumption for the proviosning Resillient C-RAN services.

Once BBU requirements have been determined, the performance of the overall system with and without NC considerations is examined for the Bristol City topology shown in Figure 5-63. In this topology, RUs are attached to the edge node through point to point links. For this topology, BBU processing for Regions A and D will be provided by Server 1 whereas BBU processing for Regions B and C by Server 2. At the same time, the main FH connectivity will be provided through links 1-5 and 3-6 for regions A, B, respectively. Protection of FH flows will be provided through paths 1-2-4-6 for Region A, 3-2-4-5 for region B, 5-4-6 for region D and 6-4-5 for region C. The encoding (replication) processes for regions A, B will be performed at node 2 (4), while for Regions C and D decoding and replication operations will be both formed at node 4.

A comparison of the optical network power consumption for the Bristol City network for the provisioning of resilient C-RAN services is shown in Figure 5-64, with and without the adoption of NC. It is observed that when NC is adopted, the protection capacity of the optical network is reduced by approximately 33% leading to an overall reduction of the power consumption.

5.7 Control plane scalability/stability analysis

5G aims at incorporating many technologies, under the same infrastructure (FH/BH network). Efficient management and operation of such a heterogeneous infrastructure can be achieved applying novel network designs that are aligned with the Software Defined Networking (SDN) open reference architecture [4]. The controller is in charge of populating the forwarding table of the switch. The communication between the two entities is carried out through a secure channel. This centralized structure makes the controller able to perform network management functions, while allowing easy modification of the network behavior through the centralized control layer. However, in such infrastructures the end to end latency is augmented. Considering that latency is critical to many network applications, a subject of current research is the size of the SDN network (controller placement problem) in order to be able to cope with the timing requirements of network services and applications.

In 5G-PICTURE, we propose a next generation network solution that includes: a) the concept of FFS between a set of servers that can offer a range of processing capabilities and can be geographically distributed across the network infrastructure, b) the employment of the MEC architecture in the form of specific purpose low processing power servers embedded in the wireless access network (also known as cloudlets) and c) a FH/BH transport network with SDN control, connecting the MEC domains with medium to large-scale DCs hosting general purpose servers placed at the optical access and metro domains. In this environment, the controller placement problem is investigated, under the scope of the stability of the whole system. To address this issue, we propose a novel mathematical model based on Evolutionary Game Theory (EGT) that allows network operators to dynamically adjust their FH split options with the objective to minimize their total operational expenditures. The stability of the proposed scheme depends on network latency, thus a metric for sizing the SDN FH/BH network is proposed.

5.7.1 Evolutionary Game Theory: Basic Concepts

Evolutionary Game Theory (EGT) studies the interactions of non-cooperative players that play repeatedly strategic games [86]. Contrary to classic Game Theory that examines the behavior of rational players, EGT focuses on how the strategies can "survive" through evolution and how they help the players who choose them to "strengthen" and better meet their needs.

Evolutionary processes are described by three main components: the population, the game and the dynamical model that describe the processes. The most common dynamics is called the Replicator Equation (RE) and can be expressed as:

$$\dot{x}_i(t) = x_i(t)\left(F_i(\boldsymbol{x}(t)) - \bar{F}(\boldsymbol{x}(t))\right), \qquad i \in S \qquad \text{Eq. 5-19}$$

where S is the set of strategies that are available to the population, $\boldsymbol{x}(t) = [\, x_1(t)\ x_2(t) \ldots\ x_i(t) \ldots\,]^{T}$ is the population state at time t with $x_i(t)$ symbolizing the proportion of the population that uses strategy i at time t, and $F_i(\boldsymbol{x}(t))$, $\bar{F}(\boldsymbol{x}(t))$ are the expected payoff of strategy i and the mean payoff respectively [86]. According to this equation the percentage growth rate $\dot{x}_i/x_i$ of the strategies that are currently used is equal to the excess of the current payoff versus the average population's payoff. This means that strategies employed at present will be spread or eliminated depending on whether their payoff is better or worse than the average.

In the above, the interaction between individuals is assumed to be instant and their results immediate. However, this is not the case in most realistic scenarios. In communication networks especially, the impact of an action may be belated, due to network latency. Thus, it is more realistic to consider a system where the strategies evolve considering the payoff values perceived in a past moment. The adjusted RE is given below [87] [88]:

$$\dot{x}(t) = x_i(t) \cdot \left(f_i\big(\boldsymbol{x}(t-\tau)\big) - \sum_{i \in S} x_j(t) \cdot f_j\big(\boldsymbol{x}(t-\tau)\big) \right) \qquad \text{Eq. 5-20}$$

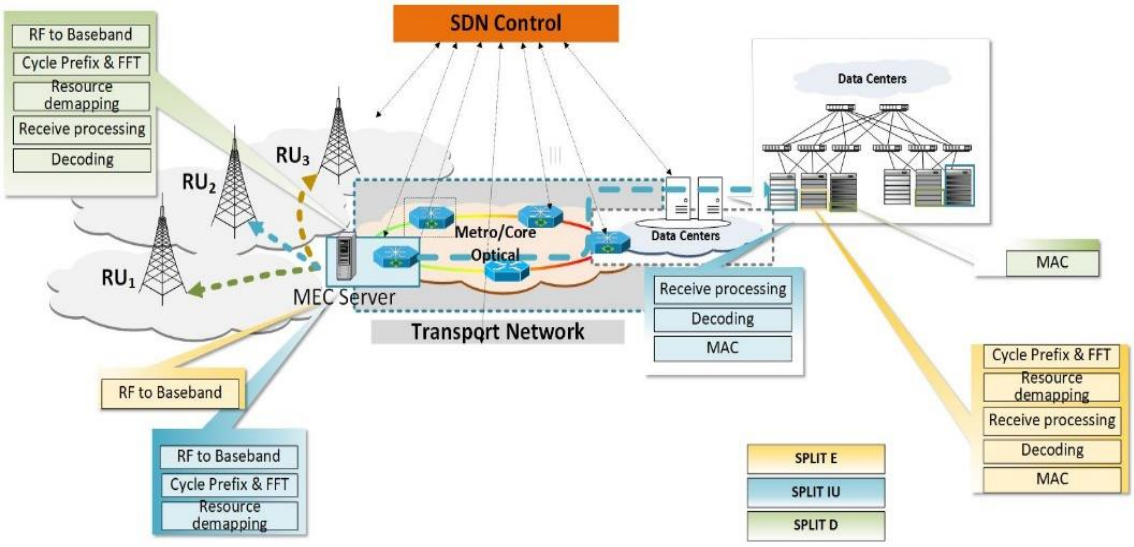

Figure 5-65: Network architecture. In the MEC, a decision about which functions should be processed locally is made for each RU. The remaining set of functions for each RU are transferred through a common network infrastructure with centralized control to a DC for further processing.

We consider the 5G network topology shown in Figure 5-65. In this scenario, the RUs are installed, managed and operated by coexisting Mobile Network Operators (MNOs). The RUs share a set of computational resources that are located both at the edge of the access network (in a MEC server) and at the metro/core network (in the Cloud). The interconnection between the MEC server and the central cloud servers is carried out by an SDN- controlled optical FH/BH transport network.

The MNOs can decide where to perform the processing of the low layer functions of the LTE protocol stack. According to the eCPRI specification, three possible functional splits can be identified [89]. In split E (split 1 for simplicity) MEC is responsible for the RF processing of the received signals and the Cloud performs the entire baseband processing. In split IU (split 2), MEC handles the per cell processing (RF processing, cyclic prefix (CP) elimination, frequency domain transformation (FFT) and resource demapping), while the remaining functions are performed at the Cloud (Equalization, IDFT, QAM, multi-antenna processing, Forward Error Correction (FEC), higher level operations (MAC, RLC, PDCP). Finally, in split D (split 3) the entire lower layer function chain is performed at the MEC server, and the higher lever functions in the Cloud. One can conclude that as the split is placed lower in the 5G protocol stack, the required transport capacity increases [90].

Each RU periodically selects one of the three possible functional splits with probability x_i, $i = 1,..,3$. The decisions are sent to the SDN controller, who is responsible for the application of the policies. We consider the scenario in which all the necessary resources are available. When the policies have been applied, the payoffs are calculated and the RUs are reviewing their split option strategy. Specifically, if a better (lower) payoff is observed, then the probability of an RU to select the specific split option increases (decreases). The new policies are sent to the controller and the same procedure is repeated. The time between each repetition is referred to as revision time. To address this scenario, EGT can provide a suitable optimization framework that can be used to support energy-aware FH service provisioning over a common infrastructure.

Denote as $\boldsymbol{x}(t) = [\, x_1(t)\ x_2(t)\ x_3(t)]^{\,T}$ the state vector of the RU, where $x_i(t)$ refers to the RU's probability of choosing split i. If the RU revises its strategy with a time rate $r_i(\boldsymbol{x})$, the change of the proportion of the probabilities is described by the following dynamical equation:

$$\dot{x}_i(t) = \sum_{j \in S} x_j(t) r_j(\boldsymbol{x}(t)) p_j^i(\boldsymbol{x}(t)) - \sum_{j \in S} x_i(t) r_i(\boldsymbol{x}(t)) p_i^j(\boldsymbol{x}(t)) \quad \text{Eq. 5-21}$$

where S is the set of strategies that consists of the three possible splits and $p_i^j(\boldsymbol{x})$ is the rule of change in the probability of choosing split i when the RU changes from split i to split j and can be expressed as:

$$p_i^j(\boldsymbol{x}(t)) = \begin{cases} x_j(t)(u(j,t) - u(i,t)) & j \neq i \\ 1 - \sum_{j \neq i} x_j(t)\big(u(j,t) - u(i,t)\big) & otherwise \end{cases} \quad \text{Eq. 5-22}$$

with $u(i,t)$ symbolizing the payoff of split i at time t. Making the assumption that all time rates are constantly equal to one $(r_i(\boldsymbol{x}) \equiv 1 \frac{revion}{time\ unit})$, the following differential equation yields:

$$\dot{x}_i(t) = x_i(t) \left[u(i,t) - \sum_{j \in S} x_j(t) u(j,t) \right] \quad \text{Eq. 5-23}$$

which satisfies the replicator dynamics model.

5.7.2 Payoff Function

The objective of the MNOs is to minimize their own service power consumption requirements and, hence, the service operational costs. Thus, the payoff function per operator is formed by summing up the power consumption of the network and compute elements required to support FH services. Table 5-4 summarizes the network and processing demands of each functional split.

Table 5-4. Network and Processing Demands of Each Functional Split

Split	*Network Rate*	*Processing Functions*	
		Local	*Remote*
1 (E)	$R_1 = N_o \cdot f_s \cdot N_Q \cdot N_R$	RF	FFT, RE Demapping, Rx Processing, DEC, MAC
2 (Iu)	$R_2 = N_{sc} \cdot {T_s}^{-1} \cdot 2 \cdot N_Q \cdot N_R \cdot \eta$	RF, FFT, RE Demapping	Rx Processing, DEC, MAC
3 (D)	$R_3 = N_{sc} \cdot {T_s}^{-1} \cdot \eta \cdot S$	RF, FFT, RE Demapping, Rx Processing, DEC	MAC

For this problem setting, the payoff of an RU operated by an MNO that chooses split i against another RU operated by a different MNO who chooses split j is described by the payoff matrix $\boldsymbol{A}$, with elements $a_{ij} = -\left(P_{PROCESSING\,ij} + P_{NET\,ij}\right) + b, \quad i,j \in S$ where $P_{PROCESSING}$ and $P_{NET_{ij}}$ refer to the total compute and network energy consumption respectively, when split i competes with split j and b is a positive constant that guarantees the robustness of the system. Technical parameters like the oversampling factor (N_o), the sampling frequency (f_s), the quantization bits per I/Q (N_Q), the number of receiving antennas (N_R), the number of subcarriers used (N_{sc}), the percentage of used resource elements (η), and the spectral efficiency (S) affect the required capacity and the power consumption of each processing function [90], [91].

Due to the nature of the SDN transport network, the payoff values are provided to the MNOs through the SDN controller. It is evident, that this kind of procedure indicates that the strategies will evolve based on information related to a past moment. This will be reflected to the expected payoff of the strategies. Network delay is mainly composed of propagation, serialization, switching/routing and queuing delay. Although propagation and switching/routing delays are constant, the rest are highly affected by the network traffic. Due to this, we expect that network delay is a random variable that is characterized by a probability density function. Specifically, if the payoff is received not instantly, but after a random delay τ, with probability distribution $P(t)$ the expected payoff of an RU using strategy i as well as the average payoff are determined by [92]:

$$u(i,t) = \int_0^{\infty} P(\tau)(\boldsymbol{A}\boldsymbol{x}(t-\tau))_i \, \bar{u} = \sum_{j \in S} x_j(t) u(j,t)$$

5.7.3 Stability Analysis

Since the above system of equations cannot be easily solved by analytical methods it is important to examine its qualitive behavior without actually solving it. We concentrate on finding the stability of a solution exploiting the Lyapunov stability theorem. This method is based on the expansion of the right part of the dynamical system as a Taylor series about an equilibrium point $\boldsymbol{x}^0$. If the initial condition $\boldsymbol{x}(0) = \boldsymbol{x}_0$ is close enough to $\boldsymbol{x}^0$, then $\boldsymbol{x}$ will be a small perturbation for some time interval extending from zero. Thus, it is acceptable to neglect the higher-order terms, and approximate the nonlinear system by the linear system:

$$\dot{\boldsymbol{x}}(t) = \boldsymbol{J_o}\boldsymbol{x}(t) + \boldsymbol{J_1}\boldsymbol{x}(t-\tau) \qquad \text{Eq. 5-24}$$

where $\boldsymbol{J}_o \in \mathbb{R}^{2x2}$ and $\boldsymbol{J}_1 \in \mathbb{R}^{2x2}$ are respectively, the Jacobian matrix, and the delayed Jacobian matrix evaluated at equilibrium at $\boldsymbol{x^0}$.

The stability of the system requires that all roots of its characteristic equation have a negative real part. The system admits to seven equilibrium points: three corner points, one interior and three corner side points. The linearization about each of the three corner critical points produces an ordinary differential equation that is independent of the delayed variables as in the non-delayed three strategies game.

At the interior critical point all the payoffs are equal. The differential system that emerges depends only on the delayed variables, thus one should anticipate that the distributed delay will affect its stability. The characteristic equation is formed as:

$$u^2 + E \cdot u + F = 0, \qquad u = \frac{\lambda}{Q} \qquad \text{Eq. 5-25}$$

The last three critical points are equilibriums where only two of the three strategies survive (corner side points). Their characteristic equation can be written as $(\lambda - l_1) \cdot (\lambda - l_2 Q) = 0$ where the parameters λ_1 and λ_2 depend on the corner side equilibrium point. As we can conclude from the above, our analysis can be restricted for finding the solution of the equation $\lambda - C\int_0^{\infty} P(\tau)e^{-\lambda\tau} = 0$. This equation is the characteristic equation of the linear differential equation $\dot{x}(t) = C\int_0^{\infty} x(t-\tau)f(t)d\tau$.
From [93] we derive the following necessary and sufficient condition for the asymptotic stability of the equilibriums:

Proposition: If $C < 0$ and the expected value (E) of the delay's probability density satisfies the condition $E(\tau) < \frac{\pi}{\gamma \cdot |C|}$, where $\gamma = 2$ when the pdf is symmetrical, or else $\gamma = \sup\{\gamma | \cos w = 1 - \frac{\gamma w}{\pi}, w > 0\}$, then the equilibrium point is stable (the proof can be found in [93]). Last but not least, as far as the variance of the distribution is concerned, the stability of the system increases as the variance grows [93].

5.7.4 SDN Controller Placement

It is well known that the SDN controller is responsible for collecting and providing to the MNOs of the RUs the required information from all controlled devices. The maximum delay corresponds to the delay of the most distant node to the controller path plus the delay of the controller-MEC path. Thus, assuming that each controlled device may host a MEC, the stability of the system is achieved only when the round-trip time (RRT) of the controller's path to the most remote device is less than $\frac{\pi}{\gamma \cdot |C|}$. Based on this limit, we propose a heuristic algorithm that tries to identify the minimum number and associated position of SDN controllers with the aim to guarantee the stability of the 5G infrastructure. This is performed with low computational complexity.

At first, the heuristic algorithm finds the maximum network radius, which is the number of hops of the longest end-to-end path. Then, for each node it calculates the maximum RRT to all the other nodes inside the network radius. If the result of all nodes is a number higher than $\frac{\pi}{\gamma \cdot |C|}$, the network radius is reduced by one, and the same procedure is repeated, until a case is found where the RRT from a node to all other nodes within the network radius. The nodes that meet this requirement, are marked as possible controller candidates. From this set, the algorithm chooses as the first controller the one that is connected to the largest number of devices within the network radius. These devices and the first controller are removed from the network, and the whole

procedure is repeated for the downscaled network. The algorithm ends when the downscaled network has no network nodes.

5.7.5 Results and Discussion

In order to see the effectiveness of our model we considered the network of Figure 5-65 with the system parameters shown in Table 5-5. The cost ratio (remote/central processing) was assumed to be equal to two. Furthermore, the relationship of the transport network's energy consumption with the required capacity for the support of the FH services was assumed to be nonlinear, since the non-linear model is best to describe the technology advancements in terms of energy efficiency of network devices

Table 5-5. Parameters of the system configuration

Symbol	Quantity	Value
B	bandwidth	20 MHz
Ant	number of the rx antennas	2
M	modulation	6 bits/symbol
R	coding rate	1/2
dt	time-domain duty-cycling	100%
f_s	sampling frequency	30.72 MHz
N_o	oversampling factor	2
N_{sc}	number of used subcarriers	1200
T_s	symbol duration	66.6 μs
N_Q	quantization bits per I/Q	10
S	spectral efficiency	3 bit/cu
η	assumed RB utilization	70%

The stability analysis indicates that the equilibrium point in such a scenario is $x_1^* = 0.2957,\ x_2^* = 0.7043, x_3^* = 0$. This means that in the non-delayed system the optimal split choice is split 2. However, as it was stated previously the SDN transport network introduces additional delay to the system. This delay can be divided to two main components, namely the processing delay of the SDN controller and the transport delay.

The SDN controller chosen for the implementation is the ODL controller, which is a scalable controller infrastructure that supports SDN implementations in modern heterogeneous networks of different vendors [96]. For measuring the processing delay of the ODL controller, we developed an application that communicates externally with the controller. For evaluations, a linear network topology with Out of Band control plane was emulated in Mininet, a tool that can emulate and perform the functions of network devices in a single physical host or virtual machine (VM) [97]. Both Mininet and ODL controller were implemented on the same machine (Intel® Core™ i5-7400U CPU @ 3.00 GHz (4 cores)) to overcome the Ethernet interface speed limitations. 7.7 GB of memory was available. The system was running Ubuntu 16.04 LTS-64 bit. The application implements at first step a mechanism for collecting data on the network topology and at second step a mechanism for sending echo messages to all switches simultaneously, and measuring the maximum time elapsed for receiving a reply. The time response of ODL is measured by averaging the results of a hundred number of tests, in order to achieve higher accuracy. The results showed an exponential relation between the controller's processing delay and the network devices.

As far as the transport delay is concerned, we used monthly delay measurements extracted from GRNET [19], in order to find the dependence of the end to end transport delay on the end to end hops. Our analysis concluded that this relationship can be well approximated with a linear function. Furthermore, the best pdf that fitted the end to end delay was the generalized t-student distribution [99].

Taking these into consideration, we expect that the total induced SDN network's delay will be a random variable that is characterized by the generalized t-student distri bution, with expected value that depends on the size of the transport network and the hops between two network nodes. Thus, the upper delay limit for our example is given by $E_{max} = 1.6449$ time units.

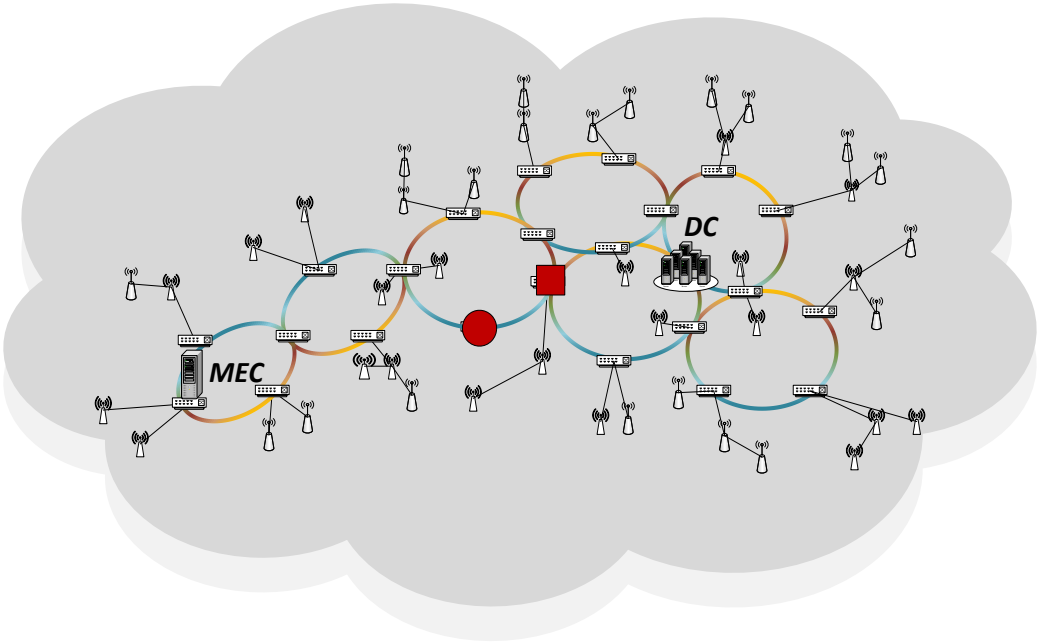

Figure 5-66. Assumed FH/BH transport network for the system described in Figure 1. The red circle represents the position of the SDN controller, after the implementation of the heuristic algorithm described in section 3.3. The red square represents the optimal position estimated according to the average propagation latency-case described in [5].

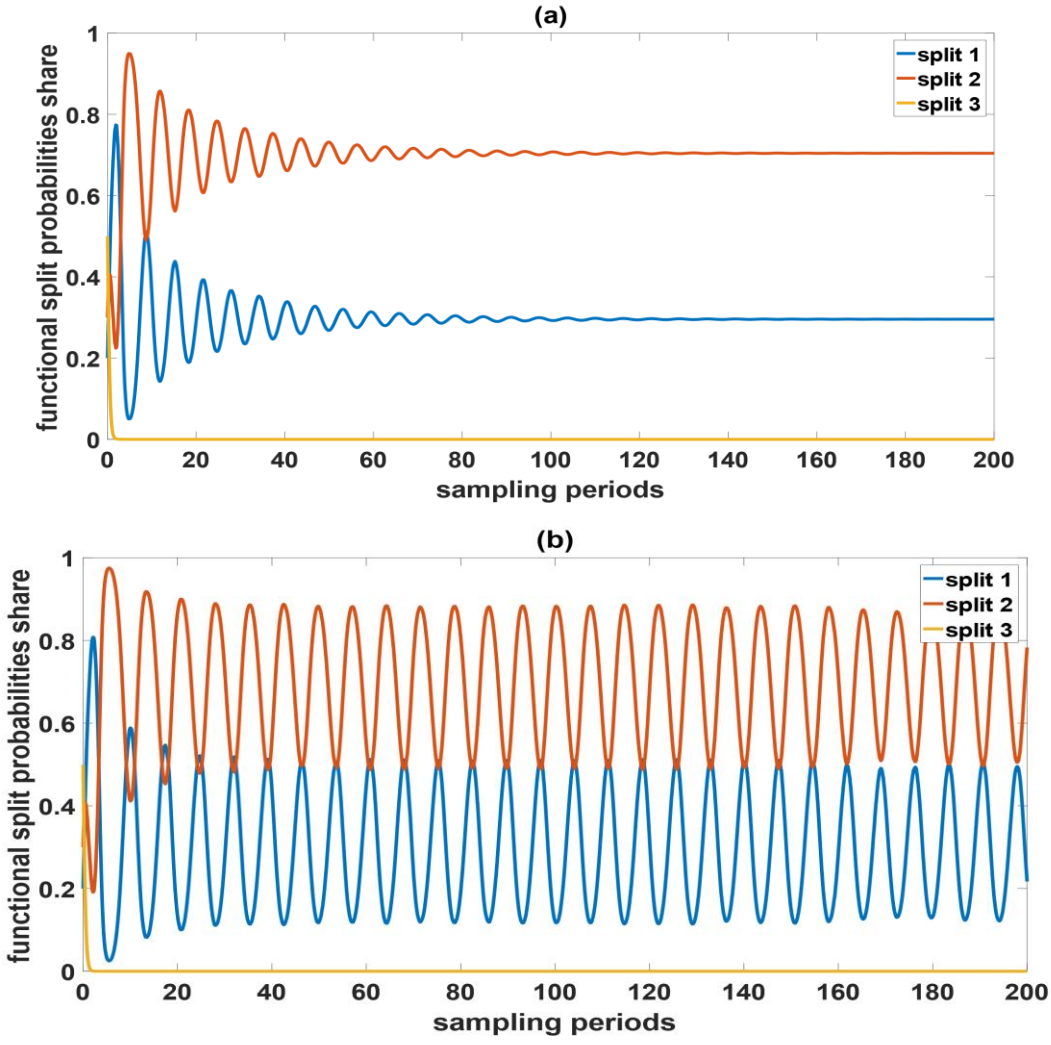

Figure 5-67.. Evolution of the probabilities of the three split options, with the parameters described in Table II, when: (a) the controller is placed in the proposed location (red circle in Figure 2) by the heuristic, b) the controller is placed in the proposed location (red square in Figure 2) of the average propagation latency-case described in [[84]].

The assumed FH/BH transport network's topology for our example is depicted in Figure 5-66. The figure also shows the possible controller placements after implementing the heuristic algorithm described in the previous section. In order to test the validity of the heuristic, we investigate the evolution of strategies in two cases: 1) when the controller is placed in one of the proposed locations by the heuristic, 2) when the controller is placed in the location identified by the average propagation latency optimization technique described in [84]. Figure 5-67 illustrates the evolution of split option selection probability under the proposed EGT based approach and the average latency minimization scheme described above. As can be seen in the former case (Figure 5-67 a) after few sampling periods the scheme converges to a mixed solution where all antennas operate under a single split option mode that will be either split 1 or split 2. However, in the second case, the placement of the SDN controller at a node that does not satisfy the stability threshold leading to an unstable operational mode for the 5G network. The reason behind this is that the increased control plane delay in this case introduces inaccurate information of the network status at the controller. Therefore, decision making is performed with outdated information that leads to an oscillation around the optimal operating point preventing it from converging to a stable solution.

5.8 5G Network Design with Reduced Computational Complexity Using AI Techniques

The concept of Mobile Edge Cloud (MEC) has been proposed as a key enabling technology that can be used to address the strict latency and processing requirements of 5G services [127]. Through the placement of servers with moderate storage and processing power at the edge of the Radio Access Network (RAN) and in close proximity to the mobile subscribers [128], the need for longer transport distances can be reduced leading to lower end-to-end latencies. This can improve end-users experience and enable the provisioning of a wide set of delay sensitive services including, positioning, connected and automated driving, augmented reality, video analytics, etc.

MEC can also assist RANs to extend their network coverage and enhance connectivity in areas where macro cell coverage is limited or not available. This concept, for example, can be realized through in-cabin/in-vehicle or even backpack installation of low-cost Remote Units (RUs) which can be coupled with softwarised implementations of the LTE protocol stack running on local MEC servers. C-RAN can address effectively the limitations of traditional RAN, reducing the cost and offering increased the scalability and flexibility. However, C-RAN requires very large transmission bandwidth and imposes strict latency and synchronization constraints. The functional split concept allows separating the signal processing functions into individual functional blocks that can be dealt with in the form of a function chain where each function can be processed independently as long as the chain order is maintained. This approach allows to handle lower layer functions locally and offload higher layer functions remotely to the RU at a Central Unit (CU). In case that this allocation of local and remote functions is performed dynamically in a flexible fashion the approach is referred to as flexible functional split.

In 5G infrastructures transport networks can be supported through integrated optical and wireless network domains offering converged backhauling and fronthauling functionalities [140]. This approach can offer high capacity transport networks interconnecting RUs with compute resources where softwarised versions of the RAN protocol stack are executed. This is enabled by a control plane that manages and optimizes the operation of a large number of highly heterogeneous network and compute elements, taking decisions related to: i) optimal embedding of service requests and creation of service chains over the converged network resources [131], [132], ii) optimal infrastructure slicing across heterogeneous network domains [133], iii) optimal sharing of common resources in support of both telecommunication and vertical industry services [134], iv) optimal fronthaul deployment strategies including optimal placing of central units with respect to remote units, functional split selection etc.[135], [136]. These problems are traditionally addressed by centralised control and orchestration platforms using a large variety of mathematical modeling frameworks, based on integer linear [137] and non-linear [127] programming, stochastic linear and non-linear formulations [138], etc.

Although these approaches can be effectively used to optimize the operational points of the whole infrastructure, they are unsuitable for real time network deployments due to their increased computational complexity and slow convergence time. The problem is further exaggerated under scenarios considering highly varying 5G topologies. A typical example is shown in Figure 5-68 where the introduction of short lived mobile base

stations (such as LTE gNBs used for emergency or transportation services) may negatively affect the performance of the whole system.

A suitable approach to enable optimal real time decision making in 5G environments is envisioned to take advantage of low computational complexity online tools based on Neural Networks (NNs) [139] exploiting optimal solutions available through offline tools based on Integer Linear Programming (ILP). The offline ILP planning models can be used to create a set containing the optimal design policies for converged 5G network environments. NNs can then use the output of these models for design and training purposes. Once the optimal NN structures have been identified, they can be used by the centralized controller or the MEC server to forecast in real time the optimal operational parameters of the 5G network.

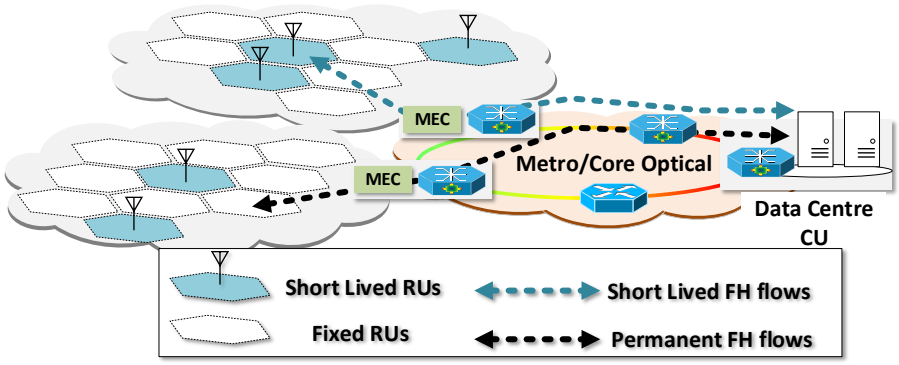

Figure 5-68: Varying 5G network topology with short lived/permanently operating RUs.

Preliminary results in this direction indicate that NNs can be effectively used to predict the optimal operational conditions of the 5G network that match the solutions obtained through the ILP models. However, this approach suffers from the increased computational complexity required to identify the optical NN architecture for every 5G network component (i.e. optical fiber, RUs, etc). This problem, also known as NN hyperparameter optimization, is hard since the number of parameters that can be selected when building a NN-based mode is extremely high. Acceleration of the NN hyper-parameter tuning process has been extensively studied in the literature and several solutions have been proposed [139], [144]. These include, exhaustive search for NN structure combinations (number of neuros, hidden layers, epochs etc) with the objective to minimize the root-mean-squared-error (RMSE) [139].

In 5G-PICTURE, we propose an alternative approach to the optimal NN hyperparameter selection problem adopting clustering techniques. Taking advantage of the correlation that exists between input traffic statistics, network topologies and routing decisions in optical clouds, a hierarchical clustering model is proposed that groups devices with similar hyperparameters. This enables the on the fly identification of the optimal NN structure for the devices compsising the 5G network taking into account actual input traffic statistics. This approach is crucial for real time optimization solutions and enables the NN model selection to become more flexible and re-constructible.

5.8.1 Problem Description

We consider the generic case of a converged 5G infrastructure interconnecting a set $\mathcal{R}$ of remote units (RUs) with a set $\mathcal{S}$ of S Central Units (CUs). $\mathcal{R}$ comprises a subset $\mathcal{R}_F$ of permanently installed (fixed) RUs and a subset $\mathcal{R}_{SL}$ of short-lived RUs (i.e., mobile gNBs in transportation environments or gNB offering services under emergency situations etc) with $\mathcal{R} = \mathcal{R}_F \cup \mathcal{R}_{SL}$ In this problem setting, the accurate number of RUs and, subsequently, the source-destination (RU-CU interconnections) FH pairs is not known in advance as the number and type of short lived RUs may greatly variate over time. A graphical representation of this concept is shown in Figure 5-68 where an integrating wireless access and optical transport network together with compute elements in support of FH flows for both short-lived and permanently operating RUs is illustrated.

To solve the service provisioning under uncertain source demands, a two-stage stochastic optimization model can be formulated, with the first-stage capturing the deterministic demands generated by $\mathcal{R}_F$and the second-stage the uncertainty introduced by $\mathcal{R}_{SL}$ In a generic form, this problem will be solved minimizing the following cost function:

$$\min_{\mathbf{x}_1 \in \mathcal{X}_1} f_1(\mathbf{x}_1) + \mathbb{E}\left[\inf_{\mathbf{x}_2 \in \mathcal{X}_2} Q(\mathbf{x}_2, \omega)\right] \quad \text{Eq. 5-26}$$

with

$$f_1(\boldsymbol{x}_1) = \sum_{s\in S}\sum_{r\in \mathcal{R}_F} c_s x_{rs} + \sum_{e\in E}\sum_{r\in \mathcal{R}_F} c_e x_{re} \quad \text{Eq. 5-27}$$

$$Q(\boldsymbol{x}_{2,}\omega) = \sum_{s\in S}\sum_{r\in \mathcal{R}_{SL}^{\omega}} c_s x_{rs}^{\omega} + \sum_{e\in E}\sum_{r\in \mathcal{R}_{SL}^{\omega}} c_e x_{re}^{\omega} \quad \text{Eq. 5-28}$$

In the first stage optimization function (Eq. 5-27), x_{rs} denotes the resources used at server s for the processing of the FH flows originating from RU $r \in \mathcal{R}_F$ while x_{re} is the network capacity used at link $e \in \mathcal{E}$ by the FH flows originating from RU $r \in \mathcal{R}_F$. The first stage problem is solved subject to a set of constraints $\mathcal{X}_1$ indicating that i) the total number of BBUs that can be assigned to server s cannot exceed its available processing capacity, ii) sufficient network and compute resources are allocated for the provisioning of FH flows and, iii) FH flows do not violate network capacity and latency constraints. In the second stage problem, the remaining network and compute capacity is allocated at the short-lived RUs with the objective to minimize cost function (**Eq. 5-28**) under a possible scenario ω. In equation (**Eq. 5-28**), x_{rs}^{ω} and x_{re}^{ω} indicate the compute and network resources allocated for the provisioning of a FH flow under a possible scenario where RU $r \in \mathcal{R}_{SL}^{\omega}$ is active. This scenario appears with a probability $p_{\omega} > 0$. The second stage problem is solved under a set of constraints $\mathcal{X}_2$ that take into account the remaining capacity from the first stage problem. This type of problems is solved using Stochastic Linear Programming (SLP) [127]. Therefore, using as inputs network topology details, traffic statistics, the probability distribution that the various scenarios may appear, the location where each function/task will be processed together with the required network and compute resources can be determined.

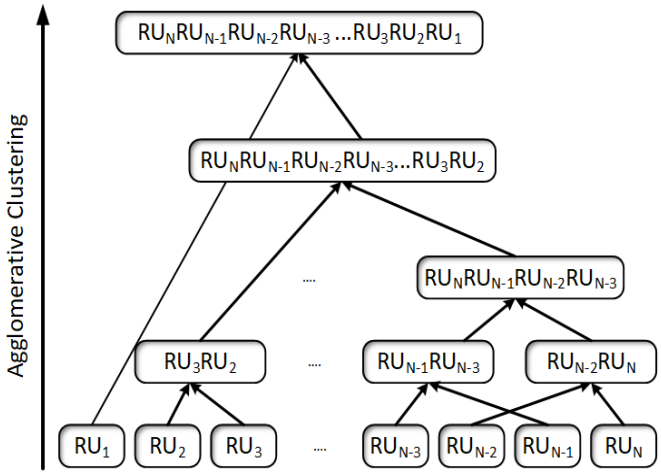

Figure 5-69: Dendrogram of the agglomerative clustering algorithm applied in our network elements.

The main limitation of this approach is related to the high computational complexity and the slow convergence of the SLP-based models. In response to this observation, we propose a two-stage neural network framework for real time service provisioning, extending our previous work in [139]. In, the first stage, long short-term memory (LSTM)-NNs are used for traffic forecasting while in the second multilayer perceptron (MLP)-NNs are adopted for the prediction of the optimal operational parameters of the 5G-Network [139]. This is achieved through the estimation of the optimal MLP-NN structure (number of neurons, the number of hidden layers, the batch size and the number of epochs) that can fit the solutions obtained using the offline optimization framework. The main limitation of this approach is related to the fact that identification of the optimal hyperparameters that characterize the NN's structure is time consuming process. Therefore, for scenarios with frequent topological changes the identification of the optimal NN structure in due time is not possible.

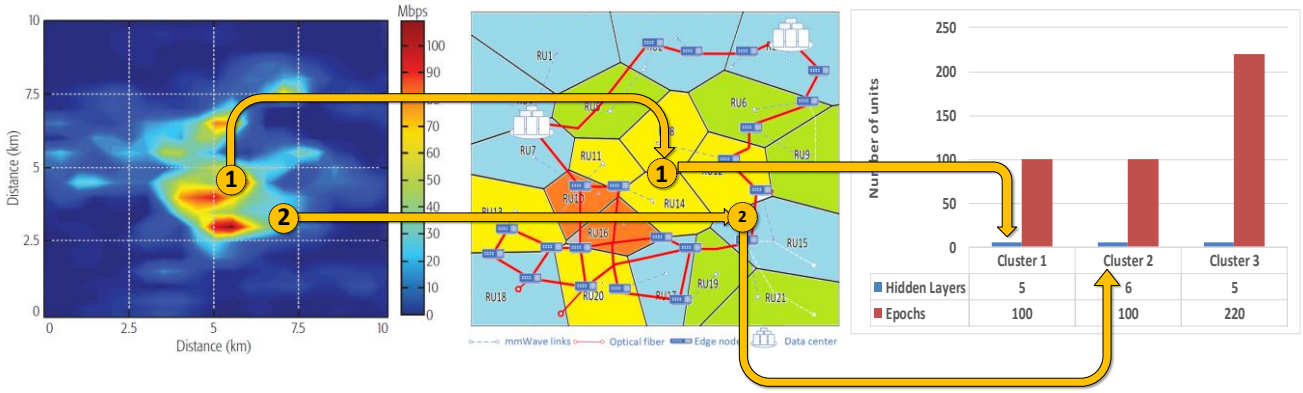

a) b) c)

Figure 5-70: Automated hyperparameter selection for two RUs a) wireless traffic statistics over a 10x10km access network, b) clustering of RUs based on their hyperparameters, c) lookup table for hyperparameter selection.

To simplify and accelerate the hyperparameter selection process, a clustering approach is proposed taking advantage of the inherent correlation that exists between input traffic statistics, 5G topology and routing decisions. To demonstrate the effectiveness of this approach, consider the simple case where the 5G network is altered by the arrival of two short-lived RUs, namely RU1 and RU2 shown in Figure 5-70.Once activated at the specific location, their optimal NN structure that can be used to determine the operational parameter of interest for the upcoming time instances can be readily obtained. To achieve this, a clustering algorithm is used to group RUs with similar NN structures. When the clustering analysis is complete RUs are classified as part of one of the resulting clusters. Once RUs have been clustered, the hidden layers and epochs are selected on the fly to determine the optical the NN model structure (Figure 5-70 c)). In the final step, the optimally extracted NN structure for each RU is trained using the traffic statistics that are available at the corresponding location. A detailed description of this process is provided in the following Section.

5.8.2 Real Time Optimization for 5G

5.8.2.1 Clustering Preliminaries

Cluster analysis is a machine learning method for identifying homogeneous groups of objects, known as clusters, based on a measure of similarity. Objects belonging to the same cluster are similar to each other, but are very dissimilar to objects belonging to different clusters. Each object can be graphically represented as a point in a n-dimensional space, where n is the number of features that characterize the object. Clustering analysis is an exploratory analysis, since many parameters of the final clustering analysis have to be investigated. Particularly, the metric which measures the correlation of objects has to be selected, while the clustering algorithm that will be used and the number of different clusters have to be determined. Most methods calculate measures of similarity or dissimilarity by estimating the distance between pairs of objects. The distance between more similar objects is small, whereas the distance between dissimilar objects is large [140]. The most convenient metric for object's similarity is the Euclidean distance. There are several clustering algorithms. These algorithms can be classified in hierarchical and partitioning methods [141]. The clustering method used in this study is the hierarchical clustering and in particular the agglomerative technique. The most popular agglomerative clustering algorithms are the single linkage, the complete linkage, the average linkage and the Ward's algorithm which are differentiated according to the way that calculate the distance between the clusters. In the present study after we have implemented a trial and error process, we select the Ward's method. This algorithm calculates the total sum of squares of the distances within each cluster and aims to minimize them. These sum of squares within the cluster are known as square error sums (ESS) and their formula is:

$$ESS = \sum_{i=i}^{n} {x_i}^2 - \frac{1}{n}\left(\sum_{i=1}^{n} x_i\right)^2$$

$$ESS_{(M\ groups)} = \sum_{j=1}^{j=M} ESS_j$$

where the x_i is the score of the individual i^{th} [142].

Initially, the number of clusters is equal to the number of objects as each object represents an individual cluster. At first the most similar objects are merged to establish a new cluster. Then another pair of objects is merged and linked to a higher level of the hierarchy. In this way a tree-like structure is constructed, each level of which is composed of a different number of clusters. In the higher levels the dissimilarity between the merged clusters is increased. Finally, since similarity decreases, all the sub-clusters are merged in a single cluster at the top of the hierarchy. This process can be visualized with a dendrogram as shown in Figure 5-69.

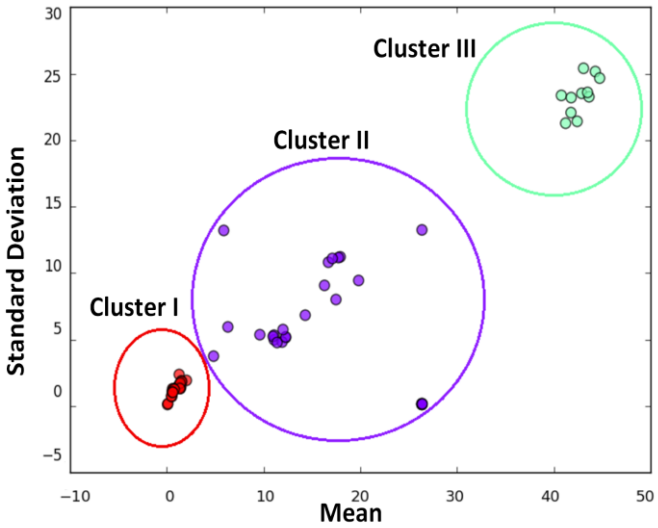

Figure 5-71: Clustering model results.

5.8.2.2 Hyper-parameter Optimization using the Agglomerative Clustering Algorithm

In [139] we proposed a LSTM-NN to forecast the input traffic at each RU and we implemented an exhaustive search in order to find the optimal LSTM's structure. This work is concentrates on identifying the parameters of LSTM-NN for each RU without having to implement an exhaustive search suffering high complexity that makes it impractical for real time network configurations. Therefore, we propose to construct another model to search the NN's hyperparameters.

Table 5-6: Agglomerative Clustering Algorithm.

Step 1: Begin with N clusters, each one composed of a single RU and a symmetric table of distances between the RUs.
Step 2: Search in the table of distances, the pair of clusters-RUs with the highest similarity, which means the smallest distance.
Step 3: If the most similar clusters are RUi and RUj., merge the clusters RUi and RUj and create a new cluster C1, that comprises the RUi and RUj objects.
Step 4: Recalculate the table of distances by removing the rows and columns related with the clusters RUi and RUj and adding a new row and column that contain the distances of the new cluster C1 and the other clusters.
Step 5: Repeat N-1 times the step 2,3, and 4. Report the clusters that were merged, the levels at which this merge was occurred.

Each RU of the dataset is characterized by a set of statistical variables associated with the traffic and its distribution. This information is sufficient for a clustering model to group similar RUs in the same cluster using the algorithm summarized in Table 5-6. Following this, each of the resulting clusters is linked with a specific

LSTM configuration. So, for the RUs belonging to the same cluster, the LSTM's parameters are selected automatically. Finally, the NN-based model is trained to predict the RU's traffic in the next time period. To assign the LSTM configurations to the appropriate clusters, we introduce a threshold value to the prediction error and we try to approximate the NN hyper-parameters instead of finding the optimal one. This relaxation enables the creation of a set of suitable LSTM configurations for each RU. Similar configurations that belongs to these sets are linked with specific clusters.

5.8.2.3 Numerical Results

5.8.2.3.1 Topology description

In our previousstudy the performance of the NN-based optimization framework was evaluated using the optical transport network topology presented in [139] over which 21 RUs are developed. Each RU serves mobile devices that generate demands according to real dataset reported in [143]. In the current study, we extend this dataset by creating more RUs with random traffic statistics based on the distributions of the real data. This extension is mandatory and efficient to produce more reliable clustering results.

5.8.2.3.2 RUs grouping using clusering approach

To group the most similar RUs in the same cluster the clustering algorithm described in Section III is applied to the dataset. This dataset is composed of a set of statistical parameters that describe the traffic of the RUs and provide the required information to perform the required RU comparison and clustering. These include the traffic distribution, the mean value and standard deviation. Figure 5-71 shows the clustering results. Based on these results three clusters are selected.

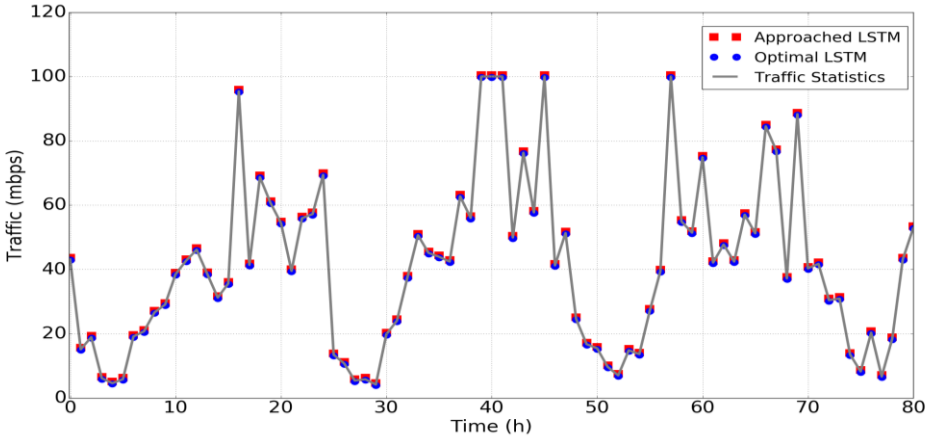

Figure 5-72: Traffic forecasting using LSTM as derived from the clustering approach.

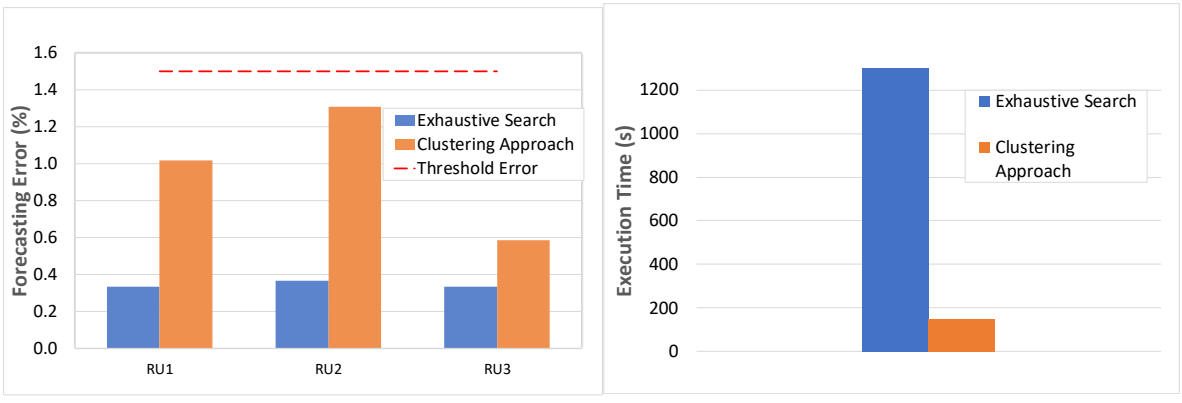

a) **b)**

Figure 5-73: a) NN forecasting error for the two different LSTM approaches. Dashed line represents the threshold error. b) Comparison between exhaustive search and clustering approach in terms of execution time.

5.8.2.3.3 Neural Network topology approximation

In [139] for each network element an exhaustive search, was performed to design the optimal NN architecture that predicts with very high accuracy the traffic for the following time period and then the optimal policies as they have been obtained by the corresponding ILP. In the present study, this optimization problem is relaxed by adding a higher error threshold in the range of (1.5%-5%), whereas the previously accepted error was in the range of (0.1%-3%). In addition, we introduce a clustering approach in order to reduce the execution time.

Once the clustering model has been produced, the NN hyper-parameters are selected as described above. The results that are obtained by these two different approaches must have similar performance. A comparison between them in terms of forecasting error is depicted in Figure 5-72 and in terms of execution time in Figure 5-73. A trade-off between execution time and prediction's accuracy are introduced with our clustering method. As shown in the first figure, we observe an increase on the forecasting error, which however is still below the threshold we have set. On the other hand, in the second figure, the gain in execution time is very high.

6 Techno-economic Analysis

The 5G-PICTURE advancements will enable the Network Operator to deliver a high quality transport network for 5G services. However, their deployment in a real network setup is not always a straightforward task, since lots of significant factors should be taken into account such as area specifics, traffic demand and growth patterns/forecasts, as well as infrastructure availability, costs and scaling capabilities. Therefore, transport network technologies deployment need to be evaluated by techno-economic analysis means, apart from direct comparison of technologies' technical characteristics.

For this purpose, techno-economic analysis has been performed in the context of 5G-PICTURE using two complementary, fully parameterized tools leveraging on the work and expertise gained from two 5G-PPP projects, namely 5G-XHaul and 5G-CROSSHAUL. The combination of these tools enables:

a. modelling transport network deployments based on 5G-PICTURE technologies and the architectural options that they support,
b. modelling various access network deployments and traffic demand/network usage scenarios,
c. dimensioning the modelled transport network deployments in an automated way and
d. obtaining comparative cost and energy efficiency results of the various deployment options, towards
    a. pre-estimating the critical, high cost factors and extracting deployment guidelines at network pre-planning stages (macro-scale strategic planning phases);
    b. at next stage (network-planning phases) performing detailed cost estimation and assessment of specific micro/medium scale mobile and fixed access network deployments.

Various scenarios can be evaluated, the list being non-exhaustive: Greenfield vs. Brownfield optical network deployment; optical vs. wireless vs. hybrid deployment options with various 5G-PICTURE technologies mixtures; multiple Functional Splits (FSs) deployments ranging from eCPRI A to eCPRI E; adoption of different Multiple-Input Multiple-Output (MIMO) schemes in the access network; multiple grades of incorporating edge or cloud computing for FS processing and/or specific application services, and so on.

6.1 Techno-economic Analysis Tools for 5G-PICTURE Solution

In general, performing techno-economic analysis is seldom a straightforward task, the underlying reasons being many and versatile. The latter ranging from the purpose/goal of the analysis, the level of detail of input information, the level of detail modelling the factors/aspects affecting the results, the scale of the system under analysis and so on. Therefore, there are usually several types of analysis applied at different stages of a commercialisation solution.

More specifically, the level of transport and access network deployment details used as input for a techno-economic analysis (such as actual/measured distances, de-facto use of protocols including functional splitting, services hosting at various network points, capability and extent of specific technologies, etc.) may differ depending on multiple factors. Some of these factors being the business entity performing the analysis, the targeted goals and the timing of the analysis. For instance:

- analysis conducted by external services (e.g. consultancy entities, equipment vendors, etc.) for consultancy purposes may not use actual network deployment details, due to confidentiality purposes;
- analysis conducted by strategic planning departments of a telecom operator at early stages of technology adoption (e.g., at pre-planning phases, for financial forecasting purposes, at early procurement phases, etc.), may not have the actual network deployment details due to timing/complexity reasons;
- analysis conducted by pure technical departments at network planning phases, where cost analysis is needed, e.g., for delivering a solution targeting a corporate customer/vertical or a specific area deployment, can and need to take into account every network deployment detail.

Similarly, the expected output of a techno-economic analysis performed by a telco provider depends highly on the business entity performing the analysis, ranging from aggregate results and guidelines provided top-down from strategy/financial department to technical department (i.e., aggregate results in terms of number of units at initial procurement phases), up to detailed Bill of Materials (BoM) and accurate cost estimation provided, e.g., from a telecom operator to a corporate customer/vertical.

From another perspective, the flexibility of assessing various scenarios is usually relevant to the scale of the deployment. Also, the assessment of a range of scenarios can be very effort and time-consuming, depending on the detail level that is needed as input information. In other words:

- In large scale deployments, the degrees of flexibility in terms of using alternative technologies/configurations is usually higher, while significant results may become more obvious compared to the case of small-scale deployments.
- However, modelling large scale deployments with high level of details requires a lot of effort, and for country-wide and nation-wide deployments can be inefficient, unless it is connected to specific corporate network planning tools.
- On the contrary, for medium/small scale deployments (corporate customer, vertical, medium city deployments, etc.) a very generic deployment modeling may provide insignificant results.
- Needless to mention that the higher the level of deployment details, the higher the accuracy/correctness of the analysis.

For all these reasons, techno-economic evaluation of various transport network deployments can be performed in many ways, ranging from macroscopic to microscopic analysis. Of course, the results/information retrieved from all types of analysis need verification: the macro deployment evaluation results need to be verified to be useful for network and cost pre-planning purposes, while the micro/medium deployment evaluation results need to be verified from a macroscopic perspective, e.g., in order to identify any hidden costs and get insights about their suitability and cost-efficiency a the longer run.

Therefore, two complementary, fully parameterized tools have been developed and used for the techno-economic analysis evaluation of 5G-PICTURE solution deployment and for cost efficient deployment of the 5G-PICTURE solution by Telecom Operators, namely:

a) **A Macroscopic Network Deployment Techno-economic Analysis Tool**, for the purposes of performing early phases and large-scale deployments cost evaluation.
b) **A Microscopic Network Deployment Techno-economic Analysis Tool**, for the purposes of performing detailed medium/small-scale deployments cost evaluation.

6.2 5G Networks Principles and 5G-PICTURE Technologies Deployment

6.2.1 Network Architecture Modeled by 5G-PICTURE Techno-economic Tools

The aforementioned techno-economic tools model the physical architecture of a converged fixed-mobile network for 5G, comprising the expected access network and the various segments of the transport network. A high level description of the modeled physical architecture has been provided in section 3.1 of the present document.

Following the widely adopted network roll-out principle, transport network deployments comprise multiple hierarchical transport network segments. Considering the current trend of minimizing the number of segments from the access to the core network nodes, the transport network model that has been used in 5G-PICTURE techno-economic analysis is the following one (see Figure 6-1):

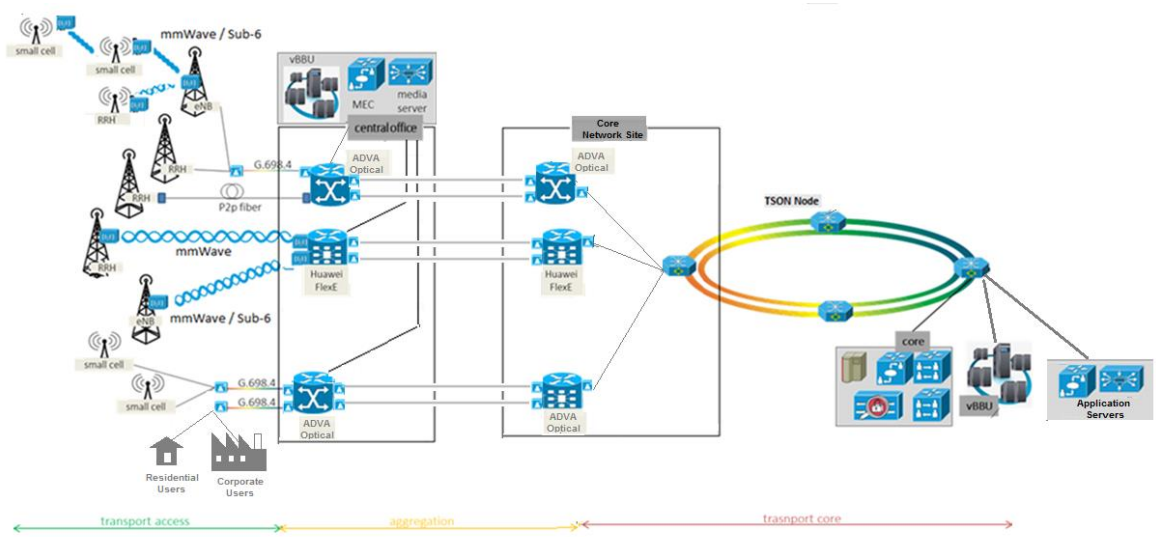

Figure 6-1: 5G-PICTURE physical architecture.

More specifically the transport network comprises 3 segments:

- **Transport access**, providing connectivity from the access network nodes to the 1st level aggregation sites (Central Offices)
- **Transport aggregation**, aggregating transport access connections at Central Offices
- **Transport core**, providing connectivity/routing between Central Offices towards the Core network.

6.2.2 Access Network Deployment Principles/Assumptions

The 5G-PICTURE data-plane architecture considers integrated optical and wireless network topology and infrastructure. The wireless domain comprises a dense layer of Small Cells (SCs) to serve high traffic demand, which is complemented by Macro-Cell Sites (MSs) layer for maximising coverage. The fixed network domain comprises a number of corporate users' fixed access network nodes, and a number of residential users' traffic access aggregation nodes.

The key technical characteristics of the SCs and MSs that have been modelled are related to:

- SCs/MSs cell capacity.
- SC/MSs maximum expected loading factor.
- Average number of cells per MS (it can be different per area type: Dense Urban, Urban, Suburban, Rural).
- Different Functional Splitting (FS) options (referring to eCPRI A to E options).
- The MSs MIMO capability and schemes.

The access network deployment is defined either as aggregate number of nodes for the macroscopic analysis or as one-by-one nodes detail, including site coordinates, and per site configuration, for the microscopic analysis. There is also the possibility to dimension the SCs deployment based on traffic demand predictions and the MSs based on generic radio-coverage calculations for a certain area.

6.2.3 Transport Access Deployment Options

The 5G-PICTURE transport access deployment options have been modelled in the context of the techno-economic analysis. These relate to the usage of different FSs, to the usage of various wireless and optical technologies and to other deployment specificities.

Deployment Option A: Multiple FSs

More specifically, the 5G-PICTURE concept, architecture and functionality support the coexistence of different FSs over the same infrastructure, namely eCPRI A, eCPRI B, eCPRI C, eCPRI D, eCPRI I_d, eCPRI II_D/I_U, eCPRI E. In practice, the throughput overhead of each functional split needs to be considered in the dimensioning of the transport links between the access network node and the BBU. A simple formula, calculating the

transport links throughput on the basis of the access network nodes data bandwidth or capacity and of the splitting option overhead, has been used as follows:

$$T_{FH} = (aT_{cell} + bC_{cell})(1 + OH_{split_i})$$

where:

- a,b = {0,1}.
- T_{cell} : data throughput of the cell.
- C_{cell} : maximum cell capacity.
- OH_{split_i} : overhead, depending by the adopted splitting option.

Indicative values of parameters for some functional splitting options are shown in Table 6-1.

Table 6-1: Indicative Functional Splits parameters

Splitting options	a	b	OH
Split E: CPRI / eCPRI	0	1	600%
Split II_D / I_U : load-dependent FH	1	0	80%
Split A: BH with centralized scheduling	1	0	25%

Deployment Option B: Usage and Placement of vBBUs and MEC

Various placements of vBBUs at the edge or core data centers, along with MEC for traffic offloading can be considered as a deployment option and modelled with the tools.

Deployment Option C: Deployment of Various Transport Access Technologies

5G-PICTURE will deliver a converged wireless/optical solution for 5G networks transport, therefore key goal of the techno-economic analysis is the evaluation of a number of deployment scenarios using 5G-PICTURE technologies. The scenarios can differ in the grade at which each of these technologies is used. In particular, the technologies considered at the access network segment are described in the following.

- **mmWave links,** with the specifications of IHP and BWT equipment, i.e.: IHP with bitrate of 1.3 Gbps and BWT with bit rate of 3.5 Gbps. These values concern average bitrates, since the actually achieved bitrate depends highly on the used frequency spectrum, on the distance between the two nodes and on the radio-environment.
- **Sub-6 GHz links,** with the specifications of i2CAT equipment, i.e., with average achieved bitrate of 0.5 Gbps (depending on used frequency spectrum, on distance between the two nodes, on the radio-environment, etc.).

The wireless transport connections (both mmWave and Sub-6 GHz) may consist of one or multiple hops, defined as deployment options in the techno-economic analysis. Moreover, multiple links per connection/hop may be considered, in case the traffic to be served exceeds the capacity limits of the equipment, or traffic can be multiplexed at some point/site, provided that aggregate throughput does not exceed transceiver capacity (see Figure 6-2).

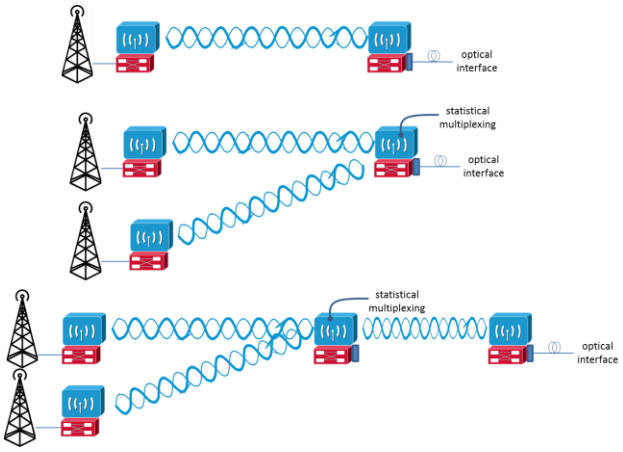

Figure 6-2: Deployment Options of 5G-PICTURE Wireless Transport Access Links (Sub-6 GHz and mmWave).

- **Point-to-point optical links** based on dark fiber plus a couple of grey transponders, aggregated to Flex-E equipment. Various P2P links can be assumed, with various specifications ranging from 1GbE up to 100GbE. In these techno-economic studies the list has been limited to 1GBE, to a massive use of 10GbE and some 25GbE as result of multiplexing. On the Flex-E client side the modeled interfaces are at 10GbE.
- **G.698.4 (ex. G.Metro) optical links**, with the specifications of ADVA equipment, multiplexed at ADVA Mux/Demux and aggregated with ADVA Muxponders. Currently the G698.4 interfaces provide 10Gbps connectivity.
- **WDM-PON links**, but in the present work this technology is considered as substituted entirely by G.Metro connections, given that it is not part of 5G-PICTURE technologies list.

Besides, other access transport scenario specifics can be modelled, such as the maximum link utilisation (usually set to 75%).

Different access transport deployment scenarios can be defined, dimensioned and evaluated.

Deployment Option D: Fiber Deployment

Given the fact that fiber deployment is not ubiquitous, instead it incurs extra costs where not present, various fiber deployment scenarios/options have been modelled.

Typically, two main scenarios types are identified:

- **Greenfield scenario**
  This scenario assumes that there is no previously deployed infrastructure and it is necessary to take into account not only the fiber as such, but also different elements that intervene like digging and trenching, law permits, technical personnel.
  The deployment cost depends highly on the type of area to be covered, as well as the applicable urban construction costs, which vary highly between countries/areas/etc.
- **Brownfield scenario**
  In this scenario, the deployment assumes an existing fiber infrastructure. At this point two different cases can be considered:
  - **Own infrastructure**: where the stakeholder that has deployed the fiber infrastructure is the same as the one deploying the 5G network; thus the costs for fiber deployment, as well as the additional costs to be applied, can be considered as zero.
  - **Third party infrastructure**: where the deployed fiber infrastructure belongs to an external company; thus the usage and cost of it are bound to agreements between the two stakeholders.

6.2.4 Transport Aggregation Deployment Options

5G-PICTURE mainly delivers two technologies applicable at transport aggregation segment, namely ADVA optical multiplexing/aggregation solution and Huawei optical Ethernet solution. Therefore key goal of the techno-economic analysis is the evaluation of a number of deployment scenarios using these technologies. The scenarios can differ in the grade at which each of these technologies is used, however this option is highly associated with the access transport deployment.

ADVA optical multiplexing/aggregation solution deployment

At the beginning of the 5G-PICTURE project two systems had to be considered as aggregator: the DWDM G.698.4 transport framework and the FUSION device.

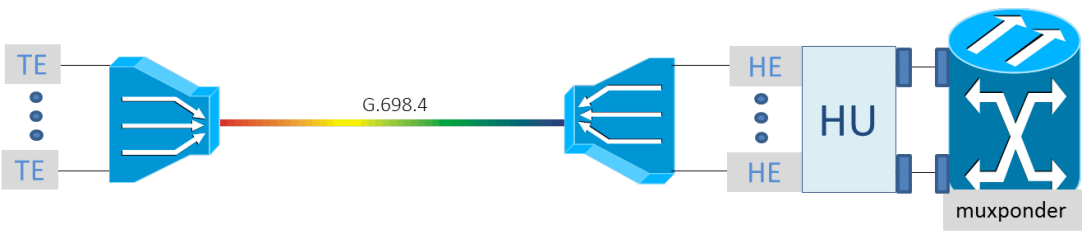

Figure 6-3: G.698.4 access transport aggregated at Muxponder.

After *TransPacket AS* leaving *the project*, the FUSION device has been substituted by ADVA Muxponder, as depicted in Figure 6-3. In brief, the G.698.4 access transport channels/interfaces are multiplexed at the G.698.4 Mux/Demux, and one G.698.4 Mux/Demux can multiplex up to 20 channels (20UL+20DL, 40 DWDM wavelengths, 100 GHz spacing). The G.698.4 access transport channels/interfaces can then be plugged to a HU shelf comprising two transponder cards and one complete HU can support up to 20 HU shelfs. Next, the HU shelfs are aggregated at the Muxponder side, the latter being capable to MUX up to 52x10 Gbps Channels.

Huawei optical Ethernet (Flex-E) aggregation solution deployment

The modelled Huawei Flex-E aggregation equipment comprises:

- tributary interfaces, at a minimum of 5GE, typically 10GE.
- a maximum of 4 x 100 GE line interfaces.
- a fully equipped matrix.
- system control, fan, power boards, etc.

A typical configuration consists of 12 10GE cards and 2 100GE cards (Flex-E interfaces), aggregating the 10GE interfaces traffic. The applied traffic dimensioning is compliant with the standards (reference document "TR-221, Technical Specifications for MPLS in Mobile Backhaul Networks" by Broadband Forum). The deployment options regarding the Flex-E equipment are shown in Figure 6-4, where it becomes obvious that the Flex-E interfaces need to be terminated to another Flex-E unit. The Flex-E 100GE interface can be used for relaying pass-through traffic (thus operating also as core transport segment solution), and/or can aggregate other 10GE interfaces' traffic in chained mode.

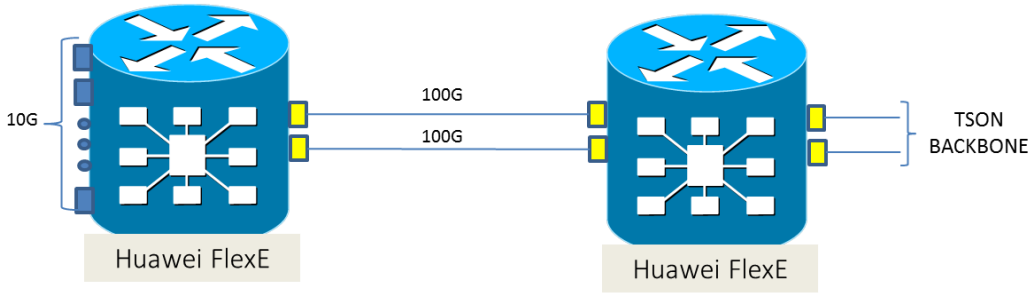

Figure 6-4: FlexE configuration.

Common aggregation solutions specifications

Besides, other transport aggregation scenario specifics must be considered, such as:

- the maximum link utilisation (usually set to 75%),
- the average loading factor of the equipment interfaces (usually set to 70%-80%),
- the expected statistical multiplexing gain, especially in the case of the Huawei Flex-E equipment.

Different deployment scenarios can be defined, dimensioned and evaluated.

6.2.5 Transport Core Deployment Options

As far as the transport core segment is concerned, TSON is the solution delivered by 5G-PICTURE.

TSON

Regarding TSON nodes, the implementation can be based on a variety of FPGA boards handling interfaces with different capacity. In the context of the project, an FPGA board capable of processing 16 x 10 G tributary ports plus 3 x 100G line ports is used. The board considered in the evaluations has by default 4 interfaces.

TSON has not a transparent optical switch similar to WSS inside it, so the "transparent" pass-through is still processed by FPGA or, even more simply, with a pair of back-to-back interfaces. In the context of 5G-PICTURE techno-economic analysis we consider TSON boards as relay core transport units with 100G interfaces.

The number of TSON edge nodes is considered on the basis of total traffic to be transported, considering also a loading factor per board of around 70%-80%.

6.2.6 Summary: 5G-PICTURE Technologies Deployment in Access, Aggregation and Core Transport

The deployment options of various transport access technologies are summarised in the following Table 6-2:

Table 6-2: Technologies Deployment Options for Access, Aggregation and Core Transport.

Network segment	Technologies / devices
Transport access	Wireless • mmWave • Sub-6 GHz Optical • Point to point fiber with grey transponder • G.698.4 (ex G.Metro). (This technologies is completely substituting TWDM-PON)
Aggregation	• Muxponder (associated to ADVA G.698.4 system) • Flex-E (*Huawei*)
Transport core	• Flex-E (*Huawei*) • TSON

6.2.7 Other Deployment Options and Input Information

Servers for Control, vBBUs, MEC and Radio Core

In the modeled deployment, compute servers are needed for Control, vBBUs, MEC and Radio Core. More specifically:

- **Servers for Controls** do not need to have excessive performance. A couple of servers (for redundancy) might be enough for a medium deployment. For instance 8 servers in the Turin use case (see section 6.4.1) can be considered in the whole metropolitan network.
- The number of **servers implementing vBBUs** depends on many factors such as: the processed traffic, the number of connected access network nodes, the adopted FS options and above all the actual vBBUs implementation specifics. The number of vBBUs necessary for the processing of the entire access transport traffic is calculated as follows:

$$N_{vBBUs} = 2 * [\![\text{ceiling}\,(\text{Max}\left(\frac{T_{FH}}{\frac{100Gbit}{s}}, \frac{N_{RRHs}}{\text{Nports}}\right)\right)$$

  In particular, 1 server is needed per 100 Gbit/s traffic (FS option E) and can serve at maximum 40 connected access network nodes.

  Depending on the FS and traffic, 1-3 CPU cores per vBBU (based on EUR solution) are needed. In brief, in the context of this analysis they are assumed 3 vcores/vCPUs per vBBU, 1 physical core that equals 3 virtual cores, and the same analogy for memory.
- **Servers for MEC**: the same dimensioning criteria used for vBBU servers can be applied also to MEC servers deployment, mathematically expressed by:

$$N_{MEC} = 2 * [\![\text{ceiling}\,(\text{Max}\left(\frac{T}{\frac{100Gbit}{s}}, \frac{N_{ports}}{40}\right)\right)$$

Storage

The cost of storage is 0.021 USD per GB per month [8]

Space in central offices – Rack Footprint Cost

The footprint cost per year (OPEX) of a rack needs to be considered, corresponding to expenses for cooling, personnel, security, etc.

[8] **Source**: https://aws.amazon.com/it/s3/pricing/

Installation

Installation costs can be either modeled as a percentage of the equipment CapEx, usually 2%. In case the value is 0%, the cost is considered embedded into the CapEx, as done in 5G-PICTURE.

Maintenance

In order to simplify the cost evaluation, expenditures for maintenance are assumed to be equal to 2% of CapEx for each year.

Energy consumption

The energy represents an important share of the OPEX. The cost of 1 kWh amounts to 7€cent.

6.2.8 Cost information and Financial Figures

To proceed with the cost estimation of a specific deployment, input is required regarding the per-unit equipment cost, installation and maintenance/service costs for each technology, along with the estimated annual prices erosion or escalation. These costs are kept as Confidential among the Project members.

Other financial figures introducing or representing extra costs such as Weighted Average Cost Of Capital (WACC) and Tax Deduction (% of Equipment Cost) are also considered.

6.3 Macroscopic Network Deployment Techno-economic Analysis Tool

The Macroscopic Network Deployment Techno-economic Analysis Tool allows:

1. Defining (as input parameters):
    a) various access network deployments, and
    b) various traffic demand/network usage scenarios.
2. Modeling various access/aggregation and core transport network deployment options based on 5G-PICTURE technologies and the architectural options that they support and, based on these:
3. Dimensioning the access/aggregation and core transport network deployments in an automated way, and
4. Providing comparative cost results of these deployments.

towards pre-estimating the critical, high cost factors and extracting deployment guidelines at network pre-planning stages (macro-scale strategic planning phases). The tool supports analysis for a certain time period, indicatively 5 –years period.

6.3.1 Deployment Scenario Definition – Input Parameters and Tool Options

The methodology to be followed in order to define the deployment scenario to be evaluated with the Tool consists of the following steps:

STEP 1. Selection of the geographical area under study (total area surface) & identification of area types (Dense Urban, Urban, Suburban, and Rural). The deployment area is also defined in terms of average range of MSs and SCs per area type.

STEP 2. Definition of 4G/5G radio coverage per year and per area type and cell overlapping factor, in order to estimate the number of MSs over the area.

STEP 3. Definition of MSs configuration, capacity and loading, in order to estimate the traffic to be served by MSs.

STEP 4. Definition of the traffic to be served by SCs, SC capacity and loading, in order to estimate the number of SCs in the deployment.

STEP 5. Definition of the fixed network traffic to be generated by corporate users/tenants and to be served by 5G-PICTURE technologies.

STEP 6. Definition of Functional Splits (Overheads and Compute resources required for their processing by vBBUs) and their distribution for a specific deployment scenario.

STEP 7. Definition of 5G-PICTURE technologies' usage distribution (on the basis of the transport network principles and options as well as 5G-PICTURE technologies' scaling models, as analyzed in the previous sections).

STEP 8. Dimensioning of access/aggregation and core transport deployment based on the aforementioned network assumptions.

STEP 9. Cost analysis using cost-related information (cost models) for each technology.

Area of Deployment Definition

The first step for the evaluation is the definition of the area of deployment. The definition refers to the total surface (Km2), and the surface covered by each area type, namely:

- Dense Urban (DU).
- Urban (U).
- Suburban (SU).
- Rural (R).

as well as the targeted radio and population coverage during the deployment time period. At this point, widely adopted radio network planning assumptions/principles shall be taken into consideration, e.g.:

- In DU: 99% area coverage corresponds to 99% population coverage.
- In U: 80% area coverage corresponds to 99% population coverage.
- In SU: 60% area coverage corresponds to 99% population coverage.
- In R: 20% area coverage corresponds to 99% population coverage.

It is evident that these area coverages can be adjusted depending on the specifics of the deployment area.

Access Network Deployment Definition

The Access Network Deployment (5-years roll-out) definition follows the 5G network architecture and access network deployment principles as described in section 6.2. The actual number of MSs and SCs for a deployment can be either calculated on the basis of rough radio-coverage estimations and traffic forecasts, or predefined (by external sophisticated radio network planning tools) and inserted as input. Further configuration information that can be considered includes:

1. The average number of cells for each MS (it can be different per type of area and per year).
2. The per cell capacity of the MSs/SCs (per year, taking into account the access network capacity expansions, e.g., due to upgrades).
3. The average maximum cell loading of MSs/SCs per area type and per year (taking into account the traffic demand increase).

Fixed Network Assumptions

The fixed network nodes to be backhauled can be considered either as nodes serving corporate fixed end-users or as nodes aggregating traffic from a number of end-users connected via existing access technologies (cable, DSL, etc.). In the first case, the dimensioning is based on the number of corporate end-users nodes (e.g., 1 node/end-user), while in the second case on the number of nodes calculated by the forecasted traffic to be backhauled.

Transport Network Deployment Definition (Assumptions/Options)

The Transport Network Deployment (5-years roll-out) options follow the 5G network architecture, the transport network deployment principles and the 5G-PICTURE technologies specifications described in section 6.2. The deployment options are defined in the following way/form:

- Distribution (%) of MSs per FS.
- Distribution (%) of MSs backhauling/fronthauling per 5G-PICTURE access transport technology, per FS and per year.
- Distribution (%) of SCs per Functional Split.
- Distribution (%) of SCs backhauling/fronthauling per 5G-PICTURE access transport technology, per FS and per year.
- Distribution (%) of Sub-6 and mmWave links that are single or multi-hops.
- Distribution of aggregation and core transport per 5G-PICTURE technology, per FS and per year.

Also the following details are configurable per scenario:

- Transport links utilization (as % of link capacity) can be defined per technology.
- Aggregation and core transport equipment loading (interfaces loading) can be defined per technology per year.
- Multiplexing gain can be defined per technology.

The tool also allows modeling of various placements (and combinations) of vBBUs at the edge, or core data centers, along with MEC for application traffic offloading.

Other Input Parameters/Assumptions

For the economic part of the analysis, input is required regarding the per-unit equipment purchase cost, installation cost and maintenance/service cost for each technology, along with the estimated annual prices erosion or escalation. The per-unit costs can be calculated then for a 5 years' timeframe.
Other financial figures introducing or representing extra costs such as Weighted Average Cost Of Capital – WACC and Tax Deduction (% of Equipment Cost) can be also considered.

6.3.2 Deployment Scenario Results

Based on the assumptions for a specific network deployment, the Tool provides:

- Access, aggregation and core transport dimensioning in terms of number of transport links, number of transport links and units of 5G-PICTURE technologies' equipment per year.
- Access, aggregation and core transport cost estimation of the deployment scenario, including CAPEX/OPEX breakdown per technology/year/etc.
- Comparative cost results of a number of deployment scenarios.

The tool output/results will be elaborated in the following sections.

6.4 Microscopic Network Deployment Techno-economic Analysis Tool

In order to evaluate cost and energy consumption of the 5G-PICTURE network, an ad-hoc tool has been developed**,** named Microscopic Network Deployment Techno-economic Analysis Tool. The tool, given traffic exigences at final users level, provides a traffic matrix and a consequent network dimensioning based on a Dijkstra algorithm with weights based on link length. As a consequence, the working path corresponds to the shortest path while the protection path is imposed to be the shortest path with links disjointed w.r.t. the working one.

The input parameters are the following:

- the list of nodes, with their ID number, their name and their geographical coordinates (latitude and longitude).
- the list of links, with their ID number, endpoint nodes and length (in km).
- the list of antennas sectors, with their ID number. For each antenna it is important to indicate:
    - the belonging node, i.e. the node directly attached to the antenna by a point to point connection,
    - the type of MIMO (2x2, 4x4, etc.),
    - the distance between antenna and belonging node (in km),
    - the type of media (optical fiber, G.698.4 or wireless),
    - the site hosting the BBU connected to the RRH present in the antenna site,
    - the user traffic and the fronthauling traffic.

In 5G KPIs the Capital Expenditures (CAPEX) and OPEX analysis is part of a more comprehensive Total Cost of Ownership (TCO) evaluation that gives, as comparison parameter between legacy and 5G-PICTURE networks, the Yearly Total Cost per bit/s (YTC):

$$YTC = \sum_{i=1}^{N} \frac{CAPEX_i}{AP_i} + \sum_{j=1}^{M} OPEX_j$$

$CAPEX_i$ and $OPEX_j$ are the i-th component and j-th component of CAPEX and OPEX respectively. In order to harmonize the sum, each CAPEX has to be annualized, splitting the investment by the appropriate *amortization*

period (*AP*). This is the easiest way to calculate the Total Cost of a system taking into account both CAPEX and OPEX, neglecting inflation and cost of the money used for investment (for example interests on outstanding debts like bonds, bank loans, etc.).

The evaluation perimeter is between the antenna, excluding the transmission system but including RRH or eNodeB, and the radio core, together with storage, servers and software. In particular, servers comprise vBBUs, hardware and software Control plane, MEC systems and Radio Core.

6.4.1 Case study in the city of Turin

The 5G-PICTURE techno-economic analysis tools have been applied to a metro case study represented by the city of Turin (Torino) in Northern Italy, where the most important verticals avalaible with the support of 5G have been considered. In specific, Rail, Stadium & Mega Events, Smart City, Industry 4.0, Large/Small Business and Residential verticals' use cases have been considered with regard to macro and small cells radio network deployment, various BBUs installation options with different FS options and various transport access, aggregation and core network deployments, adhering to the aforementioned principles and assumptions.

In particular, the metropolitan area under study is presented in Figure 6-5, along with the locations of some of the main tentative verticals in Turin and its neighbouring areas. The city population amounts to about 1.5 million inhabitants.

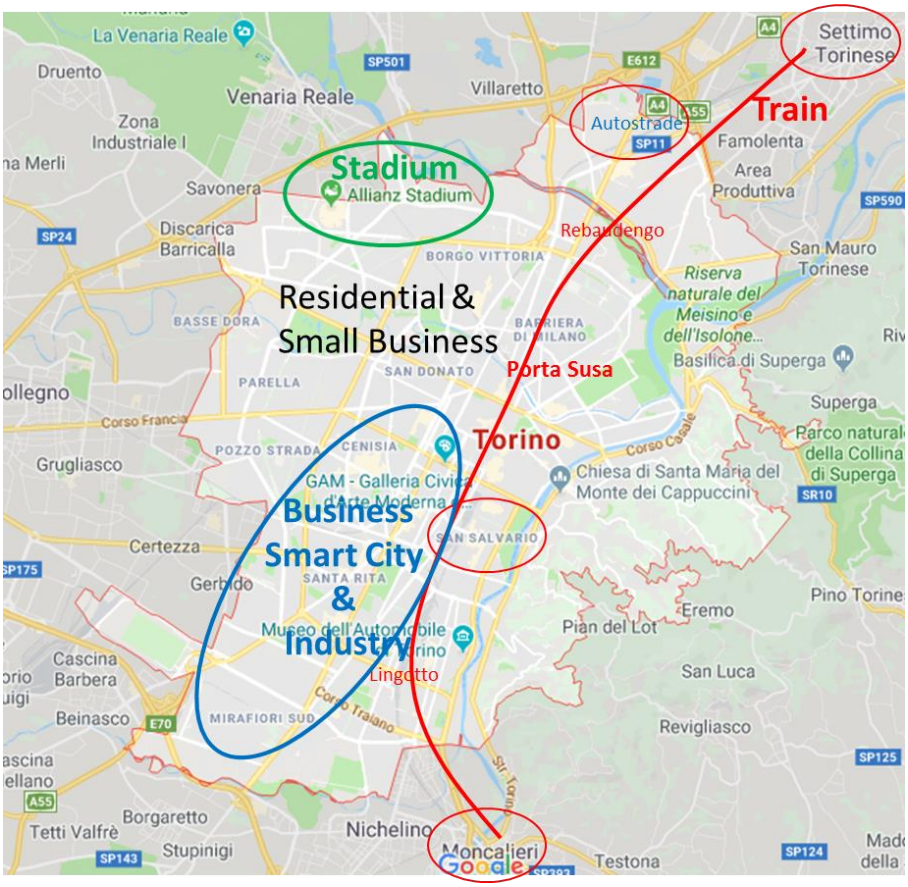

Figure 6-5: Turin map with deployment of Train, Stadium, Business/Smart City/Industry 4.0, Residential & Small Business verticals.

A 5G Mobile Network has been considered in this area, with the following access network deployment-specific assumptions:

- the average MSs' inter-site distance is 600 m.
- the average MS to SC distance is 350 m (ranging from 150 m to 600 m).
- each MS comprises 3 cells (correspondingly 3 antennas).
- each MS offers cell capacity of 5 Gbps, and each SC offers cell capacity of 0.3 Gbps.
- the radio network deployment consists of around 275 MSs with 825 cells in total and 180 SCs.

The following traffic-related assumptions have also been done:

- the network is assumed to serve about 300k users.
- the average datarate is foreseen to be 170 Mbps, according to Cisco Mobile VNI forecast in 2022 for Western Europe [1].
- applying statistical multiplexing, with a factor that can also reach one order of magnitude, the network peak bandwidth can reach 4÷5 Tbps.

6.5 Macroscopic Techno-economic Analysis

For the aforementioned radio network deployment and traffic/capacity assumptions multiple transmission network deployment scenarios have been analyzed for a 5-years period. In general, the scenarios on which our study has focused assume either static traffic and radio network deployment over this period (as afore described), or radio network capacity and traffic increase over the 5-year period. The latter assumes MSs' capacity expansion from 5 to 10 Gbps and SCs capacity expansion from 0,5 to 1 Gbps, while traffic increases also gradually over this period.

Scenarios Set 1: Optical network deployment Greenfield vs Brownfield

This set of scenarios focus on the evaluation of a Greenfield optical network deployment compared to various Brownfield options (if applicable) as presented in section 6.2. More specifically, the optical network deployment options presented in Table 6-3 have been evaluated for the support of the access transport segment of a Turin-based area model. In the scenarios we assume that optical transport is used in 97% of the MSs and 25% of the SC sites of the Turin area. The access transport optical deployment is considered static based on 10 Gbps optical connections, and results are extracted for a 5-years period.

Table 6-3: Optical Access Transport Scenarios

Optical Transport Deployment			1-Year Period			5-Year Period			
	Existing LL Fiber	Existing Transport Fiber	CAPEX	OPEX	TOTAL	CAPEX	OPEX	TOTAL	Optical Deployment %Total Cost
GF	0%	0%	4.343.060	237.842	4.580.901	21.404.443	237.842	21.642.285	81%
BF 1 0%LL - 100% Tr	0%	100%	3.557.380	214.114	3.771.494	17.476.043	1.016.722	18.492.766	77%
BF 2 75%LL - 75% Tr	75%	75%	1.575.949	154.275	1.730.223	7.568.889	717.526	8.286.415	53%
BF 3 25%LL - 25% Tr	25%	25%	3.420.689	209.986	3.630.675	16.792.592	996.082	17.788.674	76%
BF 4 12%LL - 12% Tr	12%	12%	3.900.322	224.471	4.124.793	19.190.755	1.068.507	20.259.261	79%

The comparative cost results of these deployment scenarios are presented in the following Figure 6-6.

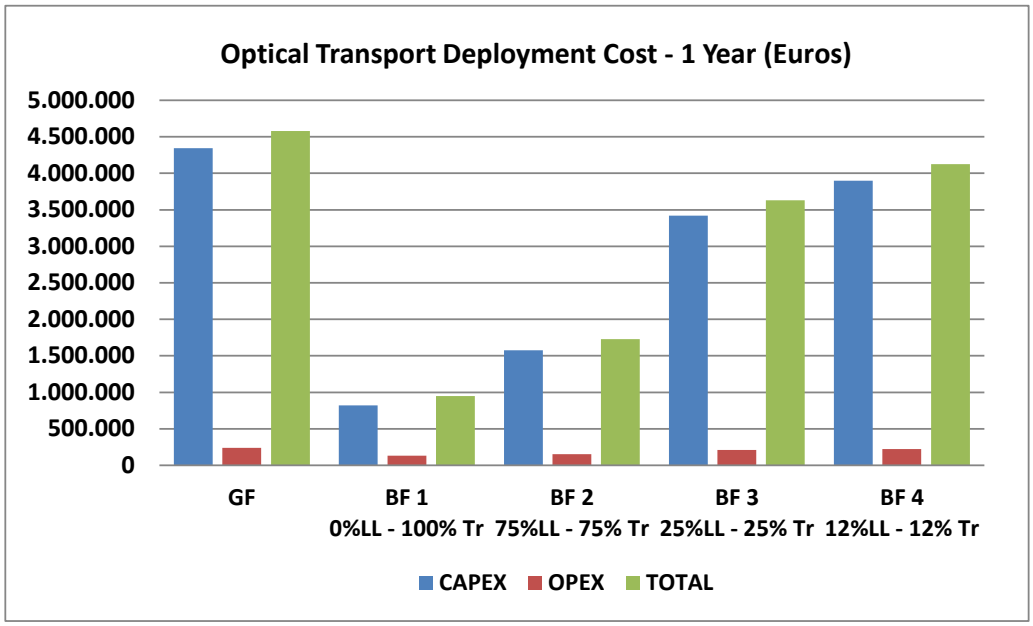

Figure 6-6: YTCO for Various Optical Transport Deployment Scenarios.

From the results, it becomes obvious that the fiber deployment cost is an extremely critical factor of the total deployment cost, as it may amount to more than 80% of the deployment in the cases of a Greenfield scenario.

Scenarios Set 2: Wireless - Optical transport deployments This set of scenarios focus on the evaluation of a variety of optical-wireless technologies mix for the transport network deployment in the area under study. More specifically, these scenarios range from pure optical deployment to multiple hybrid wireless – optical scenarios, up to a pure wireless deployment. The various network deployment options studied are presented in Table 6-4.

Table 6-4: Wireless - Optical transport deployments Scenarios.

Converged Wireless - Optical Transport Deployment				
	Optical		Wireless	
	MSs	SCs	MSs	SCs
Pure Optical	High	High	Low	Low
Hybrid 1	High	High-Medium	Low	Low-Medium
Hybrid 2	High	Low	Low	High
Hybrid 3	Medium	Medium	Medium	Medium
Hybrid 4	Low-Medium	Low	High-Medium	High
Pure Wireless	Low	Low	High	High

Converged Wireless - Optical Transport Deployment					1-Year Period			5-Year Period			Cost OH over Pure Optical
	Optical		Wireless								
Static Traffic - GF	MSs	SCs	MSs	SCs	CAPEX	OPEX	TOTAL	CAPEX	OPEX	TOTAL	
Pure Optical	100%	100%	0%	0%	4.339.624	227.007	4.566.630	21.461.914	1.087.035	22.548.950	0%
Hybrid 1	95%	75%	5%	25%	4.300.988	243.515	4.544.503	21.130.603	1.159.789	22.290.392	-1%
Hybrid 2	97%	25%	3%	75%	4.343.060	237.842	4.580.901	21.404.443	1.135.360	22.539.804	0%
Hybrid 3	50%	50%	50%	50%	4.856.014	430.083	5.286.097	22.886.682	2.001.675	24.888.358	10%
Hybrid 4	25%	10%	75%	90%	5.083.303	529.741	5.613.043	23.442.984	2.450.029	25.893.013	15%
Pure Wireless	0%	0%	100%	100%	5.343.839	630.403	5.974.242	24.177.564	2.903.523	27.081.087	20%
Static Traffic - BF2											Cost OH over Pure Optical
Pure Optical	100%	100%	0%	0%	1.457.374	139.963	1.597.336	7.050.664	651.816	7.702.480	0%
Hybrid 1	95%	75%	5%	25%	1.665.536	163.924	1.829.461	7.953.345	761.835	8.715.181	13%
Hybrid 2	97%	25%	3%	75%	1.575.949	154.275	1.730.223	7.568.889	717.526	8.286.415	8%
Hybrid 3	50%	50%	50%	50%	3.411.229	386.450	3.797.680	15.662.757	1.783.513	17.446.270	127%
Hybrid 4	25%	10%	75%	90%	4.382.870	508.588	4.891.458	19.940.822	2.344.263	22.285.085	189%
Traffic Increase - BF2											Cost OH over Pure Optical
Pure Optical	100%	100%	0%	0%	1.432.542	134.917	1.567.459	7.499.640	759.574	8.259.214	7%
Hybrid 1	95%	75%	5%	25%	1.626.184	157.849	1.784.033	8.672.988	902.238	9.575.226	24%
Hybrid 2	97%	25%	3%	75%	1.543.270	148.614	1.691.884	8.171.480	844.585	9.016.064	17%
Hybrid 3	50%	50%	50%	50%	3.264.748	370.814	3.635.562	19.643.422	2.298.482	21.941.904	185%
Hybrid 4	25%	10%	75%	90%	4.175.400	487.702	4.663.102	25.710.686	3.065.853	28.776.540	274%

In these scenarios, further assumptions, adhering to the Turin area case specifics are the following:

- SCs' transport is based on Sub-6 wireless connections, since Sub-6 equipment capacity is sufficient for this type of radio nodes, while the Sub-6 frequency band offers higher signal quality in long distances and lower indoor penetration losses than the mmWave band.
- MSs' transport is based on mmWave wireless connections, due to their capacity advantage compared to Sub-6 ones, which makes them more applicable for MSs backhauling.
- The MSs' optical transport is based mainly on G.METRO 10 Gbps links, while for the SCs P2P fiber links of 1GBE are considered.
- Regarding the splitting options:
    - All SCs have Functional Split II_D/I_U (typical for SCs equipment).
    - MSs are mainly deployed with Functional Split eCPRI II_D/I_U (more than 96%), a small portion (~2%) is deployed with Split E (for industry 4.0 deployments), and another one (~2%) with Split A (for backhauling over long distances).

The comparative cost results of these deployment scenarios are presented in the following Figure 6-7.

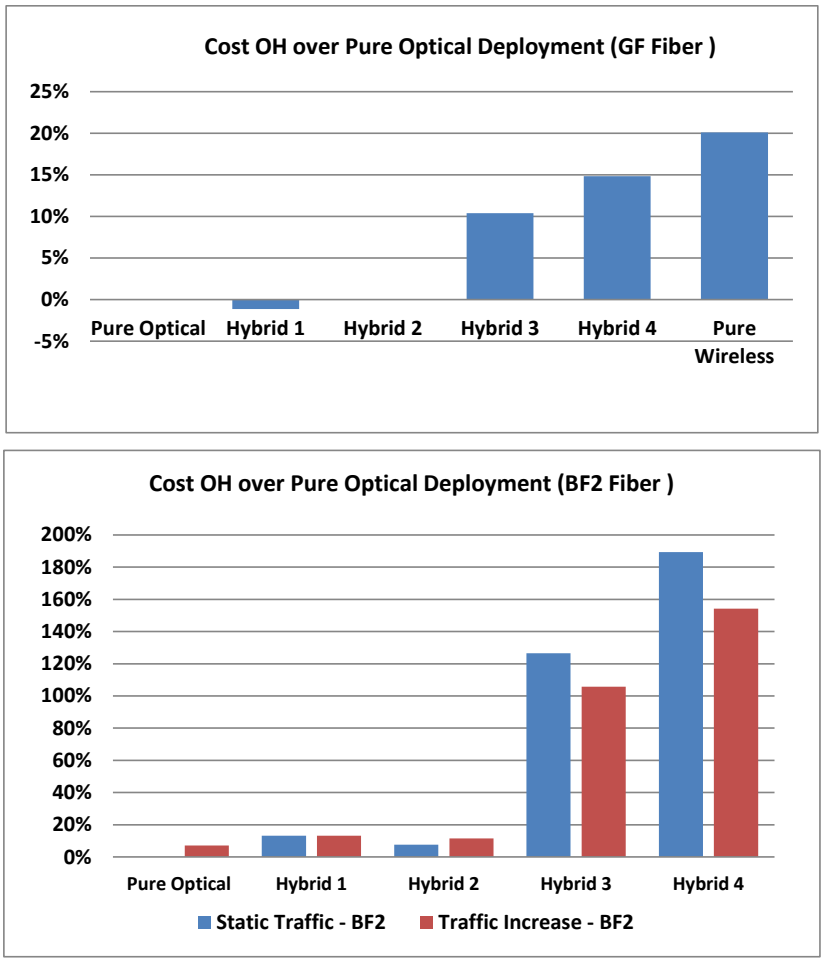

Figure 6-7: Comparison of TCO for Various Wireless-Optical Transport Deployment Scenarios.

From the results, it becomes obvious that the fiber deployment cost, as well as the wireless equipment capacity is an extremely critical factor, which can affect the decision regarding the exact wireless-optical technologies mix. More specifically:

- Scenarios based on optical network deployment are more cost efficient, even in the case of a Green-field Fiber Deployment, due to the high "cost over capacity" of the wireless equipment (with the given prices). In this case the cost increases relatively to the usage of the wireless technologies, and the overhead can reach 20%. The absolute cost of all deployments in this case is very high, above 22million Euros.
- In case of pre-existing fiber deployment footprint, the usage of optical technologies seems even more cost effective. The cost overhead of hybrid scenarios over that of the pure optical scenario is significant, and can reach even 190%.
    - The higher the usage of wireless links, the higher the deployment cost.
    - Considering future capacity/traffic increase though, the cost overhead becomes to shrink. The reason is the way optical and wireless technology equipment scales; the optical equipment scales with large steps at high prices, compared to the wireless equipment which scales with shorter steps and lower prices.
- The absolute cost in this case can be about 8 millions for a wide range of hybrid scenarios.

Scenarios Set 3: Multiple Functional Splits Transport Deployment

This set of scenarios focus on the evaluation of usage of various Functional Splits in the converged optical-wireless transport deployment under study.

More specifically, these scenarios consider various grades of usage of three main Functional Splits: A, II_D/I_U, and E presented in Table 6-5. The evaluation has been performed for hybrid deployments 1, 2, and 4.

Table 6-5: Functional Splits transport deployment Scenarios

Multiple Functional Splits Transport Deployment			
	eCPRI A	**eCPRI IIᴅ / Iu**	**eCPRI E**
FS - mix 1	High	Low	Low
FS - mix 2	Medium	High	Low
FS - mix 3	Low	High	Low
FS - mix 4	Medium	Medium	Medium
FS - mix 5	Low	Medium	High

Multiple Functional Splits Transport Deployment			
	eCPRI A	**eCPRI IIᴅ / Iu**	**eCPRI E**
FS - mix 1	95%	3%	2%
FS - mix 2	20%	75%	5%
FS - mix 3	3%	95%	2%
FS - mix 4	35%	35%	30%
FS - mix 5	5%	25%	70%

Multiple Functional Splits Deployment				1-Year Period			5-Year Period			
Hybrid 2 - GF Static Traffic	**eCPRI A**	**eCPRI IIᴅ / Iu**	**eCPRI E**	**CAPEX**	**OPEX**	**TOTAL**	**CAPEX**	**OPEX**	**TOTAL**	**Cost OH over FS mix 3**
FS mix 1	95%	3%	2%	4.306.258	226.630	4.532.888	21.284.217	1.084.745	22.368.962	0%
FS mix 2	20%	75%	5%	4.366.808	242.978	4.609.785	21.522.252	1.158.929	22.681.181	1%
FS mix 3	3%	95%	2%	4.343.060	237.842	4.580.901	21.404.443	1.135.360	22.539.804	1%
FS mix 4	35%	35%	30%	4.647.940	304.493	4.952.432	22.814.928	1.440.155	24.255.083	8%
FS mix 5	5%	25%	70%	5.125.223	409.807	5.535.029	24.978.359	1.921.261	26.899.621	20%
Hybrid 2 - BF2 Static Traffic										**Cost OH over FS mix 1**
FS mix 1	95%	3%	2%	1.466.170	140.860	1.607.030	7.083.778	655.891	7.739.670	0%
FS mix 2	20%	75%	5%	1.583.355	158.917	1.742.272	7.604.988	738.627	8.343.615	8%
FS mix 3	3%	95%	2%	1.575.949	154.275	1.730.223	7.568.889	717.526	8.286.415	7%
FS mix 4	35%	35%	30%	1.831.803	219.445	2.051.248	8.734.244	1.014.919	9.749.163	26%
FS mix 5	5%	25%	70%	2.302.745	324.568	2.627.313	10.865.971	1.495.067	12.361.039	60%
Hybrid 2 - BF2 Traffic Increase										**Cost OH over FS mix 1**
FS mix 1	95%	3%	2%	1.440.367	133.137	1.573.504	7.375.902	727.142	8.103.044	0%
FS mix 2	20%	75%	5%	1.539.084	149.374	1.688.458	8.261.613	880.898	9.142.511	13%
FS mix 3	3%	95%	2%	1.520.086	143.119	1.663.206	8.171.480	844.585	9.016.064	11%
FS mix 4	35%	35%	30%	1.801.509	212.849	2.014.358	10.218.204	1.350.515	11.568.719	43%
FS mix 5	5%	25%	70%	2.279.857	320.089	2.599.946	13.822.672	2.171.085	15.993.757	97%

The comparative cost results of these deployment scenarios are presented in the following Figure 6-8.

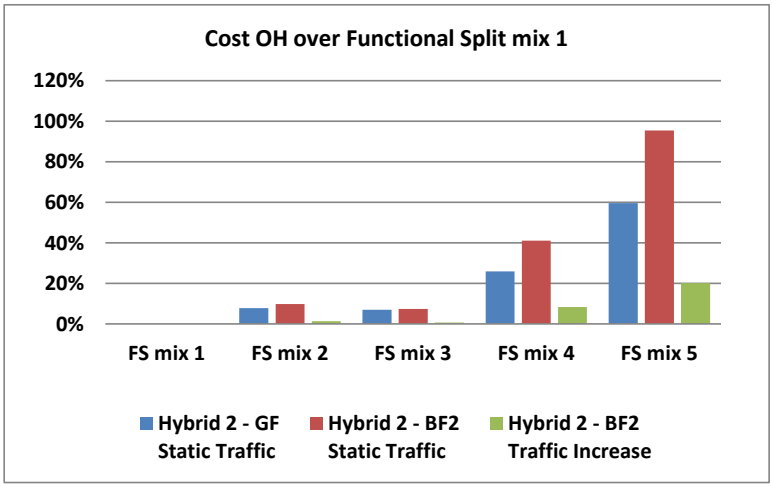

Figure 6-8: Comparison of TCO for Transport Deployment Scenarios of Various Functional Splits.

From the results, it appears that the functional splits' deployment shall be carefully selected in close association with the transport network technologies' deployment. More specifically:

- Using higher functional splits (especially Split E) incurres extra costs associated both with the required higher transport network capacity, and with the additional vBBU processing compared to lower functional splits.
- The extra cost is marginal between splits A to II_U/I_D so they can be used interchangeably depending on other deployment restrictions/requirements/factors such as access network nodes cost, available physical space for the access network node etc.
- With the traffic and capacity increase, however, the extra cost increases with the usage of higher functional splits, for the aforementioned reasons.

The use of functional splits shall always be considered along with the vBBU processing and traffic offloading options.

Scenarios Set 4: FS Processing at Edge and MEC Offloading

This set of scenarios focus on the cost analysis with regard to the benefits and overheads of FS processing at Edge and the MEC offloading. More specifically, for a range of transport technology deployments and a range of Functional Split scenarios we consider various grades of FS processing at Edge and the MEC offloading as reported in Table 6-6.

Table 6-6: FS Processing at Edge and MEC Offloading

FS Processing at Edge and MEC Offloading (Hybrid 2, FS - mix 3)			
FS offloading	**MEC Offloading**	**FS offloading**	**MEC Offloading**
Low	Low	20% IID / IU - 20% E	15%
Medium 1	Low	50% IID / IU - 50% E	15%
Medium 2	Low	90% IID / IU - 70% E	15%
High	Low	90% IID / IU - 90% E	15%
FS Processing at Edge and MEC Offloading (Hybrid 3, FS - mix 3)			
FS offloading	**MEC Offloading**	**FS offloading**	**MEC Offloading**
Low	Low	20% IID / IU - 20% E	15%
Medium 1	Low	50% IID / IU - 50% E	15%
Medium 2	Low	90% IID / IU - 70% E	15%
High	Low	90% IID / IU - 90% E	15%

The comparative cost results of these deployment scenarios are presented in the following Table 6-8:

Table 6-7: FS Processing at Edge and MEC Offloading Scenarios

FS Processing at Edge and MEC Offloading (Hybrid 2, FS - mix 3)							
		1-Year Period			5-Year Period		
FS Processing @ Edge	**MEC Offloading**	**CAPEX**	**OPEX**	**TOTAL**	**CAPEX**	**OPEX**	**TOTAL**
20% IID / IU - 20% E	15%	1.572.399	152.274	1.724.672	7.552.827	708.439	8.261.266
50% IID / IU - 50% E	15%	1.573.099	148.508	1.721.606	7.555.994	691.405	8.247.400
90% IID / IU - 70% E	15%	1.605.649	153.909	1.759.558	7.703.263	716.158	8.419.420
90% IID / IU - 90% E	15%	1.602.574	153.185	1.755.759	7.689.350	712.852	8.402.202
FS Processing at Edge and MEC Offloading (Hybrid 3, FS - mix 3)							
		1-Year Period			5-Year Period		
FS Processing @ Edge	**MEC Offloading**	**CAPEX**	**OPEX**	**TOTAL**	**CAPEX**	**OPEX**	**TOTAL**
20% IID / IU - 20% E	15%	3.415.479	386.579	3.802.058	15.681.986	1.784.134	17.466.120
50% IID / IU - 50% E	15%	3.424.729	386.227	3.810.956	15.723.836	1.782.631	17.506.467
90% IID / IU - 70% E	15%	3.440.929	386.085	3.827.014	15.797.131	1.782.144	17.579.276
90% IID / IU - 90% E	15%	3.437.854	385.361	3.823.215	15.783.219	1.778.838	17.562.057

From the results, it appears that FSs and MEC offloading have marginal impact on total transport deployment cost, due to the low cost and high capabilities of commodity servers that are needed for vBBU processing.

From the macroscopic techno-economic analysis results it became obvious that in the case of Turin area, a cost effective deployment solution would be based on Hybrid 2 technology deployment, with Functional Split mix 3. Therefore, further microscopic techno-economic analysis has been performed for these scenarios.

6.6 Microscopic Techno-economic Analysis

6.6.1 Description of the network

Considering the Macroscopic Techno-economic analysis results, the most applicable and cost-efficient scenarios have been analyzed in more detail using the Microscopic Techno-economic analysis tool. More specifically, network deployment details that have been modeled are the following ones:

- the aggregation transport segment is composed of 31 main nodes (also named belonging nodes) to which Macro-Sites are anchored,
- the BBU sites are six and located in correspondence with the belonging nodes named Porta Susa, Stadium, Polito, TIM Via Reiss Romoli, Vanchiglia and Lancia.

Fronthauling in the access segment is supported in most cases by fiber (92%), specifically:

- 34% by point-to-point fiber.
- 59% by G698.4 Multichannel bi-directional DWDM solution.

Wireless covers about 8% with the following techniques:

- Sub-6 GHz at 300 Mbps for small cells at a maximum distance of 300 m from belonging node (inside stations, stadium, factories and commercial centers).
- mmWave at 60 GHz and 10 Gbps for macro cells.

Fronthauling splitting techniques options have been chosen to be:

- in most cases eCPRI split II_D/I_U (more than 96%).
- eCPRI split E for Industry 4.0 (less than 2%).
- eCPRI split A for fronthauling over long distances (about 2%).

A complete list of nodes is reported in Table 6-8.

Table 6-8: list of node in Turin metropolitan area

Node name	latitude	longitude	Core Node	MEC Offloading Factor	location
N1	45,072	7,664	N16	10,0%	porta susa
N2	45,029	7,656	N31	10,0%	lingotto
N3	45,100	7,703	N16	10,0%	rebaudengo
N4	45,138	7,764	N16	10,0%	settimo stazione
N5	44,995	7,678	N31	10,0%	staz. Moncalieri
N6	45,056	7,681	N31	10,0%	san salvario
N7	45,103	7,727	N16	10,0%	autostrade corso giulio
N8	45,114	7,637	N16	15,0%	stadio 1
N9	45,111	7,650	N16	15,0%	stadio 2
N10	45,070	7,658	N31	15,0%	vittorio
N11	45,060	7,637	N16	7,0%	san paolo
N12	45,049	7,622	N31	15,0%	mirafiore nord
N13	45,062	7,660	N31	15,0%	poliTO
N14	45,060	7,671	N31	15,0%	re umberto
N15	45,061	7,667	N16	15,0%	galileo ferraris
N16	45,111	7,671	N16	8,0%	via reiss romoli
N17	45,093	7,664	N16	15,0%	Parco Dora
N18	45,102	7,640	N16	15,0%	toscana /sansovino
N19	45,080	7,652	N16	9,0%	regina /potenza
N20	45,128	7,707	N16	9,0%	falchera
N21	45,097	7,711	N16	15,0%	regio parco
N22	45,083	7,696	N16	15,0%	bologna
N23	45,068	7,695	N31	9,0%	vanchiglia
N24	45,071	7,693	N31	15,0%	san maurizio
N25	45,071	7,687	N31	15,0%	castello
N26	45,061	7,701	N31	15,0%	cappuccini
N27	45,072	7,752	N16	15,0%	superga
N28	45,027	7,606	N31	15,0%	corso orbassano (tangenziale)
N29	45,062	7,599	N31	15,0%	grugliasco
N30	45,073	7,573	N16	15,0%	collegno
N31	45,062	7,636	N31	15,0%	lancia

6.6.2 Rail deployment details

The network deployment has been conceived in order to support rail operational critical services, which are Ultra-Reliable, Low Latency Communication (URLLC) services, as well as enhanced Mobile Broadband (eMBB) services for train passengers and users present inside the stations.

In particular, 5 train stations (belonging nodes N1÷N5) have been taken into account, each one located at few meters from its corresponding node:

- Porta Susa station, the biggest one with an average of 50 trains and 5000 users (as supposed in D2.2 Requirements)
- Moncalieri, Lingotto, Rebaudengo and Settimo stations, having an average of about 500/1000 users inside and outside trains

Depending on stations dimensions, it has been considered a number from 1 to 10 small cells, connected in wireless to the belonging node for distances between 150 m and 300 m, while for distances higher than 300 m point-to-point fiber connections are used.

In each station 1 macro cell is present, at 20 m of distance from the belonging node.

The L2 aggregation between stations is at 100 Mbit/s, as well as the L1 DWDM TSON transport connections.

According to the demo use case prepared in WP6, two belonging nodes (N6 & N7), named “Autostrade” and “San Salvario”, are equipped with 4 towers for 60 GHz mmWave at a distance of about 500-600 m from each other, with a 10 Gbit/s capacity and maximum distance of 3 km from the corresponding belonging node. Also in these sites 1 macro cell is considered, at 20 m from the node.

In addition, in order to properly cover also the traffic requirements due to Residential and Small Business customers, in the neighborhood of this area other 35 macro cells and 10 small cells (serving for example shopping centers) have been considered.

6.6.3 Stadium & Mega Events deployment details

The network deployment has been conceived in order to support huge traffic/services demands with extreme irregular characteristics, such as a stadium during a football match or a concert event. The location considered is the Juventus stadium (named Allianz Stadium), where both high peak data rates, high capacity and high numbers of connected devices are needed for eMBB services for the audience (like Crowdsourced Video) as well as for eMMB (like CCTV) and URLLC services for business related support systems.

In particular, 2 belonging nodes in the proximity of the Stadium (N8 and N9) have been considered with:

- NI Massive MIMO, in the specific 5 macro cells connected to each node
- 40 small cells inside the stadium, connected either by wireless or fiber depending if distances are less or more than 300 m from the belonging node
- L2 Aggregation is done with 12 x 10G edgecore switches

In addition, in order to properly cover also the traffic requirements due to Residential and Small Business customers, in the neighbourhood of this area other 10 macro cells have been added.

6.6.4 Business, Smart city and Industry 4.0 deployment details

The town centre and part of the most industrial area to the south of it have been taken into account for Large Business, Smart City and Industry 4.0 use cases. Large Business requires eMMB and URLLC services, Smart City focuses primarily on mMTC services, while Industry automation particularly needs URLLC and mMTC services.

Six belonging nodes have been allocated, among them are Universities like PoliTo (belonging node N13) and Industries like FCA at Mirafiori (belonging node N12).

The antennas have been deployed as follows:

- 35 macro cells (including residential customers) and about 100 small cells for nodes N12 and N13.
- 56 macro cells for the other sites, that support also residential and small business customers located in this area.

6.6.5 Residential and Small Business deployment details

For Residential and Small Business customers, in addition to the macro cells used in the locations devoted to the previous use cases, the rest of the town and its neighbouring countries, for a total of 16 belonging nodes, have been considered for this scenario, requiring eMBB services to be highly shared by all users. For this large area there are:

- 132 macro cells in total (7÷10 for each node).
- about 10-15 small cells for commercial centers (like IKEA and huge supermarkets with shops).
- 2 belonging nodes, Cappuccini (N26) and Superga (N27), are located over the Turin hills and are connected by mmWave to the macro cells.

6.7 Results

Given the network described in section 6.4.1, adopting the technology and deployment solutions described in previous sections, the cost and energy consumption of a 5G network insisting in the Turin metropolitan area have been calculated.

It is possible to set some parameters in order to define some different use cases, as reported in Table 6-10.

Table 6-9: Use cases for 5G PICTURE network solution in Turin metropolitan area.

Use case	LL fibre already deployed	Transport fibre already deployed	Offloading factor	Statistical multiplexing at aggregation nodes
A **(green field)**	0%	0%	Average about 10% (from 7% to 15%)	60%
B (**local loop green field**, **metro deployed**)	0%	100%	Average about 10% (from 7% to 15%)	60%
C (**75% already deployed fibre**) (*)	75%	75%	Average about 10% (from 7% to 15%)	60%
D (**massive statistical multiplexing**)	75%	75%	3%	20% (**)

Notes:

(*) Realistic situation for an incumbent operator

(**) Statistical multiplexing percentage in the last column of Table 6-9 represents the traffic amount after packet processing in the point of the network (belonging node) where it is performed. In other words, 20% means a 1:5 aggregation factor.

6.7.1 Use case A results

The use case A depicts a completely green field scenario, i.e., no fiber has been deployed, neither in the connection between the antennas' sites and the closest node of the transport network nor in the transport meshed network itself. MEC offloading is about 10% and statistical multiplexing at aggregation nodes is about 60%. Synthesis and details on costs and energy consumption are shown in Table 6-10 and Table 6-11. The results of these tables are also displayed as pie-charts in Figure 6-9 and Figure 6-10.

Table 6-10: synthesis of costs and energy consumption for use case A

Total CAPEX (yearly) [€]	**4297179**
Total OPEX [€]	288241
YCO [€]	4585420
YCO per user [€]	15,28
Total Power [kW]	63882
Total Energy (per year) [kWh]	559606
Energy per user (per year) [kWh]	1,87

Table 6-11: details of costs and energy consumption for use case A.

Element	yearly Cost [€]	Power [W]	Energy [kWh]
Tributary Intefaces	13538,50	1084,00	9891,50
Line Intefaces	125260,00	508,00	4635,50
Aggregation Nodes	398570,40	40380,00	368467,50
Transport nodes	40780,00	13450,00	122731,25
Severs (vBBUs + MEC)	12900,00	3660,00	33397,50
Fibre Local loop	2735832,89	0,00	0,00
Fibre metro network	906297,21	0,00	0,00
Wireless transport	64000,00	4800,00	43800,00
OPEX Energy	39172,44	0,00	0,00
OPEX others	249068,58	0,00	0,00

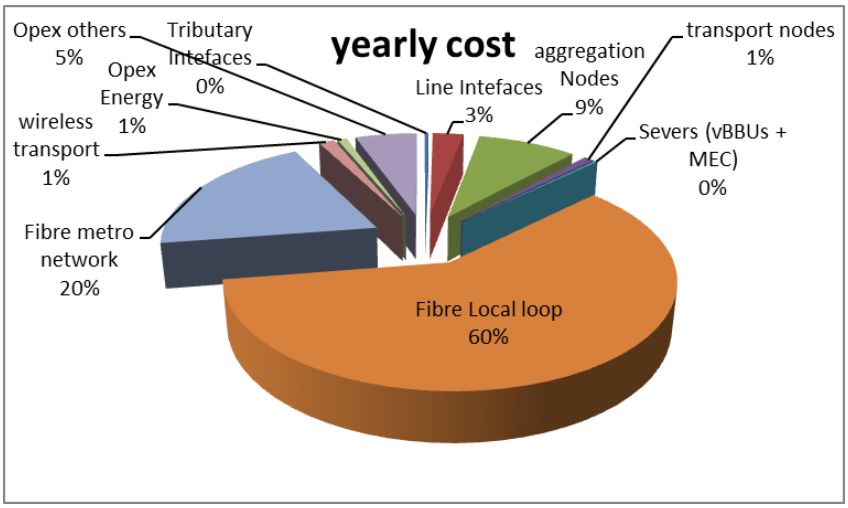

Figure 6-9: Pie-chart representing the percentage of yearly cost of different components for use case A.

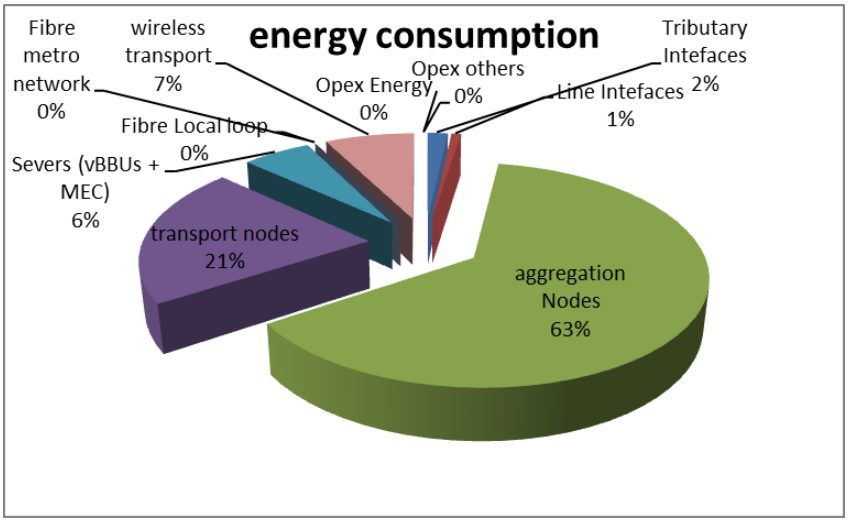

Figure 6-10: Pie-chart representing the energy consumption of different components for use case A

6.7.2 Use case B results

The use case B depicts a partially green field scenario, where no fiber has been deployed in the local loop, while it has been completely deployed in the transport meshed network. MEC offloading is about 10% and statistical multiplexing at aggregation nodes is about 60%. Synthesis and details on costs and energy consumption are shown in Table 6-12 and Table 6-13: details of costs and energy consumption for use case B. The results of these tables are also displayed as pie-charts in Figure 6-11 and Figure 6-12.

Table 6-12: synthesis of costs and energy consumption for use case B.

Total CAPEX (yearly) [€]	**3390882**
Total OPEX [€]	271747
YCO [€]	3662629
YCO per user [€]	12,21
Total Power [kW]	63882
Total Energy (per year) [kWh]	582923
Energy per user (per year) [kWh]	1,94

Table 6-13: details of costs and energy consumption for use case B.

Element	yearly Cost [€]	Power [W]	Energy [kWh]
Tributary Intefaces	13538,50	1084,00	9891,50
Line Intefaces	125260,00	508,00	4635,50
Aggregation Nodes	398570,40	40380,00	368467,50
Transport nodes	40780,00	13450,00	122731,25
Severs (vBBUs + MEC)	12900,00	3660,00	33397,50
Fibre Local loop	2735832,89	0,00	0,00
Fibre metro network	0,00	0,00	0,00
wireless transport	64000,00	4800,00	43800,00
OPEX Energy	40804,63	0,00	0,00
OPEX others	230942,64	0,00	0,00

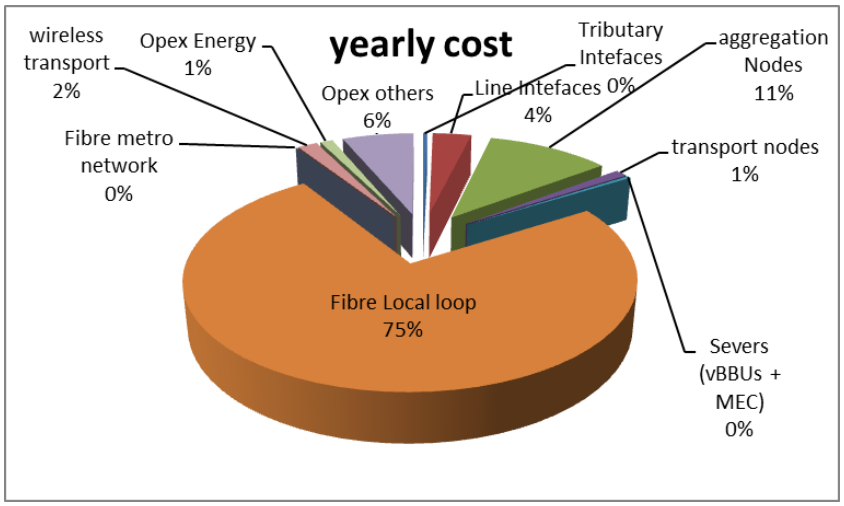

Figure 6-11: Pie-chart representing the percentage of yearly cost of different components for use case B.

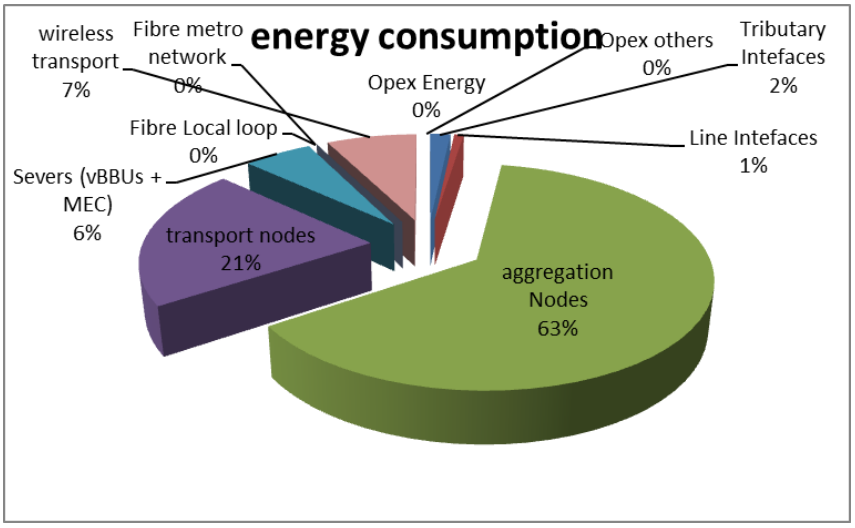

Figure 6-12: Pie-chart representing the energy consumption of different components for use case B.

6.7.3 Use case C results

The use case C depicts a realistic situation for an incumbent operator, for which the fiber is deployed at 75% both in the local loop and in the transport. MEC offloading is about 10% and statistical multiplexing at aggregation nodes is 60%. Synthesis and details on costs and energy consumption are shown in Table 6-14 and Table 6-15. The results of these tables are also displayed as pie-charts in Figure 6-13 and Figure 6-14.

Table 6-14: synthesis of costs and energy consumption for use case C

Total CAPEX (yearly) [€]	**1630269**
Total OPEX [€]	236535
YCO [€]	1866804
YCO per user [€]	6,22
Total Power [kW]	63882
Total Energy (per year) [kWh]	582923
Energy per user (per year) [kWh]	1,94

Table 6-15: details of costs and energy consumption for use case C

Element	yearly Cost [€]	Power [W]	Energy [kWh]
Tributary Intefaces	13538,50	1084,00	9891,50
Line Intefaces	125260,00	508,00	4635,50
Aggregation Nodes	398570,40	40380,00	368467,50
Transport nodes	40780,00	13450,00	122731,25
Severs (vBBUs + MEC)	12900,00	3660,00	33397,50
Fibre Local loop	799084,30	0,00	0,00
Fibre metro network	176135,83	0,00	0,00
Wireless transport	64000,00	4800,00	43800,00
OPEX Energy	40804,63	0,00	0,00
OPEX others	195730,38	0,00	0,00

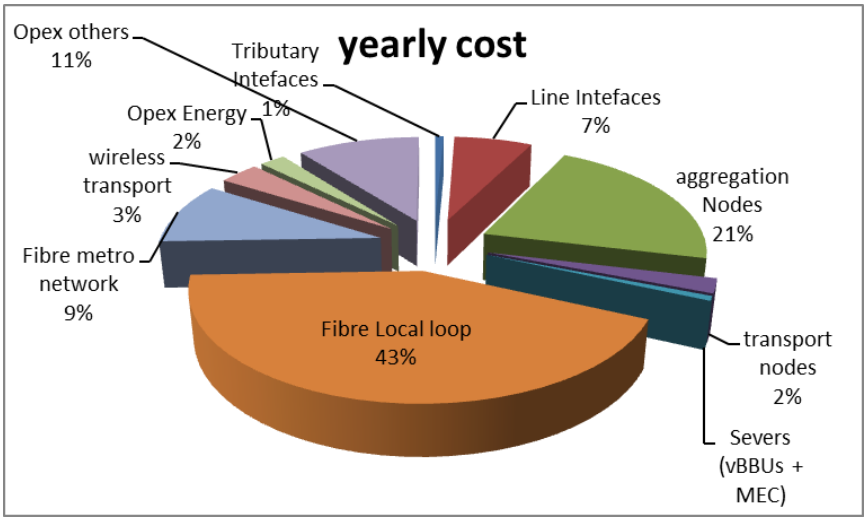

Figure 6-13: Pie-chart representing the percentage of yearly cost of different components for use case C.

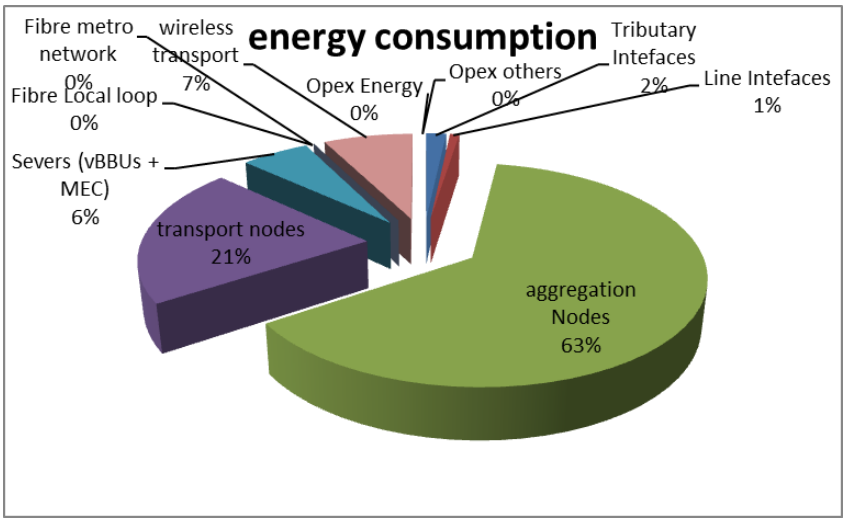

Figure 6-14: Pie-chart representing the energy consumption of different components for use case C.

6.7.4 Use case D results

The use case D depicts a scenario for an incumbent network operator, that has deployed fiber at 75% both in the local loop and at transport level, and whose network is characterized by massive statistical multiplexing (20%). MEC offloading is about 10%. Synthesis and details on costs and energy consumption are shown in Table 6-16 and Table 6-17. The results of these tables are also displayed as pie-charts in Figure 6-15 and Figure 6-16.

Table 6-16: synthesis of costs and energy consumption for use case D.

Total CAPEX (yearly) [€]	**1614167**
Total OPEX [€]	223395
YCO [€]	1837562
YCO per user [€]	6,13
Total Power [kW]	62406
Total Energy (per year) [kWh]	569455
Energy per user (per year) [kWh]	1,90

Table 6-17: details of costs and energy consumption for use case D.

Element	yearly Cost [€]	Power [W]	Energy [kWh]
Tributary Intefaces	13538,50	1084,00	9891,50
Line Intefaces	114458,00	482,00	4398,25
Aggregation Nodes	398570,40	40380,00	368467,50
Transport nodes	36780,00	12250,00	111781,25
Severs (vBBUs + MEC)	11600,00	3410,00	31116,25
Fibre Local loop	799084,30	0,00	0,00
Fibre metro network	176135,83	0,00	0,00
Wireless transport	64000,00	4800,00	43800,00
OPEX Energy	39861,83	0,00	0,00
OPEX others	183533,34	0,00	0,00

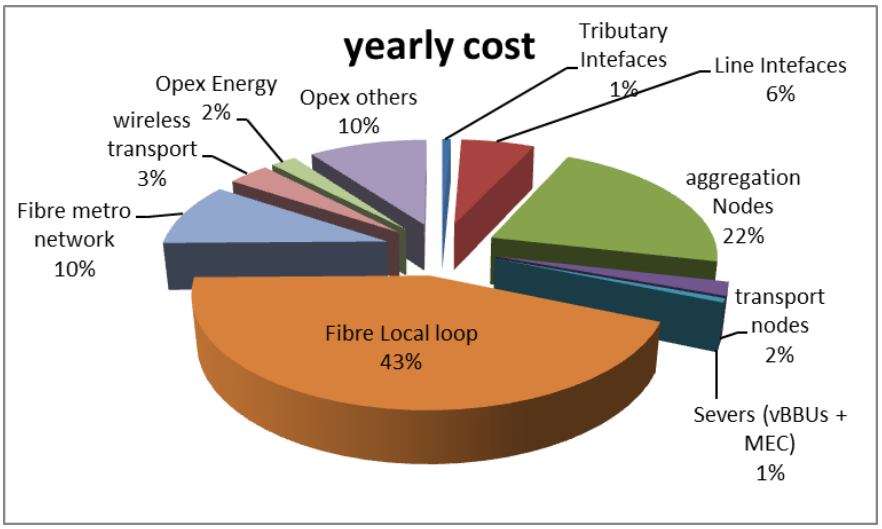

Figure 6-15: Pie-chart representing the percentage of yearly cost of different components for use case D.

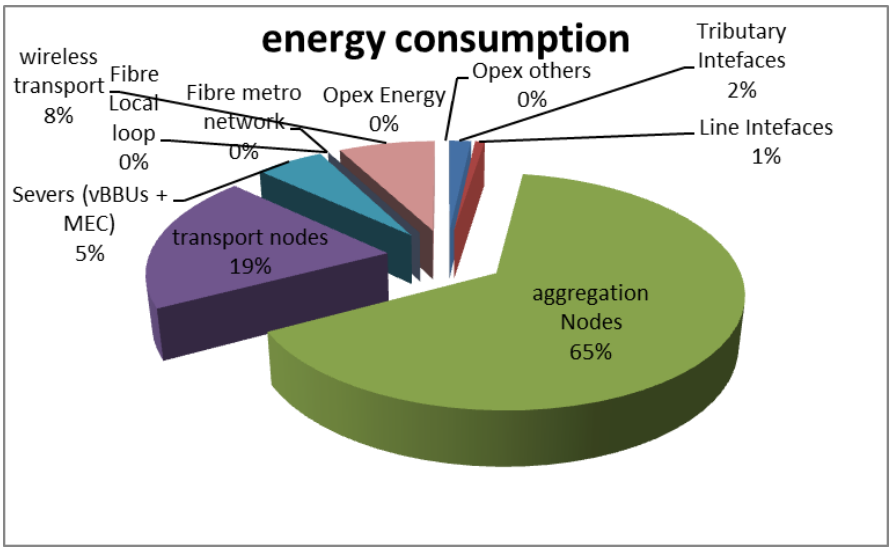

Figure 6-16: Pie-chart representing the energy consumption of different components for use case D.

6.7.5 Use cases results analysis

This cost and energy consumption analysis has evidenced some important results:

- The yearly total cost per 5G service and per device ranges from 6 € to 15 €, considering only the network segment, i.e., excluding the antenna;
  This is a confirmation that 5G is a commercially viable technology, with annual costs that can be estimated to be about 100-200 € per user, considering multiple devices per user
- The fiber in the local loop is the biggest cost share, so that incumbent operators, owning fibre and digs, are commercially advantaged;
- The analysis confirms that wireless system, even if they have been used in a small percentage in this specific analysis, have a not negligible impact on costs;
- Aggregation nodes for transport are the most energy hungry elements, followed by transport nodes and then by wireless systems and servers for vBBUs and MEC;
- Massive statistical multiplexing does not bring significant cost savings (see YCO results in case C and D, which are almost the same value). This means that the network investment can be future-proof against dramatic volume increase.

7 Conclusions

5G-PICTURE, in aligment with the overall 5G vision, targeted to develop a generic architecture that is able to support a set of stringent requirements in terms of latency, reliability and density, along with tight constraints on geographical and population coverage and mobility capabilities. The project focuses on the development and demonstration of a transport network infrastructure supporting converged fronthaul and backhaul services integrating advanced wireless and novel optical and packet network solutions. The requirements that the architecture needs to support have been identified and studied through the generic 5G KPIs defined as part of the 5G PPP KPI WG activites and also the specific use cases planned to be showcased in the framework of the project. These use cases include a Rail related demonstarion in Catalonia, Spain, a Smart City demonstration in the city wide test-bed in Bristol, UK and a Stadium event demo also located in Bristol, UK, exploiting the generic 5G-PICTURE architecture and technology developments.

The main architectural principles that 5G-PICTURE have focused on include convergence and integration of network and compute technologies, network softwarisation, hardware programmability and dissagregation of compute/storage and network resources. Adopting these concepts, the project has proposed the architectural approach of Dissagggregated – Radio Access Network (DA-RAN) – to facilitate provisioning of any service across the infrastructure by flexibly and efficiently mixing-and-matching network, compute and storage resources. The overall architectural approach of the project involves a layered structure comprising a programmable data plane that exposes a set of physical and virtual funtions to the control plane. Services are provisioned through the orchestration layer responsible to combine physical and/or virtual functions adopting the notion of service chaining. In this generic framework, 5G-PICTURE relies on a set of hardware and software innovations associated with the data plane, the control plane and the orchestration layer.

In terms of the data plane, the 5G-PICTURE vision involves a set of highly configurable wired/wireless infrastructures and interfaces, integrated in a single transport solution. Therefore, the 5G-PICTURE network is highly heterogeneous, being composed by passive and high capacity elastic optical networks, packet/Ethernet based networks, mmWave and massive MIMO wireless transport technologies. Since this heterogeneity can be a limiting factor to the integration of the various network segments, 5G-PICTURE leverages the concept of data plane programmability to seamlessly merge the various technologies and to offer a set of network functions that can be deployed among the programmable elements of the network to efficiently realize the required network services. Specific technologies that have been developed, extended and integrated to include: (a) aggregation of 10Gb clients to 40/100Gb is added to the architecture, (b) TSON frame slice are modified to become transparent to other packet processing devices maintainign the time-slices frames visible for processing, (c) all TSON wavelengths (i.e. 10G, 40G, and 100G) are supporting elastic bandwidth allocation mode, (d) TSON supports the eCPRI protocol frame, which is either native Ethernet frame with VLAN, IPV4 packet with VLAN, or IPV6 packet with VLAN with eCPRI Ethertype (IEEE1914.3) and (e) TSON has been extended with encoding and decoding capabilities to support Network Coding for Resilient C-RANs. In addition, the 5G-PICTURE wireless transport and access network adopt massive MIMO, mmWave, and Sub-6 technologies that leverage much greater numbers of antennas at the radio units to improve data rates, reliability as well as energy efficiency. In 5G-PICTURE, these technologies feature programmability and upgradability, with the goal of being able to satisfy the demands of 5G. The mMIMO RU architecture developed in 5G-PICTURE provides the following benefits: (a) peak capacity up to 8x compared to 2x2 RRH, (b) FH capacity requirement only 3x of CPRI 2x2 RRH, or 1/3 of 16x16 CPRI RRH, (c) maximum allowed delay variation increased from 5 µs to >100 µs, (d) Beamforming weight update time reduced by 10x, and (e) high degree of reconfigurability, updatability, alarm reporting through M-Plane. A mmWave solution developed in the framework of the project addresses the rapid prototyping in the micro- and mmWave frequency region using an SDR approach. This is supported by the real-time capabilities that this platform feauters making it a good candidate for use in running and upcoming 5G-related projects. In terms of wireless technologies theTyphoon Platform supproting data plane programmability has been extended towards virtualized synchronisation functions in support of the deployment of mmWave Typhoon nodes along the track as part of the Railway demonstration activities 6. The BWT IP that is included within the Typhoon module consists in the patented HYDRA technology (Hybrid Defined Radio Architecture). A key feature of the HYDRA is that both the PHY and the MAC layer of its IEEE 802.11ad modem combine optimized hardware accelerators with programmable parallel processing. Namely both MAC and PHY are software-defined, which allows the performance of novel mmWave wireless algorithms to be explored and continuously tailored in the context of advanced research platforms. The Typhoon utilises the latest integrated electronic beam steering phased array antenna, RF and baseband technologies and is available in various configurations. The 5G-PICTURE transport also includes packet-based technologies such

as Flex-E and X-Ethernet. Flex-E enables Ethernet-based services to be mapped over a next-generation optical transport network with the most efficient utilization of capacity. X-Ethernet on the other hand stands for extended distance, expanded granularity and extremely low latency and introduces Ethernet PCS switching based on the interface offered by Flexible-Ethernet. The basic switching unit is Flex-E Client but with enhanced desing that allows removing all the time-consuming procedures, such as encapsulation/decapsulation, queuing and table lookup. Finally, The packet level programmable dataplane aims to provide the following main capabilities: (a) protocol independence, thus managing programmable parsing of the protocol stack for generic field extraction, (b) extended rule matching capabilities providing programmable flow level stateful behaviors and (c) programmable packet level actions for generic packet generation, encapsulation/decapsulation. 5G-PICTURE developed several building blocks to achieve these objectives, namely (i) V-PMP, a VLIW (Very Long Instruction Word) processor called V-PMP tailored for packet manipulation task; (ii) FlowBlaze, a programmable data plane focused on the implementation of stateful per-flow functionalities based on eXtended Finite State Machine (XFSM) and (iii) a P4 compiler to configure high speed Mellanox Ethernet switches.

5G-PICTURE focused on demonstrating how programmable hardware platforms can be used to instantiate several physical and virtual functions, which can then be dynamically orchestrated by an operating system (5G OS) to deploy connectivity services on demand. A number of the aforementioned functions classified in three groups, namely: *RAN*, *Transport*, and *Synchronization* functions have been developed that make use of specialized processors developed in WP3, e.g. the AIR Massive MIMO platform, various FPGAs platforms, the CNIT Open Packet Processor (OPP), or the I2CAT Sub-6 and BWT mmWave wireless platforms. In addition, we have other software functions that make use of generic x86 compute resources. Looking at how the various functions are integrated with the 5G OS developed three main cases have been identified: (a) functions that are part of the 5G OS, i.e. a control function of the 5G OS, (b) physical network functions that are controlled by the 5G OS through a well-defined API or descriptor, and (c) software functions that are virtualized (VM/container) and are dynamically instantiated by the 5G OS. In addition, there are some functions that are physical transmission technologies, and therefore do not interact with the 5G OS.

One of the very central targets for the 5G-PICTURE architecture is to support multi-tenancy, different strategies can be applied to support slicing for both the RAN and transport network. Specifically, for the RAN, slicing can rely on slicing at the spectrum level, the ICIC level, the packet scheduling level, and at the admission control level. For a disaggregated RAN environment such as in the 5G-PICTURE infrastructure, three overlapping service levels have been identified. First, Infrastructure-as-a-Service, which provides programmable software-defined infrastructure for hosting RAN services. Second, Platform-as-a-Service that extends the former mentioned service in monitoring and orchestrating the functions of RAN slices. And finally, Software-as-a-Service including control applications such as RRM and SMA to provide control logics. RAN runtime that belongs to the category of Platform-as-a-Service, provides a multiservice execution environment for customized functioning and sharing of radio resources at RAN. RAN runtime allows slice owner or service provider to perform the following tasks, providing individual control for multiple tenants or operators over their specific resources: (a) managing the RAN slices, (b) performing controlled logics, (c) operate on virtual resource level, e.g., resource block groups, and (d) access the state of a plane revealed by RAN runtime. In 5G-PICTURE slicing related use cases will be shown as part of the Bristol stadium and the Spanish Rail demonstrations.

The final evaluation and benchmarking of the 5G-PICTURE architecture was performed using mathematical models, simulation frameworks that have been purposely developed. In this deliverable we present our final evaluation tools as they have been developed in the second year of the project, and a set of scenarios and use cases that have been defined and analysed using these tools. The architecture evaluation focuses on the data and control planes proposed by the generic 5G-PICTURE architecture. In terms of data plane the topics/scenarios considered address performance of the 5G wireless access communications to trains and the adoption of Sub-6 GHz LTE Massive MIMO technologies, multi-technology access network solutions in railway systems and the benefits these can provide in terms of reliability and throughput. In terms of the optical transpot the extesnion of TSON to provide rellient C-RAN services is also discussed. The adoption of network coding in support of resilient C-RAN services have been proposed and showcased and the performance of the corresponding solution is assessed experimentaly in a lab environment and theoretically at network level. Possible approaches for efficient dynamic placement of softwarised RAN functions in Data Centres adopting the disaggregated 5G-PICTURE architecture have been studied and evaluated and suitable solutions are proposed. Emphasis is also given on scalability topics where a novel service chaining approach is proposed that can significantly reduce service provisioning times. Control plane scalability issues are investigated through optimal SDN placement approaches relying on Evolutionary Game Theory. Investigation and proposal of suitable approaches to enable scalable service chaining in MEC-assisted 5G Networks exploiting Artificial Intelligence,

and finally scalable multi-service placement is also examined. The performance of these schemes is examined over realistic topologies using actual traffic statistics.

Finally, the 5G-PICTURE architecture has been assessed in terms of energy and cost efficiency through a detailed techno-economic analysis taking into consideration real traffic statistics and equipement costs. The analysis was performed using two complementary, fully parameterized tools leveraging on the work and expertise gained from two 5G-PPP projects, namely 5G-XHaul and 5G-CROSSHAUL. The combination of these tools enables: (a) modelling transport network deployments based on 5G-PICTURE technologies and the architectural options that they support, (b) modelling various access network deployments and traffic demand/network usage scenarios, (c) dimensioning the modelled transport network deployments in an automated way and (d) obtaining comparative cost and energy efficiency results of the various deployment options. These are adopted with the aim to: a) pre-estimate the critical, high cost factors and extracting deployment guidelines at network pre-planning stages (macro-scale strategic planning phases) and b) at next stage (network-planning phases) perform detailed cost estimation and assessment of specific micro/medium scale mobile and fixed access network deployments. Using these tools various scenarios have be evaluatedin terms of their energy consumption and cost including Greenfield vs. Brownfield optical network deployment; optical vs. wireless vs. hybrid deployment options with various 5G-PICTURE technologies mixtures; multiple Functional Splits (FSs) deployments ranging from eCPRI A to eCPRI E; adoption of different MIMO schemes; and multiple grades of incorporating edge or cloud computing for FS processing and/or specific application services.

8 References

[1] Cisco Visual Networking Index: Global Mobile Data Traffic Forecast Update, 2017–2022, Available: https://www.cisco.com/c/en/us/solutions/collateral/service-provider/visual-networking-index-vni/white-paper-c11-738429.pdf

[2] 5G-PICTURE, Deliverable D2.2 System architecture and preliminary evaluations, 31st July 2018.

[3] 3GPP TS 22.261 V16.1.0 (2017-09) 3rd Generation Partnership Project; Technical Speci-fication Group Services and System Aspects; Service requirements for the 5G system; Stage 1 (R16)

[4] 3GPP, TR 22.861, "Feasibility Study on New Services and Markets Technology Enablers for massive Internet of Things; Stage 1"

[5] 3GPP, TR 22.862, "Feasibility study on new services and markets technology enablers for critical communications; Stage 1"

[6] 3GPP, TR 22.863, "Feasibility study on new services and markets technology enablers for enhanced mobile broad-band; Stage 1"

[7] 3GPP, TR 22.864, "Feasibility study on new services and markets technology enablers for network operation; Stage 1"

[8] 3GPP, TR 22.891, "Feasibility study on new services and markets technology enablers; Stage 1"

[9] Recommendation ITU-R M.2083-0 (09/2015): IMT Vision - Framework and overall objectives of the future development of IMT for 2020 and beyond.

[10] NGMN 5G Initiative Team, "A Deliverable by the NGMN Alliance", NGMN 5G White Paper, Feb.17, 2015 - https://www.ngmn.org/5g-white-paper/5g-white-paper.html

[11] Euro-To5G project, Deliverable D2.6, "Final report on programme progress and KPIs", https://5g-ppp.eu/wp-content/uploads/2017/10/Euro-5G-D2.6_Final-report-on-programme-progress-and-KPIs.pdf

[12] 5G PPP, 5G PPP phase II KPIs – Annex to Programme Management Report, August 2019.

[13] 5G empowering vertical industries, brochure available online at https://5g-ppp.eu/wp-content/uploads/2016/02/BROCHURE_5PPP_BAT2_PL.pdf

[14] 5G-PICTURE, Deliverable D2.1 5G and Vertical services, use cases and requirements, January 2018.

[15] 5G-PICTURE, Deliverable D6.2 Vertical Demo and Testbed setup and initial validation results, July 2018.

[16] METRO-HAUL, Deliverable D2.1 Definition of Use Cases, Service Requirements and KPIs, Feb 2018

[17] 5G-PICTURE deliverable D3.3, “Final report on Data Plane Programmability and infrastructure components”, submission date November 2019.

[18] 5G-PICTURE deliverable D2.2, “System architecture and preliminary evaluations”, 2018.

[19] O-RAN Fronthaul Working Group, “Control, User and Synchronization Plane Specification”, Technical Specification, 2019.

[20] O-RAN Fronthaul Working Group, “Management Plane Specification”, Technical Specification, 2019.

[21] 5G-PICTURE D3.2, “Intermediate report on data plane programmability and infrastructure components,” 30 2018 November. [Online]. Available: https://www.5g-picture-project.eu/publication_deliverables.html. [Accessed 30 November 2018].

[22] 5G-PICTURE D3.1, “Initial report on data plane programmability and infrastructure components,” 4 2018 April. [Online]. Available: https://www.5g-picture-project.eu/publication_deliverables.html. [Accessed 11 April 2018].

[23] M. Grandi, D. Camps-Mur, A. Betzler, J. J. Aleixendri, and M. Catalan, "SWAM: SDN-based Wi-Fi Small Cells with Joint Access-Backhaul and Multi-Tenant Capabilities", IEEE IWQoS 2018.

[24] 5G-PICTURE D4.1, “State of the art and initial function design,” 28 February 2018. [Online]. Available: https://www.5g-picture-project.eu/publication_deliverables.html. [Accessed 9 September 2018].

[25] 5G-PICTURE D4.2, “Complete design and initial evaluation of developed functions,” 30 November 2018. [Online]. Available: https://www.5g-picture-project.eu/publication_deliverables.html. [Accessed 30 November 2018].

[26] 5G-PICTURE D4.3, “Integration of developed functions with 5G-PICTURE orchestrator”, submission date November 2019.

[27] 5G-PICTURE deliverable D5.1, “Relationships between Orchestrators, Controllers, slicing systems”, November 2018.

[28] 5G-PICTURE deliverable D5.2, “Auto-adaptive Hierarchies”, May 2019.

[29] 5G-PICTURE deliverable D5.3, “Support for multi-version services”, May 2019.

[30] A. Tulumello, G. Belocchi, M. Bonola, S. Pontarelli and G. Bianchi, "Pushing Services to the Edge Using a Stateful Programmable Dataplane," 2019 European Conference on Networks and Communications (EuCNC), Valencia, Spain, 2019, pp. 389-393.

[31] Miano, Sebastiano, et al. "Creating complex network service with eBPF: Experience and lessons learned." High Performance Switching and Routing (HPSR). IEEE (2018).

[32] Pontarelli, Salvatore, Roberto Bifulco, Marco Bonola, Carmelo Cascone, Marco Spaziani, Valerio Bruschi, Davide Sanvito et al. "FlowBlaze: Stateful Packet Processing in Hardware." In NSDI, pp. 531-548. 2019.

[33] Y. Piasetzky, M. Kadosh, M. Pritsak, O. Shabtai, A. Lo and G. Lu, "Switch ASIC Programmability in Hybrid Mode," 2018 IEEE 26th International Conference on Network Protocols (ICNP), Cambridge, 2018, pp. 448-449.

[34] O. Sallent, J. Perez-Romero, R. Ferrus and R. Agusti, "On radio access network slicing from a radio resource management perspective," *IEEE Wireless Communications,* vol. 24, no. 5, pp. 166-174, 2017.

[35] X. Foukas, M. Marina and K. Kontovasilis, "Orion: RAN Slicing for a Flexible and Cost-Effective Multi-Service Mobile Network Architecture," in *International Conference on Mobile Computing and Networking - MobiCom*, 2017.

[36] C. Chang and N. Nikaein, "Closing in on 5G Control Apps: Enabling Multiservice Programmability in a Disaggregated Radio Access Network," *IEEE Vehicular Technology Magazine,* vol. 13, no. 4, pp. 80-93, 2018.

[37] X. Foukas, N. Nikaein, M. M. Kassem, M. K. Marina and K. Kontovasilis, "FlexRAN: A flexible and programmable platform for software-defined radio access networks," in *12th International on Conference on emerging Networking EXperiments and Technologies*, 2016.

[38] NGMN Alliance, "NGMN 5G White Pape," 2015. [Online]. Available: https://www.ngmn.org/fileadmin/ngmn/content/downloads/Technical/2015/NGMN_5G_White_Paper_V1_0.pdf. [Accessed September 2019].

[39] X. Zhou, R. Li and T. Z. H. Chen, "Network slicing as a service: enabling enterprises' own software-defined cellular networks," *IEEE Communications Magazine,* vol. 54, no. 7, pp. 146-153, 2016.

[40] 3GPP, "Study on management and orchestration of network slicing for next generation network," in *3GPP TR 28.801, v15.1.0*, 2018.

[41] G. Brown, “Mobile Edge Computing Use Cases & Deployment options,” Juniper White paper, July 2016.

[42] ETSI White paper, MEC Deployments in 4G and Evolution Towards 5G, No. 24, Feb. 2018.

[43] Q. Zheng, Y. Chen, R. Dreslinski, C. Chakrabarti, A. Anastasopoulos, S. Mahlke, and T. Mudge, “Wi-Bench: An Open Source Kernel Suite for Benchmarking Wireless Systems”, 2013 IEEE International Symposium workload Characterization (IISWC), Portland, OR, 2013, pp.123-132.

[44] J. Perelló et al., "All-optical packet/circuit switching-based data center network for enhanced scalability, latency, and throughput," in IEEE Network, vol. 27, no. 6, pp. 14-22, November-December 2013.

[45] A. Tzanakaki et al., "Wireless-Optical Network Convergence: Enabling the 5G Architecture to Support Operational and End-User Services," *IEEE Communications Magazine*, vol. 55, no. 10, pp. 184-192, Oct. 2017.

[46] M. Anastasopoulos, A. Tzanakaki and D. Simeonidou, "Service Chaining in MEC – Assisted Large Scale 5G Networks," *2018 European Conference on Optical Communication (ECOC)*, Rome, pp. 1-3, 2018.

[47] A. Tzanakaki, M. P. Anastasopoulos, and D. Simeonidou, "Converged Optical, Wireless, and Data Center Network Infrastructures for 5G Services," *Journal of Optical Communications and Networking* 11, A111-A122, 2019.

[48] F. Musumeci, C. Bellanzon, N. Carapellese, M. Tornatore, A. Pattavina, and S. Gosselin, "Optimal BBU Placement for 5G C-RAN Deployment Over WDM Aggregation Networks," IEEE Journal of Lightwave Technology, 34, 1963-1970, 2016.

[49] C. Ranaweera, E. Wong, A. Nirmalathas, C. Jayasundara and C. Lim, "5G C-RAN With Optical Fronthaul: An Analysis From a Deployment Perspective," IEEE Journal of Lightwave Technology, vol. 36, no. 11, pp. 2059-2068, 1 June, 2018.

[50] B. M. Khorsandi, C. Raffaelli, M. Fiorani, L. Wosinska and P. Monti, "Survivable BBU Hotel placement in a C-RAN with an Optical WDM Transport," in Proc. of *Design of Reliable Communication Networks (DCRN) 2017,* Munich, Germany, pp. 1-6, 2017.

[51] M. Shehata, O. Ayoub, F. Musumeci and M. Tornatore, "Survivable BBU Placement for C-RAN over Optical Aggregation Networks," *in Proc. of 20th International Conference on Transparent Optical Networks (ICTON)*, Bucharest, 2018, pp. 1-4.

[52] M. Klinkowski, "Planning of 5G C-RAN with Optical Fronthaul: A Scalability Analysis of an ILP Model," *2018 20th International Conference on Transparent Optical Networks (ICTON)*, Bucharest, pp. 1-4, 2018.

[53] A. Tzanakaki, M. P. Anastasopoulos and D. Simeonidou, "Optical networking: An Important Enabler for 5G," *2017 European Conference on Optical Communication (ECOC)*, Gothenburg, pp. 1-3, 2017.

[54] D. Sabella, N. Nikaein, A. Huang, J. Xhembulla, G. Malnati and S. Scarpina, "A Hierarchical MEC Architecture: Experimenting the RAVEN Use-Case," *2018 IEEE 87th Vehicular Technology Conference (VTC Spring)*, Porto, pp. 1-5, 2018.

[55] A.M. Geoffrion. Generalized Benders decomposition. Journal of Optimization Theory and Applications, Vol. 10, No. 4. pp. 237–260, 1972.

[56] A. Clauset et al., Hierarchical structure and the prediction of missing links in networks, Nature 453, 98–101, 2008

[57] D. J. Garcia, F. You, Supply chain design and optimization: Challenges and opportunities, Computers & Chemical Engineering, Vol. 81, pp. 153-170, 2015.

[58] J.-F. Cordeau, G. Stojković, F. Soumis, and J. Desrosiers, Benders Decomposition for Simultaneous Aircraft Routing and Crew Scheduling Transportation Science, Vol. 35: No. 4, 375-388, 2001.

[59] B. Vignac, B. F. Vanderbeck, and B. Jaumard, *Reformulation and Decomposition Approaches for Traffic Routing in Optical Networks*, Networks, Vo.. 67, No. 4, 2016.

[60] A. Tzanakaki et al., "5G infrastructures supporting end-user and operational services: The 5G-XHaul architectural perspective," IEEE ICC, 2016.

[61] M. Ruffini, Multi-Dimensional Convergence in Future 5G Networks. IEEE/OSA JLT, Vol. 35, No. 3, March 2017.

[62] B. Khorsandi, F. Tonini, C. Raffaelli, "Design methodologies and algorithms for survivable C-RAN," *ONDM* 2018, pp. 106-111.

[63] B. M. Khorsandi, C. Raffaelli, M. Fiorani, L. Wosinska and P. Monti, "Survivable BBU Hotel placement in a C-RAN with an Optical WDM Transport," *DRCN 2017* 2017, pp. 1-6.

[64] M. Shehata, O. Ayoub, F. Musumeci and M. Tornatore, "Survivable BBU Placement for C-RAN over Optical Aggregation Networks," *2018 20th ICTON*, Bucharest, 2018, pp. 1-4.

[65] S. Mohamed et al., "Resilient BBU placement in 5G C-RAN over optical aggregation networks", Photonic Network Commin., Jan. 2019

[66] E. Wong, E. Grigoreva, L. Wosinska and C. M. Machuca, "Enhancing the survivability and power savings of 5G transport networks based on DWDM rings," in *IEEE/OSA Journal of Optical Communications and Networking*, vol. 9, no. 9, pp. D74-D85, Sept. 2017.

[67] C. Colman-Meixner, G. B. Figueiredo, M. Fiorani, M. Tornatore and B. Mukherjee, "Resilient cloud network mapping with virtualized BBU placement for cloud-RAN," *in proc. of ANTS*, Bangalore, 2016, pp.

[68] A. Tzanakaki, M. P. Anastasopoulos and D. Simeonidou, "Optical networking: An Important Enabler for 5G," *2017 European Conference on Optical Communication (ECOC)*, 2017, pp. 1-3.

[69] T. K. Dikaliotis, A. G. Dimakis, T. Ho and M. Effros, "On the delay of network coding over line networks," *IEEE ISIT* 2009, pp. 1408-1412.

[70] 5G-XHaul Project, Deliverable D2.2, ” System Architecture Definition”, submitted on July 1st, 2016.

[71] “IEEE Standard for a Precision Clock Synchronization Protocol for Networked Measurement and Control Systems”, IEEE Std 1588-2008.

[72] Y. Yan. et al, “FPGA-based Optical Network Function Programmable Node”, in Proc. OFC (2014)

[73] A.-F.Beldachi. et al, ‘Experimental Demonstration of 5G Fronthaul and Backhaul Convergence based on FPGA-based Active Optical Transport’. in proc of ECOC 2018.

[74] http://www.ieee802.org/1/pages/tsn.html

[75] https://www.xilinx.com/products/intellectual-property/axi_10g_ethernet.html

[76] https://www.xilinx.com/support/documentation/ip_documentation/axi_10g_ethernet/v3_1/pg157-axi-10g-ethernet.pdf

[77] 5G-XHaul Project, Deliverable D3.1 ” Evaluation of wireless-optical converged functionalities at UNIVBRIS testbed”, June 31st, 2016

[78] N. Gkatzios, M. Anastasopoulos, A. Tzanakaki and D. Simeonidou, "Compute Resource Disaggregation: An Enabler for Efficient 5G RAN Softwarisation," *2018 European Conference on Networks and Communications (EuCNC)*, Ljubljana, Slovenia, 2018, pp. 1-5.

[79] X. Chen et al., “Analyzing and modeling spatio-temporal dependence of cellular traffic at city scale,” in Proc. of IEEE International Conference on Communications (ICC), 2015.

[80] A. Tzanakaki et al., "Wireless-Optical Network Convergence: Enabling the 5G Architecture to Support Operational and End-User Services," in IEEE Communications Magazine, vol. 55, no. 10, pp. 184-192, Oct. 2017.

[81] M. Kamel, W. Hamouda and A. Youssef, "Ultra-Dense Networks: A Survey," in IEEE Communications Surveys & Tutorials, vol. 18, no. 4, pp. 2522-2545, Fourthquarter 2016.

[82] H. Liu, F. Eldarrat, H. Alqahtani, A. Reznik, X. de Foy and Y. Zhang, "Mobile Edge Cloud System: Architectures, Challenges, and Approaches," in IEEE Systems Journal, vol. 12, no. 3, pp. 2495-2508, Sept. 2018.

[83] Software-Defined Networking”, https://www.opennetworking.org/sdn-definition/ .

[84] B. Heller, R. Sherwood and N. McKeown, “The Controller Placement Problem”, in Proceedings of Hot Topics in Software Defined Networking (HotSDN), 2012.

[85] D. Hock, M. Hartmann, S. Gebert, M. Jarschel, T. Zinner and P. Tran-Gia, "Pareto-optimal resilient controller placement in SDN-based core networks," Proceedings of the 2013 25th International Teletraffic Congress (ITC), Shanghai, 2013, pp. 1-9.

[86] J. W. Weibull, “Evolutionary Game Theory”, MIT Press, 1997.

[87] Tao Yi and Wang Zuwang, “Eject of Time Delay and Evolutionarily Stable Strategy”, Academic Press Limited, 1997.

[88] Germán Obando et.al., “Replicator dynamics under perturbations and time delays”, Springer Mathematics of Control, Signals, and Systems, Vol 28, no 3, 2016.

[89] eCPRI Specification V1.1 (2018-01-10), http://www.cpri.info/

[90] Wübben et.al., "Benefits and Impact of Cloud Computing on 5G Signal Processing", in IEEE Signal Processing Magazine, pp. 35-44, November 2014.

[91] C. Desset et.al., "Flexible power modeling of LTE base stations", in IEEE Wireless Communications and Networking Conference (WCNC), Shanghai, China, April, 2012.

[92] N. Ben-Khalifa, R. El-Azouzi and Y. Hayel, "Random time delays in evolutionary game dynamics," 2015 54th IEEE Conference on Decision and Control (CDC), Osaka, 2015, pp. 3840-3845.

[93] S. Bernard et.al., “Sufficient conditions for stability of linear differential equations with distributed delay”, Discrete & Continuous Dynamical Systems -series B, vol 1, no 2, pp. 233-256, 2001.

[94] J. Baliga, R. Ayre, K. Hinton, W. V. Sorin and R. S. Tucker, "Energy Consumption in Optical IP Networks," in Journal of Lightwave Technology, vol. 27, no. 13, pp. 2391-2403, 2009.

[95] Internet2 Layer 2 services. https://www.internet2.edu/products-services/advanced-networking/layer-2-services/

[96] Platform Overview. www.opendaylight.org

[97] Mininet Overview. http://mininet.org/overview/

[98] https://grnet.gr/infrastructure/network-and-topology/

[99] Student's t-distribution. https://en.wikipedia.org/wiki/Student%27s_t-distribution

[100] “5G Vision. The 5G Infrastructure Public Private Partnership: the next generation of communication networks and services.,” 2015. [Online]. Available: [Online] https://5g-ppp.eu/wp-content/uploads/2015/02/5G-Vision-Brochure-v1.pdf.

[101] “GSMA Intelligence, Understanding 5G: Perspectives on future technological advancements in mobile.,” Dec 2015. [Online]. Available: https://www.gsmaintelligence.com/research/?file=c88a32b3c59a11944a9c4e544fee7770&download.

[102] “3GPP Release 12. (E-UTRAN), Overall description, Stage 2 (Release 12). TS36.300, v12.6.0.”.

[103] “3GPP Release 10. Architecture enhancements for non-3gpp accesses. Technical specification TS 23.402, 2012. Release 10.”.

[104] “ETSI GS NFV-SWA 001 V1.1.1 (2014-12), “Network Functions Virtualisation (NFV); Virtual Network Functions Architecture”,” 2014.

[105] Wang, Y., Haas, H., 2015. Dynamic Load Balancing With Handover in Hybrid Li-Fi and Wi-Fi Networks, Journal of Lightwave Technology, Volume: 33, Issue: 22.

[106] “CHINA mobile White paper, C-RAN: The Road Towards Green RAN,” [Online]. Available: http://labs.chinamobile.com/cran/.

[107] “Meet LTE-R, the network responsible for next-generation smart trains,” [Online]. Available: https://www.rcrwireless.com/20161115/fundamentals/smart-trains-lte-tag31-tag99.

[108] R. He and et. al, “High-Speed Railway Communications: from GSM-R to LTE-R,” IEEE Vehicular Communications Magazine, 2016.

[109] “Connected Rail Solution Design Guide,” November 2016. [Online]. Available: https://www.cisco.com/c/dam/en_us/solutions/industries/docs/cts-dg.pdf.

[110] “Cisco Wireless Controller Configuration Guide, Release 8.2,” [Online]. Available: https://www.cisco.com/c/en/us/td/docs/wireless/controller/8-2/config-guide/b_cg82/b_cg82_chapter_0101101.html.

[111] Haas, H., et. al, 2016. “What is LiFi,” Journal of Lightwave Technology, Volume: 34 , Issue: 6

[112] Chen, C., Basnayaka, D., Haas, H., 2016. “Downlink Performance of Optical Attocell Networks,” Journal of Lightwave Technology, Volume: 34, Issue: 1

[113] Epple, B., 2007. “Performance Optimization of free space optical communication protocols based on results from FSO demonstrations,” SPIE 6709, Free-Space Laser Communications VII, 670915.

[114] Refai, H., Sluss, J., Refai, H., 2005. “The transmission of multiple RF signals in free-space optics using wavelength division multiplexing,” SPIE 5793, Atmospheric Propagation II.

[115] Ninos, M., et. al., 2018. CDMA Radio on FSO links over Gamma Turbulence Channels with Nonzero Boresight Pointing Errors, Int. Conf. on Modern Circuits and Systems Technolgy, 2018.

[116] Mai, V., et. al, 2013. Performance of TCP over free-space optical atmospheric turbulence channels, Journal of Optical Communications and Networking, Volume: 5 , Issue: 11, pp. 1168 - 1177.

[117] Hasegawa, Y., 2017. A Transmission Control Protocol for Free-Space Optical Communications, IEEE Global Communications.

[118] “Huawei, Building 4G on High-Speed Railways,” [Online]. Available: http://www1.huawei.com/en/static/HW-371912.pdf.

[119] Tzanakaki, A., et.al., 2016. 5G infrastructures supporting end-user and operational services: The 5G-XHaul architectural perspective, In proc. of IEEE ICC, 2016.

[120] Sivaraman, A., 2016, Packet Transactions: High-Level Programming for Line-Rate Switches, ACM SIGCOMM

[121] Brebner, G., 2015. Programmable hardware for high Performance SDN, OFC

[122] “ETSI GS NFV-EVE 005 V1.1.1, Network Functions Virtualisation (NFV); Ecosystem; Report on SDN Usage in NFV Architectural Framework. 2015-12.”.

[123] Jin H., et al, 2013, “OpenFlow-Based Flow-Level Bandwidth Provisioning for CICQ Switches, IEEE Transaction on Computers, vol. 62.

[124] Tzanakaki, A., et al., 2013. Virtualization of heterogeneous wireless-optical network and IT support of cloud and mobile Services, IEEE Communications Magazine, Volume: 51, Issue: 8.

[125] Chen X., et al, 2015. Analyzing and modeling spatio-temporal dependence of cellular traffic at city scale, IEEE ICC

[126] Fang, Y., Chlamtac, I., 2002. Analytical Generalized Results for Handoff Probability in Wireless Networks, IEEE Trans Communications, Volume: 50, Issue: 3.

[127] M. Anastasopoulos, A. Tzanakaki and D. Simeonidou, "Service Chaining in MEC – Assisted Large Scale 5G Networks," 2018 European Conference on Optical Communication (ECOC), Rome, 2018, pp. 1-3.

[128] ETSI White Paper No. 11, Mobile Edge Computing A key technology towards 5G, Sep. 2015.

[129] A. Tzanakaki et al., "5G infrastructures supporting end-user and operational services: The 5G-XHaul architectural perspective," 2016 IEEE International Conference on Communications Workshops (ICC), Kuala Lumpur, 2016, pp. 57-62.

[130] Common Public Radio Interface:eCPRI Interface Specification, D01, Aug. 2017.

[131] A. Gupta et al., |On service-chaining strategies using Virtual Network Functions in operator networks”, Computer Networks, Vo. 133, 14 March 2018.

[132] 5G Vision. The 5G Infrastructure Public Private Partnership: the next generation of communication networks and services. 2015. [Online].

[133] A. Tzanakaki et al., "Wireless-Optical Network Convergence: Enabling the 5G Architecture to Support Operational and End-User Services", IEEE Commun. Mag., pp. 184 – 192, Aug. 2017.

[134] M. Anastasopoulos et al., “ICT platforms in support of future railway systems”, in proc. of TRA 2018, Apr. 2018.

[135] F. Musumeci, C. Bellanzon, N. Carapellese, M. Tornatore, A. Pattavina, and S. Gosselin, "Optimal BBU Placement for 5G C-RAN Deployment Over WDM Aggregation Networks," J. Lightwave Technol. 34, 1963-1970 (2016).

[136] T. Pfeiffer, "Next generation mobile fronthaul and midhaul architectures [Invited]," in IEEE/OSA Journal of Optical Communications and Networking, vol. 7, no. 11, pp. B38-B45, November 1 2015.

[137] M. Fiorani, S. Tombaz, J. Martensson, B. Skubic, L. Wosinska and P. Monti, "Modeling energy performance of C-RAN with optical transport in 5G network scenarios," in IEEE/OSA Journal of Optical Communications and Networking, vol. 8, no. 11, pp. B21-B34, Nov. 2016.

[138] M. Anastasopoulos, A. Tzanakaki and D. Simeonidou, "Stochastic Energy Efficient Cloud Service Provisioning Deploying Renewable Energy Sources," in IEEE Journal on Selected Areas in Communications, vol. 34, no. 12, pp. 3927-3940, Dec. 2016.

[139] Antonia Pelekanou, Markos Anastasopoulos, Anna Tzanakaki, Dimitra Simeonidou, “Provisioning of 5G Services Employing Machine Learning Techniques”, International Conference on Optical Network Design and Modeling, May 2018.

[140] Jure Leskovec, Anand Rajaraman, Jeffrey D. Ullman, “Mining of Massive Datasets”, Cambridge University Press New York, NY, USA 2011

[141] M. Starstedt and E. Mooi, “Cluster Analysis”, Springer-Verlag, Berling 2014.

[142] Joe H. Ward, Jr, “Hierarchical Grouping to Optimize an Objective Function”, Journal of the American Statistical Association, vol. 58, no. 301, pp. 236-244, March 1963.

[143] X. Chen et al., “Analyzing and modeling spatio-temporal dependence of cellular traffic at city scale,” in proc. of IEEE ICC, pp.3585-3591, 2015

[144] Jinn-Tsong Tsai, Jyh-Horng Chou, Tung-Kuan Liu, “Tuning the Structure and Parameters of a Neural Network by Using Hybrid Taguchi-Genetic Algorithm”, IEEE Transactions on Neural Networks, vol. 17, no. 1, January 2006.

[145] H.K. Lam, S.H. Ling, F.H.F. Leung, P.K.S. Tam, “Tuning of the structure and Parameters of Neural Networks using Improves Genetic Algorithm”, IEEE Transactions on Neural Networks, vol. 14, no. 1, January 2003.

[146] Dinesh P. Pitambare, “Survey on Optimization of Number of Hidden Layers in Neural Networks, International Journal of Advances Research in Computer and Communication Engineering, November 2016.

[147] Hossein Valavi, Peter J. Ramadge, “An Upper-Bound on the Required Size of a Neural Network Classifier”, ICASSP, 2018.

[148] James Bergstra, Yoshua Bengio, “Random Search for Hyper-Parameter Optimization”, Journal of Machine Learning Research, February 2012.

9 Acronyms

Acronym	Description
5G OS	5G Operating System
AI	Artificial Intelligence
AoA	Angle of Arrival
API	Application Programming Interface
APs	Access Points
ATC	Automatic Train Control
BBU	Baseband Unit
BIO	Bristol Is Open
BMC	best master clock
BN	Best Node
BS	Base Station
BVT	Bandwidth Variable Transponder
CAPEX	CApital Expenditures
CBR	Constant Bit Rate
CG	Candidate Group
CO	Central Office
CoMP	Coordinated Multi-Point
CP	Cyclic Prefix
C-RAN	Cloud-RAN
CSI	Channel State Information
CU	Central Unit
DAC	Digital-to-Analogue Converter
DA-RAN	Dis-Aggregated RAN
DC	Domain Controller
DL	Downlink
DMP	Data Management Platform
DO	Domain Orchestrator
D-RAN	Distributed-Radio Access Network
DU	Distributed Unit
eMBB	enhanced Mobile Broadband
ER	Eligible Region
ETB	Ethernet Train Backbone
ETB	Ethernet Train Backbone level
F1AP	F1 Application Protocol
FCS	Frame Check Sequence
FEC	Forward Error Correction
FFT	Fast Fourier Transform
FPGA	Field Programmable Gate Array
GOPS	giga operation per second
GPP	general-purpose processors

GST	Guaranteed Service Transport
GTP	GPRS Tunnelling Protocol
HRG	Hierarchical Random Graph
HW	hardware
IAB	integrated Access and Backhaul
ICIC	Inter-Cell Interference Coordination
IFFT	Inverse Fast Fourier Transform
IoT	Internet of Things
IPS	instructions per second
ISG	Industrial Specification Group
ITU	International Telecommunications Union
KPI	Key Performance Indicators
LLR	Logarithmic Likelihood Ratios
LoS	Line of Sight
LSTM	Long Short-Term Memory
LTE	Long Term Evolution
LUT	Look up table
M2M	Machine to Machine
MAC	Medium Access Control
MCM	Markov Chain Monte Carlo
MDO	Multi-Domain Orchestrator
MEC	Mobile Edge Computing
MEF	Metro Ethernet Forum
MIMO	Multiple-Input Multiple-Output
MLP	Multilayer Perceptron
mMTC	massive Machine Type Communications
MNO	Mobile Network Operator
MPI	Multi-protocol interfaces
NAT	Network Address Translation
NEST	Network Slice Template
NFV	Network Function Virtualization
NIC	Network Interface Card
NMS	Network Management System
NN	Neural Network
NR	New Radio
NSD	Network Service Descriptor
NSO	Network Service Orchestrator
OAI	OpenAirInterface
OCC	Operations and Control Centre
ODM	Operational Data Management
OLT	Optical Line Terminal
ONU	Optical Network Unit
OPEX	OPerational EXpenditure
OPP	Open Packet Processor

OS	Operating System
OSS	Operations Support System
PCS	Physical Coding Sublayer
PDCP	Packet Data Convergence Protocol
PDU	Protocol Data Unit
PMA	Physical Medium Attachment
PNF	Physical Network Function
PRB	Physical Resource Block
PTP	Precision Time Protocol
QoS	Quality of Service
RB	Resource Block
RBIR	Received Bit mutual Information Rate
REC	Radio Equipment Control
REST	REpresentational State Transfer
RLC	Radio Link Control
RMSE	Root-Mean-Square Error
RN	Remote Node
RO	Resource Orchestrator
RoE	Radio over Ethernet
RRC	Radio Resource Control
RTT	Round-Trip-Time
RU	Remote Unit
SC	service chaining
SC-FDMA	Single Carrier Frequency Diversity Multiple Access
SDAP	Service Data Adaptation Protocol
SDR	software-defined radio
SLA	Service Level Agreements
SoC	System on Chip
SPP	specific-purpose processors
SW	software
TCN	Train Communication Network
TSN	Time Sensitive Networking
TSON	Time Shared Optical Network
UHD	ultra-high definition
UL	Uplink
URLLC	Ultra-Reliable and Low Latency Communications
VLIW	Very Long Instruction Word
VNF	Virtual Network Function
VOQ	Virtual Output Queues
VR	Virtual Reality
WACC	Weighted Average Cost Of Capital
WG	Working Group